

**Engineered Spider Silk Fusion
Proteins for Enhanced Functionality
in Tissue Engineering and Medical
Applications**

by

Kai Mayer

Born in Heidelberg

ORCID: 0000-0002-5914-3677

October 2023

Submitted in total fulfillment of the requirements of the
degree of a jointly awarded Doctor of
Philosophy (PhD / DR. RER. NAT)

between the

*Bayreuther Graduiertenschule für Mathematik und
Naturwissenschaften (BAYNAT)
University of Bayreuth*

and the

Department of Biomedical Engineering
The University of Melbourne

This doctoral thesis was prepared jointly at the department of Biomaterials at the University of Bayreuth and the department of Biomedical Engineering at the University of Melbourne from June 2019 until June 2023 and was supervised by Prof. Dr.Thomas Scheibel and A/Prof Daniel E. Heath.

Form of the dissertation: monograph

Date of submission: 29.09.2023

Admission by the executive board: 10.10.2023

Date of defense: 15.05.2024

Acting director: Prof. Dr. Jürgen Köhler

Doctoral committee:

Prof. Dr.Thomas Scheibel (reviewer)

A/Prof Dr.Daniel E. Heath (reviewer)

Prof Dr. Daniela Loessner (reviewer)

Prof. Dr.Anna Schenk (chair)

Juniorprof. Dr. Meike Leiske

Abstract

Tissue engineering and cardiovascular disease management are essential in regenerative medicine, addressing the pressing need for functional tissue regeneration and improved treatment options for cardiac conditions. This thesis explores the potential of recombinant spider silk proteins as versatile biomaterials for tissue engineering applications and stent coating technology, aiming to advance the fields and offer innovative solutions to critical medical challenges.

In the realm of tissue engineering, the design and fabrication of biomimetic scaffolds play a pivotal role in guiding cell behavior and promoting tissue regeneration. Due to their structural similarity to the extracellular matrix and ability to support cell growth and function, hydrogels have emerged as promising scaffolds for tissue engineering applications. This thesis presents eADF4(C16)-CBD, a modified spider silk fusion protein processed into an injectable hydrogel with enhanced mechanical properties and stability compared to the unmodified spider silk variant. By modifying the recombinant spider silk with a cellulose-binding domain, the hydrogel achieves increased mechanical strength and improved cell adhesion, making it a valid scaffold for tissue regeneration. The eADF4(C16)-CBD hydrogel exhibits excellent biocompatibility, tunable mechanical properties, and the ability to support cell proliferation, presenting a versatile approach for tissue engineering in various clinical applications.

In the domain of cardiovascular disease management, the development of improved coatings for drug-eluting stents is of utmost importance. Current stents face significant challenges, including inflammation or limited endothelialization. To overcome these limitations, this thesis investigates the potential of eADF4(C16) as a coating material for stents. By genetically coupling the cell-selective peptide REDV, the eADF4(C16)-REDV coating promotes cellular attachment and rapid endothelialization, mitigating inflammation and enhancing the formation of a functional endothelial layer. The eADF4(C16)-REDV coating demonstrates excellent hemocompatibility, tunable degradation properties, and the ability to release therapeutic agents in a controlled manner, offering a promising solution to improve stent performance and patient outcomes.

Experimental investigations, encompassing cell culture studies, mechanical characterization, biocompatibility assessments, and *in vitro* evaluations, substantiate the potential of recombinant spider silk proteins in tissue engineering and cardiovascular disease management. The exceptional versatility, biocompatibility, and tunable properties of eADF4(C16)-CBD and eADF4(C16)-REDV make them highly attractive biomaterials for various biomedical applications. These proteins provide opportunities to address the complex challenges associated with tissue regeneration, such as the development of functional tissues with appropriate mechanical properties and the improvement of stent coatings to achieve enhanced endothelialization, reduced inflammation, and improved hemocompatibility.

Developing and utilizing these biomaterials will offer new possibilities for addressing the complex challenges associated with tissue regeneration and cardiovascular diseases, ultimately leading to enhanced patient outcomes, improved quality of life, and the advancement of biomedical science.

Kurzzusammenfassung

Geweberegeneration (engl. Tissue Engineering) und die Behandlung von kardiovaskulären Erkrankungen sind essentiell in der regenerativen Medizin und zielen darauf ab, den dringenden Bedarf an funktionellen Geweben und verbesserten Behandlungsmöglichkeiten für Herz-Kreislauf-Erkrankungen zu decken. Diese Dissertation erforscht das Potenzial von rekombinanten Spinnenseidenproteinen, insbesondere eADF4(C16)-CBD und eADF4(C16)-REDV, als vielseitige Biomaterialien für Anwendungen im Bereich des *Tissue Engineering* und der Beschichtung von Stents, mit dem Ziel, innovative Lösungen für wichtige medizinische Herausforderungen anzubieten.

Im Bereich des *Tissue Engineering* spielen das Design und die Herstellung von biomimetischen Gerüsten eine entscheidende Rolle bei der Steuerung des Zellverhaltens und der Förderung der Geweberegeneration. Aufgrund ihrer strukturellen Ähnlichkeit zur extrazellulären Matrix und ihrer Fähigkeit, das Zellwachstum und die Funktion zu unterstützen, haben sich Hydrogele als vielversprechende Gerüste für Anwendungen im *Tissue Engineering* herauskristallisiert. Diese Dissertation fokussiert sich auf eADF4(C16)-CBD, ein modifiziertes Spinnenseiden-Fusionsprotein, als injizierbares Hydrogel mit verbesserten mechanischen Eigenschaften und Stabilität im Vergleich zur unmodifizierten Variante. Durch die Modifikation der rekombinanten Spinnenseide mit einer Cellulose-Bindungsdomäne erreicht das Hydrogel eine erhöhte mechanische Festigkeit und verbesserte Zelladhäsion, was es zu einem geeigneten Gerüst für die Geweberegeneration macht. Das eADF4(C16)-CBD Hydrogel zeichnet sich durch exzellente Biokompatibilität, anpassbare mechanische Eigenschaften und die Fähigkeit zur Unterstützung der Zellproliferation aus, was eine vielseitige Verwendungsmöglichkeit für *Tissue Engineering* in verschiedenen klinischen Anwendungen darstellt.

Im Bereich der Behandlung von kardiovaskulären Erkrankungen ist die Entwicklung verbesserter Beschichtungen für medikamentenfreisetzende Stents von größter Bedeutung. Aktuelle Stents stehen vor erheblichen Herausforderungen, wie Entzündungen oder begrenzter Endothelialisierung. Um diese Einschränkungen zu überwinden, untersucht diese Dissertation das Potenzial von eADF4(C16) als Beschichtungsmaterial für Stents. Durch die genetische

Kopplung des zellselektiven Peptids REDV fördert die eADF4(C16)-REDV Beschichtung die Zelladhäsion und eine schnelle Endothelialisierung, was Entzündungen mindert und die Bildung einer funktionalen Endothelschicht verbessert. Die eADF4(C16)-REDV Beschichtung zeigt eine ausgezeichnete Hämokompatibilität, anpassbare Abbau-Eigenschaften und die Fähigkeit, therapeutische Wirkstoffe kontrolliert freizusetzen, was eine vielversprechende Lösung zur Verbesserung der Stent-Leistung und der Patientenergebnisse bietet.

Experimentelle Untersuchungen, einschließlich Zellkulturstudien, mechanischer Charakterisierung, Biokompatibilitätsbewertung und *in vitro*-Evaluationen, belegen das Potenzial der rekombinanten Spinnenseidenproteine im *Tissue Engineering* und im Management von kardiovaskulären Erkrankungen. Die außergewöhnliche Vielseitigkeit und Biokompatibilität von eADF4(C16)-CBD und eADF4(C16)-REDV machen sie zu äußerst attraktiven Biomaterialien für verschiedene biomedizinische Anwendungen. Diese Proteine bieten Möglichkeiten, die Entwicklung funktionaler Gewebe mit geeigneten mechanischen Eigenschaften und die Verbesserung von Stent-Beschichtungen zur Erzielung einer verbesserten Endothelialisierung, einer reduzierten Entzündung und einer verbesserten Hämokompatibilität voranzutreiben.

Declarations

(§ 9 Satz 2 Nr. 3 PromO BayNAT)

Hiermit versichere ich eidesstattlich, dass ich die Arbeit selbstständig verfasst und keine anderen als die von mir angegebenen Quellen und Hilfsmittel benutzt habe (vgl. Art. 64 Abs. 1 Satz 6 BayHSchG).

(§ 9 Satz 2 Nr. 3 PromO BayNAT)

Hiermit erkläre ich, dass ich die Dissertation nicht bereits zur Erlangung eines akademischen Grades eingereicht habe und dass ich nicht bereits diese oder eine gleichartige Doktorprüfung endgültig nicht bestanden habe.

(§ 9 Satz 2 Nr. 4 PromO BayNAT)

Hiermit erkläre ich, dass ich Hilfe von gewerblichen Promotionsberatern bzw. -vermittlern oder ähnlichen Dienstleistern weder bisher in Anspruch genommen habe noch künftig in Anspruch nehmen werde.

(§ 9 Satz 2 Nr. 7 PromO BayNAT)

Hiermit erkläre ich mein Einverständnis, dass die elektronische Fassung meiner Dissertation unter Wahrung meiner Urheberrechte und des Datenschutzes einer gesonderten Überprüfung unterzogen werden kann.

(§ 9 Satz 2 Nr. 8 PromO BayNAT)

Hiermit erkläre ich mein Einverständnis, dass bei Verdacht wissenschaftlichen Fehlverhaltens Ermittlungen durch universitätsinterne Organe der wissenschaftlichen Selbstkontrolle stattfinden können.

Kai Mayer

This is to certify that

- i. this thesis comprises only my original work towards the PhD,
- ii. due acknowledgement has been made in the next to all other material used, and
- iii. the thesis is less than 100,000 words in length, exclusive of tables, figures, bibliography and appendices.

Kai Mayer

Preface

The entire research of this thesis was conducted by its author, Kai Mayer, with the supervision of Thomas Scheibel and Daniel Heath, where not otherwise stated. Individual experiments were conducted as service work and are acknowledged throughout the text. As such,

- Dr Martin Humenik and Andreas Schmidt conducted MALDI-TOF measurements at the University of Bayreuth.
- Dr Yukie O'Brian conducted Gas chromatography measurements as service work requested from the TrACEES platform of the University of Melbourne.
- Alexander Ruhoff conducted the UV-dependent platelet plasma assays (Factor XIIa and turbidity) at the Heart Research Institute of the University of Sydney.
- Athulya Wickramasingha, under the supervision of Prof. Luke Henderson, observed the polyacrylamide coatings as intermediate layer between steel and spider silk.

Lastly, Prof. Anna Waterhouse provided extensive knowledge about blood-surface interactions and kindly offered her help by hosting a research stay at her Cardiovascular Medical Devices group at the University of Sydney to conduct these experiments.

Parts of chapters 4 and 5 are used to prepare the manuscript "REDV-functionalised recombinant spider silk for next-generation coronary artery stent coatings: hemocompatible, drug-eluting, and endothelial cell-specific materials."

This manuscript is still in the editing phase, and at the time of the submission of this thesis, it has not been submitted to any journal.

Furthermore, the eADF4(C16)-CBD protein discussed in this thesis was used in a cooperative research effort with the technical university Munich (TUM) to create biocompatible light waveguides. This research was funded by the bavarian environmental ministry within the BayBionik project frame (FKZ: TUT01UT-73843) and is published as:

M. Reimer, K. Mayer, D. Van Opdenbosch, T. Scheibel, C. Zollfrank, Biocompatible Optical Fibers Made of Regenerated Cellulose and Recombinant Cellulose-Binding Spider Silk. *Biomimetics (Basel)* **8**, (2023).

This publication is not included in this thesis.

Acknowledgements

This incredible journey, which extended across continents, was imbued with tremendous and, oftentimes, overwhelming experiences that I could not have navigated without the emotional and professional support of cherished friends, former colleagues, and family. I have crossed paths with remarkable individuals throughout these four years, and to them, mere words on paper will not be adequate thanks. Nevertheless, I will try to do them justice as I recount our encounters.

This journey began during my master studies when I applied to the nascent Biofabrication program at the University of Bayreuth. The dean of the program and my future supervisor, Thomas Scheibel, not only enabled me to complete half of my master studies at the University of Melbourne, Australia but also offered a PhD candidacy at his department after that. He continued as my primary supervisor for the next four years. Concurrently, I had the privilege of meeting Andrea O'Connor and Daniel Heath, who acted as my supervisors in Australia, extending a warm welcome and supporting me acclimatizing to this new environment. My deepest appreciation goes out to you three for fostering my academic growth across these two extraordinary research groups, and for your unwavering support and insightful feedback. You were there for me in every instance, lending a willing ear and helping me overcome many hurdles this joint PhD presented. On that note, there must be special thanks to Irina Heschner, who supported me with all the paperwork this journey presented.

The laboratories I worked in were a confluence of brilliant colleagues, many of whom became dear friends. In Bayreuth, I was fortunate to share office space with my first Julia Jasinski and Shakir Bin Zainuddin, who embarked on this journey alongside me. Together, we grappled with research conundrums and navigated the administrative IT-labyrinth of our department. During my Melbourne breaks, I bonded with my office mate Tim Schiller, as we balanced our research endeavors with recreational activities. Further, I want to extend my gratitude to the entire lab ensemble: Martin and Hendrick for their insightful feedback, our secretaries Sabrina and Andrea for their indispensable roles in running the department smoothly, the TA-team comprising Nicole, Alex, JD, and Anderl, and all fellow PhD candidates, past and present.

Thank you Xuen, Tebbi, Dr. Sommer, Ashish, Christina, Suphun, Kathrin and Julia C, Vanessa T and N, Anika D and W, Sarah, Fabian and Christian.

In Melbourne, my lab group was a tremendous source of support and camaraderie. Your individual and collective contributions to this incredible experience are indelible. In particular, I want to thank Hazem, Mike, Matt, Tao, Wiktor, Nick, and Anna for their engaging professional and casual conversations. Additionally, our spirited group - Courtney, Xin, Anna-Lena, Shirin, Anita, Claire, Andrea, and Shaveen - was always up for activities, creating memorable moments like the futsal cup and trivia-wins at PA's.

The unique structure of the University of Melbourne and its cross-departmental collaborations significantly bolstered the quality of my work. Special thanks to Roger Curtain from the Bio21 facility for offering me the quintessential Australian experience with his SEM inductions. I hold those moments dear, may his soul rest in peace!

Networking opportunities at the ASBTE were crucial in enriching my work. At a conference in Melbourne in April 2022, Daniel introduced me to Anna Waterhouse who graciously invited me to her lab at the University of Sydney to conduct human whole-blood tests. I gathered valuable data and made meaningful connections alongside her students Alex Ruhoff, Tiffany Goh, and Jasneil Singh. Thanks for the warm welcome, complete with a fire alarm on the first day.

I am sure I have inadvertently missed some names in this gratitude roll call, but please know that every one of you has enriched my journey immeasurably. You've all played your part in making my dream a reality; I am eternally grateful for that.

Away from the academic world, my friends from back home, especially my partner, Svenja, have been a constant source of support. Svenja, your patience, love, and strength, particularly during my travels, are beyond comparison. And finally, to my parents Martina and Ralph, who have backed my every decision from the very beginning, my deepest gratitude. Your constant support and love helped me not give up many times along the road.

Once again, thanks to everybody I met along this journey!

Publication List

M. Reimer, K. Mayer, D. Van Opdenbosch, T. Scheibel, C. Zollfrank, Biocompatible Optical Fibers Made of Regenerated Cellulose and Recombinant Cellulose-Binding Spider Silk, *Biomimetics* (Basel). 2023;8(1):37.

DOI: 10.3390/biomimetics8010037.

Strassburg, S., Mayer, K., Scheibel, T. (2021). 7 Functionalization of biopolymer fibers with magnetic nanoparticles. In S. Odenbach (Ed.), *Magnetic Hybrid-Materials: Multi-scale Modelling, Synthesis, and Applications* (pp. 167-194). Berlin, Boston: De Gruyter. DOI: 10.1515/9783110569636-007.

C. Haynl, J. Vongsivut, K.R.H. Mayer, H. Bargel, V.J. Neubauer, M.J. Tobin, M.A. Elgar, T. Scheibel, Free-standing spider silk webs of the thomisid *Saccodomus formivorus* are made of composites comprising micro- and submicron fibers, *Sci Rep*, 10 (2020) 17624. DOI: 10.1038/s41598-020-74469-z.

These publications are not related to this thesis and are therefore not included.

Conference Proceedings

27. September 2019	SPP 1681 meeting in Benediktbeuern, Germany	oral presentation
17. October 2019	kick-off event BayBionik in Nürnberg, Germany	oral presentation
13. February 2020	Ideenforum 2020 in Nürnberg, Germany	oral presentation
24. November 2021	Public showcase of BayBionik projects in the planetarium Nürnberg, Germany	oral presentation
20-22. April 2022	ASBTE conference in Melbourne, Australia	poster presentation
9. December 2022	ASBTE showcase Victoria, Melbourne, Australia	oral presentation
28-31. March 2023	TERMIS-EU, Manchester, UK	oral presentation

Awards during PhD candidature

Best oral presentation at the 2022 ASBTE regional showcase Victoria, Australia.

2022 Eugen Singer Award for outstanding Polymer research.

Table of Contents

Abstract	I
Kurzzusammenfassung	III
Declarations.....	V
Preface	VII
Acknowledgements	VIII
Publication List	X
Conference Proceedings.....	XI
Awards during PhD candidature	XI
Table of Contents.....	XII
List of Figures	XVII
List of Tables.....	XXIX
List of Abbreviations.....	XXX
Chapter 1 Literature Review	1
1.1 Introduction / Background	1
1.2 Tissue Engineering.....	3
1.3 Scaffolds	5
1.3.1 Scaffold materials: Biomaterials in Tissue Engineering and Medicine... 9	
1.3.2 Hydrogels in Tissue Engineering	10
1.3.3 Protein coatings for scaffolds and biomedical devices	16
1.4 Recombinant Spider Silk as Biomaterial	20
1.5 Applications of Recombinant Spider Silk in Tissue Engineering.....	25
1.5.1 Silk Materials in Bone Tissue Engineering	36
1.6 Recombinant fusion Proteins	38
1.6.1 Spider silk fusions	38
1.6.2 Cellulose blended Biomaterials.....	43
1.6.3 The role of Cellulose binding domains	45

1.7 State of the Art: CBD fusions	48
1.8 Peptide Modification of Biomaterials	51
1.8.1 Spider silk peptide modifications	55
1.9 State of the art: Drug-eluting stents (DES)	60
1.10 Objectives	67
1.10.1 Objective: design, production, purification and characterisation of novel eADF4(C16) based proteins	68
1.10.2 Objective: eADF4(C16)-CBD Hydrogels	69
1.10.3 Objective: eADF4(C16)-REDV Coatings.....	70
1.11 Scope of work	72
Chapter 2 Recombinant cellulose-binding spider-silk fusion protein: production and characterisation.....	75
2.1 Introduction.....	75
2.2 Materials and Methods	76
2.2.1 Genetic engineering of the fusion protein eADF4(C16)-CBD.....	76
2.2.2 Protein expression and purification	79
2.2.3 SDS polyacrylamide gel electrophoresis, silver staining and Western Blot	82
2.2.4 MALDI-TOF.....	84
2.2.5 Circular Dichroism (CD) spectroscopy	85
2.2.6 Fluorescence spectroscopy	86
2.2.7 Cellulose-binding assay.....	86
2.2.8 Spin-coating.....	86
2.2.9 QCM-D measurements	87
2.3 Results and Discussion	87
2.3.1 Designing eADF4(C16)-CBD.....	87
2.3.2 Proper folding of the CBD	89
2.3.3 Cellulose binding.....	93

2.4 Conclusion.....	95
Chapter 3 Hydrogels from recombinant cellulose-binding spider-silk fusion proteins	97
3.1 Introduction.....	97
3.2 Material and Methods	98
3.2.1 Hydrogel preparation	98
3.2.2 Rheology	99
3.2.3 3D printing.....	99
3.2.4 Cell culture: viability and proliferation of MG63 cells.....	99
3.2.5 SEM imaging	101
3.2.6 Statistical analysis	101
3.3 Results and discussion.....	101
3.3.1 Hydrogel formation	101
3.3.2 Enhanced Stiffness of eADF4(C16)-CBD Hydrogels through Cellulose Microfiber Blending	103
3.3.3 Application in Tissue Engineering: Injectable hydrogels for bone defects	109
3.4 Conclusion.....	113
Chapter 4 Endothelial cell-selective recombinant spider silk fusion protein: production and characterisation	116
4.1 Introduction.....	116
4.2 Material and Methods	117
4.2.1 Cloning of the REDV-modified eADF4(C16) protein.....	117
4.2.2 Protein Production and inclusion body purification	117
4.2.3 Preparation of aqueous eADF4(C16) solutions	121
4.2.4 Protein characterisation	122
4.2.5 Cell culture: adhesion and proliferation	122
4.2.6 Statistical analysis	123
4.3 Results and discussion.....	124

4.3.1 Protein characterisation	124
4.3.2 Cell selectivity	125
4.3.3 HUVEC proliferation	127
4.4 Conclusion.....	130
Chapter 5 Endothelial cell-selective recombinant spider silk fusion protein: application as a coating for DES.....	131
5.1 Introduction.....	131
5.2 Material and Methods	132
5.2.1 Coating of 316L stainless steel	132
5.2.2 AFM	133
5.2.3 Bending/scratching assay	133
5.2.4 SEM	134
5.2.5 Water contact angle	134
5.2.6 Gas chromatography	134
5.2.7 Polyacrylamide functionalisation and lap shear test	135
5.2.8 QCM-D measurements.....	137
5.2.9 Factor XIIa activation	137
5.2.10 Turbidity assay.....	137
5.2.11 Whole blood rocking assay.....	138
5.2.12 Modified Chandler loop	139
5.2.13 Enzymatic degradation	139
5.2.14 Everolimus elution	140
5.2.15 HPLC-MS.....	140
5.2.16 Statistical analysis.....	142
5.3 Results and discussion.....	143
5.3.1 Protein processing and coating of 316L stainless steel	143
5.3.2 Hemocompatibility	149
5.3.3 Enzymatic degradation of the coating.....	156

5.3.4 Drug elution properties	159
5.4 Conclusion.....	163
Chapter 6 Summary and future outlook	165
6.1 Summary	165
6.2 Future perspectives	169
References.....	174

List of Figures

Figure 1-1: Illustration of the traditional approach of Tissue Engineering. Cells suitable for the target applications are extracted and isolated from the patient, cultivated in vitro, seeded onto scaffolds and re-implanted into the patient. Adapted from reference [37] (© M. Asadin et al., published by MDPI, distributed under the terms of the Creative Commons Attribution 4.0 International License (CC BY 4.0), <http://creativecommons.org/licenses/by/4.0/>)..... 4

Figure 1-2: A): A hydrogel schematic showing a three-dimensional structure with a dense polymer network. B): Photograph of an actual protein hydrogel. In this case, a hydrogel from recombinant spider silk eADF4(C16)..... 8

Figure 1-3: A): A schematic of a thin polymer film. B): A photograph of a film cast from regenerated cellulose. Adapted from reference [93] (© M. Reimer et al., published by MDPI, distributed under the terms of the Creative Commons Attribution 4.0 International License (CC BY 4.0), <http://creativecommons.org/licenses/by/4.0/>) 8

Figure 1-4: Various chemical and physical cross-linking mechanisms. A) Showcases the active cross-linking, initiated mainly by adding a reaction partner. B) Demonstrates the creation of hydrogels via polymer-polymer interactions. C) Reveals photo cross-linked hydrogels formed by covalent bonds created by photoinitiated reactions. D) Features enzyme-mediated chemical cross-linking. In physical cross-linking, E) highlights the role of hydrophobic moieties annealing, while F) illustrates chain entanglement mediated through ionic interactions. G) Depicts hydrogen bonding as a form of physical attraction between polymer molecules, and lastly, H) shows the role of the formation of inter- or intramolecular crystalline regions. Figure inspiration from [110]..... 14

Figure 1-5: A selection of relevant coating techniques for polymer coatings in TE. A) A drop casting approach where a polymer solution is cast into a mold (or surface). Once cast, the solvent evaporates and a solid polymer coating forms. B) Demonstrates dip-coating. A substrate is immersed into the polymer solution and removed at a controlled speed to ensure reproducibility and homogeneous coatings. C) Depicts spin-coating, where the substrate rotates at high speed so the cast solution gets evenly and thinly distributed across the substrate. Suitable

for very thin films. D) illustrates electro spraying. Here two opposite charges are deployed at the substrate and solution, respectively. The attracting charges lead to droplets being ejected towards the surface, creating a thin and well-adjustable film on the substrate. E) highlights Electro-coating. Like electro spraying, two opposite charges are deployed between the solution and substrate. However, the substrate is immersed, and by applying several charge cycles, the thickness of the coating can be well-defined. 18

Figure 1-6: Illustration of the different spider silk variants found in orb webs of *A. diadematus*. Pyriform silk is used as attachment material on surfaces; Cylindriform silk is used as a protective shell for eggs; minor ampullate silk is used for the auxiliary spiral in the centre of the web; flagelliform silk forms the catching prey-catching spiral; major ampullate silk forms the frame and radii of the web and serves as dragline silk of the spider; Aggregate silk serves as a glue and is distributed across the surface of the web, and actiniform silk is used for wrapping living prey. Adapted and modified from reference [182] (© L. Eisoltd et al., published by Elsevier, distributed under the terms of the Creative Commons Attribution 3.0 International License (CC BY 3.0), <https://creativecommons.org/licenses/by-nc-nd/3.0/>) 21

Figure 1-7: Overview of *A. diadematus*' major ampullate silk structure. The red-framed boxes guides towards the protein of interest of this study, ADF4. Focusing on the MA silk, a highly repetitive core sequence flanked by NRN and NRC is illustrated. The core domain usually comprises MaSp-typical motifs, which, in turn, can form secondary protein structures such as β -sheets, -helices and -turns, as well as 3_{10} helices, yielding the fibres mechanical properties when spun. 22

Figure 1-8: Hierarchical structure of the dragline thread of *A. diadematus*. The fibre's outer shell is a lipid layer, surrounding a layer made of glycoproteins and minor ampullate silk. The fibre's core consists of multiple fibrils made of the MaSp proteins. Figure inspiration from [13]. 23

Figure 1-9: Amino acid sequence of eADF4(C16). The C-module is repeated 16 times, mimicking the properties of natural MaSp2 protein. Dark blue highlights the glutamic acid residue, adding a negative charge to each module. 25

Figure 1-10: Overview of the different recombinant spider silk morphologies used in TE. Natural spider silks serve as a blueprint for recombinant spider silk production. The production hosts bacteria, yeast, eukaryotic and insect cells are shown, as well as morphologies of recombinant spider silk (foam, fiber, film, hydrogel, and non-woven mesh) for potential applications in TE. Figure and caption adapted from reference [158] (© S. Salehi et al., published by MDPI, distributed under the terms of the Creative Commons Attribution 4.0 International License (CC BY 4.0), <http://creativecommons.org/licenses/by/4.0/>)..... 26

Figure 1-11: Shape fidelity assay of printed spider silk bioinks. A) Strands of each bioink formulation were printed on a pillar row with defined distances to observe the breaking point of an extruded ink line. B) Stereo microscopy images of the hanging lines of spider silk hydrogels with and without cell culture media (scale bars: 200 μm). Adapted from reference [58] (© A. Lechner et al., published by Wiley-VCH, distributed under the terms of the Creative Commons Attribution 4.0 International License (CC BY 4.0), <http://creativecommons.org/licenses/by/4.0/>) 30

Figure 1-12: A): Photograph of the AVL operation. The AVL was placed between two layers of spider silk hydrogel. B) Microcomputer tomography (μCT). After 2 and C) 4 weeks. Adapted from reference [59] (© S. Steiner et al., published by IOP publishing, distributed under the terms of the Creative Commons Attribution 4.0 International License (CC BY 4.0), <http://creativecommons.org/licenses/by/4.0/>) 31

Figure 1-13: A): Foam processing with cell incorporation. Media containing cells (pink) was blended with the fibronectin-modified spider silk solution (blue) (I). The introduction of air bubbles with pipette tip (II), induced the foam formation. B): mCherry was detected after 48 h, indicating the presence and incorporation of the differentiated human embryonic stem cells (hESC) into the foam structure. C+D): Immunostaining of the endodermal markers SOX17 (green) and FOX2A (red) was supported by RTqPCR analysis. Expression of the genes SOX17, CER1, NANOG for hESC in the silk foam versus that of a 2D culture. Bars represent the mean fold change \pm standard deviation (n = 4). E): Differentiation of human mesenchymal stem cells within the-silk foam into adipogenic lineage, showing lipids droplets stained by Red Oil (red) (n = 2, n = 4). Originally adapted from reference

[92] (© U. Johansson et al., published by IOP publishing, distributed under the terms of the Creative Commons Attribution 4.0 International License (CC BY 4.0), <http://creativecommons.org/licenses/by/4.0/>). Copyright 2019, Nature Research. Modified image and caption adapted from reference [158] (© S. Salehi et al., published by MDPI, distributed under the terms of the Creative Commons Attribution 4.0 International License (CC BY 4.0), <http://creativecommons.org/licenses/by/4.0/>). 32

Figure 1-14: Schematic of the spider silk-coated silicone implants, which are supposed to minimize fibrosis, cell proliferation, contractures and encapsulation by ECM proteins. Adapted from reference [52](© P. Zeplin et al., published by WILEY-VCH and reprinted with permission under license number 5558781272790.) 34

Figure 1-15: Calcium crystal deposition by differentiating human mesenchymal stem cell on the recombinant silk and silk-silica films. Calcium crystals (red) staining by alzarin red S was performed on hMSCs cells grown on nh-15mer (N-terminal his6 tag), nh-15mer-R5 (N-terminal his6 tag, C-terminal R5 protein), 15mer-ch (C-terminal his6 tag), R5-15mer-ch (C-terminal his6 tag, N-terminal R5 protein) and TCP (Tissue culture plate) four (A) and eight (B) weeks post seeding. Scale bars are 300 µm. (C) Quantification of calcium deposition of hMSCs grown on recombinant silk-silica constructs after 4 weeks (white bars) and 8 weeks (grey bars) in culture. Results for nh-15mer, nh-15mer-R5, 15mer-ch and R5-15mer-ch silk-silica constructs and TCP no osteogenesis and TCP osteogenesis are shown. Data are represented as the average ± standard deviation (n = 3, *p < 0.05). Figure and caption adapted from reference [246](© R. Plowright et al., published by Royal Society of Chemistry and reprinted with permission under license number 1397909-1.). 35

Figure 1-16: A): Test of formation of hydrogels by R4C (4 repeats of reisilin module with c-terminal spider silk) and R8C. Vials containing 15% (w/v) protein solutions were incubated for 10 min at the indicated temperatures and then inverted for image collection; (b) Oscillatory rheological analysis of R4C and R8C at a protein concentration of 20% (w/v). The temperature sweeps were performed with a heating rate of 2 °C min⁻¹. Figure and caption adapted from reference [272] (© F. Luo et al., published by MDPI, distributed under the terms of the

Creative Commons Attribution 4.0 International License (CC BY 4.0), <http://creativecommons.org/licenses/by/4.0/>)..... 40

Figure 1-17: Cellulose nanofibres (CNF)-based composite films show bioactivity. A): Optical microscopy images of CNF and composite CNF/silk films (top panel). Scale bars:4 mm. Fluorescence microscopy images show the binding of fluorophore-labeled IgG (green, bottom panel). Scale bars: 1 mm. B): Fluorescence images of IgG-fluorophore bound to casted films (top panel) and coatings on CNF films(bottom panel)of CNF and the Z domain alone (CNF/Z),CNF premixed with Z-silk (CNF/Z-silk) or pure CNF, respectively Scalebars: 1 mm. C): Human dermal fibroblasts cultured on CNF or CNF/FN-silk films for 7 days. Top panel: live/dead staining (green,living cells; red, dead cells/ autofluorescence from CNF). Bottom panel: F-actin staining (green, F-actin; blue, nuclei/autofluorescence from CNF). Scale bars: 500µm for 2×and 100µm for 10×. D): Number of Human dermal fibroblasts (mean + SD) per mm² on free-standing films of CNF (white bar) and CNF/FN-silk (grey bar), at 2, 4 and 6 days, as evaluated by DAPI staining and manual counting of nuclei. Statistically significant differences according to Student's t-test:**p< 0.01,***p< 0.001, and*****p< 0.00001. E): Representative Alamar blue viability graph of three independent experiments with Human dermal fibroblasts growing on CNF and CNF/FN-silk films (n=3) during 1 week. Statistically significant differences according to Student's t-test:*p< 0.05. Error bars show standard deviation. Figure and caption adapted from reference [273] (© N. Mittal et al., published by ACS Nano, distributed under the terms of the Creative Commons Attribution 4.0 International License (CC BY 4.0), <http://creativecommons.org/licenses/by/4.0/>) 42

Figure 1-18: Structure of CBD_{CEX} from C .fimi. Yellow highlights the tryptophan residues 17, 54 and 72, forming the comb to bind to cellulose molecules. 47

Figure 1-19: Viability of BxPC-3 cells (10 mio cells per milliliter) in printed constructs comprising 4% eADF4(C16), 3% eADF4(C16)-RGD, or 3% eADF4(C16)-RGE. Spider silk bioinks were printed using a RegenHU Bioplotter with a 22G tapered tip at room temperature and cultivated for up to 14 days at 5% CO₂, 95% relative humidity, and 37 °C. A) For CLSM imaging, live cells were stained with Calcein A/M (green) and dead cells with EthD-I (red). Background staining occurs due to interaction of hydrogels with EthD-I (scale bars: 100 µm).

B) Quantification of viable cells on day 1 and day 14 (**p ≤ 0.05). Figure and caption adapted from reference [336](© A. Lechner et al., published by WILEY-VCH and reprinted with permission under license number 5591210309508. 56

Figure 1-20: Fibroblasts form focal adhesions on peptide-modified silk films within 3 h. a) Representative micrograph of F-actin (red), vinculin (green) and nuclei (blue) stained fibroblasts allowed to adhere for 3 h on different films. b) Percentage of cells with apparent focal adhesions (n = 4, duplicates). Cells cultured on RGD ranked significantly better than WT (*=p < 0.05). Figure and caption adapted from reference [338](© M. Widhe et al., published by Elsevier and reprinted with permission under license number 5632990050324. 58

Figure 1-21: Pancreatic Islets maintained on RGD foam show improved in vivo survival and vascularization. A:) Percentage of islets that showed a stable or positive increase in size over a 4 week period. (5 mice, 1–6 islets per eye). B): Percentage of control islets (white bars) and islets from RGD foam (black bars) that showed clear vascularization by transmitted light imaging 4 weeks post-transplantation. (n = 3 separate transplantation experiments, 12 recipient mice, 1–6 islets per eye). C): Representative (n= 3) bright field micrographs of control islet (left) and islet from RGD foam (right) during in vivo imaging of the eye, where vasculature can be seen as grey areas. Scale bars = 50 µm. D): Morphology by H/E (hematoxylin and eosin staining) (left panel) and insulin (green, right panel) staining of eye sections showing representative (n=3) control islet (upper graphs) and islet from RGD foam (lower graphs). Vasculature was seen in islets from both culture conditions (white arrowhead), although vessels with erythrocytes were more common in islets from RGD foam. Areas of visual cell death were sometimes present in the control islet (white-lined circle). Scale bars = 50 µm. Figure and caption adapted from reference [339](© U. Johansson et al., published by PLOS ONE, distributed under the terms of the Creative Commons Attribution 4.0 International License (CC BY 4.0), <http://creativecommons.org/licenses/by/4.0/>) 60

Figure 1-22: Schematic of stent deployment showing a nearly closed blood vessel. A metal stent on an inflatable balloon is inserted into the target area, where the balloon is inflated, and the metal stent expands. After stent deployment, the

balloon gets deflated and removed from the system, leaving an expanded stent mesh. 61

Figure 1-23: Schematic of a stented vessel with a monolayer of EC forming to avoid neointimal hyperplasia. 72

Figure 1-24: Schematic of this thesis' structure. Both approaches start with a similar starting point: genetic spider silk modification. Once the novel proteins are created, the approaches divide into processing the protein into hydrogels for eADF4(C16)-CBD and into coatings for the REDV variant. Then, both morphologies will be evaluated on their potential use in Tissue Engineering applications..... 74

Figure 2-1: Workflow of combining two cut pCS parts to yield one closed pCS vector with the modified eADF4(C16) sequence. All involved restriction sites are shown, while the used sites are highlighted for each step. BamHI and HindIII are required for the next cloning step and are therefore included in this scheme. The two sequence-bearing vectors are digested with BseRI/BsaI and BsaI/BsgI, respectively. These fragments are then ligated to create a new pCS vector comprising the fused sequence. 78

Figure 2-2: Workflow of the eADF4(C16)-target-sequence transfer into an expression vector (pET). BamHI/HindIII digested the fused sequence in the pCS vector. The sequence is then transferred into a pET vector which has been treated the same. The sticky-ends facilitate improved ligation specificity, and the kanamycin resistance of the pET vector serves as a selection marker for successful cloning attempts. A general pET vector, not including the 6-His-tag is shown.... 79

Figure 2-3: Representative fermentation profile of overnight cultivation followed by a 1.5-hour induction window of eADF4(C16)-CBD. 80

Figure 2-4: A representative chromatogram of the IMAC-purification of eADF4(C16)-CBD..... 82

Figure 2-5: A: Silver stained SDS-gel of samples taken from IMAC-purification of eADF4(C16)-CBD and B: corresponding Westen Blot with T7-HRP-antibody detection. 84

Figure 2-6: MALDI-TOF of eADF4(C16)-CBD in aqueous solution showing a +1 peak at 60716 m/z and a +2 peak at 30361 m/z..... 85

Figure 2-7: A) The amino acid motifs of the hybrid spider silk-cellulose binding protein. B) Schematic structure of the fusion protein eADF4(C16)-CBD. Domain structure reproduced by PDB ID 3.2.1.91. The exposed tryptophan residues W17, W54, and W72, responsible for binding cellulose, are highlighted yellow. The proline-linker is demonstrated as a red string, and eADF4(C16) is shown in block form with the attached T7- and His-tag at the n-terminus 89

Figure 2-8: Far-UV CD spectra of eAD4(C16) and the CBD-modified variant. ... 90

Figure 2-9: Near UV- CD spectra of eADF4(C16)-CBD denatured by a temperature gradient (A) and a GdmCL gradient (B). The vertical dotted line represents the tryptophan peak at 290 nm, which decreases in intensity by proceeding denaturation. 91

Figure 2-10: Fluorescence spectra of eADF4(C16)-PL-CBD in the presence of different GdmCl concentrations. 92

Figure 2-11: Cellulose-binding assay. Concentration change after a 30-minute incubation of cellulose fibres with eADF4(C16) based protein solutions. 93

Figure 2-12: QCM-D measurements of 0.125 mg/mL eADF4(C16)-CBD and eADF4(C16) on cellulose films. Dashed red lines indicate a change of the introduced solution. The first line shows the change from the buffer to the protein solution, and the second line indicates the buffer wash following protein incubation. Dashed lines indicate the Sauerbrey approximation for adsorbed protein mass on the surface of the chip. (n=3) 95

Figure 3-1: 3D-bioprinted hydrogels from eADF4(C16)-CBD (A+B) and eADF4(C16) (C+D). Both gels are at 2% w/v protein concentration and were printed as a hollow cylinder with 5 mm in diameter. E: Silver stained SDS-gel of eADF4(C16)-CBD in reducing and non-reducing conditions. 103

Figure 3-2: SEM micrographs of the used CF to blend with eADF4(C16)-CBD for size analysis. Scale bars: A+B: 200 µm;C:20 µm. 104

Figure 3-3: Amplitude sweep of 2% w/v eADF4(C16) (A) and eADF4(C16)-CBD (B) with and without 3 mg/mL cellulose fibres (CF). (n=2) 105

Figure 3-4: Stiffness of 2% w/v hydrogels of eADF4(C16) and CF-enhanced eADF4(C16)-CBD (n=3).....	106
Figure 3-5: A: Stress-strain behaviour, and B: Viscosities of the different hydrogel blends. n=2	107
Figure 3-6: Schematic of the hypothesised gelation process. i): The eADF4(C16)-CBD protein (blue: eADF4(C16) moiety, green with purple cloud: CBD) binds to cellulose particles (black) in the solution. ii): The dense protein-cellulose network is further cross-linked via hydrophobic interactions of the protein fibrils (blue boxes).	108
Figure 3-7: SEM images of the freeze-dried bioink formulations. A)+C) eADF4(C16); B)+D) eADF4(C16)-CBD. Red dotted lines highlight incorporated cellulose fibres; scale bars: A)+B): 100 μm ; C)+D): 50 μm	109
Figure 3-8: MG63 cell culture on 2% (w/v) eADF4(C16) and eADF4(C16)-CBD (blended with 0.3% (w/v) cellulose fibres) hydrogels. A): Proliferation assay of MG63 cells in the bioink formulations over 8 days; *** $p\leq 0.001$. B)-E): Confocal micrographs of Live (green)/Dead (red) stained MG63 cells in the bioinks after 1 and 7 days; Scale bar:200 μm . F)+G): magnified micrographs of the cell morphology at day 7; scale bar: 200 μm	112
Figure 4-1: Representative fermentation profile of overnight induction for the high-yield production of eADF4(C16)-REDV.	118
Figure 4-2: A) A schematic of the fusion protein eADF4(C16)-REDV. The individual C-modules are shown in light and dark blue, the N-terminal T7-tag is highlighted in orange and the C-terminal REDV peptide in red. B) The silver-stained SDS-PAGE gels of eADF4(C16) (left) and eADF4(C16)-REDV (right) show the purity of the product and similar molecular weights.	120
Figure 4-3: MALDI-TOF was used to determine the molecular weight of eADF4(C16) (green) and the REDV variant (red). Results indicate that eADF4(C16) and eADF4(C16)-REDV molecular weights are 47.7 kDa and 48.7 kDa, respectively. A smaller peak at one-half the molecular weight corresponds to molecules with a z value of 2.....	121

Figure 4-4: A): The CD-spectra of both eADF4(C16) variants from 195 to 260 nm show no significant changes caused by the peptide modification. B): Fluorescence spectra of eADF4(C16)-REDV displaying a Thyrosine peak and no Tryptophane emission peak. 124

Figure 4-5: 4-hour adhesion of A) human smooth muscle cells, B) fibroblasts, and C) endothelial cells. Normalized to TCP-adhesion. *** $p \leq 0.001$ 127

Figure 4-6: A) 7-day proliferation of human endothelial cells on fibronectin-coated TCP and films of the spider silk variants. *** $p \leq 0.001$. B) Representative fluorescence images of endothelial cells on various surfaces over 7 days. Cell nuclei were stained blue (DAPI), f-actin was stained red (rhodamine-conjugated phalloidin), and CD31 was stained green (Alexa Fluor 488-conjugated rat anti-human CD31 antibody) (on day 7 only). Scale bar for all images identical: 200 μm 129

Figure 5-1: EVE-standard for HPLC-MS and UV 280nm. A) Chromatogram of EVE at 975.7 m/z with B) the standard derived from the peak values. C) the compound's photodiode array (PDA) signal at 280 nm, and D) the standard derived from the peak values thereof. Computed with the linear fit function of the Origin 2020b software. 142

Figure 5-2: Surface characterization of spider silk coatings on 316L stainless steel. The surface topography of pristine 316L stainless steel (left) and eADF4(C16)-REDV-coated 316L stainless steel (right) was visualised scanning electron microscopy 143

Figure 5-3: A: AFM image of a partly delaminated eADF4(C16)-REDV coating on 316L stainless steel with indication of measurement lines used to calculate the thickness of the coating. B: thickness profile obtained from 1 (black line) and the average of 100 (red line) lines of the AFM image. 144

Figure 5-4: The hydrophilicity of the various surfaces was investigated by measuring the water contact using sessile droplet tensiometry. Contact angle data is presented as mean \pm standard error (n=10 and) and *** indicates that $p \leq 0.001$ 145

Figure 5-5: Gas chromatography of pre-determined HFIP concentrations in methanol and an overnight leaching sample of an eADF4(C16)-REDV coated 316L stainless steel sheet. A: Total ion chromatogram. B: Multiple ion chromatogram of the sum of ions $m/z = 51, 69, 99,$ and 129 as determined by a library search for the peak in A. 146

Figure 5-6: Scratching and bending behaviour of eADF4(C16)-REDV coatings. The left side inserts demonstrate how the mechanical force acted on the coatings. A: A scratch on a wet protein coating showing protein removal along the scratched path, B: A scratch on a dry protein coating, displaying large areas of delamination C: Bending of a wet and D: a dry protein coating where no apparent defects are observable..... 147

Figure 5-7: Lap-shear test of polyacrylamide functionalised steel plates glued with eADF4(C16)-REDV solution. A: photograph of a glued specimen for testing, B: Specimens after the lap-shear test, C) The experimental setup and D) Normalised adhesive strengths of pristine and functionalised steel plates coated with spider silk. . $n=3, ***p\leq 0.001$ 148

Figure 5-8: QCM-D measurements of human fibrinogen on gold (Au) QCM-D chips and eADF4(C16)-based coated chips. Graph cut to exclude equilibration time. Fibrinogen introduction after ~ 1 minute, PBS washing step after ~ 18 minutes. 150

Figure 5-9: . Hemocompatibility assays on spider silk coatings and control surfaces. A) Clotting was assessed by measuring the turbidity change when the various surfaces were exposed to platelet poor plasma (PPP), as an increase in turbidity indicates fibrin formation ($n=4$). B) Factor XIIa activation rate was assessed on various surfaces as it is involved in the coagulation cascade. ($n=4$). C) Representative Factor XIIa activation profiles used for determination of the slopes in panel B.. $***p\leq 0.001$ 152

Figure 5-10: Photograph of the coagulated samples after 15-, 30-, and 60-minutes exposure to human whole blood, and E) Quantification of the whole blood coagulation by measuring the fluorescence intensity of the fibrin network formed from PPP that was spiked with fluorescently labelled fibrinogen. Data is presented

as mean \pm standard error (n = 3 donors) $p \leq 0.001$ for all statistical analyses.
 *** $p \leq 0.001$ 153

Figure 5-11: Representative scanning electron micrographs of 316L stainless steel and eADF(C16)-based surfaces after 15, 30, and 60 minutes of exposure to whole blood. Red squares highlight fibrin network formations, arrows point at activated platelets and circles denote fixed red blood cells. 154

Figure 5-12: Representative photograph of samples after 30 minutes of whole blood exposure in the Chandler Loop assay. B) Quantification of modified Chandler Loop data by assessing mass gain of samples after exposure to blood. * $p \leq 0.05$, *** $p \leq 0.001$. n=9..... 155

Figure 5-13: A) Degradation of eADF4(C16)-REDV coatings shown as mass loss from protein coatings over time. B) Scanning electron micrographs of silk coatings exposed to either a proteinase solution or buffer (negative control). Scale bar: 10 μm 158

Figure 5-14: Magnified SEM micrographs from Figure 5-13B. Enzyme-degraded (MMP-2/elastase mix) after 15 days of incubation. 159

Figure 5-15: A) Drug elution of everolimus (EVE) from spider silk coatings fitted to a Pappas-Sahlin model. B) Fraction of Fickian diffusion (F; black) and polymer relaxation (R/F; red) over the time of drug elution according to the Peppas-Sahlin fit. Percentage estimated based on the total amount of drug from independent measurements. n=2..... 163

List of Tables

Table 1-1: Overview of exemplary studies using naturally derived polymer hydrogels for Tissue Engineering applications.	15
Table 1-2: Overview of exemplary polymer coatings used in Tissue Engineering applications.	19
Table 1-3: Exemplary overview of Tissue Engineering applications using spider silk proteins. Compiled from [233] and [158].	27
Table 1-4: Exemplary overview of possible cellulose-blended composite materials in Tissue Engineering.	43
Table 1-5: CBD families and their properties. Adapted from [289].....	46
Table 1-6: Exemplary overview of CBD fusion proteins and their uses.....	48
Table 1-7: Catalogue of known and commonly used cell-adhesion peptides.	52
Table 5-1: Buffer gradient used in HPLC-MS data acquisition	141

List of Abbreviations

µm	Micrometre (1 x 10 ⁻⁶)
ADF3	<i>Araneus diadematus</i> fibroin 3
ADF4	<i>Araneus diadematus</i> fibroin 4
AFM	Atomic force microscopy
ANOVA	Analysis of variance
APTES	(3-Aminopropyl)triethoxysilane
AVL	Arteriovenous loop
BSA	Bovine serum albumin
CAD	Coronary artery disease
CBD	Cellulose-binding domain
CD	Circular dichroism
CF	Cellulose fibres
CLSM	Confocal laser scanning microscopy
cm	Centimetre (1 x 10 ⁻²)
DES	Drug-eluting stents
DPBS	Dulbecco's phosphate-buffered saline
DTT	Dithiothreitol
eADF4(C16)	Engineered <i>Araneus diadematus</i> fibroin 4 (16 repeats of the "C-module")
EC	Endothelial cell
ECM	Extracellular matrix
EDTA	Ethylenediaminetetraacetic acid
EMEM	Eagle's minimum essential medium
EVE	Everolimus

FCS	Fetal calf serum
FDA	Food and Drug Administration
GC	Gas chromatography
GdmCl	Guanidinium chloride
GdmSCN	Guanidium thiocyanate
GelMA	Gelatin methacryloyl
GFP	Green fluorescent protein
GPa	Gigapascal (1×10^9)
HCASMC	Human coronary artery smooth muscle cells
HFIP	Hexafluoroisopropanol
HPLC	High-pressure liquid chromatography
HSD	Honestly significant difference
HUVEC	Human umbilical vein endothelial cell
IgG	Immunoglobulin G
IMAC	Immobilized metal affinity chromatography
IPTG	Isopropyl β -d-1-thiogalactopyranoside
ISR	In-stent restenosis
kDa	Kilodalton (1×10^3)
L	Litre
LC	Liquid chromatography
m	Metre
M	Mole (unit)
MA	Major ampullate
mA	Milli ampere

MaSp1	Major ampullate spidroin 1
MaSp2	Major ampullate spidroin 2
MIC	Multiple ion chromatogram
MJ	Megajoule (1×10^6)
mm	Millimetre (1×10^{-3})
MMP-2	Matrix metalloprotease - 2
MQ-H ₂ O	Ultrapure water
MS	Mass spectrometry
mS	milliSiemens (conductivity)
NHDF	Normal human dermal fibroblasts
nm	Nanometre (1×10^{-9})
NRC	Non-repetitive C-terminus
NRN	Non-repetitive N-terminus
OD	Optical density
PBS	Phosphate-buffered saline
PDA	Photodiode array
PDLLA	Poly(D-L-lactic acid)
PLGA	Poly(lactic-co-glycolic acid)
PLLA	Poly(L-lactic acid)
pO ₂	Oxygen partial pressure
PPP	Platelet-poor plasma
PRP	Platelet-rich plasma
PVDF	Polyvinylidene fluoride
QCM-D	Quartz crystal microbalance and dissipation
rpm	Rounds per minute

rps	Rounds per second
SDS	Sodium dodecyl sulphate
SEM	Scanning electron microscopy
SMC	Smooth muscle cell
TE	Tissue engineering
TIC	Total ion chromatogram
V	Volt
W	Watt
w/v	Weight/volume
w/w	Weight/weight
λ	Lambda (symbol for wavelength)

Chapter 1 Literature Review

1.1 Introduction / Background

Tissue engineering (TE) represents a beacon of hope in the realm of regenerative medicine, offering potential solutions to the monumental challenge of repairing or replacing damaged or lost tissues and organs. While many approaches of TE are possible, the most prominent one hinges on using scaffolds that dictate the course of the desired tissue formation. A particular scaffold structure that has been at the centre of attention in recent years is hydrogels, owing to their adaptability to the target site's geometry and close mimicking of the physical environment. Furthermore, their injectability directly into the patient's target site reduces the need for extensive surgical procedures [1, 2]. Hydrogels can be either laden with cells or designed to serve as scaffolds providing cell attachment points [3]. Despite the promise of hydrogels, their stiffness often limits physically cross-linked hydrogels, being mostly in the range of 10 Pa to single-digit kPa values, making them unsuitable for numerous applications, including bioprinting multilayered structures or their usage in TE applications involving high mechanical stress [2, 4]. Chemically cross-linked hydrogels, although stiffer, ranging in the realm of several kPa to even MPa, tend to disintegrate under injection pressure or when printed as pre-formed gels [5]. Consequently, the optimal injectable TE scaffold combines relatively high stiffness, suitable pore size for culturing the target tissue's cells, injectability, and, ideally, the provision of cell attachment points [2].

Cardiovascular and arterial diseases hold the status of the leading cause of mortality worldwide [6, 7], accentuating the significance of exploring advanced treatment options to alleviate the colossal healthcare burden. Among arterial diseases, coronary artery disease has been a focal point of concern, necessitating surgical intervention involving stent implantation for a substantial number of patients globally [8]. The intervention is required to alleviate the detrimental effects of stenosis, a narrowing of blood vessels supplying oxygenated blood to the heart due to plaque accumulation [9, 10]. Despite the widespread use and success of modern drug-eluting stents (DES), these devices still present considerable challenges, such as inflammation, weak hemocompatibility, and,

Chapter 1: Literature Review

most crucial, limited endothelialisation [11], demanding the development of novel materials to overcome these limitations and enhance stenting technology. These two diverse fields, tissue engineering focused on hydrogel applications and cardiovascular interventions, represent distinct medical challenges yet share a common goal of improving patient outcomes.

Drawing on the need to improve upon these two diverse but crucial medical fronts, this thesis set out with two over-arching goals: enhancing scaffold designs for tissue engineering applications and developing materials for cardiovascular stents with enhanced functionality. The common thread binding the endeavours in both approaches is the exploration of recombinant spider silk proteins, specifically the MaSp2-derived eADF4(C16) [12, 13].

Therefore, this thesis presents a novel hydrogel formulation, marrying the beneficial qualities of elevated stiffness, injectability, and potential cell adhesion points by modifying a recombinant spider silk protein with a cellulose-binding domain (CBD). Especially spider silk fibres have been lauded for their remarkable mechanical properties [12, 14-19], biocompatibility [12, 17, 20-22], degradability [22], bacteriostatic [23] and hypoallergenic [13] characteristics throughout many studies. Moreover, the recombinant spider silk protein eADF4(C16) has proven its versatility, being processable into various morphologies, including physically cross-linked hydrogels [24]. A mechanical enhancer in the form of cellulose, an abundant, renewable, and biocompatible biopolymer [25], was introduced to enhance the stability of these hydrogels. To strengthen the mechanical properties of the resulting hydrogels, cellulose-binding domains derived from cellulose-degrading microorganisms [26, 27], were genetically modified onto the eADF4(C16) protein sequence, marking a first in the production and processing of such a fusion protein into hydrogels.

Turning to the cardiovascular front, the aim was to broaden the field of current stent coating materials by developing a natural material that minimises inflammation, slowly degrades into non-toxic and non-inflammatory products, exhibits excellent hemocompatibility, facilitates rapid endothelialisation, and offers a tunable, elongated degradation rate. The proposed solution involved leveraging the promising qualities of eADF4(C16) for stent coating and building on these to mitigate the challenges associated with the current DES.

Chapter 1: Literature Review

Therefore, the cell-selective peptide REDV [28-30] was genetically coupled to the spider silk protein to promote cellular attachment and thus facilitate the rapid endothelialisation of the stent.

The research efforts have offered potential advancements in TE and cardiovascular disease management, leveraging the multifaceted recombinant spider silk protein eADF4(C16) as one central solution.

This concise literature review delves into the realm of hydrogels and coatings in TE, emphasising their distinctive properties and importance in these applications. By unravelling the fundamental principles and critical factors that govern their performance, the aim is to illuminate the path towards developing innovative materials and strategies that enhance their functionality and broaden their use in the field. With a particular focus on cellulose-binding materials and drug-eluting stents (DES), this review sets the stage for the research chapters of the thesis, highlighting the immense potential of these applications in advancing the field of TE.

1.2 Tissue Engineering

TE and regenerative medicine have garnered significant interest in recent years, offering promising solutions to address the growing need for tissue repair and replacement in various clinical applications. Ancient civilisations utilised wound dressings from natural sources [31, 32], which could be considered as first rudimentary forms of TE. In the late 19th and early 20th centuries, pioneering researchers such as Wilhelm Roux, Leo Loeb, and Konrad Heim laid the foundation for modern tissue culture techniques [33]. However, it was not until the early 1980s that the term *Tissue Engineering* was defined in medical and science publications, marking the beginning of its recognition as a distinct discipline [34, 35]. Fast forwarding to today's advances, numerous research societies have been established, making TE a staple in medical research, defining it as an interdisciplinary biomedical engineering field that leverages the synergy between cells, engineering techniques, material science, and relevant biochemical and physicochemical factors to restore, maintain, improve, or replace various types of biological tissues [36].

Chapter 1: Literature Review

TE mainly involves using cells and tissue scaffolds to create new, viable tissue for medical applications. The textbook procedure for doing so is displayed in **Figure 1-1**. Here, It is depicted that the conventional way of TE starts with the extraction (isolation) and cultivation (expansion) of patient cells, followed by the seeding in a pre-designed scaffold (tissue development) and, lastly, the re-implantation of the patient's cells [37]. In an optimal case, this circumvents the issue of donor rejection as commonly observed with donor organs and avoids the need for immunosuppressive treatment. However, the field is not limited to only those components. In modern practice, TE encompasses a wide range of applications to repair or replace portions of or entire tissues, such as bone, cartilage, blood vessels, bladder, skin, and muscle [38]. In addition, these tissues typically demand specific mechanical and structural properties for proper functioning [39].

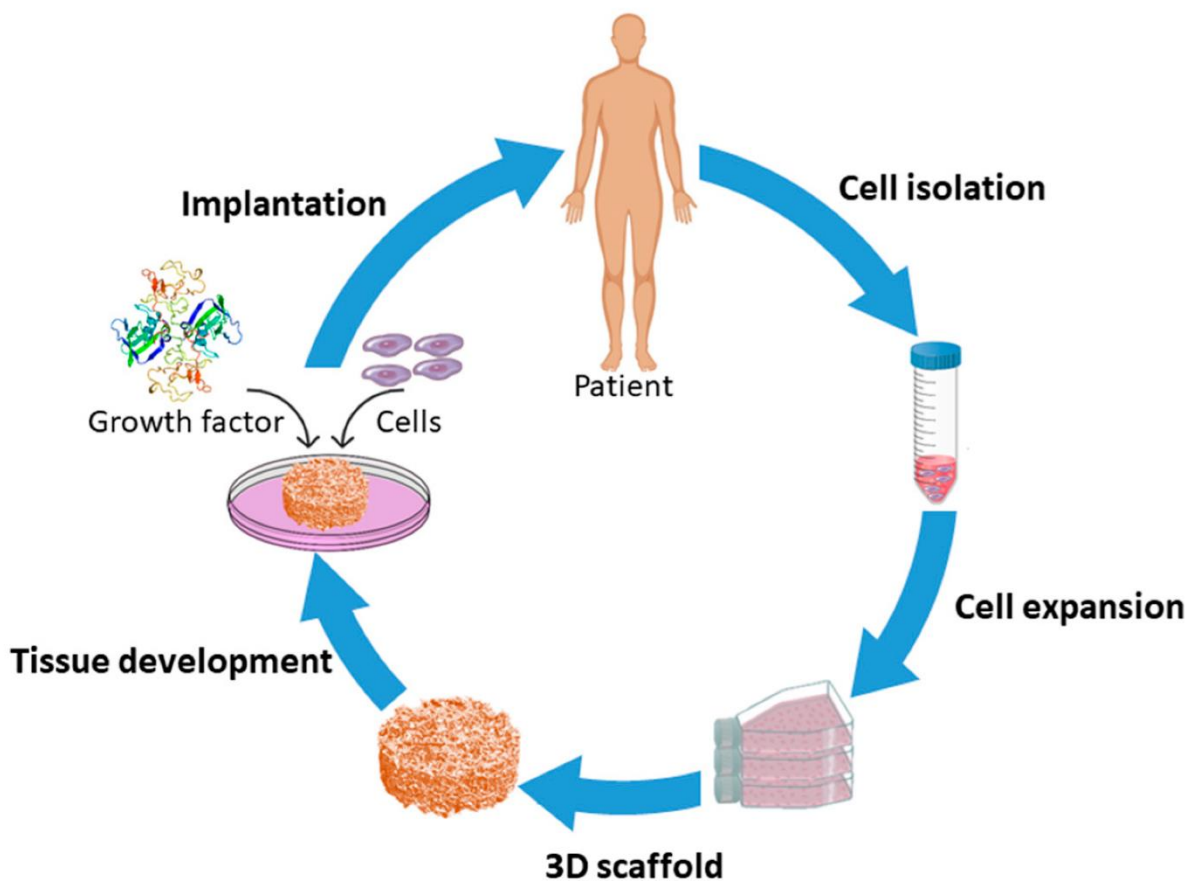


Figure 1-1: Illustration of the traditional approach of Tissue Engineering. Cells suitable for the target applications are extracted and isolated from the patient, cultivated in vitro, seeded onto scaffolds and re-implanted into the patient. Adapted from reference [37] (© M. Asadin et al., published by MDPI, distributed under the terms of the Creative Commons Attribution 4.0 International License (CC BY 4.0), <http://creativecommons.org/licenses/by/4.0/>)

Chapter 1: Literature Review

It is important to note that, in addition to scaffold-based strategies, non-scaffold approaches in TE have gained considerable attention. These techniques often rely on the self-organizing ability of cells to form functional tissues without the need for a predefined scaffold structure. One prominent method is the use of cell sheets, where layers of cells are cultured and then stacked or rolled to create three-dimensional tissue constructs [40]. Another approach involves organoids, which are miniaturized and simplified versions of organs, grown from stem cells or organ-specific progenitor cells [41]. These organoids can recapitulate the complex architecture and functionality of native tissues. Additionally, decellularization techniques are employed to strip cells from donor tissues or organs, leaving behind an extracellular matrix that can be repopulated with patient-specific cells [42]. These non-scaffold methods offer unique advantages, such as preserving the native tissue architecture and reducing potential issues related to scaffold degradation. They hold great promise for advancing regenerative medicine and developing new therapeutic strategies but are not covered in further detail throughout this thesis.

1.3 Scaffolds

In TE, scaffolds serve as three-dimensional cell carriers and/or provide a cell-friendly environment to induce cellular growth upon implantation at the target site. Ceramics, metals and alloys, natural and synthetic polymers, and composites are usually the materials of choice, as the scaffold must meet specific conditions depending on the target application [38]. As such, material sciences play a crucial role in scaffold design to fulfil the general guidelines of a suitable TE scaffold as follows:

1. Scaffolds should be biocompatible to ensure seamless integration with the host body while avoiding mutagenic, carcinogenic, or cytotoxic responses that may trigger severe inflammation [43].
2. The scaffold should exhibit appropriate mechanical properties to provide temporary structural support until the formation of new tissue [44].
3. The surface properties of the scaffold must enable cell attachment, migration, proliferation, and differentiation [45].

Chapter 1: Literature Review

4. Biodegradability is crucial for the scaffold to avoid additional surgery for implant removal, with an ideal degradation rate matching the pace of new tissue formation [46].
5. High porosity and surface-to-volume ratio of the engineered 3D scaffold are necessary for promoting cell attachment, offering cell growth sites, and facilitating nutrient exchange during *in vitro* and *in vivo* culture [47].
6. The scaffold should mimic the native extracellular matrix (ECM) in structure and biological function [48].

To meet these criteria, a wide array of morphologies for scaffolds has emerged, including but not limited to films/coatings [49-52], fibres [53-55], hydrogels [56-59], foams [43, 60], (micro)spheres [22, 61-63], non-woven meshes [20, 21, 64] or decellularised tissues [65-67]. These scaffolds are made from different processing techniques, such as (bio)printing [68-71], additive manufacturing [72], solvent casting [73], electrospinning [20, 21, 64] or self-assembly [74-78]. Recently, combinations of different techniques yielded even more sophisticated scaffolds [79, 80], paving the way for more complex applications.

TE has shown significant advancements in recent years, offering promising solutions for various clinical applications. However, current scaffold production approaches face several challenges and limitations that must be addressed to unlock their full potential.

One of the primary challenges lies in replicating the complex nature of the native extracellular matrix (ECM) [81], which provides an attractive environment for cell growth and tissue specificity. In addition, achieving precise control over scaffold architecture, including pore size, shape, and interconnectivity, is essential for promoting cell infiltration and nutrient exchange, yet remains a significant hurdle [58].

Another challenge is the balance between mechanical properties and biodegradation rates, as materials with suitable mechanical properties may not always exhibit the desired biodegradation rates [22, 82]. Ensuring biocompatibility and avoiding negative immune responses or inflammation is also crucial, especially when using synthetic polymers [83-85].

Chapter 1: Literature Review

Furthermore, integration between the scaffold and host tissue is vital for TE success [86]; however, current approaches may struggle with seamless integration, leading to potential mechanical instability and tissue-engineered construct failure [87]. Another critical aspect is vascularisation, as developing an adequate blood supply for tissue survival and functionality is often challenging to achieve with existing scaffold production methods [88].

Lastly, the scalability, reproducibility, and cost are additional challenges faced by TE. Many scaffold fabrication techniques are time-consuming, labour-intensive, and unsuitable for large-scale manufacturing. Furthermore, developing, producing, and validating tissue-engineered constructs can be expensive, limiting their widespread clinical adoption [89, 90].

Hydrogels and coatings of biomaterials have emerged as essential components in TE, playing a critical role in addressing the diverse requirements of regenerating and repairing damaged or lost tissues. These versatile morphologies can provide a platform for cellular attachment, proliferation, and differentiation, which are vital factors in the successful regeneration of functional tissues [5, 56, 91].

Hydrogels are three-dimensional, polymeric networks that closely resemble the native extracellular matrix (ECM) of many tissues. The primary principle behind hydrogel formation is a dense, hydrophilic network, mostly consisting of polymers, capable of captivating and retaining water molecules, resulting in a liquid-like yet stable structure, as shown in **Figure 1-2**. The distinctive properties of hydrogels, including their inherent biocompatibility, adaptable mechanical strength, and capacity to incorporate cells and bioactive molecules, render them optimal selections for a broad range of TE applications [1, 92].

Chapter 1: Literature Review

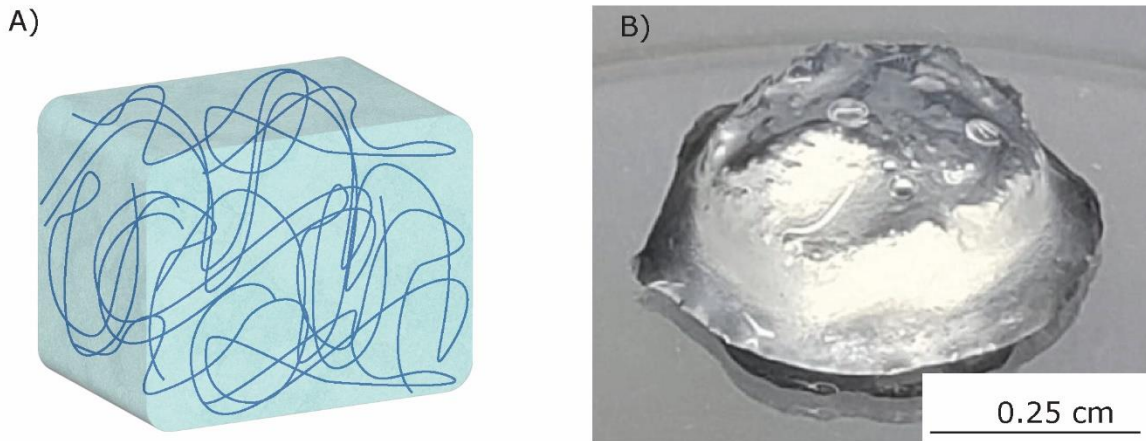


Figure 1-2: A): A hydrogel schematic showing a three-dimensional structure with a dense polymer network. **B):** Photograph of an actual protein hydrogel. In this case, a hydrogel from recombinant spider silk eADF4(C16).

Coatings, respectively films, as depicted in **Figure 1-3**, on the other hand, are thin layers of biomaterials, typically with a thickness ranging from nanometers to a few micrometres, applied to the surface of implants, scaffolds or medical devices to enhance their performance and biocompatibility. These films exhibit structural integrity and can be tailored to exhibit specific mechanical, chemical, or physical characteristics and often provide a barrier, controlled release of substances, or improved biocompatibility when used in TE applications [16].

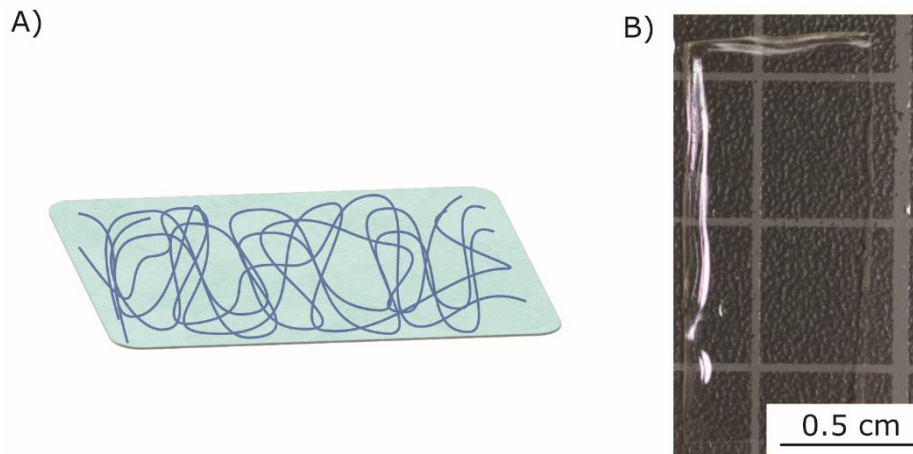


Figure 1-3: A): A schematic of a thin polymer film. **B):** A photograph of a film cast from regenerated cellulose. Adapted from reference [93] (© M. Reimer et al., published by MDPI, distributed under the terms of the Creative Commons Attribution 4.0 International License (CC BY 4.0), <http://creativecommons.org/licenses/by/4.0/>)

Chapter 1: Literature Review

1.3.1 Scaffold materials: Biomaterials in Tissue Engineering and Medicine

To delve deeper into the processing of hydrogels and films, this section will briefly introduce different biomaterials, focusing specifically on polymers and proteins.

Biomaterials are materials designed to interact with biological systems for various medical applications, such as tissue repair and replacement. They are engineered to be biocompatible, ensuring minimal adverse reactions when in contact with living tissues or cells [94]. Various biomaterials are employed in TE, including metals, ceramics, and polymers.

Metals such as stainless steel [95], titanium [96, 97], or cobalt-chromium alloys [98] have been widely used in various medical applications due to their high mechanical strength and durability. For example, metallic materials are primarily employed in orthopedic [99] and dental implants [100], as well as cardiovascular stents [101, 102] and other load-bearing applications owing to their ability to withstand the mechanical demands of these applications. However, metals also have limitations, such as the potential for corrosion [103] and a lack of bioactivity, which can hinder their integration with surrounding tissues [38].

Ceramics, on the other hand, are inorganic, non-metallic materials that include bioceramics such as hydroxyapatite, calcium phosphate, and bioactive glass [97]. These materials exhibit excellent biocompatibility, bioactivity, and osteoconductivity, making them suitable for bone TE and dental implants [104]. Ceramics can be processed into various forms, such as porous scaffolds [99] and coatings [4], to promote cell adhesion, proliferation, and differentiation. However, ceramics are often brittle and have limited mechanical strength [45], restricting their use in load-bearing applications.

Polymers have garnered substantial interest in TE due to their remarkable versatility, customisable properties [105], and often straightforward fabrication processes. Polymers can be classified as either synthetic or natural in origin. Synthetic polymers offer superior control over their mechanical and degradation properties [82], whereas natural polymers, such as proteins, facilitate improved biological interactions [106] and often demonstrate inherent biocompatibility [107].

Chapter 1: Literature Review

A crucial aspect to consider when selecting biomaterials for TE applications is their degradation behaviour. Synthetic polymers can be engineered with controlled degradation rates, allowing them to align with the pace of tissue regeneration [82, 83]. This enables a progressive transfer of load from the scaffold to the newly formed tissue, ensuring proper tissue development. Conversely, protein-based biomaterials typically exhibit more intricate degradation profiles, as they are subject to enzymatic degradation by proteases present within the body [108]. This enzymatic degradation process can result in more rapid and potentially less predictable disintegration of the scaffold. However, the degradation products consist of amino acids, which can be directly metabolised by the body, thereby eliminating the risk of inflammation [22].

The following sections will focus on the characteristics and applications of naturally derived protein hydrogels and coatings in TE, providing a comprehensive understanding of their roles and potential in advancing the field.

1.3.2 Hydrogels in Tissue Engineering

Hydrogels have gained significant attention among the various scaffold morphologies due to their inherent biocompatibility, bioactivity, and ability to mimic native extracellular matrix (ECM) properties [1, 92]. Their high water content accentuates their resemblance to biological tissues, making them an ideal choice for TE [109]. The formation of these hydrogels relies on cross-linking, creating an interconnected network capable of retaining water [110], which can be classified into two main types: physical and chemical, as depicted in Figure 1-4. Understanding the differences between these cross-linking methods is crucial in designing protein hydrogels with tailored properties to suit specific TE applications. The following sections discuss the fundamental aspects of physical and chemical cross-linking and how they influence the properties of protein hydrogels.

Chemical cross-linking involves the formation of covalent bonds between polymer chains, creating a more stable and permanent hydrogel network. Chemical cross-linking can be achieved through various methods:

For instance, cross-linking reagents (**Figure 1-4A**) create a direct, covalent bond between the polymer chains in the hydrogel via a chemical reaction such as the polymerisation of acrylamide being initiated by the addition of free radicals (such

Chapter 1: Literature Review

as ammonium persulfate) [111]. This strategy is commonly used for its simplicity and effectiveness, generating a highly stable network that can withstand various physical and biological conditions.

Polymer interactions (**Figure 1-4B**), which involve the interaction of functional groups on different polymer chains (for example, ionic bonding between the amino groups of chitosan and the carboxyl groups of alginate [112]), represent another approach. These reactions can be tuned to create a wide range of mechanical and degradation properties, enabling a high degree of control over the resulting hydrogel.

Photo-cross-linking (**Figure 1-4C**) is a distinctive mechanism that employs light energy to induce covalent bonding between polymer chains (GelMA cross-linking with a photoinitiator, e.g. Irgacure [113]). This approach is particularly valuable due to its capacity for spatiotemporal control, allowing for the precise manipulation of hydrogel formation and structure.

Lastly, enzymatic cross-linking (**Figure 1-4D**) capitalises on the remarkable specificity of enzyme-substrate interactions. By facilitating the formation of covalent bonds between polymer chains (as shown with transglutaminase catalysing the amide formation between amine and acyl in gelatin hydrogels [114]), this technique can give rise to highly specialised and biologically relevant hydrogel structures. However, the complexity of these systems can pose a challenge, necessitating careful design.

The resulting chemically cross-linked hydrogels exhibit enhanced mechanical stability compared to their physically cross-linked counterparts. However, they often lack the dynamic, self-healing properties of physically cross-linked hydrogels and therefore, experience disruption upon shear [5], rendering them generally unfeasible for injection-based applications. Chemically cross-linked hydrogels are ideal for applications where long-term stability and robust mechanical properties are essential [79].

On the other hand, physical cross-linking and entanglement involves the formation of non-covalent interactions between polymer chains, such as hydrophobic interactions, hydrogen bonding, and ionic interactions and are therefore often reversible [1].

Chapter 1: Literature Review

Hydrophobic interactions (**Figure 1-4E**) come into play when hydrophobic segments of polymer chains self-assemble in an aqueous environment, minimising their water exposure and leading to a three-dimensional network structure (as seen in hydrophobic effects of methyl-rich regions of methylcellulose hydrogels [115]). This type of hydrogel demonstrates stimuli-responsiveness, as temperature, pH or solvent alterations may change the hydrophobic associations and modify the hydrogel structure [115].

Furthermore, ionic interactions (**Figure 1-4F**), which involve the attraction between oppositely charged ions, also contribute to forming physically cross-linked hydrogels. Charged polymers, or polyelectrolytes, can form a physical network via ionic cross-linking through multivalent cations bridging negatively charged sites along polymer chains or through cooperative interaction of polyanions and polycations, as demonstrated with cationic K^+ and Na^+ ions within anionic recombinant spider silk matrices [56]. Ionic hydrogels respond to changes in pH or ionic strength, affecting the charge density and altering these ionic interactions [116].

Supplementing this, hydrogen bonding (**Figure 1-4G**), another non-covalent interaction involving intermolecular attraction between a partially positive hydrogen atom bonded to an electronegative atom (like nitrogen, oxygen, or fluorine) and another nearby electronegative atom, also plays a pivotal role in physically cross-linked hydrogel formation. Hydrogels formed through hydrogen bonding respond to changes in pH and temperature, which can disrupt the hydrogen bonds, adjusting the hydrogel's properties. One such type of hydrogel is composed of a blend of poly(vinyl alcohol) and DNA [117].

Lastly, crystalline formation (**Figure 1-4H**) is another mechanism where specific polymers can form semi-crystalline regions within their structure. In aqueous environments, the often intermolecular crystalline regions act as physical cross-links, acting as nucleation points for the hydrogel network, as seen in dextran hydrogels [118]. These hydrogels show thermoresponsive behaviour, as heating can alter the crystalline regions, leading to hydrogel changes.

Moreover, particularly in the case of physically cross-linked hydrogels, it is common to see a convergence of these mechanisms [56, 119]. This is mainly

Chapter 1: Literature Review

because many of these effects are interdependent. For instance, hydrophobic interactions can lead to the condensation of the polymer chain, setting the stage for the emergence of hydrogen bonds yielding crystalline regions. In this manner, crystallization can occur due to strong intermolecular forces such as hydrogen bonding, van der Waals interactions, ionic interactions, hydrophobic interactions, dipole-dipole interactions, and π - π stacking between polymer chains [120]. Hydrogen bonding involves the attraction between a hydrogen atom covalently bonded to a highly electronegative atom (such as oxygen or nitrogen) and another electronegative atom with a lone pair of electrons. Van der Waals interactions are weak attractions between molecules or parts of molecules resulting from transient local partial charges. Ionic interactions occur between oppositely charged ions, leading to strong electrostatic attraction. Hydrophobic interactions arise when nonpolar groups aggregate to avoid contact with water, leading to an organized structure. Dipole-dipole interactions involve attractions between polar molecules with permanent dipoles. π - π stacking refers to the attractive, non-covalent interactions between aromatic rings, where the electron clouds of π bonds interact, leading to a stacked configuration. Together, these interactions facilitate the alignment and organization of polymer chains into a crystalline structure. This interplay of mechanisms underscores the complex and multifaceted nature of physically cross-linked hydrogel formation.

Physically cross-linked hydrogels are often characterised by their ability to self-heal [1], as the reversible cross-links can rearrange and reform at specific conditions after the hydrogel was subjected to stress or damage. This characteristic makes physically cross-linked hydrogels particularly attractive for applications requiring adaptability and dynamic responsiveness to environmental stimuli, such as being injected directly into the target site in a patient's body without needing large incisions [1, 2]. This allows for cell-laden hydrogels or plain hydrogels that serve as scaffolds and cell attachment points [3]. However, physically cross-linked hydrogels often exhibit limited stiffness, rendering them too unstable for many applications, including bioprinting multilayered structures or TE applications involving high mechanical stresses [2, 4].

Chapter 1: Literature Review

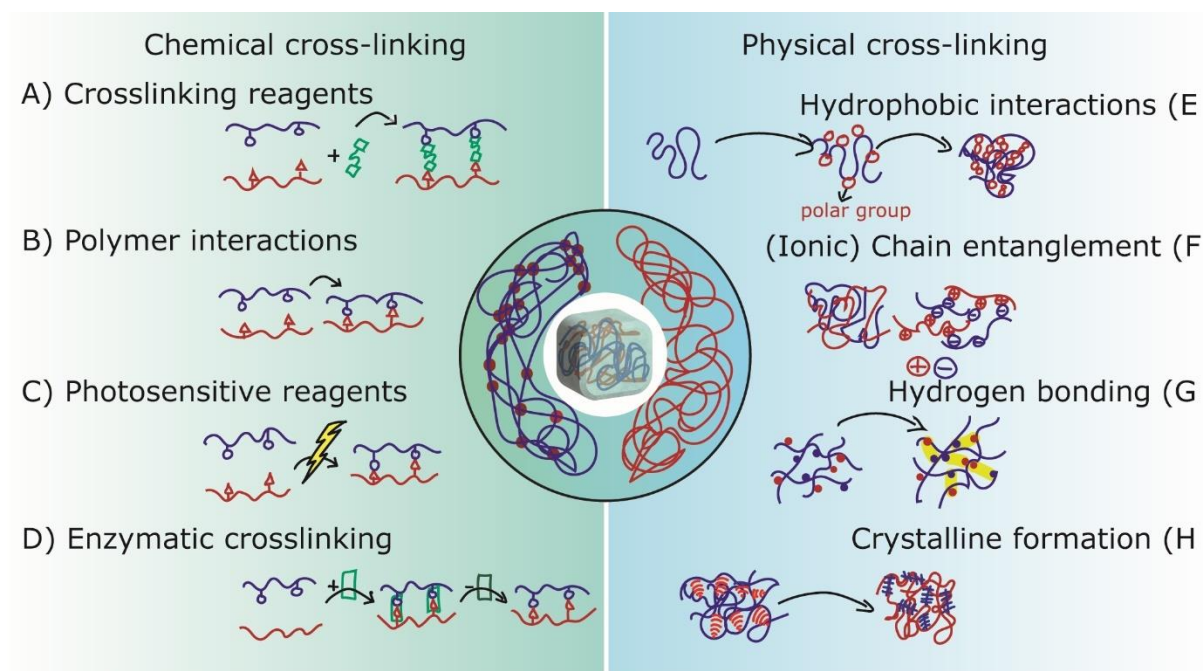


Figure 1-4: Various chemical and physical cross-linking mechanisms. A) Showcases the active cross-linking, initiated mainly by adding a reaction partner. B) Demonstrates the creation of hydrogels via polymer-polymer interactions. C) Reveals photo cross-linked hydrogels formed by covalent bonds created by photoinitiated reactions. D) Features enzyme-mediated chemical cross-linking. In physical cross-linking, E) highlights the role of hydrophobic moieties annealing, while F) illustrates chain entanglement mediated through ionic interactions. G) Depicts hydrogen bonding as a form of physical attraction between polymer molecules, and lastly, H) shows the role of the formation of inter- or intramolecular crystalline regions. Figure inspiration from [110]

The extensive range of available processing techniques opens up an immense spectrum of possibilities for hydrogels, allowing for the exploration of diverse materials and applications. **Table 1-1** provides a concise snapshot of some recent studies using hydrogels from naturally derived materials for TE applications to underscore the significance and potential of these bio-based substances. Notably, many of these materials are subject to further modification prior to processing into hydrogels.

Chapter 1: Literature Review

Table 1-1: Overview of exemplary studies using naturally derived polymer hydrogels for Tissue Engineering applications.

Application	Base material	Cross-linking	Ref.
Bone TE	Gelatin-methacryloyl	Chemical (photo)	[121]
	Hyaluronic acid	Chemical (photo)	[122]
	Chitosan	Physical (ion)	[123]
	Collagen	Physical (ion)/chemical (reaction-based)	[124]/ [124, 125]
	dopamine-caffeic acid	Physical (ion)	[126]
	Alginate/Gelatin	Physical (ion)	[127]
	Silk fibroin/Hydroxyapatite	Physical (hydrophobic)	[4]
	Gelatin-methacryloyl	Chemical (photo)	[128, 129]
Cardiac/Vascular TE	Hyaluronic acid	Chemical (reaction-based)	[130]
	Alginate	Physical (ion)	[131]
	Recombinant spider silk	Physical (hydrophobic)	[59]
	Silk fibroin	Physical (hydrophobic)	[132]
	Alginate	Physical (ion)	[121, 133]
Cartilage TE	Gelatin	Physical (hydrophobic)	[134]
	Silk fibroin	Physical (hydrophobic)/chemical (photo)	[135]/ [136]
	Agarose/Silk fibroin	Physical (crystalline)	[137]
	Chitosan/Silk fibroin	Chemical (photo)	[138]
	Collagen	Physical (ion)	[139]
	Fibrin/Collagen	Physical (ionic/entanglement)	[140, 141]
Skin TE	Silk fibroin	Physical (hydrophobic)	[142]

Chapter 1: Literature Review

Drug delivery	Recombinant spider silk	Physical (hydrophobic)	[57, 119]
	Hyaluronic acid/Silk fibroin	Physical (ionic/entanglement)	[143]
Neural TE	Silk fibroin	Physical (hydrophobic)	[144]

As the broad spectra of applications suggests, the mechanical properties of hydrogels play a significant role in TE to meet the distinct needs of the application and must be tuned carefully. This tuning can also alter cell adhesion, thus fostering the interaction between cells and hydrogel [144], and helps to mimic physiological conditions.

In summary, the versatility and adaptability of hydrogels, emphasised by their diverse cross-linking mechanisms and tunable mechanical properties, have made them indispensable tools in TE. Their ability to mimic the ECM, interact with cells, and respond to environmental stimuli enables the design of more physiologically relevant systems. Despite the challenges, the continuous innovation and research in developing and improving hydrogel systems underscore their tremendous potential. Therefore, their further study and refinement promise to unlock new avenues for advances in TE, pushing the boundaries of what is currently achievable.

1.3.3 Protein coatings for scaffolds and biomedical devices

While three-dimensional structures such as hydrogels are often focused for applications due to their ability to mimic the ECM, two-dimensional films and coatings also play vital roles in TE. While films may seem less relevant due to their two-dimensional nature in a field where the natural environment is inherently three-dimensional, their application as coatings on devices and scaffolds is a significant area of exploration. Coatings, although they may not directly emulate an ECM or target tissue, primarily serve to enhance the surface properties of scaffolds and devices. This enhancement can include rendering them more biocompatible [16, 52, 145], promoting cell adhesion [146], bestowing antimicrobial properties [147, 148], or altering their mechanical properties and degradation profiles [103]. A typical strategy to achieve these improvements involves the incorporation of growth factors [149], peptides [10, 150], or other

Chapter 1: Literature Review

drugs [151, 152] into the coating material. Various techniques are available for coating deposition, each with advantages and considerations. **Figure 1-5** shows some of the most frequently used techniques.

For example, casting (**Figure 1-5A**) is a versatile method for adding a liquid solution or suspension onto a substrate, allowing it to solidify into a thin film by solvent evaporation [153]. This technique is especially suitable for large-area coatings, accommodating hydrophilic and hydrophobic materials, but may result in uneven surfaces [154].

Dip-coating (**Figure 1-5B**) involves immersing a substrate into a liquid or suspension and then withdrawing it at a controlled rate. As the substrate is withdrawn, a film forms on its surface through solvent evaporation or chemical reaction. Dip-coating is a versatile method suitable for various materials, enabling uniform coatings. However, achieving precise control over coating thickness at large substrates can be challenging, and the method is limited by high viscosities [52].

Spin coating (**Figure 1-5C**) entails depositing a liquid solution or suspension onto a rapidly rotating substrate. The centrifugal force spreads the liquid into a thin, uniform layer, solidifying through solvent evaporation. This technique offers precise control over coating thickness and is commonly used for thin films in the nanometer regime [49, 155]. However, it is limited to small areas.

Electrospraying (**Figure 1-5D**) utilises an electric field to generate charged droplets from a liquid solution or suspension, which are directed onto the substrate, forming a coating. It offers precise control over droplet size and distribution, enabling uniform coatings and is well-suited for delicate or porous substrates. Besides electrospraying, this method can also be conducted without using an electric field by utilising defined gas streams to deposit the solution. This method is then called spray-coating and is less precise but more feasible for nonconductive solvents [156].

Electro-coating (**Figure 1-5E**), also known as electrodeposition, involves the application of an electric field to deposit charged molecules or ions onto a conductive substrate. This technique controls coating thickness, yields excellent

Chapter 1: Literature Review

adhesion, and is commonly used for metal coatings. However, it is limited to conductive substrates [157].

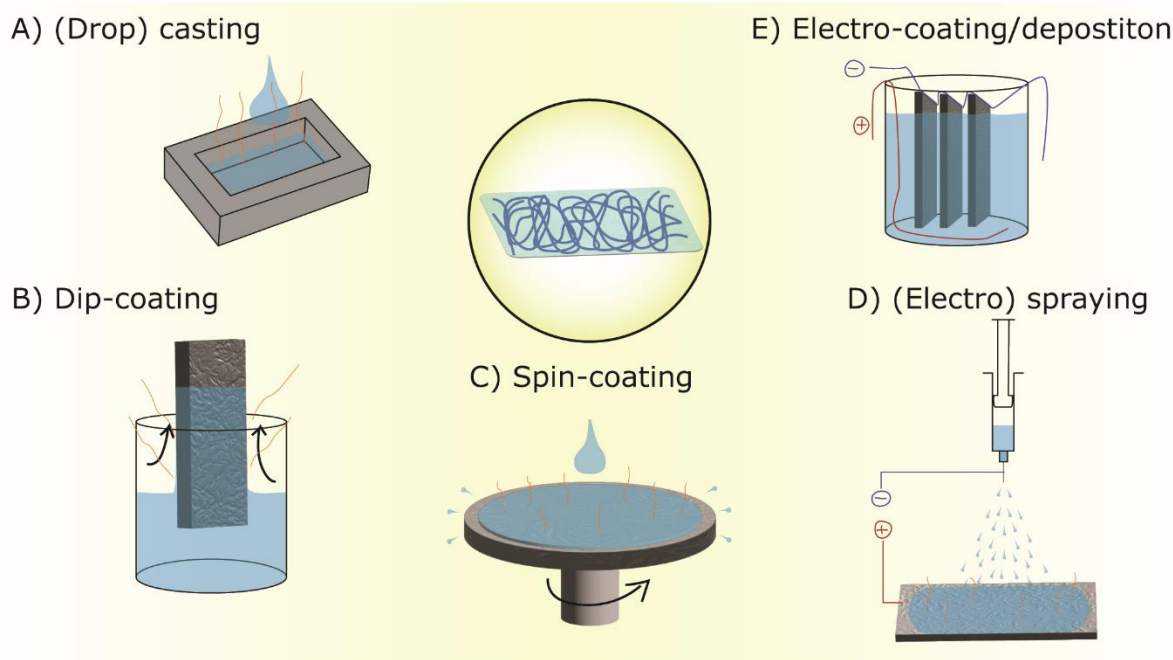


Figure 1-5: A selection of relevant coating techniques for polymer coatings in TE. A) A drop casting approach where a polymer solution is cast into a mold (or surface). Once cast, the solvent evaporates and a solid polymer coating forms. B) Demonstrates dip-coating. A substrate is immersed into the polymer solution and removed at a controlled speed to ensure reproducibility and homogeneous coatings. C) Depicts spin-coating, where the substrate rotates at high speed so the cast solution gets evenly and thinly distributed across the substrate. Suitable for very thin films. D) illustrates electrospraying. Here two opposite charges are deployed at the substrate and solution, respectively. The attracting charges lead to droplets being ejected towards the surface, creating a thin and well-adjustable film on the substrate. E) highlights Electro-coating. Like electrospraying, two opposite charges are deployed between the solution and substrate. However, the substrate is immersed, and by applying several charge cycles, the thickness of the coating can be well-defined.

Selecting a suitable coating technique is critical to achieving the desired functional and mechanical properties. Factors such as coating thickness, uniformity, adhesion, and material interactions must be considered. Furthermore, the processing parameters and conditions, such as solvent evaporation speed, play a crucial role in determining the mechanical properties of the coating, particularly in protein-based coatings where these parameters influence secondary structure self-assembly [158]. Careful consideration of these aspects is vital to optimise the coating process and tailor the properties of the coatings to meet the specific requirements of TE applications.

Despite being less versatile than hydrogels in terms of scaffold specific properties, their ease of application and the many possibilities to alter surface properties led

Chapter 1: Literature Review

to coatings being used in many TE applications. **Table 1-2** provides a very brief overview of studies employing possible applications thereof, highlighting the great variability of coatings used in TE.

Table 1-2: Overview of exemplary polymer coatings used in Tissue Engineering applications.

Application	Base material	Processing	Ref.
Bone TE	dopamine/ silk fibroin	Dip-coating	[159]
	polydopamine	Dip-coating	[160]
	Gelatin/nano-hydroxyapatite	Dip-coating	[161]
	Nanohydroxyapatite	Electrodeposition	[162]
	Heparin	Electro-coating	[163]
Cardiac/Vascular TE	Recombinant spider silk	Casting	[146]
	Recombinant protein C	Casting	[164]
	mRNA	Casting	[165]
	polycaprolactone	Electrospraying	[166]
	Recombinant tropoelastin	Electrospraying	[167]
Skin TE	collagen	Electrospraying	[168]
	Recombinant spider silk	Casting	[169]
Neural TE	Polypyrrole	Dip-coating	[170]
	Chitosan	Electrodeposition	[171]
	Polydopamine	Dip-coating	[172]
Other Devices/Implants	Recombinant spider silk	Casting	[16, 52, 148]
	Silk fibroin	Casting	[10]
	Titanium dioxide	Dip-coating	[173]

1.4 Recombinant Spider Silk as Biomaterial

Proteins, as a subclass of polymers, offer high versatility and often show excellent biocompatibility, making them a compelling choice for biomaterial applications [14]. With the advent of genetic engineering, the library of proteins that can be created to mimic natural proteins with specific properties has expanded significantly [174]. Moreover, the production of proteins in large-scale bioreactors provides an independent and sustainable source of material [13].

Among various protein-based materials, silk has garnered significant interest throughout history. Silk has been utilised in diverse cultures for its textiles and traditional biomedical applications, such as wound dressings [175]. Silk can be defined as fibril-like proteins with highly repetitive domains processed into stable fibres by animals [176].

Spiders are one example of the many species capable of producing silk, alongside silkworms, moths, honey bees, wasps, and lacewing flies [175]. In the world of spiders, approximately 50% of known species utilise silk to weave intricate webs for capturing prey, resulting in over 130 different web shapes [177].

One of the most extensively studied spider silk web types is the orb web produced by *Araneus diadematus*, commonly known as the European garden spider. This web consists of several silk types, as depicted in **Figure 1-6**, with the major ampullate (MA) silk being of particular interest due to its exceptional mechanical properties [178, 179]. The MA silk is responsible for the frame and radii of the orb web, bearing the majority of its weight. These fibres exhibit remarkable extensibility (27%) and toughness (180 MJ m^{-3}), coupled with moderate strength (1.1 GPa) [180]. Furthermore, *A. diadematus* produces other silk types, including flagelliform silk for catching prey, minor ampullate silk for web stability, piriform silk for architectural purposes, and aggregate silk for coating the catching fibres with sticky silk aggregates. The cylindrical and aciniform silks wrap eggs and enclose prey [177, 181].

Chapter 1: Literature Review

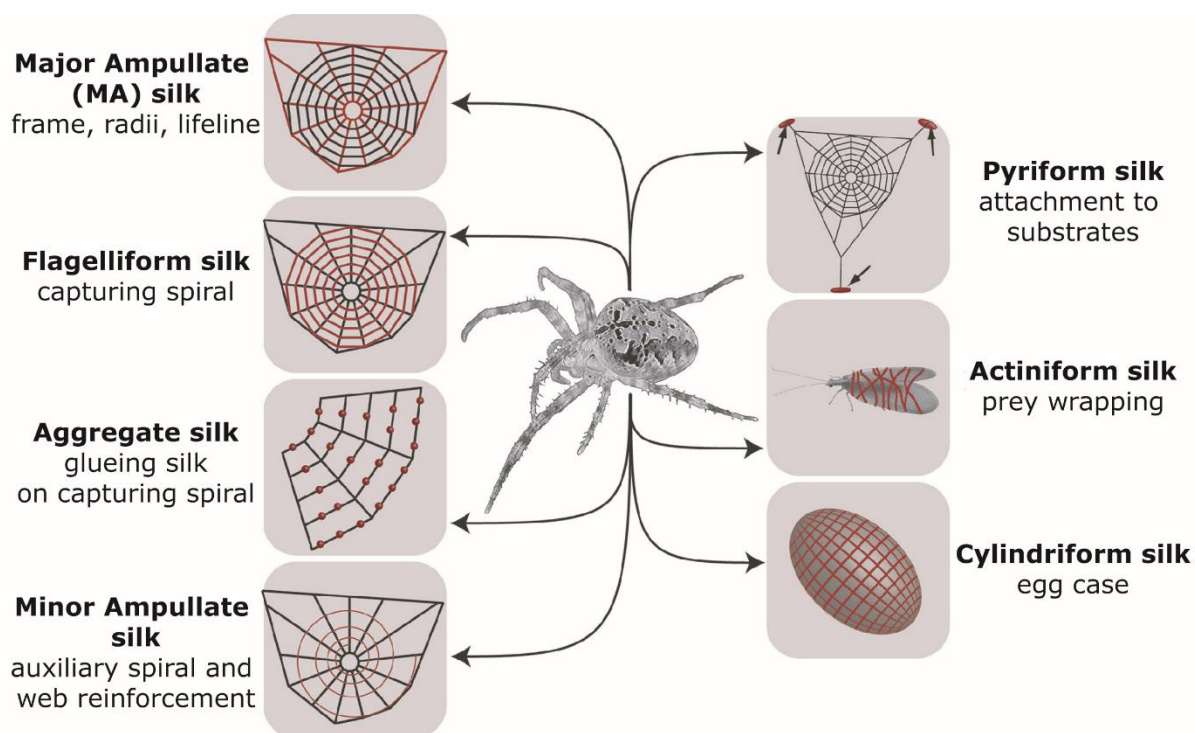


Figure 1-6: Illustration of the different spider silk variants found in orb webs of *A. diadematus*. Pyriform silk is used as attachment material on surfaces; Cylindriform silk is used as a protective shell for eggs; minor ampullate silk is used for the auxiliary spiral in the centre of the web; flagelliform silk forms the catching prey-catching spiral; major ampullate silk forms the frame and radii of the web and serves as dragline silk of the spider; Aggregate silk serves as a glue and is distributed across the surface of the web, and actiniform silk is used for wrapping living prey. Adapted and modified from reference [182] (© L. Eisoltd et al., published by Elsevier, distributed under the terms of the Creative Commons Attribution 3.0 International License (CC BY 3.0), <https://creativecommons.org/licenses/by-nc-nd/3.0/>)

The remarkable mechanical properties of MA silk can be attributed to the major ampullate spidroin (MaSp) proteins, which have an average molecular weight of 250-350 kDa [183]. Among these proteins, major ampullate spidroin 1 and 2 (MaSp1 and MaSp2) have received considerable research attention [15, 184, 185]. These two proteins differ significantly in their proline contents, which play a crucial role in determining the mechanical properties of the silk fibre. MaSp1 exhibits a low proline content (<0.4%), while MaSp2 is rich in proline residues (>10%) [13, 184].

The specific composition of MaSp1 and MaSp2 proteins varies among spider species and is directly linked to the mechanical properties of the resulting silk fibres [183]

Chapter 1: Literature Review

In the case of *A. diadematus*, two types of MaSp2 proteins are present in the MA silk: *Araneus diadematus* fibroin 3 and 4 (ADF3 & ADF4). **Figure 1-7** gives an overview of the origins and the structure of the MaSp proteins of *A. Diadematus*.

The repetitive domains of MA spidroins in *A. diadematus* are predominantly shaped by poly-alanine stretches, $(GGX)_n$ and $(GPGXX)_n$ (X= variable amino acid residue) regions [13, 186]. As a result, the poly-alanine regions form β -sheet crystallites, contributing to the fibre's high tensile strength [187]. The $(GGX)_n$ and $(GPGXX)_n$, on the other hand, form 3_{10} -helices [188] and β -turn spirals, donating to the fibre's elasticity by posing an amorphous matrix [174, 189, 190].

Recently, more spidroins, such as the MaSp3 [191], which lacks the MaSp-typical poly-Ala stretches, the MaSp4 [192], with the unique GPGPQ motif, or the very small MaSp5 [193] proteins have been identified in *Araneus ventricosus*, *Caerostris darwini* and *Caerostris darwini* respectively; however, their contribution to fibre performance in these species is yet to be defined.

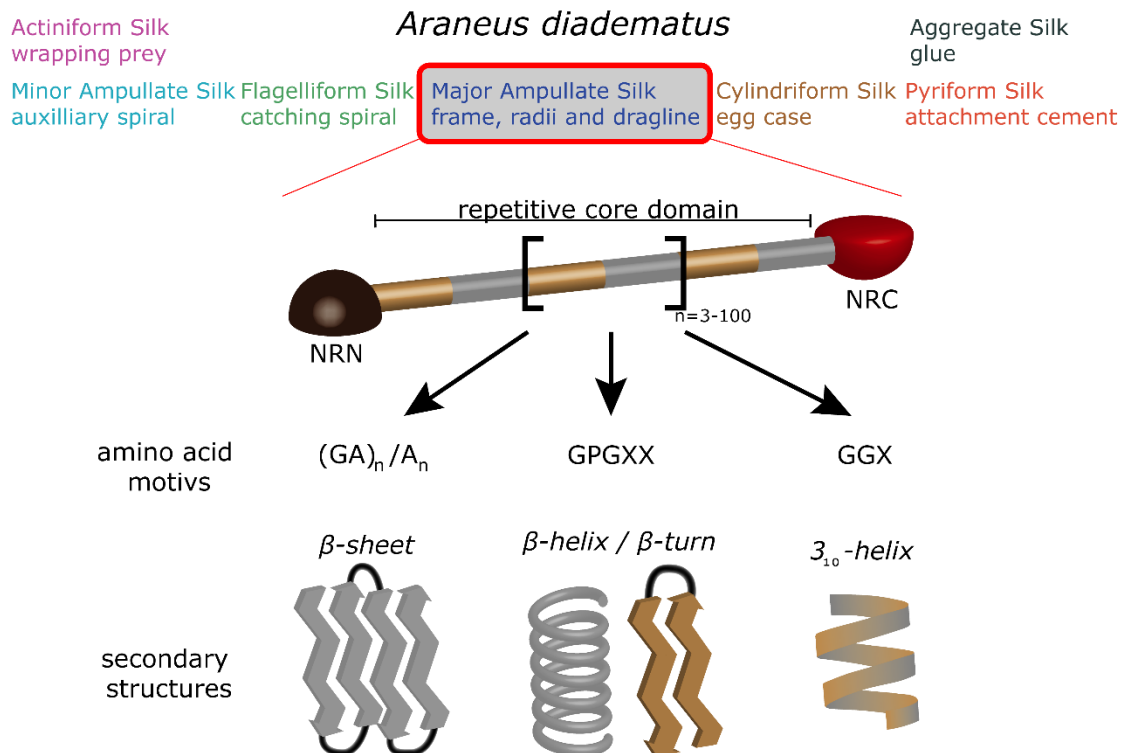


Figure 1-7: Overview of *A. diadematus*' major ampullate silk structure. The red-framed boxes guides towards the protein of interest of this study, ADF4. Focusing on the MA silk, a highly repetitive core sequence flanked by NRN and NRC is illustrated. The core domain usually comprises MaSp-typical motifs, which, in turn, can form secondary protein structures such as β -sheets, -helices and -turns, as well as 3_{10} helices, yielding the fibres mechanical properties when spun.

Chapter 1: Literature Review

The non-repetitive domains flanking the repetitive core domains consist of 40-200 amino acids and show predominantly α -helical structures [13, 15]. Due to the ability to form dimers through intramolecular disulphide bonds, the termini enable the storage of high protein concentrations in spiders' silk glands via the formation of micelle-like structures [181]. Furthermore, these termini play a vital role in the coordination of fibre formation as it triggers a salting-out effect and the formation of β -sheets during the shear-induced spinning process [76, 194-197].

Besides the molecular structures, spider silk's extraordinary mechanical properties stem from its multilevel organisation, as depicted in **Figure 1-8**. Protective layers of minor ampullate silk, glycoproteins and lipids surround the fibril core consisting of ADF3 & 4.

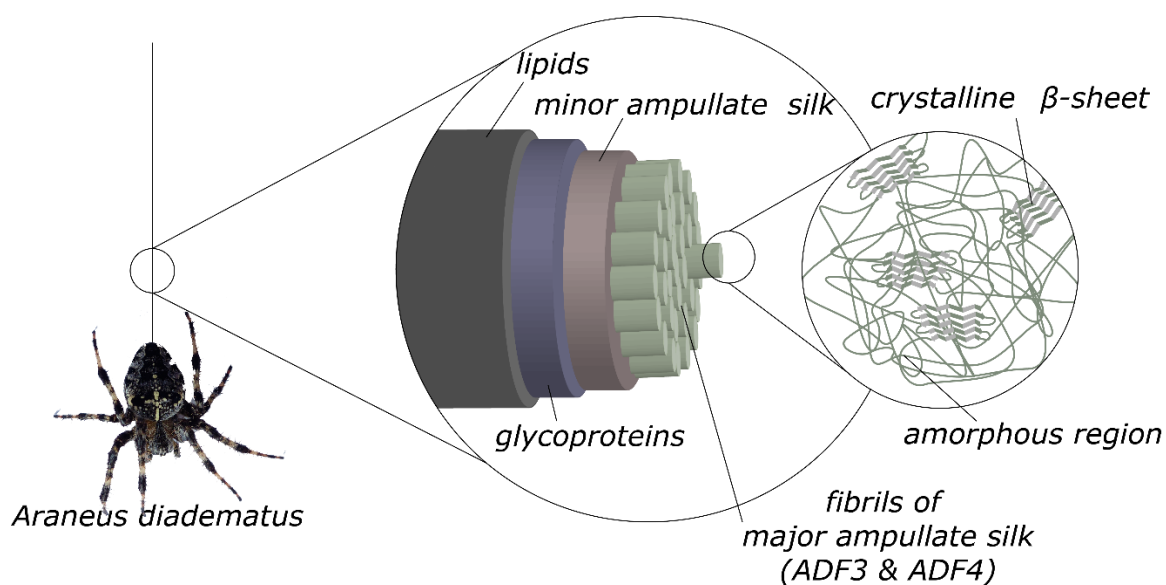


Figure 1-8: Hierarchical structure of the dragline thread of *A. diadematus*. The fibre's outer shell is a lipid layer, surrounding a layer made of glycoproteins and minor ampullate silk. The fibre's core consists of multiple fibrils made of the MaSp proteins. Figure inspiration from [13].

Due to its biocompatibility [12, 17, 20-22] and mechanical properties [12, 14-19], spider silk has garnered significant interest in medical and technical applications. Therefore, a sustainable supply of raw materials is necessary. However, unlike other silks, such as the silkworm *Bombyx mori* produces [198], spider silk can not be harvested by conventional means. Due to spiders' aggressive and sometimes cannibalistic territorial behaviour, natural spider silks' mass production and harvest are unsustainable [199].

Chapter 1: Literature Review

One commonly used technique is the recombinant production of proteins, where the target protein's known amino acid sequence is codon-optimised for a host organism and translated into a DNA sequence. Therefore, fully synthetic genes that differ from the natural model but encode proteins with the key features and structures of natural MaSp proteins have been designed. These synthetic copies of various silk-coding genes were expressed by several expression organisms, including transgenic animals such as *B. mori* [200], mice [201] or goats [202]. Other eukaryotic hosts such as yeast [203-207], plants [208, 209] or insect cells [19, 210-213] have also been used to produce recombinant spider silk. Lastly, a more practical approach is using bacterial host organisms to enable large-scale production in bioreactors. Amongst these hosts are *Salmonella typhimurium* [214, 215], *Bacillus subtilis* [203] and the most popular host organism, *Escherichia coli*, which has been extensively used for recombinant spider silk proteins [12, 14, 18, 174, 177, 194, 203, 216-226].

In the case of the ADF4-mimicking recombinant spider silk variant eADF4(C16), so-called "C-modules", as depicted in **Figure 1-9** were designed to enable a facile cloning approach. Every module possesses the key motifs of the core domain of the MaSp2 gene and has been codon-optimised for the expression in *E. coli*. Using relatively small (105 bp) repeatable modules, precise control over the final protein size is achievable [12]. Using a seamless cloning strategy [227], these modules can be combined freely, and further modifications, such as the non-repetitive termini, can later be integrated [15, 228].

Recombinant "engineered *Araneus diadematus* fibroin 4" (eADF4) comprises 16 repeats of the C-module, giving it the name eADF4(C16). The protein sequence results in a 47 kDa protein, which is smaller than the natural model, but large-sized proteins still pose a critical problem in the expression with *E. coli*. Also, the eADF4(C16) protein does not include the C- or N-termini found in the natural protein [19, 177].

Consensus-sequence: the C-module

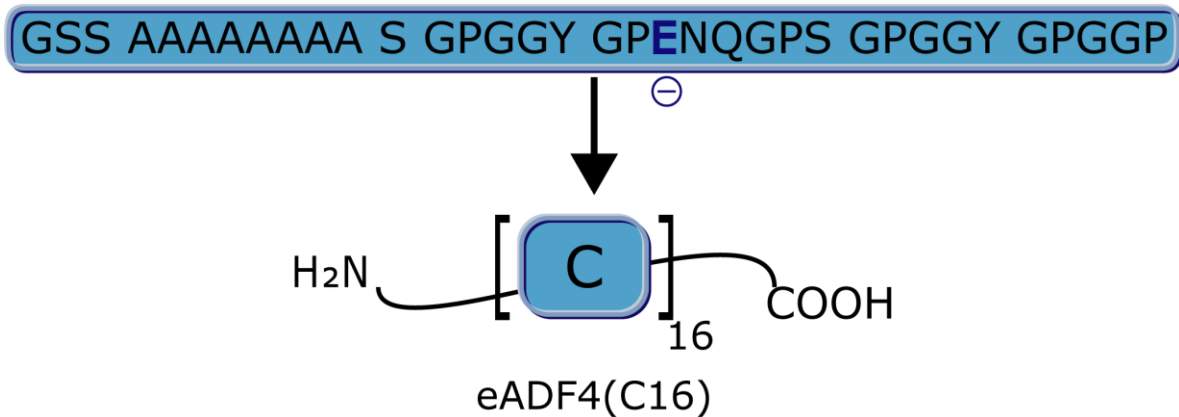


Figure 1-9: Amino acid sequence of eADF4(C16). The C-module is repeated 16 times, mimicking the properties of natural MaSp2 protein. Dark blue highlights the glutamic acid residue, adding a negative charge to each module.

After fermentation and purification, this protein can be lyophilised and stored until further processing into various morphologies [229]. Furthermore, molecular biological means can further modify the protein due to its recombinant nature. This can change the protein in terms of single amino acids, such as modifying its default negative charge or adding new peptides or proteins to create novel fusion proteins [78].

eADF4(C16) has shown great potential as a biomaterial and new approaches to using this excellent material for various applications have emerged. For example, fibres, coatings and non-woven meshes can be used as filter matrices [230, 231] in more technical-oriented applications.

1.5 Applications of Recombinant Spider Silk in Tissue Engineering

TE, in particular, poses an exciting field of application for recombinant spider silk. It was also shown that recombinant spider silk is a fantastic material for implant technology as it acts as a bacteriostatic bio-shield and avoids fibrous capsule formation [52]. Furthermore, through the advancements in genetic engineering and cloning techniques, it is possible to modify spider silk proteins to enhance their functionality for specific applications. One such modification involves the incorporation of cell adhesion peptides onto the spider silk protein, which can

Chapter 1: Literature Review

transform the naturally cell-rejecting material into one that promotes cell attachment and proliferation [223]. This tailoring of spider silk through genetic modifications, combined with the variety of available morphologies, opens up exciting possibilities for expanding its potential in TE and regenerative medicine, enabling precise control over its interactions with cells and tissues [232].

Figure 1-10 overviews the most prominent recombinant spider silk morphologies used in TE, and **Table 1-3** briefly summarizes applications thereof, highlighting the versatility of this material.

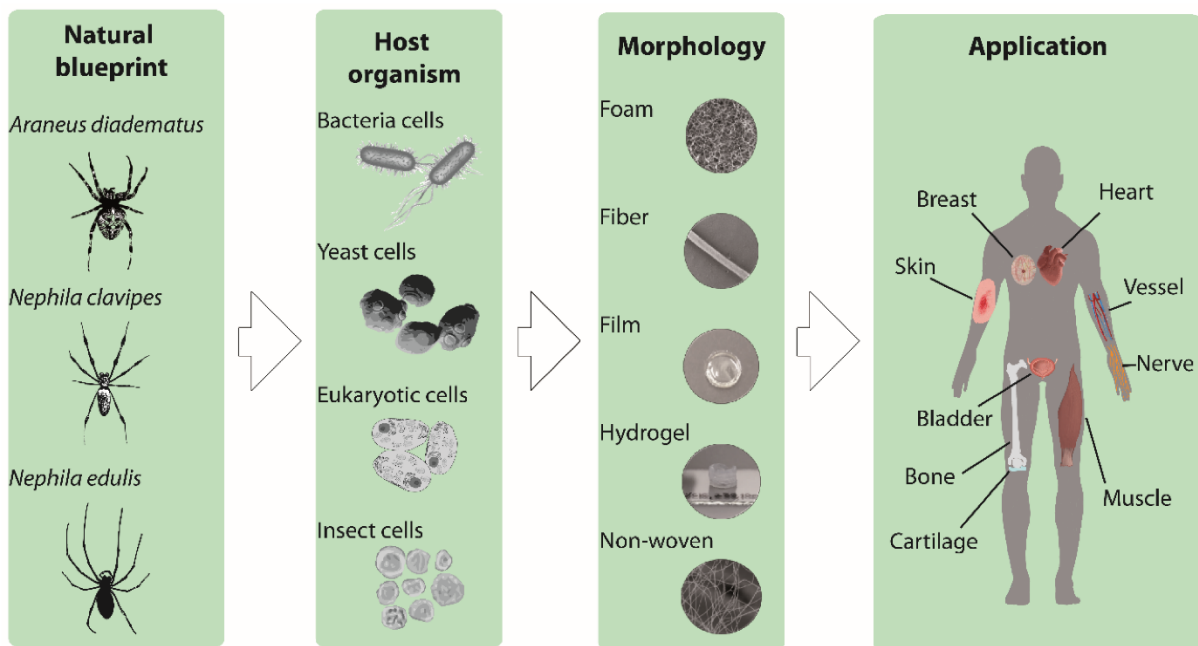


Figure 1-10: Overview of the different recombinant spider silk morphologies used in TE. Natural spider silks serve as a blueprint for recombinant spider silk production. The production hosts bacteria, yeast, eukaryotic and insect cells are shown, as well as morphologies of recombinant spider silk (foam, fiber, film, hydrogel, and non-woven mesh) for potential applications in TE. Figure and caption adapted from reference [158] (© S. Salehi et al., published by MDPI, distributed under the terms of the Creative Commons Attribution 4.0 International License (CC BY 4.0), <http://creativecommons.org/licenses/by/4.0/>)

Chapter 1: Literature Review

Table 1-3: Exemplary overview of Tissue Engineering applications using spider silk proteins. Compiled from [233] and [158].

Application	Morphology	Content of study	Ref.
Heart TE	coatings	Cardiomyocytes seeded on coated glass substrates. Observation of contraction and electrical signalling.	[146, 234]
	films	Showed different cell morphologies depending on the spider silk variant used.	[235]
Vascular TE	Fibres and non-woven hydrogels	AV-loops <i>in vivo</i> in rat models.	[20] [59]
	foams	Observed of vessel-like structures within 14 days.	[92]59
	Rolled non-woven tubes	Observation of the formation of synapses and membrane potentials along the tubes.	[236]
Neural TE	Self-rolling chitosan/spider silk tubes	Observation of directed neuron differentiation.	[237]
	<i>Natural</i> silk fibres	Parallel fibres used as nerve guiding scaffold	[238, 239]
	<i>Natural</i> silk fibres	Ridging of long nerve defects in sheep.	[240]
	foams	Observation of neuronal stem cell attachment and differentiation into astrocytes.	[241]
Muscle TE	Patterned films	Mayoblasts <i>in vitro</i> culture showed surface topography dependency.	[232]
Cartilage TE	Gradient films	Observation of gradient-dependent cell adhesion.	[242]
	Coatings (blends with spider silk and other polymers)	Differentiation from MSC to osteoblasts.	[243]

Chapter 1: Literature Review

Bone TE	Coating/ film	Differentiation from MSC to osteoblasts.	[244, 245]
	coatings	significantly increased differentiation of bone marrow hMSCs.	[246]
	Coatings of a blend of recombinant and <i>natural</i> spider silk	Observation of guided osteoblastic differentiation of MC3T3-E1 cells.	[247]
Bladder TE	Cross-weaved <i>natural</i> silk fibres	Observation of primary human urothelial cell adhesion without fibrosis-associated gene expression.	[248]
Skin TE	Coatings/ films	Elevated wound healing rate <i>in vivo</i> rat models.	[169]
	Woven <i>natural</i> silk fibres	Multilayer epidermis model.	[249]
	fibres	<i>In vivo</i> implants in rats showed fibroblast ingrowth and angiogenesis.	[250]
	coating	Showed enhanced cell-binding activity and cellular growth of skin-derived human dermal fibroblasts of neonatal origin.	[251]
Breast TE	Coating	Coating for breast implants showed decreased fibrosis and inflammation response.	[52]
TE devices	<i>Natural</i> silk fibres	Braided fibres used as sutures.	[252]
	coatings	Antifouling coating for polyurethane catheters.	[105]
Undefined	foams	Mesenchymal stem cell ingrowth with endodermal differentiation.	[253]
	foams	Observation of good fibroblast adhesion and distribution.	[60], [254]

Chapter 1: Literature Review

hydrogels	Characterization as bioink with varying concentrations and cell types.	[24, 255] [58]
-----------	--	----------------

Table 1-3 does not showcase a high utilization of hydrogels derived from recombinant spider silk in precisely defined TE applications besides the AV-loop [59] and general printing studies [24, 58, 255]. Nonetheless, initial investigations focusing on their mechanical properties, printability, and cellular interactions have begun to shed light on their overall potential.

Specifically, *Lechner et al.* conducted a pioneering study to explore the behaviour of Arg-Gly-Asp (RGD)-modified spider silk hydrogels. They found that these hydrogels undergo physical cross-linking when cells are incorporated, indicating an active interaction between the hydrogel and the cells. In contrast, untagged spider silk proteins showed no such interaction with cells.

Importantly, the study revealed that cell viability remained remarkably high following extrusion-based printing, even at high cell densities of up to ten million cells per millilitre. This finding is a crucial prerequisite for developing spider silk hydrogels in TE. **Figure 1-11** shows a shape fidelity assay of printed constructs using a filament collapse test in both the absence and presence of cell culture media, further confirming the structural integrity of the printed constructs [58].

Chapter 1: Literature Review

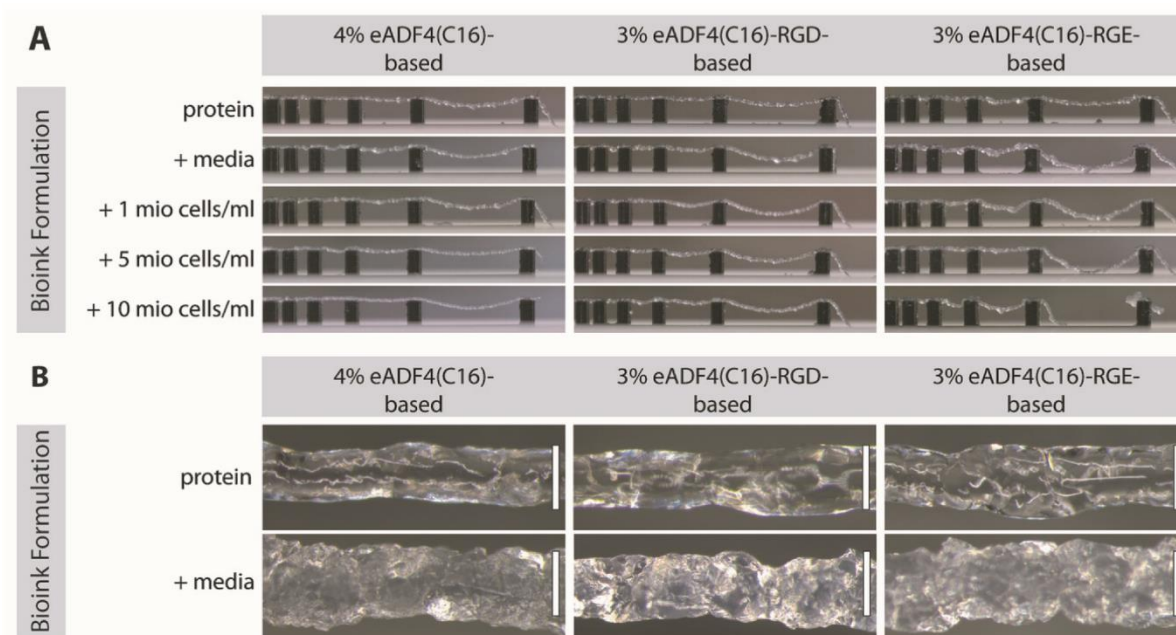


Figure 1-11: Shape fidelity assay of printed spider silk bioinks. A) Strands of each bioink formulation were printed on a pillar row with defined distances to observe the breaking point of an extruded ink line. B) Stereo microscopy images of the hanging lines of spider silk hydrogels with and without cell culture media (scale bars: 200 μm). Adapted from reference [58] (© A. Lechner et al., published by Wiley-VCH, distributed under the terms of the Creative Commons Attribution 4.0 International License (CC BY 4.0), <http://creativecommons.org/licenses/by/4.0/>)

Furthermore, *in vivo* experiments conducted by Steiner et al. represented a significant advancement in the utilization of hydrogels composed of eADF4(C16). In these experiments, the hydrogels were transferred into teflon isolation chambers, as depicted in **Figure 1-12A** and implanted in a rat arteriovenous loops (AVL) for 4 weeks. In addition, they also implanted RGD-modified eADF4(C16) hydrogels in the AVL model to enhance vascularisation after 2 and 4 weeks.

Upon explantation, histological and microcomputed tomography analyses (**Figure 1-12B+C**) were performed on the specimens. The results confirmed the biocompatibility of the hydrogels and revealed the progressive formation of functional tissue over time. Notably, the functionalization of eADF4(C16) with RGD motifs proved to be a powerful strategy to improve hydrogel stability and enhance vascularization. In fact, the RGD-functionalized eADF4(C16) hydrogels outperformed other hydrogels, including fibrin gels, in terms of promoting vascularization [59]. Johansson et al. [92] observed a similar response in the presence of spider silk foams during a co-culture experiment involving endothelial cells and connective tissue cells. The mixture contained 2-10% endothelial cells.

Chapter 1: Literature Review

Over a two-week culture period, the endothelial cells aggregated and generated branched sprouts measuring several millimetres in length.

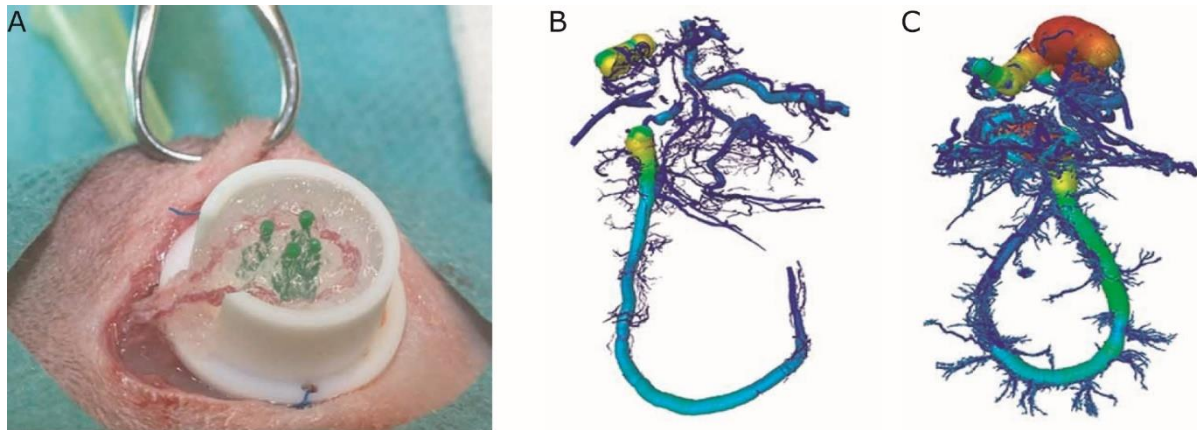


Figure 1-12: A) Photograph of the AVL operation. The AVL was placed between two layers of spider silk hydrogel. B) Microcomputer tomography (μ CT). After 2 and C) 4 weeks. Adapted from reference [59] (© S. Steiner et al., published by IOP publishing, distributed under the terms of the Creative Commons Attribution 4.0 International License (CC BY 4.0), <http://creativecommons.org/licenses/by/4.0/>)

These findings demonstrate the feasibility of recombinant spider silk hydrogels for TE and underscore their potential for advanced fabrication techniques such as 3D bioprinting. The ability of spider silk hydrogels to support cell viability, exhibit cell-interacting behaviour, and maintain structural integrity during the printing process holds great promise for developing complex tissue constructs with enhanced biological functionality. Further research in this field will undoubtedly unlock the full potential of recombinant spider silk hydrogels and propel their integration into a wide range of TE applications.

In a research study conducted by *Johansson et al.* [92], they utilized a scaffold composed of recombinant spider silk protein known as 4RepCT, which underwent genetic modification through the inclusion of a cell adhesion motif from fibronectin. The scaffold was generated from a silk solution and mouse mesenchymal stem cells. The assembly triggered by the gentle introduction of air bubbles into the solution formed a wet foam structure (**Figure 1-13A**). Careful control of the air-water interface facilitated the homogeneous distribution of cells within the silk material, leading to the even dispersion of cells throughout the three-dimensional silk foam network. After a three-day incubation, the cells were well-distributed within the 3D silk foam structure. The study demonstrated the successful distribution and integration of human embryonic stem cells, within the silk foam.

Chapter 1: Literature Review

Notably, cell aggregates within the 3D foam became apparent after 48 hours (**Figure 1-13B**). Subsequent induction of endodermal differentiation led to the formation of dense layers of cells, as confirmed by mRNA analysis. A comparison of gene expression profiles between 2D and 3D samples revealed a significant upregulation of SOX17 and CER1, along with a downregulation of pluripotency marker NANOG, indicating the successful initiation of differentiation (**Figure 1-13C+D**). Additionally, the study explored the differentiation potential of human bone marrow-derived mesenchymal stem cells when mixed with the spider silk foam by observing the presence of lipid droplets throughout the scaffolds containing integrated cells after expansion and differentiation induced by adipocyte-specific media, as shown in **Figure 1-13E**.

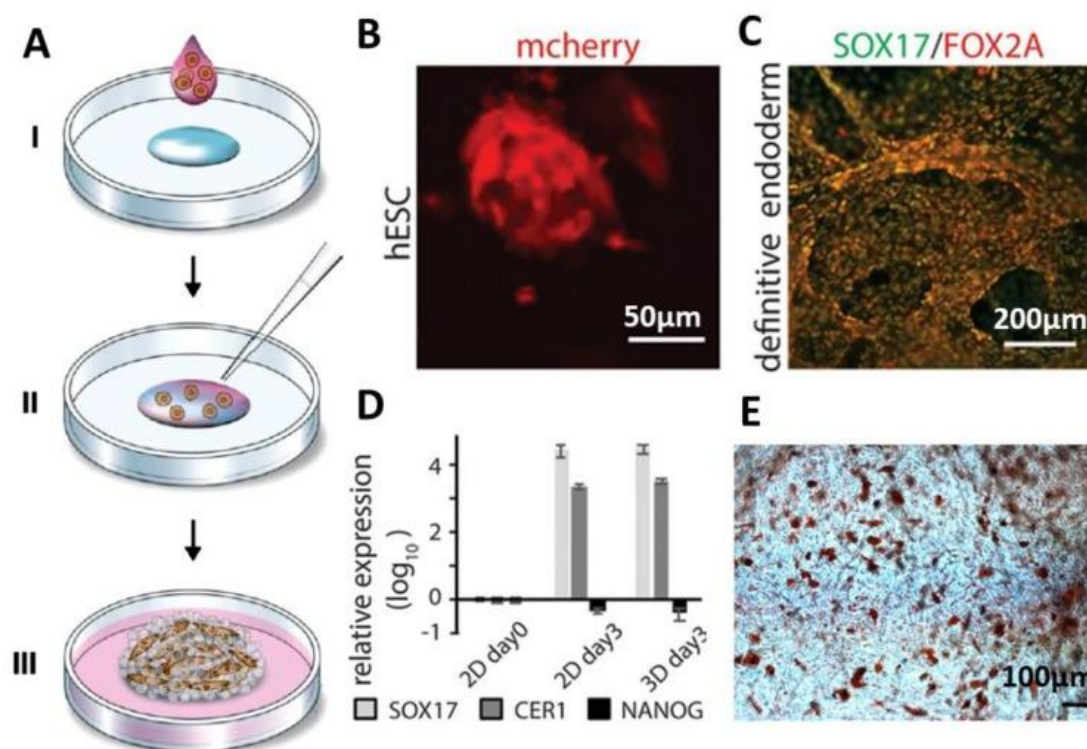


Figure 1-13: A): Foam processing with cell incorporation. Media containing cells (pink) was blended with the fibronectin-modified spider silk solution (blue) (I). The introduction of air bubbles with pipette tip (II), induced the foam formation. B): mCherry was detected after 48 h, indicating the presence and incorporation of the differentiated human embryonic stem cells (hESC) into the foam structure. C+D): Immunostaining of the endodermal markers SOX17 (green) and FOX2A (red) was supported by RTqPCR analysis. Expression of the genes SOX17, CER1, NANOG for hESC in the silk foam versus that of a 2D culture. Bars represent the mean fold change \pm standard deviation ($n = 4$). E): Differentiation of human mesenchymal stem cells within the-silk foam into adipogenic lineage, showing lipids droplets stained by Red Oil (red) ($n = 2, n = 4$). Originally adapted from reference [92] (© U. Johansson et al., published by IOP publishing, distributed under the terms of the Creative Commons Attribution 4.0 International License (CC BY 4.0), <http://creativecommons.org/licenses/by/4.0/>). Copyright 2019, Nature Research. Modified image and caption adapted from reference [158] (© S. Salehi et al., published by MDPI, distributed under

Chapter 1: Literature Review

the terms of the Creative Commons Attribution 4.0 International License (CC BY 4.0), <http://creativecommons.org/licenses/by/4.0/>.

Finally, the study investigated the differentiation of adult precursor cells known as human skeletal muscle satellite cells encapsulated within the spider silk foam. After a two-week culture period in myogenic differentiation media, the HSkMSCs exhibited full alignment and coverage of the fibrillar network within the foam.

Coatings, on the other hand, have already been used in TE applications extensively, and some even reached clinical trials. One such approach was designed by *Zepelin et al.*, as shown in **Figure 1-14**. In this study, medical-grade silicone implants were coated with a thin layer of recombinant spider silk proteins, and the biocompatibility of these coated implants was thoroughly analyzed both *in vitro* and *in vivo*. Quantitative methods were employed to determine marker-specific gene expression and protein concentration, allowing insights into the effects of the silk coating on various cellular processes. The results revealed that the silk coating exerted inhibitory effects on fibroblast proliferation, collagen I synthesis, and the differentiation of monocytes into CD68-positive histiocytes.

Furthermore, the silk coating significantly reduced capsule thickness, post-operative inflammation, synthesis and remodelling of the extracellular matrix, and the expression of factors mediating contracture. These findings are of great importance as they demonstrate that coatings made of recombinant spider silk proteins have the potential to effectively mitigate major post-operative complications associated with the introduction of implants, specifically capsular fibrosis and contraction [52].

Chapter 1: Literature Review

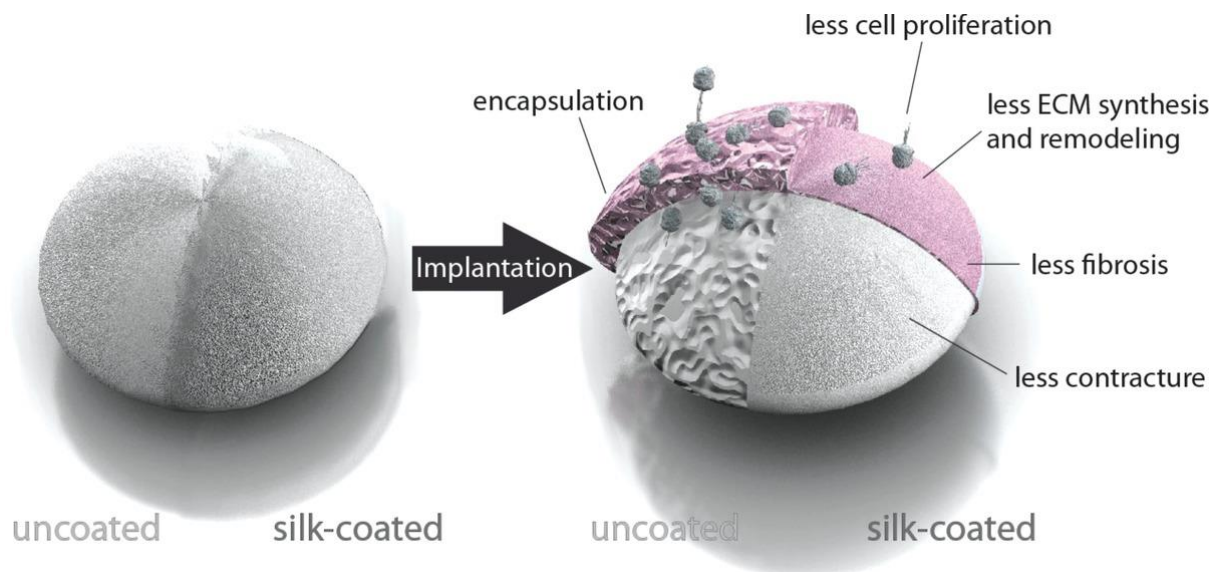
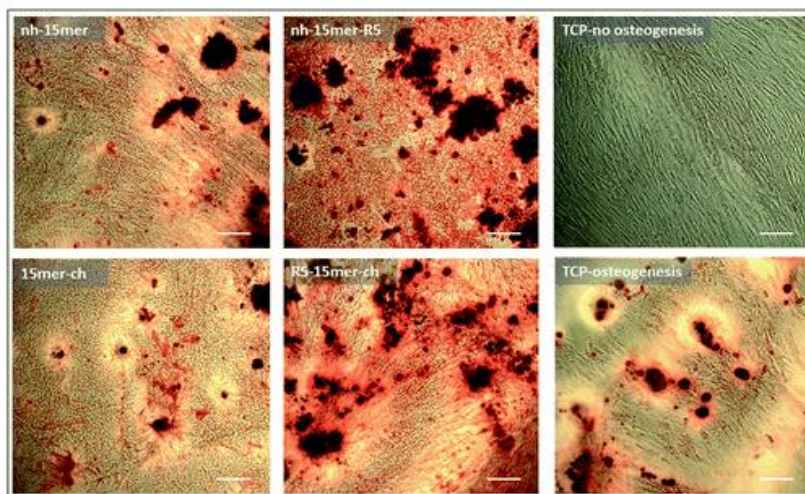


Figure 1-14: Schematic of the spider silk-coated silicone implants, which are supposed to minimize fibrosis, cell proliferation, contractures and encapsulation by ECM proteins. Adapted from reference [52](© P. Zeplin et al., published by WILEY-VCH and reprinted with permission under license number 5558781272790.)

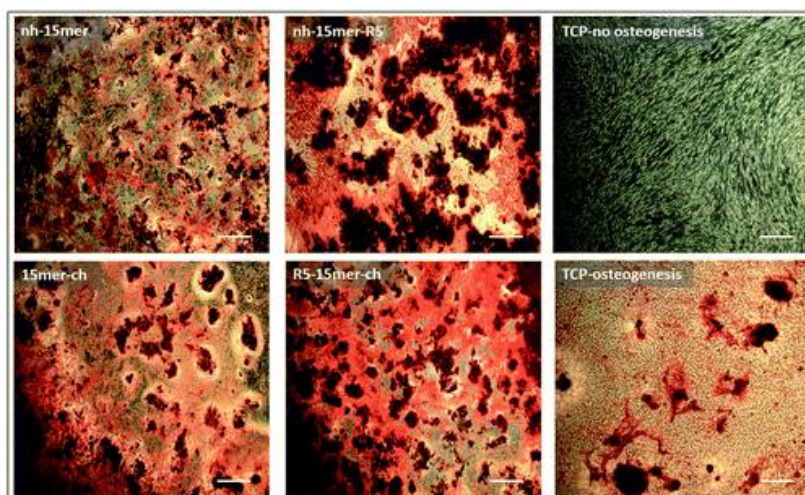
Besides implant coatings, more fundamental research in regard to biomineralization has been conducted. For example, *Gomes et al.*[245] demonstrated the potential of recombinant spider silk proteins derived from the major ampullate spidroin (MaSp1) from *Nephila clavipes* in the context of bone regeneration. Therefore, they genetically fused it with a bone sialoprotein. This functionalization aimed to promote cellular attachment, differentiation, and the deposition of calcium phosphate on the surface of a film. Their experiments resulted in an accelerated calcification *in vitro*, observed after as little as 6 hours at 37°C. Furthermore, films composed of this fusion protein facilitated calcium phosphate deposition and exhibited excellent adhesion properties for human mesenchymal stem cells, significantly enhancing their differentiation. Next, *Plowright et al.*[246] utilized the same base recombinant spider silk, however, they designed a new fusion of the spider silk with the silica-binding peptide R5 (SSKKSYSYSGSKGSKRRIL), sourced from silaffin of *Cerithiopsis fusiformis*, at both termini of the silk sequence to observe bio silicification as shown in **Figure 1-15**. Adding the silica domain to the carboxyl-terminal end demonstrated superior and more controlled silica precipitation after 4 and 8 weeks when compared to unmodified silk films and tissue culture plate substrates. Moreover, this modified silk significantly promoted the differentiation of bone marrow-derived human mesenchymal stem cells.

Chapter 1: Literature Review

a) 4 weeks



b) 8 weeks



c) 4 and 8 weeks

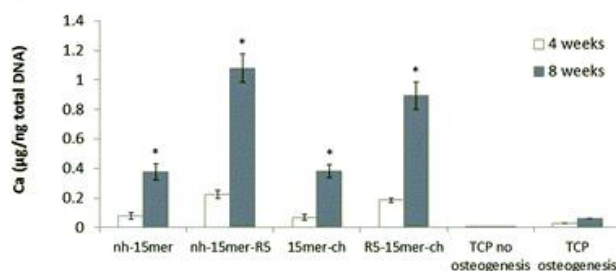


Figure 1-15: Calcium crystal deposition by differentiating human mesenchymal stem cell on the recombinant silk and silk-silica films. Calcium crystals (red) staining by alzarin red S was performed on hMSCs cells grown on nh-15mer (N-terminal his6 tag), nh-15mer-R5 (N-terminal his6 tag, C-terminal R5 protein), 15mer-ch (C-terminal his6 tag), R5-15mer-ch (C-terminal his6 tag, N-terminal R5 protein) and TCP (Tissue culture plate) four (A) and eight (B) weeks post seeding. Scale bars are 300 μm . (C) Quantification of calcium deposition of hMSCs grown on recombinant silk-silica constructs after 4 weeks (white bars) and 8 weeks (grey bars) in culture. Results for nh-15mer, nh-15mer-R5, 15mer-ch and R5-15mer-ch silk-silica constructs and TCP no osteogenesis and TCP osteogenesis are shown. Data are represented as the average \pm standard deviation ($n = 3$, $*p < 0.05$). Figure and caption adapted from reference [246](© R. Plowright et al., published by Royal Society of Chemistry and reprinted with permission under license number 1397909-1.).

Chapter 1: Literature Review

Lastly, in this group of exemplary spider silk usage in TE, *Baoyong et al.* conducted a study to evaluate the wound-healing properties of two types of recombinant spider silk proteins, pNSR-16 and pNSR-32, compared to collagen as a control in an *in vivo* rat model. The experiment involved applying these proteins on the wound, with an additional group left untreated as a negative control. Various assessments were performed on days 3, 5, 7, 14, and 21, including wound-healing rate, histological tests, measurement of hydroxyproline synthesis, and immunohistochemical staining to detect basic fibroblast growth factor. The results of the implantation testing demonstrated that the treatment groups receiving the recombinant spider silk proteins, pNSR-16 and pNSR-32, exhibited significantly improved wound healing compared to the control group ($p < 0.01$). On the 7th, 14th, and 21st days, there was a higher expression of bFGF, which is known to be crucial in promoting tissue regeneration. Additionally, the levels of hydroxyproline, an essential component of collagen synthesis and an indicator of tissue remodelling, increased in the treatment groups' skin samples. These findings collectively indicated successful regeneration of the wound skin in the groups treated with the recombinant spider silk proteins [169].

1.5.1 Silk Materials in Bone Tissue Engineering

One particularly interesting discipline of TE utilizing spider silk or silk fibroin is Bone tissue engineering as a promising method for bone regeneration, potentially replacing existing clinical therapies.

Besides being processed and used as a graft, tissue-engineered constructs also open the door for three-dimensional tissue models that aid in the detection of tissue malfunctions and their analysis at the cellular and molecular levels [256, 257]. By combining cells, scaffolds, and, to some extent, growth factors or mechanical stimuli, the objective is to create and help regenerating 3D bone tissues using the patient's own cells. Selecting an appropriate biomaterial that can mimic the mechanical and biological properties of the natural bone tissue matrix to support tissue development is one of the main challenges. Due to its exceptional mechanical qualities, silk materials, which are a promising biomaterial for scaffold fabrication in general, is well suited for use in bone TE [258]. For example,

Chapter 1: Literature Review

Hennecke et al. [252] utilized braided natural spider silk fibres as suture material for tendons, minimizing foreign body reactions.

Lastly, silks have shown great promise in prior studies regarding bone TE and the beneficial biomineralization. *Hardy et al.* [243] and *Yang et al.* [259] observed biomineralization and increased alkaline phosphatase activity when human mesenchymal stem cells were cultivated on these materials. The calcium ions could bind and speed up the mineralization because the used spider silk contained several carboxylic acid moieties. Calcium carbonate was preferentially deposited on eADF4(C16), but not on the synthetic polymer phases of the blend films from the composite polymer solution of eADF4(C16) and poly(butylene terephthalate) or poly(butylene terephthalate-co-poly(alkylene glycol) terephthalate). Finally, as discussed before (**Chapter 1.5.1**), *Gomes et al.* [245] could further enhance bone regeneration with a fusion protein of recombinant MaSp1 protein and a sialoprotein.

Generally speaking, clinical practice has shown that most bone fractures heal naturally and do not require TE strategies. Therefore, bone TE strongly focuses on supporting the regeneration of intricate or non-uniform fractures. Therefore, next to the apparent choice of silk fibres due to their mechanics, hydrogels have also found their way into bone TE. Hydrogels can serve as networks, which offer impressive options for delivering cells and cytokines to target sites, which can be hard to reach in deeply located bone or tendon injuries. Additionally, they are advantageous, especially for clinical applications, because they benefit from being injectable [260-262] if physically cross-linked.

While the usage of hydrogels from recombinant spider silk in bone TE is not established yet, several studies showed progress in utilizing hydrogels formed from silk fibroin. For example, human MSCs could be successfully encapsulated in sonication-induced silk fibroin hydrogels, which also supported their cellular processes of proliferation, growth, and maintenance [263]. Furthermore, even without adding osteogenic stimulants to the cell culture medium, hydrogels induced osteogenic differentiation of human MSCs [264]. And lastly, it has been shown that injectable silk fibroin hydrogels speed up the remodelling processes in rabbit distal femurs [265]. One *in vivo* study with injectable silk fibroin hydrogels in rats showed that incorporated growth factors in these hydrogels promoted

Chapter 1: Literature Review

angiogenesis and new bone formation [266]. Such gels highlighted a minimally invasive manner to deliver growth factors, drugs or cells to regenerate irregular or difficult-to-access cavities in bone.

1.6 Recombinant fusion Proteins

As mentioned earlier, recombinant proteins offer tremendous potential for further modifications and functional enhancements. This innovative approach gives rise to entirely new fusion proteins that possess the combined properties of the fused partners. These hybrid proteins have become invaluable medical research tools for drug-targeting applications.

By linking specific functional proteins, such as single-chain antibodies or cell surface receptor ligands, to a protein, fusion proteins can be designed to target and interact with particular cell types selectively. This targeted approach holds great promise in various therapeutic applications, as fusion proteins can deliver payloads, such as toxins or cytokines, to desired cell populations [267, 268]. Notably, several fusion protein drugs, including Enbrel® (tumour necrosis factor/Fc-IgG1), Ontak® (interleukin-2/diphtheria toxin), Orencia® (cytotoxic T-lymphocyte antigen-4/Fc-IgG1), Amevive® (leukocyte function antigen-3/Fc-IgG1), Arcalyst® (interleukin-1 receptor extracellular domain/Fc-IgG1), and Nplate® (thrombopoietin/Fc-IgG1), have already been approved by the FDA [269-271], underscoring the clinical significance of this approach.

1.6.1 Spider silk fusions

Consequently, genetic modifications can be utilized for recombinant spider silk to create fusion proteins that possess both spider silk's exceptional mechanical properties and the fused domain's specific functionalities. In that manner, various spider silk fusions have been created to date.

For example, *Neubauer et al.* have created a collagen-binding spider silk fusion protein to initiate biomineralization on spider silk films and showed enhanced MC3T3-E1 mouse pre-osteoblasts adhesion on the mineralized surface [242].

Chapter 1: Literature Review

Similar to this approach, *Dinjaski et al.* fused a hydroxyapatite binding domain to both terminals of the spider silk and could show increased biomineralization [244]. Lastly, the biomineralisation could be further improved by an approach by *Gomes et al.*, where they fused bone sialoprotein to a spider silk protein and archived mineralisation of films through deposition of calcium phosphate by the selectively adhered and differentiated human mesenchymal stem cells [245], as discussed in section **1.5**.

Luo et al. fused repeating units of resilin with a spider silk c-terminal domain from *N. clavipes* to obtain a thermoresponsive copolymer that could reversibly form hydrogels at a temperature threshold [272]. The thermoresponsive properties of the terminal domain enabled gel formation at low ($\sim 2^{\circ}\text{C}$) and high ($\sim 65^{\circ}\text{C}$) temperatures in prior studies and was observed for conservation of this property when fused to multiresponsive resilin protein with 4 and 8 repeats in this study. As depicted in their results shown in **Figure 1-16A**, both protein solutions (15% v/w) of either R4C, with 4 repeats of the resilin sequence, or R8C, with 8 repeats were able to form reversible hydrogels at lower temperatures between 4 and 15°C , which is higher than for gels of the unmodified terminal domain at 2°C . Both formulations melted above 15°C and formed irreversible hydrogels at 65°C for R4C and 85° for R8C, attributed to the proteins' denaturation. The rheological evaluation shown in **Figure 1-16B** confirmed this behaviour of 20% w/v gels with both gels crossing the sol-gel point around 20°C and again upon heating at 65°C and 75°C , respectively. This study highlighted the interplay of the fusion partners properties to yield similar, but differently tunable properties of the fusion protein.

Chapter 1: Literature Review

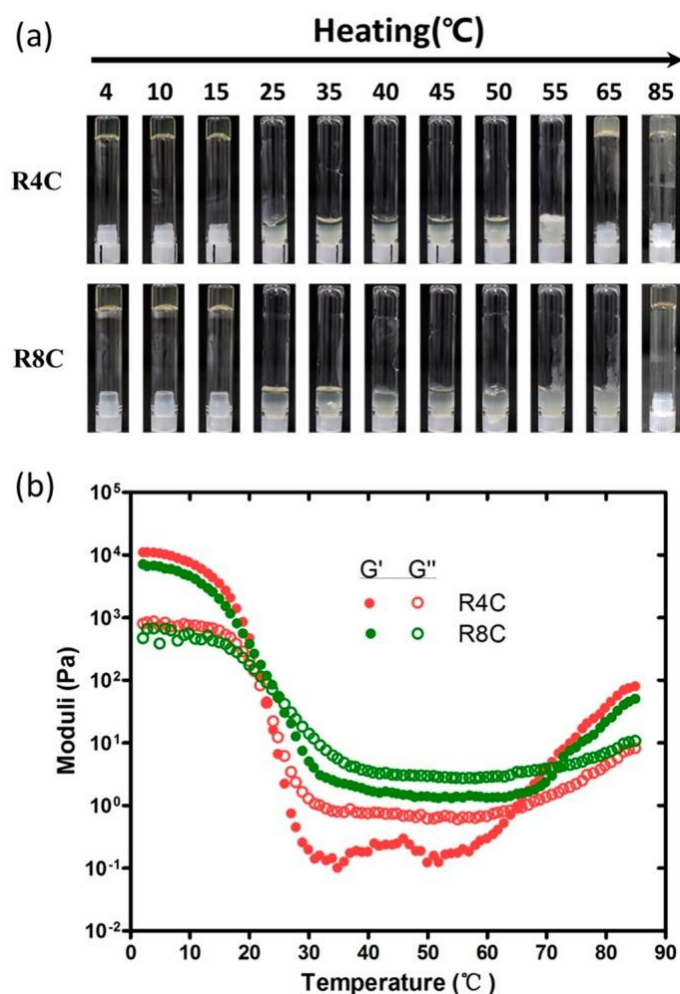


Figure 1-16: A): Test of formation of hydrogels by R4C (4 repeats of reisin module with c-terminal spider silk) and R8C. Vials containing 15% (w/v) protein solutions were incubated for 10 min at the indicated temperatures and then inverted for image collection; (b) Oscillatory rheological analysis of R4C and R8C at a protein concentration of 20% (w/v). The temperature sweeps were performed with a heating rate of 2 °C min⁻¹. Figure and caption adapted from reference [272] (© F. Luo et al., published by MDPI, distributed under the terms of the Creative Commons Attribution 4.0 International License (CC BY 4.0), <http://creativecommons.org/licenses/by/4.0/>).

Another study by *Humenik et al.* fused the green fluorescent protein (GFP) to the recombinant spider silk protein eADF4(C16). By doing so, they achieved a recombinant spider silk that is fluorescent and, at the same time, retains the properties of the spider silk, such as the gelation into physically cross-linked hydrogels [78]. Fundamental research to fuse GFP to spider silk proteins was conducted by *Zhang et al.*; where they mainly focused on the host organism and the production parameters in general but could already produce the functional fusion protein in small amounts [213].

Chapter 1: Literature Review

By trying to mimic a complete natural spider silk molecule more closely, *Thamm et al.* recombinantly produced a short major ampullate spidroin as a fusion construct between *Latrodectus hesperus* terminal domains and the *Cyrtophora moluccensis* core domain to obtain more insight into the molecular assembly of spider silk fibres [183].

One approach by *Mittal et al.* fused spider silk proteins with an affinity domain Z, which binds immunoglobulin G (Z-silk), as well as a fusion protein with the RGD peptide derived from fibronectin (FN-silk). These proteins were blended with cellulose nano fibres to create composite materials that exhibit bioactivity regarding antibody binding and cellular attachment [273]. **Figure 1-17A+B** demonstrates the ability of free-standing and cast films, as well as coatings processed from the CNF/Z-silk blend, to bind to fluorescently labelled IgG antibodies, while the controls of CNF and CNF/FN-silk do not show any fluorescent signals, indicating the functionality of the fusion protein. Furthermore, **Figure 1-17C** shows bioactivity regarding cell adhesion to the FN-silk variant functionalized with RGD. Here, it can be seen that human dermal fibroblasts adhere to the CNF/FN-silk blend films, while no cellular attachment could be observed for CNF films., which is supported by cell counts (**Figure 1-17D**) and Alamar blue assays (**Figure 1-17E**).

Chapter 1: Literature Review

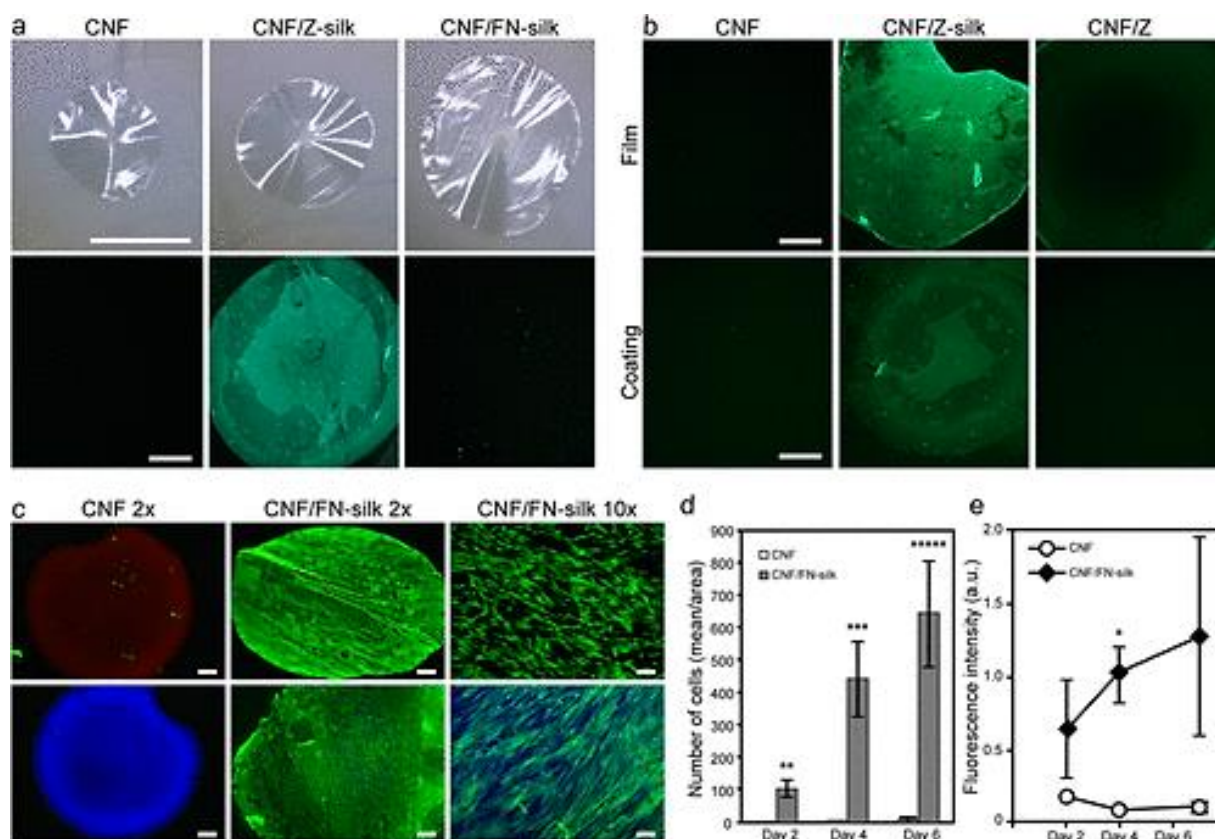


Figure 1-17: Cellulose nanofibres (CNF)-based composite films show bioactivity. A): Optical microscopy images of CNF and composite CNF/silk films (top panel). Scale bars: 4 mm. Fluorescence microscopy images show the binding of fluorophore-labeled IgG (green, bottom panel). Scale bars: 1 mm. B): Fluorescence images of IgG-fluorophore bound to casted films (top panel) and coatings on CNF films (bottom panel) of CNF and the Z domain alone (CNF/Z), CNF premixed with Z-silk (CNF/Z-silk) or pure CNF, respectively. Scale bars: 1 mm. C): Human dermal fibroblasts cultured on CNF or CNF/FN-silk films for 7 days. Top panel: live/dead staining (green, living cells; red, dead cells/ autofluorescence from CNF). Bottom panel: F-actin staining (green, F-actin; blue, nuclei/autofluorescence from CNF). Scale bars: 500 μ m for 2 \times and 100 μ m for 10 \times . D): Number of Human dermal fibroblasts (mean + SD) per mm² on free-standing films of CNF (white bar) and CNF/FN-silk (grey bar), at 2, 4 and 6 days, as evaluated by DAPI staining and manual counting of nuclei. Statistically significant differences according to Student's t-test: ** $p < 0.01$, *** $p < 0.001$, and **** $p < 0.00001$. E): Representative Alamar blue viability graph of three independent experiments with Human dermal fibroblasts growing on CNF and CNF/FN-silk films ($n=3$) during 1 week. Statistically significant differences according to Student's t-test: * $p < 0.05$. Error bars show standard deviation. Figure and caption adapted from reference [273] (© N. Mittal et al., published by ACS Nano, distributed under the terms of the Creative Commons Attribution 4.0 International License (CC BY 4.0), <http://creativecommons.org/licenses/by/4.0/>)

Lastly, two distinct approaches involving cellulose-binding spider silk fusion proteins to enhance the mechanical properties of spider silk materials have been researched and will be explained in detail in Chapter 1.7. Briefly, Meirovic et al. and Mohammadi et al. have both explored the incorporation of cellulose nanoparticles to improve the resulting morphology of spider silks, specifically films and sponges [216], as well as fibres [274] and films [275], respectively.

Chapter 1: Literature Review

These studies demonstrate the potential of utilizing cellulose-binding spider silk fusion proteins to enhance the mechanical properties of spider silk materials by showing that incorporating cellulose particles presents a valuable strategy for reinforcing spider silk-based films, sponges, fibres, and potentially other morphologies, possibly expanding their applications in biomaterials, TE, and beyond.

1.6.2 Cellulose blended Biomaterials

Cellulose, derived from plants and bacteria, is a versatile and abundant biopolymer with immense potential in biomaterials research. Its unique properties, including renewability, biocompatibility, and mechanical strength, make it an attractive candidate for various applications [25]. In the field of TE, cellulose-based materials have shown promising outcomes, demonstrating their ability to provide mechanical support and scaffolding in 3D cell cultures as hydrogels from cellulose nanofibres [276] and bone grafting scaffolds from composite materials [277-281].

Table 1-4 briefly overviews studies using cellulose materials as blend partners, mostly utilizing its low cost, abundance, and mechanical properties.

Table 1-4: Exemplary overview of possible cellulose-blended composite materials in Tissue Engineering.

Blend material	Application	Effect of cellulose	Ref.
Bacterial cellulose + hydroxyapatite	Enhanced bone regeneration in membranes.	Matrix material for mechanical properties.	[277]
Bacterial cellulose + hydroxyapatite + growth factor peptides	Enhanced bone regeneration in membranes.	Matrix material for mechanical properties.	[278]
Cellulose nanofibres + silk fibroin	Highly transparent, strong, elastic films.	Matrix material for transparency mechanical properties (strength).	[282]
Cellulose+ nanohydroxyapatite	Electrospun meshes for bone regeneration.	Material for electrospinning.	[279]
Carboxymethylcellulose + nanofibrous silk fibroin	Hydrogels with high biomineralization capabilities for bone TE.	Yields to higher hydrophilicity, supporting cell growth and biomineralization.	[281]
Cellulose nanofibres + silk fibroin	Nanostructures with „ultrafast“ water transport.	Mechanical properties and	[283]

Chapter 1: Literature Review

Nanohydroxyapatite + cellulose nano crystals + silk fibroin	Freeze-dried scaffold for bone TE with enhanced osteoconductivity compared to dual blends of these materials.	hygroscopy for water transport. Enhanced mechanical and thermal properties in the composite.	[284]
Cellulose + silk fibroin	Mechanically strong electrospun mats for cell culture.	Matrix used for material sustainability without compromising properties of silk fibroin.	[285]
Cellulose nanofibres + recombinant spider silk variants	Films and coatings with maintained bioactivity from the fusion proteins.	Cheap and strong filler material for the films, contributing mechanical properties.	[273]

One remarkable aspect of cellulose is its capacity to enhance the mechanical properties of other materials when used as a filler or additive. Studies have revealed that incorporating cellulose particles into silk-based materials can significantly improve their mechanical performance, resulting in tunable composites with increased strength and durability [282, 283]. The combination of cellulose's inherent strength and its ability to reinforce other materials makes it an intriguing prospect for biomaterial research.

Following this approach, *Cho et al.* and *Xiong et al.* blended cellulose nanofibres with silk fibroin to produce films with elevated mechanical properties while maintaining the transparency of silk films at low concentrations [282, 283]. *Chen et al.* blended silk fibroin with hydroxyapatite and cellulose nanocrystals for freeze-dried scaffolds in bone TE [284]. "Ultrastrong" fibres have been produced by *Mittal et al.* by blending cellulose nanofibrils with recombinant spider silk [273]. *Gzuman-Puyol et al.* processed a silk fibroin/cellulose powder solution into electrospun non-woven mats to increase mechanical properties and observe fibroblast proliferation rates [285].

1.6.3 The role of Cellulose binding domains

While these studies have explored cellulose-based and -blended materials in combination with silks, the interactions between these materials were not well-defined. However, nature provides a solution through molecular binding sites that can facilitate strong interactions between cellulose and other molecules, potentially leading to enhanced mechanical properties through recombinant protein production.

Cellulose-degrading microorganisms, such as *Clostridium cellulovorans* [286] and *Cellulomonas fimi* [26, 27], produce cellulase enzymes that possess a unique structure comprising a catalytic domain, a linker sequence, and a non-catalytic cellulose-binding domain. This cellulose-binding domain (CBD) is crucial in establishing prolonged contact between the cellulose molecule and the catalytic domain [287, 288].

CBDs have cellulose recognition sites linked to a catalytic domain via a proline-rich linker. Over time, more than 200 CBD sequences have been identified, and they are categorized into 13 families based on their structure and binding mechanisms, as summarized in **Table 1-5** [289]. Families 1-3 contain the majority of known CBDs, ranging from 30 to 180 amino acids, and are typically located at a terminus of the parent protein [290].

Family 1 comprises fungal binding domains among the CBD families, while family 2 encompasses the extensively studied bacterial cellulose-binding domains, making it particularly relevant for this study as protein production will occur in *E. coli*. Family 2 CBDs share common features such as a low content of charged amino acids, a high content of hydroxyamino acids, conserved tryptophan residues, and two cysteines positioned near the C- and N-termini. The conserved tryptophan residues adopt a comb-like structure, as depicted in **Figure 1-18**, and play a critical role in the binding ability of CBDs through an entropically driven process [291].

Chapter 1: Literature Review

Table 1-5: CBD families and their properties. Adapted from [289]

Family	Size (amino acids)	Characteristics
I	33-36	Exclusively CBDs from fungal enzymes. >40 members. Some also bind to chitin.
II	~100	Two sub-families (IIa and IIb). IIa contains two chitin-binding domains. ~ 40 members. Some IIa CBDs bind chitin, IIb CBDs show affinity for xylan.
III	130-170	Two sub-families (IIIa and IIIb). ~25 members. Some bind to chitin.
IV	125-170	5–6 members. Does not bind crystalline cellulose.
V	63	CBD from <i>Erwinia chrysanthemi</i> only.
VI	85-90	6 members. Low affinity for crystalline cellulose.
VII [292]	~240	CBD from <i>Clostridium thermoce</i> only
VIII	152	CBD from <i>Dictyostelium discoidem</i> only.
IX	170-180	9 members, from thermostable xylanases. CBDs occur mainly as tandem repeats.
X	50-55	7 members almost exclusively from <i>Ps. fluorescens</i>
XI	120-180	4 members, mainly from <i>Clostridium</i> and <i>Fibrobacter</i> enzymes.

Chapter 1: Literature Review

XII	~50	10 members. Mainly sequences derived from <i>Bacilli</i> endoglucanases and from various chitinases.
XIII	40-45	Contains triple repeated CBDs from xylanases and lectin-like domains with different specificities.

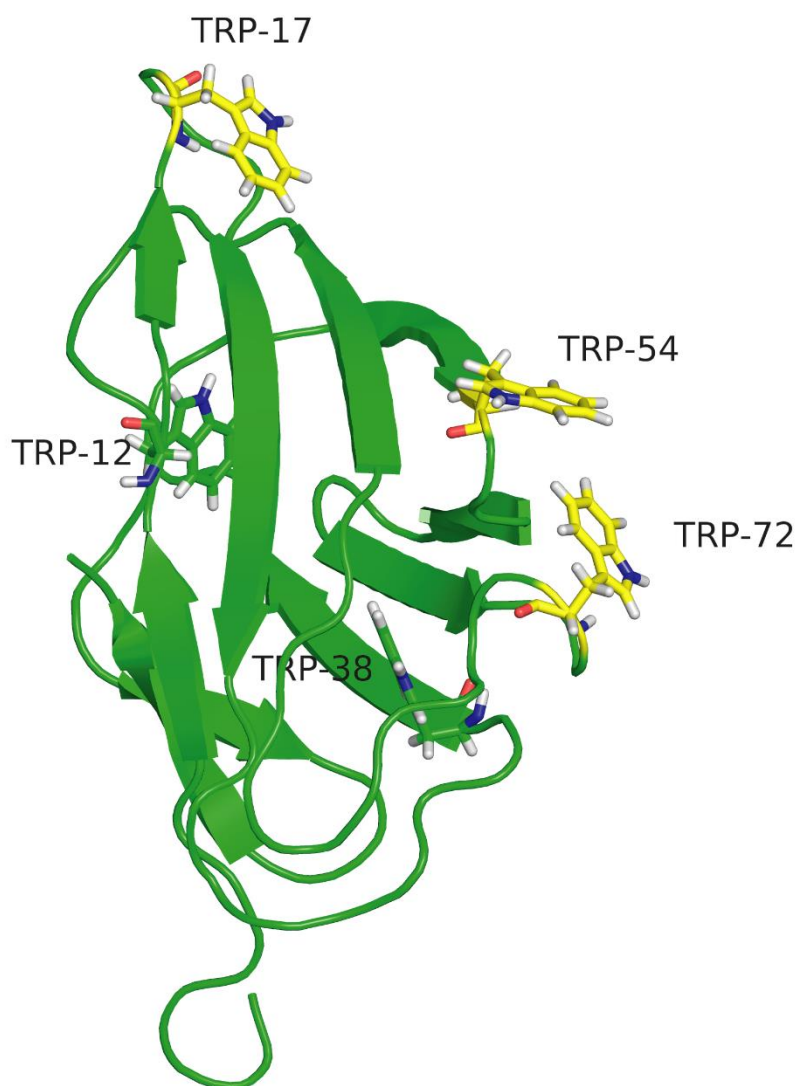


Figure 1-18: Structure of CBD_{CEX} from *C. fimi*. Yellow highlights the tryptophan residues 17, 54 and 72, forming the comb to bind to cellulose molecules.

Chapter 1: Literature Review

1.7 State of the Art: CBD fusions

Recombinant protein production, especially fusion proteins, shows great promise in developing novel materials for medicine and technology. The coupling of CBDs has found significant usage since the late 1990s [293], when the first structures were discovered and characterized. As most recombinant production procedures in the laboratory scale utilize bacterial cultures such as *E.coli*, the most used and researched CBDs belong to family 2, which comprises mainly bacterial CBDs. Because the field of CBD fusions itself emerged not recently, the area of applications is widespread across various disciplines. Due to the fundamental method and the CBDs being discovered not recently, the array of applications is vast, as suggested by **Table 1-6**, where it can be deduced that CBD fusion proteins are used throughout many research areas.

Table 1-6: Exemplary overview of CDB fusion proteins and their uses.

Application	Fusion partners	Effect	Ref.
Tissue Engineering	CBD-RGD peptide	Improved fibroblast affinity.	[294]
Emulsification	CBD-Hydrophobin	Improved oil-in-water emulsions when combined with cellulose nanofibres.	[295]
Protein purification	metallothionein (MT)-CBD-superfolder GFP (sfGFP).	Simplified protein identification and purification.	[296]
Analytcs	CBD-rcSso7d (engineered protein for binding to various antigens)	Utilized in a paper-based dignostic approach for binding antigens.	[297]
Analytcs	CBD-Protein A	IgG binding tests with CBD as immobilizing moiety.	[298]
Material Engineering	CBD-recombinant spider silk	Composite material with high strength and stiffness combined with increased toughness.	[274]
Material Engineering	CBD-recombinant spider silk	Self-assembly into nanofibrils. Processed into sponges and films with increased thermal and structural characteristics.	[216]

Chapter 1: Literature Review

Material Engineering	CBD-recombinant spider silk N-terminus	pH sensitive tunable viscosity of blends with cellulose nano fibres.	[299]
Adhesives	CBD-recombinant spider silk	Adhesive for delignified wood.	[300]
Adhesives	CBD-recombinant spider silk	Adhesive for cellulosic materials.	[275]

One main application until today remains the fusion of a target protein, such as alkaline phosphatase, with a CBD for protein purification. By using traditional cellulose-affinity chromatography, the fusion protein is immobilized on the column. Yields of up to 85% could be achieved after elution. However, the elution condition might partly denature the protein [289]. For a native structure, the linker sequence can be cleaved as it is very susceptible to proteases [301].

More modern and application-driven approaches include the fusion of a CBD with a cell affinity peptide-bearing fusion partner. The most commonly used cell-adhesion peptide is Arg-Gly-Asp (RGD) [222, 302, 303]. In this manner, *Andrade et al.* coated bacterial cellulose fibres with a CBD-RGD fusion to create highly biocompatible and proliferation-enhancing scaffolds for fibroblasts without any chemical modifications [294].

Varjonen et al. showed improved self-assembly of cellulose nanofibrils by fusing a CBD with the surface active protein hydrophobin. By harnessing the unique properties of the fusion, cellulose nanofibrils were successfully organized into densely packed thin films at both the air/water and oil/water interfaces. This approach significantly enhanced the formation and stability of oil-in-water emulsions, remaining unchanged for several months [295].

Another interesting approach for the detection and purification of heavy metal contaminations was presented by *Xiao et al.* The fusion protein consisted of three distinct components: metallothionein (MT), cellulose binding domain (CBD), and superfolder GFP (sfGFP). Metallothionein, known for its high affinity for heavy metals, was incorporated to chelate contaminants efficiently. The CBD enabled the fusion protein (MT-CBD-sfGFP) to bind to cellulose selectively, simplifying the purification and immobilization process. Including superfolder GFP facilitated the fusion protein's detection during expression and immobilization stages [296].

Chapter 1: Literature Review

Lastly, *Miller et al.* designed an antigen-binding domain with a CBD to create paper-based diagnostic systems. They showed that the high binding affinity combined with the available test area should be capable of capturing target antigens with nearly 100% efficiency [297].

Narrowing down the application pool to recombinant spider silk fusion proteins with CBDs, only a few studies have successfully created and applied the fusion. *Lemetti et al.* used an eADF3-based fusion molecule containing a CBD from *Clostridium thermocellum* as a biological water-based adhesive for delignified wood [300]. The same protein was used by *Mohammadi et al.*, where they processed it into films and fibres with elevated mechanical properties when blended with cellulose nanoparticles compared to unmodified silk variants [274]. Furthermore, the same protein was used in another adhesive study by the same team for cellulosic materials [275].

Meirovic et al. employed a cellulose-binding MaSp1 spider silk protein blended with cellulose nanoparticles to create films and sponges with enhanced mechanical properties. The incorporation of cellulose nanoparticles into the spider silk matrix led to improved strength and toughness, thereby reinforcing the resulting materials [216]. This approach represents a promising strategy for enhancing the performance of spider silk films and sponges by harnessing the mechanical properties of cellulose.

Voutilainen et al. fused CBDs to spider silk N-terminal domains and showed how the pH-sensitive switching of the N-terminus into dimers affected the cellulose binding affinity. By blending the protein solution with cellulose nanofibres, the viscosity of the solution could be precisely tuned by altering the ratio and concentration of their fusion variants [299].

In these studies, spider silk-CBD fusions have been utilized to investigate their potential in various applications. These investigations have primarily focused on two core domain fusions, namely from ADF3 and MaSp1, and one fusion incorporating an N-terminus. Each of these fusion proteins has provided valuable insights into the properties and functionalities of spider silk-CBD constructs. However, there remains a gap in the literature regarding exploring alternative spider silk proteins in combination with CBDs, especially for generating TE-feasible

Chapter 1: Literature Review

hydrogels, which have not been reported for ADF3 and MaSp1 proteins in the literature.

1.8 Peptide Modification of Biomaterials

Another way to genetically modify a recombinant protein is to incorporate small peptide sequences, often called tags. These proteins can also be referred to as fusions, but mostly, when discussing fusion proteins, they combine two complete protein structures with distinct functions [301].

These small tags are most often used for protein purification or identification means. Two of the most commonly used ones are the T7-tag and the 6His-tag. The T7 tag MASMTGGQMG [304] stems from bacteriophage T7 [305] and is mainly used to detect a protein by antibody conjugation. The 6His tag comprises six histamine residues (HHHHHH) and is extensively used for immobilized metal affinity chromatography (IMAC) on a Ni²⁺-NTA column [306]. Combining the two tags for identification in, e.g. Western Blot after purification via IMAC Ni²⁺-NTA column chromatography is one of the gold standards in recombinant protein production and purification [307].

In a more application-oriented perspective, short peptide modifications in the form of cell adhesion or attraction sequences have emerged, especially for applications in TE. These short amino acid sequences are primarily identified from the target tissue and the surrounding ECM. The RGD peptide mentioned above, the most prominent representative, is present in the sequences of fibronectin vitronectin, osteopontin, collagens, thrombospondin and fibrinogen [308]. Cell-specific integrins, consisting of two membrane-spanning subunits, bind adhesion molecules and trigger various signalling pathways depending on the specific integrin targeted [308].

In combination with biomaterials that show excellent scaffold properties but lack cell adhesion, this hurdle can be overcome by modification with these peptides.

Focusing on this approach, many cell adhesion peptides have emerged over time. Even though RGD is still by far the most incorporated sequence, it is not always the best choice as it attracts many types of cells, whereas in TE, the attraction of specific cells to specific target locations might be favourable. Therefore, cell type-

Chapter 1: Literature Review

specific peptides are becoming increasingly important in modern TE approaches. **Table 1-7** displays a catalogue of known cell-adhesion peptides used in TE research.

Table 1-7: Catalogue of known and commonly used cell-adhesion peptides.

Sequence	Effect	Ref.
RGD (<i>Arg-Gly-Asp</i>)	Recognized by several integrins. Crucial for cell migration, differentiation, and survival. Derived from fibronectin.	[302, 309-311]
LRE (<i>Leu-Arg-Glu</i>)	Promotes neuron adhesion Derived from laminin.	[312]
IKVAV (<i>Ile-Lys-Val-Ala-Val</i>)	$\alpha_3\beta_1$ receptor. Promotes cell adhesion and neurite growth. Derived from laminin.	[313]
DGEA (<i>Asp-Gly-Glu-Ala</i>)	$\alpha_2\beta_1$ receptor. Similar function to RGD. Derived from collagen.	[314]
REDV (<i>Arg-Glu-Asp-Val</i>)	Selectively binds to endothelial cells and is often used in research related to vascular biology. Receptor for $\alpha_4\beta_1$ integrin. Capturing of endothelial precursor cells.	[29, 150, 310, 315]
HGGVRLY (<i>His-Gly-Val-Arg-Leu-Tyr</i>)	$\alpha_4\beta_1$ receptor. Capturing of endothelial precursor cells. Promotes adhesion of bone marrow stromal cells.	[29]

Chapter 1: Literature Review

<p>YIGSR (<i>Tyr-Ile-Gly-Ser-Arg</i>)</p>	<p>Inhibits tumor metastasis. $\alpha_4\beta_1$ and $\alpha_2\beta_1$ receptor. Derived from laminin.</p>	<p>[316] [317]</p>
<p>KGD (<i>Lys-Gly-Asp</i>)</p>	<p>Promotes keratinocyte, epithelial cell and fibroblast adhesion. Reduced platelet aggregation. Derived from collagen.</p>	<p>[318]</p>
<p>QHREDGS (<i>Gln-His-Arg-Glu-Asp-Gly-Ser</i>)</p>	<p>Promotes survival of heart cells and attachment and survival of keratinocytes and osteoblasts. Derived from angiopoietin</p>	<p>[319]</p>
<p>PHSRN (<i>Pro-His-Ser-Arg-Asn</i>)</p>	<p>Works together with RGD to enhance the adhesion of cells. $\alpha_5\beta_1$ and $\alpha_{IIb}\beta_3$ receptor. Derived from fibronectin</p>	<p>[320]</p>
<p>NGR (<i>Asn-Gly-Arg</i>)</p>	<p>Can target drug delivery to tumor vasculature by binding to aminopeptidase N, an enzyme overexpressed on the surface of tumor blood vessels.</p>	<p>[321]</p>
<p>GFOGER (<i>Gly-Phe-Hyp-Gly-Glu-Arg</i>)</p>	<p>$\alpha_{10}\beta_1$, $\alpha_{11}\beta_1$, $\alpha_2\beta_1$ and $\alpha_1\beta_1$ receptor. Often used in osteogenic approaches. Derived from collagen.</p>	<p>[322] [323] [324]</p>
<p>KQAGDV (<i>Lys-Gln-Ala-Gly-Asp-Val</i>)</p>	<p>Variant of the RGD motif with improved selectivity for integrin $\alpha_{IIb}\beta_3$. $\alpha_{IIb}\beta_3$ and $\alpha_5\beta_1$ Derived from fibronectin.</p>	<p>[325]</p>
<p>CRETAWAC (<i>Cys-Arg-Arg-Glu-Thr-Ala-Trp-Ala-Cys</i>)</p>	<p>$\alpha_5\beta_1$ receptor . Promotes adhesion of endothelial cells.</p>	<p>[326]</p>
<p>DGEA (<i>Asp-Gly-Glu-Ala</i>)</p>	<p>$\alpha_2\beta_1$ receptor. Promotes platelet adhesion.</p>	<p>[327]</p>

Chapter 1: Literature Review

<p>SIKVAV (<i>Ser-Ile-Lys-Val-Ala-Val</i>)</p>	<p>$\alpha_3\beta_1$, $\alpha_6\beta_1$ receptor. Increases protease activity of a human salivary gland adenoid cystic carcinoma cell line. Derived from laminin.</p>	<p>[328]</p>
<p>IKLLI (<i>Ile-Lys-Leu-Leu-Ile</i>)</p>	<p>$\alpha_3\beta_1$ receptor. Derived from laminin.</p>	<p>[329]</p>
<p>SINNR (<i>Ser-Ile-Asn-Asn-Asn-Arg</i>)</p>	<p>Promotes adhesion of type II alveolar and HT1080 cells. $\alpha_6\beta_1$ receptor. Derived from laminin.</p>	<p>[330]</p>
<p>NPWHSIYITRFG (<i>Asn-Pro-Trp-His-Ser-Ile-Tyr-Ile-Thr-Arg-Phe-Gly</i>)</p>	<p>Regulation of Melanoma Invasion. $\alpha_6\beta_1$ receptor. Derived from laminin.</p>	<p>[331]</p>
<p>TWYKIAFQRNRK (<i>Thr-Trp-Tyr-Lys-Ile-Ala-Phe-Gln-Arg-Asn-Arg-Lys</i>)</p>	<p>Regulation of Melanoma Invasion. $\alpha_6\beta_1$ receptor. Derived from laminin.</p>	<p>[331]</p>
<p>KAFDITYVRLKF (<i>Lys-Ala-Phe-Asp-Ile-Thr-Tyr-Val-Arg-Leu-Lys-Phe</i>)</p>	<p>Promotes angiogenesis. $\alpha_5\beta_1$, $\alpha_v\beta_3$ receptor. Derived from laminin.</p>	<p>[332]</p>
<p>IDAPS (<i>Ile-Asp-Ala-Pro-Ser</i>)</p>	<p>$\alpha_4\beta_1$ receptor. Derived from fibronectin.</p>	<p>[333]</p>
<p>LDV (<i>Leu-Asp-Val</i>)</p>	<p>Promotes support melanoma cell adhesion. $\alpha_4\beta_1$, $\alpha_4\beta_7$ and $\alpha_4\beta_P$ receptor. Derived from fibronectin.</p>	<p>[334]</p>

Chapter 1: Literature Review

KQAGDV	$\alpha_{IIb}\beta_3$ and $\alpha_5\beta_1$ receptor.	[335]
(Lys-Gln-Ala-Gly- Asp-Val)	Derived from fibronectin.	

1.8.1 Spider silk peptide modifications

Given recombinant spider silk proteins' well-suited nature for TE applications, numerous short peptide modifications have been developed to enhance their naturally cell-unattractive surface properties.

Several studies incorporating eADF4(C16)-RGD have been conducted to date, including the observation of rheological behaviour of RGD-functionalized hydrogels [58], *in vivo* observations of vascularization in rat models as previously mentioned [59], cultivation of contracting human cardiomyocytes on film morphologies [50, 146], or comparison between chemically linked RGD and recombinantly coupled modifications with subsequent fibroblast adhesion observations [303]. Interestingly, the recombinant variant showed superior cell adhesion in the last study.

Furthermore, *Trossmann et al.* conducted an extensive study using several known adhesion peptides modified to the eADF4(C16) recombinant spider silk and tested the resulting cell reactions on cast films [336]. They observed that the resulting spider silk film can show significantly varying attachment behaviours depending on the peptide modification. The RGD-modified variant showed the expected outcome, with all tested cell lines attaching very well to the films. However, for example, on eADF4(C16)-YIGSR, NG108 cells from rat nerves attached very well, while they were only very poorly attached on the QHREDGS modified variant. This broad study impressively demonstrates just how flexible the recombinant spider silk protein eADF4(C16) is when modified with the respective peptide tags for TE.

Chapter 1: Literature Review

Focusing on the RGD-modified silk, *Lechner et al.* demonstrated high viability of BxPC-3 cells (epithelial pancreas cell line) in both eADF4(C16) and eADF4(C16)-RGD after bioprinting. **Figure 1-19** shows the results of their live/dead staining and proliferation data after 14 days. It can be seen that cells in both hydrogel formulations were viable after the printing procedure. However, for the unmodified silk, the cell number decreased over time, whereas for the RGD-modified variant, no decrease in cell number occurred, suggesting some form of attachment of the cells within the hydrogel. Notably, although the cell number did not decrease, the round cell morphology of the encapsulated cells does not hint at a functional tissue generation and remains the subject of further research to be improved upon.

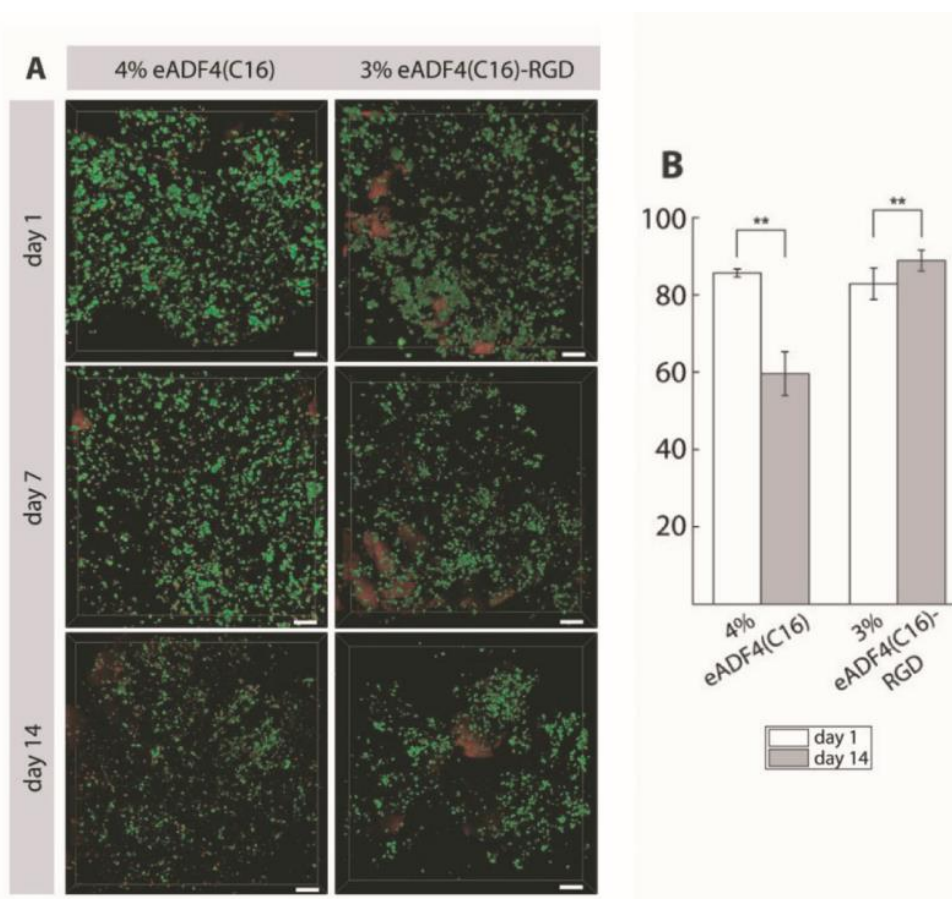


Figure 1-19: Viability of BxPC-3 cells (10 mio cells per milliliter) in printed constructs comprising 4% eADF4(C16), 3% eADF4(C16)-RGD, or 3% eADF4(C16)-RGE. Spider silk bioinks were printed using a RegenHU Bioplotter with a 22G tapered tip at room temperature and cultivated for up to 14 days at 5% CO₂, 95% relative humidity, and 37 °C. A) For CLSM imaging, live cells were stained with Calcein A/M (green) and dead cells with EthD-I (red). Background staining occurs due to interaction of hydrogels with EthD-I (scale bars: 100 μm). B) Quantification of viable cells on day 1 and day 14 (**p ≤ 0.05). Figure and caption adapted from reference [336](© A. Lechner et al., published by WILEY-VCH and reprinted with permission under license number 5591210309508.

Chapter 1: Literature Review

In a similar vein to eADF4(C16)-based approaches, *Widhe et al.* specifically observed the morphology and adhesion of primary fibroblasts, keratinocytes, endothelial cells and Schwann cells on films of the recombinant spider silk protein, 4RepCT modified with different peptides [337]. Again, they showed that the peptide motifs are available for cell attachment on the surface of stiff protein films and distinct differences based on the used peptide modification were observable.

Figure 1-20A demonstrates their observations for fibroblast on differently modified surfaces of WT (4RepCT), NRC (4RepCT with N-terminal domain), RGD, RGE, IKVAV, YIGSR (4RepCT with respective peptide) films. After three hours, cells on RGD-modified films displayed significant focal adhesion point formation and highly ordered actin fibres, comparable the morphology seen on fibronectin fibronectin (FN). In contrast, cells on films from WT and RGE silks did not form distinct actin cytoskeleton and showed diffused vinculin staining. Few focal adhesions could be seen on cells cultured on films functionalized with the other motifs, however, to a significantly lesser extent, while still superior to WT films (**Figure 1-20B**). Lastly, most fibroblasts cultured on IKVAV and YIGSR variants displayed some stress fibres, while actin filaments were rarely observed on WT and RGE film cultures.

Chapter 1: Literature Review

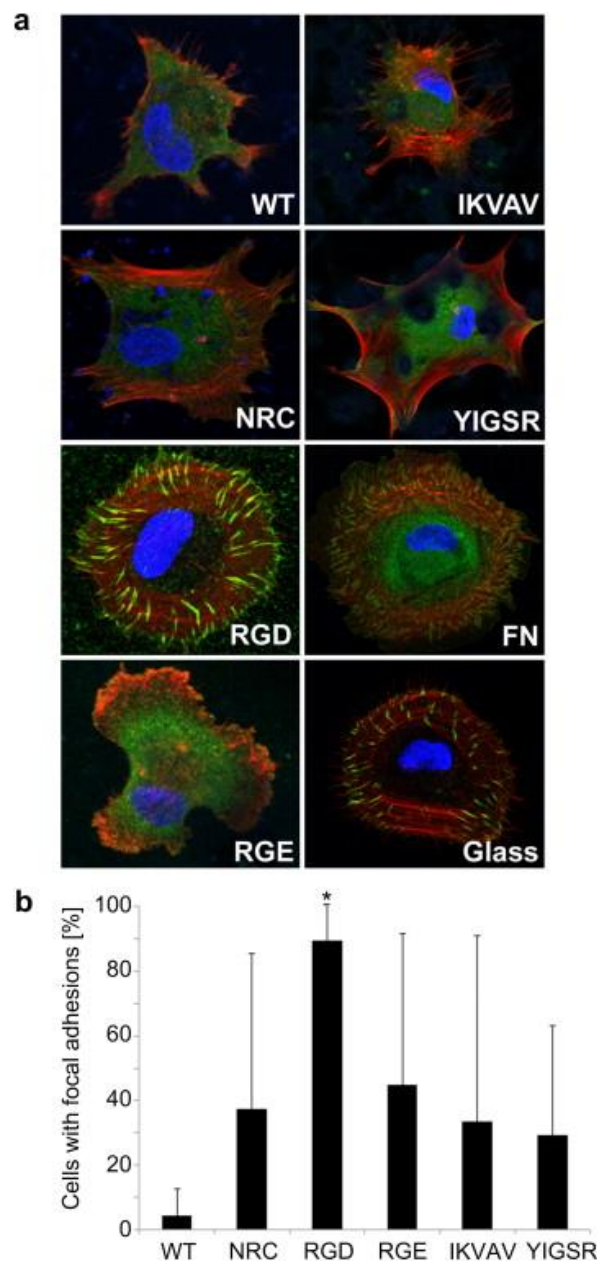


Figure 1-20: Fibroblasts form focal adhesions on peptide-modified silk films within 3 h. a) Representative micrograph of F-actin (red), vinculin (green) and nuclei (blue) stained fibroblasts allowed to adhere for 3 h on different films. b) Percentage of cells with apparent focal adhesions ($n = 4$, duplicates). Cells cultured on RGD ranked significantly better than WT ($*=p < 0.05$). Figure and caption adapted from reference [338](© M. Widhe et al., published by Elsevier and reprinted with permission under license number 5632990050324).

Johansson et al. [339] used these 4repCT-RGD variants to observe their potential as foams to create pancreatic islets for potential diabetes treatments. They observed that during *in vitro* culture, islets on silk foams displayed better revascularization. The potential for long-term preservation of human islets was also assessed for the matrices. Human islet maintenance was increased (from 36% to 79%) by matrices containing the cell-binding motif RGD compared to

Chapter 1: Literature Review

unmodified silk foams. Furthermore, islet architecture and function were maintained for more than 3 months *in vitro*. Within the silk structure, the islets created vessel-like structures and produced cell-matrix connections. Lastly, RGD matrices encouraged the development of additional insulin-positive islet-like clusters connected to the primary islets via endothelial cells. **Figure 1-21** highlights some of their *in vivo* results, with panel **A** showing that foams were processable from both silk variants; however, the RGD-modified foams were more stable and showed greater growth over 4 weeks. **Figure 1-21B+C** highlight the formation of new vasculature throughout the implanted foams, with a higher degree of revascularization occurring in the RGD-variant. Lastly, the images presented in panel **D** demonstrate the high cell viability for both foam formulations; however, patches of apoptotic cells could be detected for the unmodified variant, whereas the RGD-variant displayed homogeneous cell growth and vascularization.

Lastly, *Bini et al.* produced a recombinant MaSp1-RGD protein and showed improved human mesenchymal stem cell attachment and proliferation on electrospun non-woven mats of the silk variant [222]. Furthermore, they observed that when compared to tissue culture plastic, recombinant spider silk and recombinant spider silk modified with RGD both supported higher osteogenic outcomes from human bone marrow-derived mesenchymal stem cells. Surprisingly, when compared to the identical protein containing RGD, the unmodified recombinant spider silk protein showed improved bone-related results determined by calcium deposition.

These studies on various types of recombinant spider silk further solidify its high potential for TE application, especially when further modified with peptides for enhanced cellular interactions. However, as noted before, most studies focus on RGD-modified silk or incorporate other tags for general studies without specific final applications, a research gap still waiting to be targeted.

Chapter 1: Literature Review

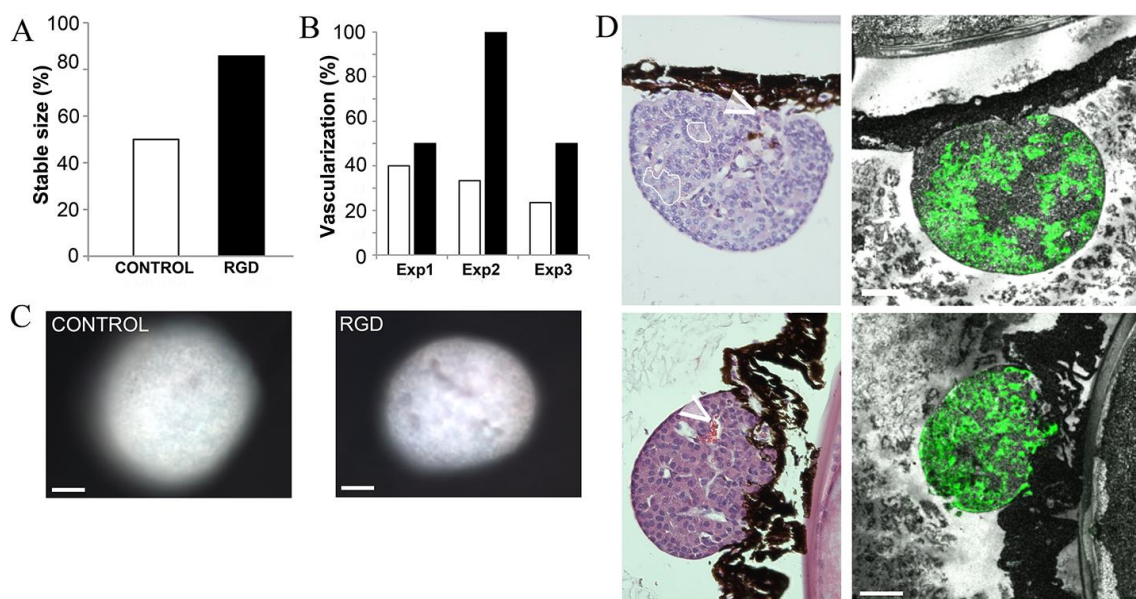


Figure 1-21: Pancreatic Islets maintained on RGD foam show improved in vivo survival and vascularization. A:) Percentage of islets that showed a stable or positive increase in size over a 4 week period. (5 mice, 1–6 islets per eye). B:) Percentage of control islets (white bars) and islets from RGD foam (black bars) that showed clear vascularization by transmitted light imaging 4 weeks post-transplantation. ($n = 3$ separate transplantation experiments, 12 recipient mice, 1–6 islets per eye). C:) Representative ($n = 3$) bright field micrographs of control islet (left) and islet from RGD foam (right) during in vivo imaging of the eye, where vasculature can be seen as grey areas. Scale bars = 50 μm . D:) Morphology by H/E (hematoxylin and eosin staining) (left panel) and insulin (green, right panel) staining of eye sections showing representative ($n=3$) control islet (upper graphs) and islet from RGD foam (lower graphs). Vasculature was seen in islets from both culture conditions (white arrowhead), although vessels with erythrocytes were more common in islets from RGD foam. Areas of visual cell death were sometimes present in the control islet (white-lined circle). Scale bars = 50 μm . Figure and caption adapted from reference [339](© U. Johansson et al., published by PLOS ONE, distributed under the terms of the Creative Commons Attribution 4.0 International License (CC BY 4.0), <http://creativecommons.org/licenses/by/4.0/>)

1.9 State of the art: Drug-eluting stents (DES)

Following the approach of cell-selective tailoring of a spider silk-based material, the application as a coating for DES poses an exciting field of application. Therefore, DES and their development will be highlighted for perspective. Cardiovascular medicine uses stents to treat coronary artery diseases (CAD). CADs are characterised by the narrowing of blood vessels, mainly caused by plaque attached to the vessel walls, which ultimately leads to blocked vessels and insufficient oxygenation of the system, often culminating in death. With approximately 1 out of 5 deaths [340], CADs are the leading cause of death worldwide. The first coronary stent was successfully implanted in 1977 by Gruentzig of Switzerland [341]. The typical treatment for CADs is using coronary

Chapter 1: Literature Review

stents to re-open a clogged vessel, thus preventing elastic recoil. **Figure 1-22** shows a schematic of the procedure. First, a catheter with an inflatable balloon and the crimped stent is inserted into the artery, into the centre of the plaque clogging. The balloon is inflated, simultaneously plastically deforming the stent and elastically deforming the vessel, including the plaque layer. Finally, the balloon deflates, and the catheter with the mounted balloon is removed from the vessel and the patient's body. The stent inhibits sufficient stiffness and strength to counteract the vessel's urge to recoil, keeping it open. In the ideal case of a correctly functioning stent, the blood vessel is entirely remodelled after 12-24 months [342]. Historically, stents are made of metal, primarily stainless steel 316L [101], or in more modern approaches, titanium [343] and cobalt-chromium [98] alloys.

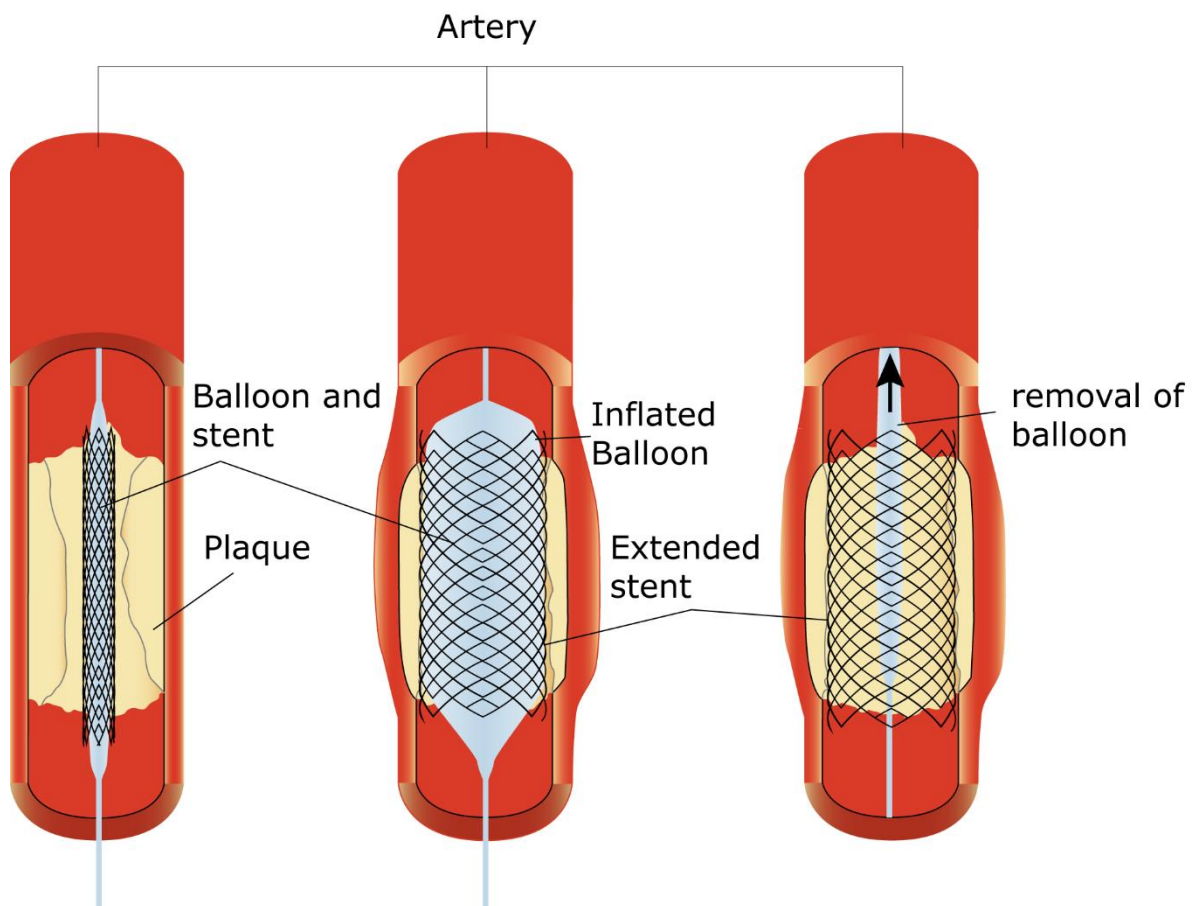


Figure 1-22: Schematic of stent deployment showing a nearly closed blood vessel. A metal stent on an inflatable balloon is inserted into the target area, where the balloon is inflated, and the metal stent expands. After stent deployment, the balloon gets deflated and removed from the system, leaving an expanded stent mesh.

Chapter 1: Literature Review

The introduction of bare-metal stents enhanced the safety of angioplasty, the surgical intervention to re-open blocked blood vessels [344], but long-term outcomes were limited due to neointimal hyperplasia that led to in-stent restenosis [345]. Neointimal hyperplasia is the condition of re-narrowing vessels due to the infiltration of smooth muscle cells (SMC), which build the structural support around blood vessels.

To address this issue, drug-eluting stents (DES) were developed to deliver antiproliferative drugs at the injury site during the early phase of vessel healing to prevent the over-proliferation of the vascular smooth muscle cells [337-339]. Developing effective DES entails addressing several more challenges, including selecting appropriate drug and polymer combinations, optimizing polymers' biodegradability and mechanical integrity, ensuring coating uniformity, preventing thrombosis and hypersensitivity reactions and promoting endothelialization of the vessel.

DES are metallic stents coated with a biodegradable polymer coating containing an anti-proliferative drug such as sirolimus, paclitaxel, everolimus, or zotarolimus [346].

First-generation drug-eluting stents, such as sirolimus-eluting stents (e.g. Cypher [347, 348]) in 2003 and paclitaxel-eluting stents (e.g. Taxus [349]) in 2004, significantly decreased in-stent restenosis compared to bare-metal stents.

Sirolimus, also known as rapamycin, was identified initially as an antifungal agent on Easter Island [350] and has shown great potential as an anti-inflammatory and antiproliferative drug. This has led to its application in cancer therapy and transplant rejection treatment. The ability of sirolimus to inhibit leukocyte and smooth muscle cell proliferation has made it an appealing option for preventing neointimal hyperplasia and restenosis [351].

On the other hand, Paclitaxel is derived from the bark of the Pacific yew tree and inhibits the breakdown of microtubules during cell synthesis, thereby hindering cellular replication. Additionally, like sirolimus, paclitaxel's antiproliferative effects have been harnessed to reduce smooth muscle proliferation and mitigate the occurrence of in-stent restenosis [352].

Chapter 1: Literature Review

Many comparative studies [353-356] have tried to find the more suitable of the two candidates. One of these studies identified some minor advantages for sirolimus [348]; however, they could not determine a significant difference in the long-term outcomes after five years [355].

Second-generation drug-eluting stents, such as everolimus-eluting (e.g. Xience [346]) and zotarolimus-eluting (e.g. Endeavor [357]) variants, showed various improvements over first-generation stents. For one, these stents use smaller struts that enhance stent flexibility and deliverability and have been shown to improve endothelialization in animal models [358]. They have also reduced late-stage thrombosis [359, 360]. On the other hand, they incorporated more advanced drug formulations such as everolimus and zotarolimus. However, the drug-containing polymer layers remained a concern as foreign-body-induced inflammatory responses and delayed re-endothelialization remained significant issues in cardiovascular stents, including second-generation DES.

Zotarolimus is a more lipophilic derivative of sirolimus, further leveraging the desirable properties of the parent drug. On the other hand, everolimus, closely related to sirolimus, exhibits similar antiproliferative and immunosuppressive effects. However, its increased lipophilicity enables rapid absorption into the arterial wall at the site of vessel injury [357].

The clinical program known as the SPIRIT trials [361-364] played a crucial role in developing and approving everolimus-eluting stents. These trials demonstrated the superior efficacy of the everolimus-eluting stent compared to bare metal stents and paclitaxel-eluting stents, showing significant reductions in late lumen loss and improved safety profiles. The SPIRIT III [365] and SPIRIT IV [364, 366] trials further confirmed the benefits of the everolimus-eluting stent, including lower rates of target lesion revascularization, myocardial infarction, and stent thrombosis. The COMPARE [359] trial also showcased the favourable outcomes of the everolimus-eluting stent compared to a second-generation paclitaxel-eluting stent. The X-SEARCH [367] registry and the EXCELLENT [368] trial provided additional evidence supporting the clinical advantages of everolimus-eluting stents over bare metal stents, paclitaxel-eluting stents, and sirolimus-eluting stents. The development of a second-generation zotarolimus-eluting stent (Resolute) [369]

Chapter 1: Literature Review

addressed the restenosis issues associated with the early version of the stent and demonstrated noninferiority to the everolimus-eluting stent in terms of major cardiac events. These advantages, combined with the vast amount of clinical trials, made everolimus one of the gold standards for modern drug-eluting stents.

Besides the incorporated drug, the polymer matrix is essential when designing a drug-eluting stent. Therefore, significant advancements have been made in developing biocompatible permanent polymer coatings for DES. The Xience DES [370] and the PROMUS Element DES (everolimus-eluting) [368] incorporate a polymer composition consisting of an initial layer of poly(n-butyl methacrylate) and a second layer of the highly fluorinated polymer poly(vinylidene fluoride-co-hexafluoropropylene). Similarly, the Resolute Integrity (zotarolimus-eluting) [371] and the Resolute Onyx [371] (zotarolimus-eluting) utilize a BioLinx polymer, which is a blend of hydrophobic C10 polymer and polyvinylpyrrolidone C19 polymer with both hydrophobic and hydrophilic groups, and hydrophilic polyvinylpyrrolidone polymers [372]. However, despite advancements in the biophysical properties of polymers, they continue to exhibit drawbacks, such as delayed endothelialization and hindered arterial healing within the stented segment. [373]. To mitigate these challenges, biodegradable polymer coatings have been engineered to enhance long-term stent outcomes by minimizing polymer-associated adverse effects.

To date, a series of randomized trials have demonstrated the higher efficacy and safety of biodegradable-polymer-coated drug-eluting stents (DESs) compared to first-generation DESs, and their non-inferiority to second-generation DESs [374].

The most commonly researched polymer coatings for DES are poly-L-lactic acid (PLLA), poly-D,L-lactic acid (PDLLA), and poly(lactic-co-glycolic acid) (PLGA) [375]. PLLA, derived from lactic acid, stands out for its biocompatibility, decent mechanical strength, and cost-effectiveness. It has been widely employed as a drug-eluting layer or platform in DESs, demonstrating favourable outcomes regarding safety and efficacy. Clinical trials have shown promising results with PLLA-based DESs, such as Excel [376], Orisiro, and BioMime [377], which exhibit improved biocompatibility and reduced thrombosis rates compared to earlier-generation DESs.

Chapter 1: Literature Review

PDLLA, another synthetic biodegradable polymer, exhibits lower crystallinity and faster degradation than PLLA. Its amorphous structure allows for favourable drug distribution and prolonged release profiles. PDLLA-based DESs, such as Nobori [378], Yukon Choice PC [379], Firehawk [380], and Ultimaster [381], have demonstrated promising clinical outcomes, including reduced thrombosis rates and improved safety.

PLGA, a lactic and glycolic acid copolymer, provides further versatility in DES design. By controlling the molar ratio of monomers, the physicochemical properties of PLGA can be tailored to meet specific requirements. DES incorporating PLGA, such as Tivoli [382], Synergy [383], Mistent [384], and BuMa [385], have shown promising safety and efficacy profiles. The fast degradation of PLGA compared to PLLA and PDLLA offers potential benefits in reducing the incidence of very-late thrombosis. However, its rapid degradation can also induce arterial inflammation due to acidic by-products [11], necessitating controlled degradation strategies and careful consideration of drug release behaviour.

Despite their successful implementation and undoubted suitability as DES coatings, these polymers have specific considerations. PLLA, despite its excellent biocompatibility and mechanical strength, has a slow degradation rate, which may lead to a prolonged presence of the polymer in the vessel. This extended presence can hinder the endothelialization process and potentially contribute to a higher incidence of in-stent thrombosis [386]. PDLLA, on the other hand, exhibits faster degradation than PLLA, but it can still induce arterial inflammation due to its acidic degradation products and coating defects [387]. PLGA, known for its faster degradation, has been associated with releasing acidic by-products, leading to inflammation and adverse tissue reactions. The acidic nature of these polymers can hinder proper healing and potentially contribute to complications such as chronic inflammation and neoatherosclerosis [388]. In addition, hydrophobic polymers used as stent coatings present another challenge related to delayed endothelialization. These hydrophobic surfaces are limited to facilitating endothelial cell migration, adhesion, and proliferation onto the stent surface [166, 389]. As a result, the process of endothelialization, which is crucial for restoring the normal function of the vessel and preventing thrombosis, may be hindered.

Chapter 1: Literature Review

To overcome this limitation, it is necessary to develop new materials that address the shortcomings of current stent coatings, especially regarding endothelialization. By improving the surface properties and promoting better endothelial cell interactions, these innovative materials can enhance stenting technology, improve clinical outcomes, and reduce the reliance on prolonged antiplatelet therapies, thereby minimizing the associated bleeding risk.

In accordance with this thesis' projects, the focus of novel materials lies within silk protein materials. The two significant studies leading to the objective of this study will now be discussed briefly.

The first study by *Xu et al.* focused on silk fibroin from *B. mori* as a coating for sirolimus-eluting magnesium stents. They aimed to enhance the corrosion resistance of Mg-based stents while increasing biocompatibility. After dip-coating their surfaces in a 1% wt protein solution in HFIP, they characterized their coating by observing endothelial cell (EC) attachment, conducting initial blood compatibility tests with platelet-rich plasma (PRP) from rabbits, and detecting sirolimus elution. Their findings showed a near ~70% release of sirolimus after 1-3 days and good human umbilical vein endothelial cell (HUVEC) attachment while minimizing platelet aggregation on the surface [151].

However, their results seem inconclusive due to several aspects. First, their detection of sirolimus was conducted by uv-spectrometry at a wavelength of 280 nm with no proof that their protein coating is not degrading. As the protein would also be detected at 280 nm, it cannot be deduced that the measured values were solely determined by drug release. Furthermore, according to the manufacturer, their measured concentration in phosphate-buffered saline (PBS) is higher than the solubility of sirolimus in water. Furthermore, the measured supernatant was used as an incubation buffer for the next measurement step, making it impossible to determine the end point of the elution.

Regarding the Hemocompatibility, their results seem to be in accordance with the literature for silk fibroin in a blood environment [390]. However, due to the minimalized approach with PRP, other coagulation factors of whole blood might have been overlooked.

Chapter 1: Literature Review

Wang et al. presented a study using silk fibroin blended with the REDV peptide and heparin on magnesium surfaces as DES coatings. Their approach was utilizing an aqueous silk fibroin solution to enhance EC selectivity while minimizing blood clotting. Their surface modification resulted in remarkable improvements in hemocompatibility, as evidenced by reduced platelet adhesion, decreased hemolysis rate, and prolonged blood coagulation time. Additionally, the cell culture of human umbilical vein endothelial cells (HUVEC) and vascular smooth muscle cells (SMC) demonstrated a higher number of attached HUVECs on the functionalized samples compared to the unmodified Mg alloy surfaces [10].

However, their results still showed a significant number of SMC being attached to the surface, which might have adverse effects regarding neointimal hyperplasia in a theoretical *in vivo* translation.

Combining the results of these two approaches towards silk-based stent coatings, one major downside is the non-selectivity of silk fibroin. Both studies showed suitable HUVEC attachment; however, also SMC grew favourable on the substrate when tested. The REDV peptide might shift the selectivity slightly, but if the base material is cell-attractive such as silk fibroin [391-393], the general attractiveness seems to outweigh.

So while silk fibroin showed extremely promising first results, the research gap lies within a material combining these previously discussed features and extending towards the more selective adhesion of HUVEC while still exhibiting excellent biocompatibility, Hemocompatibility, and drug release properties.

1.10 Objectives

The objectives of this thesis are two-sided. The first objective is the creation of novel fusion proteins based on the recombinant spider silk eADF4(C16). After the successful production and characterization, the proteins from objective 1 are applied in two ways: The evaluation as TE materials as cellulose-enhanced hydrogels and as a coating material for DES, Giving rise to the objectives as follows:

Chapter 1: Literature Review

1. The design, production, purification and characterization of the novel recombinant spider silk variants eADF4(C16)-CBD and eADF4(C16)-REDV.
2. The processing of eADF4(C16)-CBD in hydrogels and their evaluation for use in Tissue Engineering.
3. The processing and evaluation of eADF4(C16)-REDV into metal coatings for their future use as DES coatings.

1.10.1 Objective: design, production, purification and characterisation of novel eADF4(C16) based proteins

The overarching first objective is a prerequisite for both projects; the creation of the novel protein at hand. The REDV-modified protein was designed, produced and purified in the same manner as other small peptide-modified eADF4(C16)-based proteins before [303]. Briefly, the desired REDV sequence, including a short linker sequence was modified onto the spider silk sequence by a seamless cloning approach [174], the sequence containing vector was then transferred into *e.coli* for protein production and purified via an inclusion body purification.

Characterization of the protein was carried out by CD spectroscopy, SDS-PAGE, and cell culture experiments.

The cellulose-binding variant was designed in the same manner, via a seamless cloning approach, however proved more challenging in terms of the production parameters. Due to the complex tertiary structure of the cellulose-binding domain, the fermentation parameters had to be adjusted carefully to exclude the possibility of overexpression. Consequently, inclusion body purification could not be conducted but a lower yield supernatant purification had to be carried out followed by IMAC chromatography. The produced protein was then assessed additionally by far-UV CD spectroscopy and QCM-D measurements to confirm the intact

Chapter 1: Literature Review

tertiary structure of the CBD as well as the capability to bind to cellulose substrates.

1.10.2 Objective: eADF4(C16)-CBD Hydrogels

The first stand-alone part of this thesis aims to widen the array of injectable hydrogels in bone TE applications by developing a novel cellulose-binding recombinant spider silk protein and investigating its mechanical properties and performance as a hydrogel scaffold. Injectable hydrogels offer numerous advantages in TE, including their ability to be directly administered to the target site, eliminating the need for extensive surgical procedures [1, 2]. As such, there is a need for a hydrogel that combines elevated stiffness, suitable pore size for cell cultivation, injectability, and the provision of cell attachment points [3].

The production of a cellulose fibre-enhanced hydrogel with improved mechanical and cell adhesion properties was hypothesised to be capable of filling this gap. Therefore, this first part of the thesis focuses on a cellulose-binding recombinant spider silk protein to work towards that aim. As mentioned before, spider silk is known for its remarkable mechanical properties [12, 14-19], biocompatibility [12, 17, 20-22], degradability [22], and hypoallergenic nature [13]. The previously observed mechanical enhancements provided by cellulose particle blending [216, 281, 282, 284, 394] were utilised by fusing the cellulose-binding domain CBD_{CEX}, derived from *C. fimi*, onto the recombinant spider silk protein eADF4(C16). This fusion enabled specific binding between spider silk and cellulose molecules, resulting in a more robust and more stable hydrogel than traditional eADF4(C16) gels, rendering them more suitable for TE applications.

Furthermore, the performance of the hydrogels as scaffolds for TE applications was evaluated. Cell viability and proliferation assays assessed biocompatibility and confirmed the hydrogels' ability to support cell growth and tissue regeneration.

This approach offered distinct advantages compared to various biodegradable polymer-based materials tested in processing bone replacement implants. Collagen, for example, is of special interest because it is present in the natural bone structure. However, it falls behind because it lacks mechanical stability *in vitro*, and disintegrates over time [395].

Chapter 1: Literature Review

Turning to spider silks, other fusion proteins, such as engineered ADF3 and recombinant MaSp1 proteins cannot be processed into viable hydrogels. The literature lacks reports of eADF3-based hydrogels and recombinant MaSp1 proteins requiring high temperatures for hydrogel formation, which is unsuitable for cell culture [272, 396]. In contrast, this approach utilizing the cellulose-binding fusion protein based on an ADF4 protein [397, 398] presented a unique opportunity to develop injectable hydrogels with good mechanical properties at 37°C.

By pursuing this objective, this study seeks to contribute to the field of TE by introducing a novel cellulose-binding spider silk hydrogel. The outcomes of this study have the potential to advance the development of innovative biomaterials, improve TE strategies, and ultimately enhance clinical outcomes in regenerative medicine.

1.10.3 Objective: eADF4(C16)-REDV Coatings

The second objective of this study is to develop and evaluate the performance of a novel coating for DES using the eADF4(C16)-REDV fusion protein. DES have significantly improved the treatment of coronary artery disease by releasing drugs that prevent restenosis and promote vessel healing. However, current DES coatings still face challenges such as delayed endothelialization and increased risk of thrombosis and inflammation [386-388].

To overcome these limitations, this project focused on the recombinant spider silk eADF4(C16)-REDV fusion protein as a coating for DES by incorporating the REDV peptide, which exhibits a specific affinity towards endothelial cells. A fusion protein instead of a polymer/peptide blend could ensure that the small peptide does not prematurely elute out of the matrix and is homogeneously distributed. Furthermore, the production of the coating material occurred in one step, minimizing eventual chemical modifications.

Through this innovative coating approach, the biocompatibility of DES could be improved and facilitated early endothelialization, leading to reduced risk of thrombosis and improved long-term clinical outcomes. The eADF4(C16)-REDV coating was thoroughly characterized and evaluated for its ability to promote

Chapter 1: Literature Review

endothelial cell adhesion, proliferation, and migration and its capacity to minimize thrombogenicity and prevent restenosis.

Furthermore, drug elution of the antiproliferative drug everolimus was assessed as a countermeasure to neointimal hyperplasia.

The recombinant spider silk protein eADF4(C16) promises to be an excellent material for a stent coating because it is biocompatible with low to no immune response [14, 20, 180]. Furthermore, it showed slow biodegradation rates depending on the processing method and the ability to coat implants to protect them from forming a fibrotic capsule [14]. Another beneficial property in medical applications is eADF4(C16), being bacteriostatic and, most importantly, repellent against most human cell types, including blood cells [14, 399].

REDV, on the other hand, binds $\alpha_4\beta_1$ integrins, which are abundant in EC, while scarce on SMC membranes [400]. This enabled the fast formation of an EC monolayer covering the stent, which is beneficial for covering coronary stents as in-stent restenosis (ISR) often occurs when cells carried by the bloodstream adhere to the stents [342, 401-403]. Furthermore, it has been shown that the REDV peptide supports angiogenesis [28, 30, 404], which could also prove beneficial as surrounding spreads of the artery are most likely damaged by the plaque. **Figure 1-23** shows the theoretical layers of an artery opened by an eADF4(C16)-REDV coated stent. The blood vessel is held open by the mechanics of the stent, which is coated with the endothelial cell-selective fusion protein to support the formation of a monolayer of endothelial cells.

Building upon the findings from *Wang et al* [10] and *Xu et al* [151], this approach presented eADF4(C16) as a base material for DES coatings to exploit its inherent cell-repellent surface to improve upon the uncontrolled cell growth on silk fibroin materials. Furthermore, incorporating drug release and a degradation study with relevant protease environments *in vitro* was used to determine how feasible this material is in drug elution. Lastly, hemocompatibility observations conducted with fresh human whole blood were utilized to gain valuable insights into the behaviour of eADF4(C16) in an appropriate blood environment.

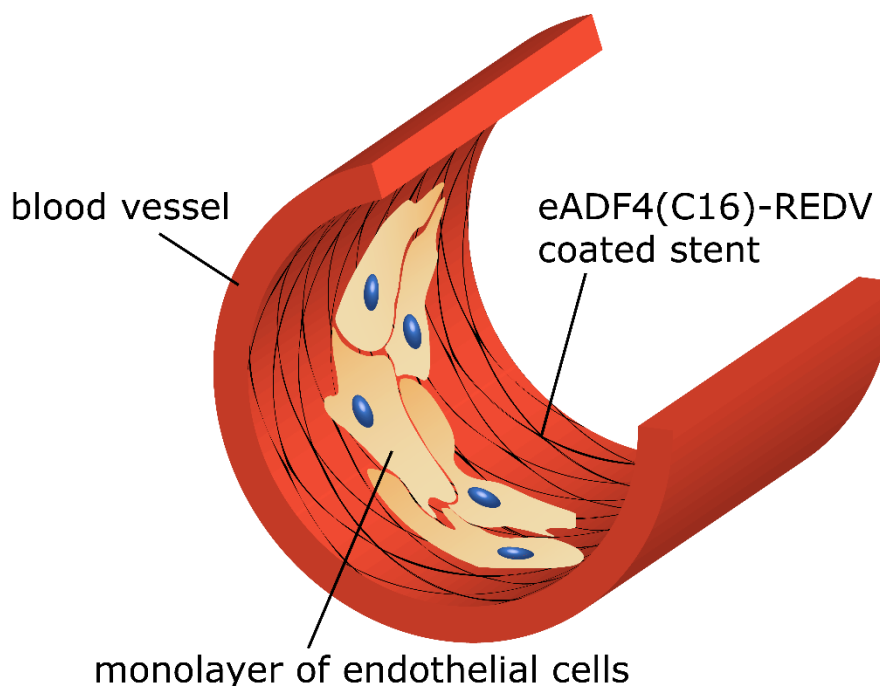


Figure 1-23: Schematic of a stented vessel with a monolayer of EC forming to avoid neointimal hyperplasia.

1.11 Scope of work

Figure 1-24 serves as a visual demonstration of how the individual chapters are arranged and intertwined.

Chapters 2 and 3, cover the creation and application of the cellulose-binding recombinant spider silk protein eADF4(C16)-CBD and chapter 4 and 5 focus on the production, characterization and application of eADF4(C16)-REDV as DES coating material.

Both approaches start with identifying the correct fusion sequence for the modification of eADF4(C16). Therefore, **chapter 2** describes identifying a suitable CBD sequence, the genetic modification of eADF4(C16), and protein production and purification. Lastly, it focuses on the characterization of the protein, including the detection of its cellulose binding capability.

Similarly, **chapter 4** focuses on the genetic modification of eADF4(C16) with the REDV endothelial cell-specific adhesion peptide. After modification, the

Chapter 1: Literature Review

production, purification and characterization will be described, including determining its EC selectivity and endothelialization possibilities *in vitro*.

Next, both proteins will be processed into their respective morphologies and assessed for use in TE applications. While the approach of cellulose-enhanced hydrogels follows the principle of mechanical cell signalling for attachment, the REDV variant covers the chemical route of cell attraction.

Chapter 3 will describe the processing of eADF4(C16)-CBD into cellulose fibre-enhanced hydrogels, their printability, rheological characterization and application as TE scaffolds *in vitro*.

Chapter 5 concludes with applying eADF4(C16)-REDV as a potential coating material for DES. Therefore, dip-coated stainless steel sheets are characterized by their thickness, hydrophobicity and surface homogeneity. Furthermore, the results of various human whole blood assays are discussed to deepen the knowledge of the Hemocompatibility of recombinant spider silk proteins. Lastly, everolimus elution over 29 days and enzymatic degradation in physiologically relevant wound healing conditions are occupied to observe the long-term stability of the coating.

Lastly, **chapter 6** summarises the findings and elaborates on future prospects for these TE approaches.

Chapter 1: Literature Review

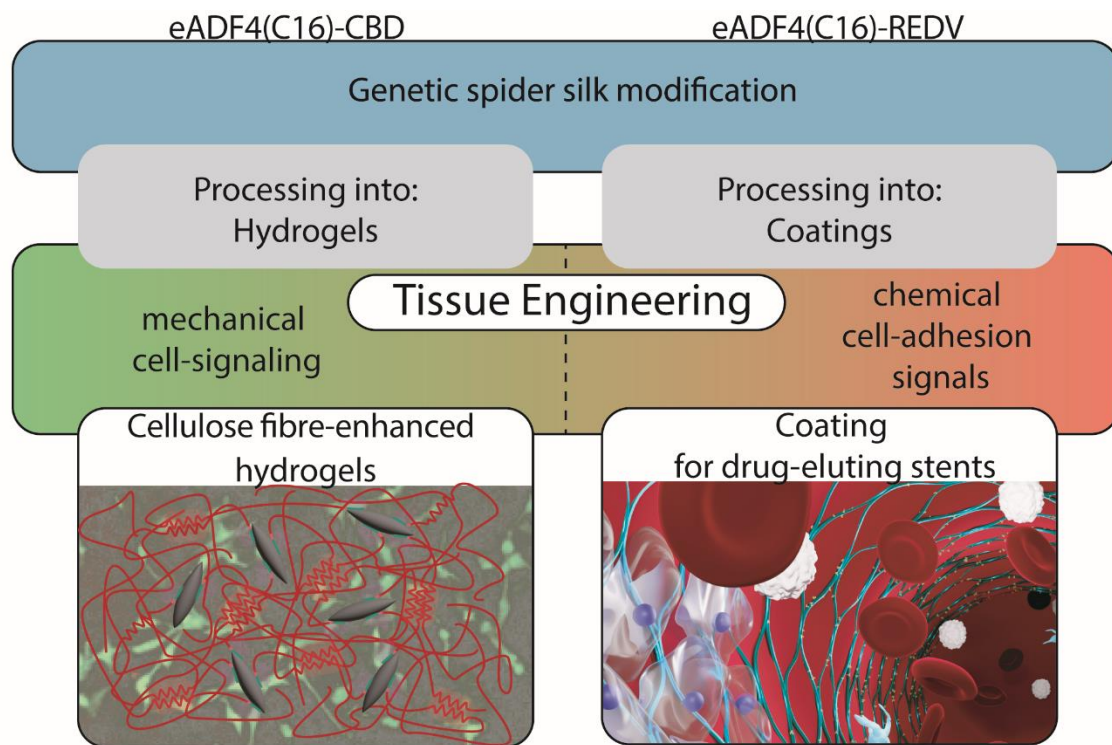


Figure 1-24: Schematic of this thesis' structure. Both approaches start with a similar starting point: genetic spider silk modification. Once the novel proteins are created, the approaches divide into processing the protein into hydrogels for eADF4(C16)-CBD and into coatings for the REDV variant. Then, both morphologies will be evaluated on their potential use in Tissue Engineering applications.

Chapter 2 Recombinant cellulose-binding spider-silk fusion protein: production and characterisation

2.1 Introduction

This Chapter serves as the foundation for processing cellulose-fibre enhanced eADF4(C16)-based hydrogels. Therefore, it first describes the design and production of the fusion protein, followed by experimental observations and discussions regarding the purification and characterisation of the cellulose-binding eADF4(C16)-CBD.

The examination commences with an exploration of the design process underpinning this protein variant's creation. Next, the procedures involved in producing and purifying eADF4(C16)-CBD, essential to ensuring a high-quality protein for subsequent investigations, are discussed. Therefore, the cloning, fermentation and purification via IMAC are described. Next, The resulting product is characterized via SDS-PAGE and MALDI-.TOF.

Continuing forward, an investigation is conducted into the crucial aspect of proper folding of the cellulose-binding domain within the fusion. This step is conducted via circular dichroism and fluorescence spectroscopy and holds immense significance in ensuring the functional binding properties of the fusion protein. Subsequent exploration revolves around the protein's binding capabilities to cellulose, utilising quartz crystal microbalance measurements on cellulose substrates. This discussion delves into theoretical foundations and experimental results, shedding light on the interaction between the protein and cellulose.

Through an analysis of these aspects, this chapter lays the groundwork for future applications of the eADF4(C16)-CBD fusion protein. It sets the tone for Chapter 3, which delves deeper into its potential across Tissue Engineering.

Chapter 2: Recombinant cellulose-binding spider-silk fusion protein: production and characterisation

2.2 Materials and Methods

Chemicals used in the experiments of this chapter were purchased from Roth (Karlsruhe, Germany) if not stated otherwise. eADF4(C16) was purchased from AMSilk GmbH (Planegg/ Munich, Germany). All nucleotide sequences were acquired from Eurofins Genomics (Germany). Enzymes were acquired from New England Biolabs (Germany) and used according to the manufacturer's protocol.

2.2.1 Genetic engineering of the fusion protein eADF4(C16)-CBD

To produce eADF4(16)-CBD, first, a modified nucleotide sequence, optimised for expression in *E. coli* [405], was created by fusing the cellulose-binding domain CBD_{ceX} with the eADF4(C16) sequence. The full protein sequence comprises of: (GSSAAAAAASGPGGYGPENQGPSGPGGYGPGGP)₁₆ G PTPTPTTPTPTTPTPTPTPT G SGPAGCQVLWGVNQWNTGFTANVTVKNTSSAPVDGWTLTFSFSGQQVTQASSTVTQS GSAVTVRNAPWNGSIPAGGTAQFGFNGSHTGTNAAPTAFSLNGTPCTVGG. The CBD_{ceX} [406] domain, including its PT-rich linker sequence, was derived from the exoglucanase enzyme found in *C. fimi*, and a seamless cloning approach, as described previously [19], was used for creating this fusion. In short, as depicted in **Figure 2-1**, the eADF4(C16) protein modification began with both the eADF4(C16) and the target sequence (CBD) being processed from individual cloning vectors (pCS). For the modification with peptides or fusion domains to the C- or N-terminus of the insert, the vector containing the eADF4(C16) sequence was cut with BsaI/BsgI for C-terminal modification. Another pCS vector containing the targeted modification sequence within the "insert region" (between BamHI and HindIII restriction sites) was cut oppositely with BsaI and BseRI for its N-terminal modification. This generated two complementary parts of the pCS vector, one carrying the eADF4(C16) sequence and the other containing the targeted modification. The restriction products were then isolated by agarose gel electrophoresis. After ligation, the newly formed pCS vectors were transformed into *E. coli* DHb10 (Novagen, Germany) for high DNA yield following a 20 mL overnight culture in LB-media at 37°C and subsequent DNA extraction (Promega,

Chapter 2: Recombinant cellulose-binding spider-silk fusion protein: production and characterisation

Wizard® Genomic DNA Purification kit, # TM050). When cut with BsaI, the vector was cleaved within the ampicillin resistance-coding sequence, enabling the identification of the correctly ligated vectors by their ampicillin resistance on ampicillin containing substrates. Identified colonies were selected for overnight culture, and correctly assembled constructs were identified through sequencing conducted by Eurofins Genomics, Germany.

Once the modification of eADF4(C16) in a pCS vector was confirmed by sequencing, the insert (in this case eADF4(C16)-CBD) was cleaved with BamHI/HindIII and transferred into the expression vector pET28a [407], as shown in **Figure 2-2**. In this procedure, the cut fusion-protein sequence was ligated with a BamHI/HindIII digested pET vector, which serves as a commonly used expression vector. Unlike the pCS vector, the pET28a vector is designed for protein expression, which, besides the lac operon necessary for induction, includes a 6-His tag (not shown in **Figure 2-2**) and a T7 tag at the protein's N-terminus. Kanamycin resistance was used as selection tool for ligated vector colonies. The accuracy of the DNA sequence was again confirmed through sequencing conducted by Eurofins Genomics, Germany.

Chapter 2: Recombinant cellulose-binding spider-silk fusion protein: production and characterisation

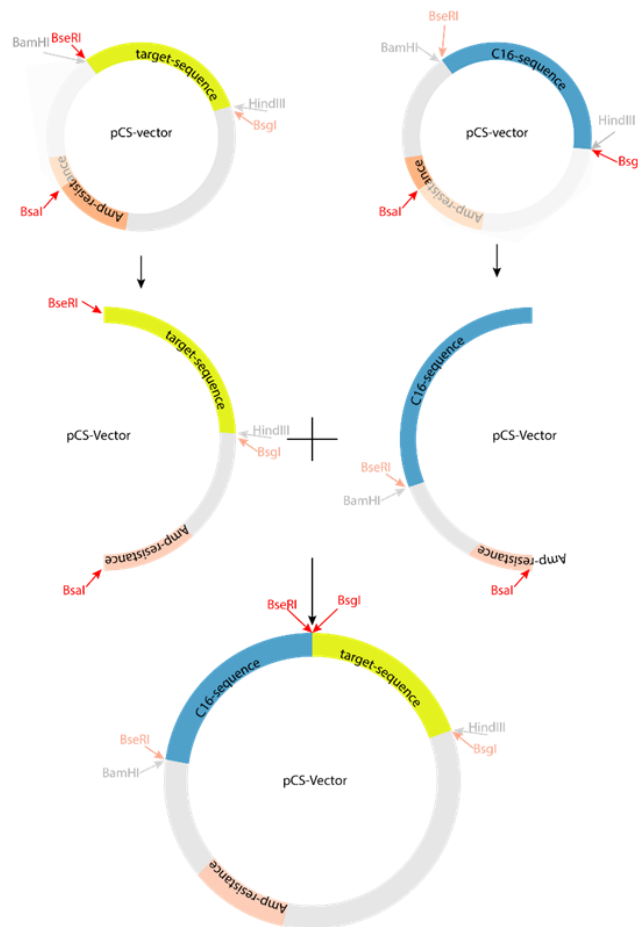


Figure 2-1: Workflow of combining two cut pCS parts to yield one closed pCS vector with the modified eADF4(C16) sequence. All involved restriction sites are shown, while the used sites are highlighted for each step. BamHI and HindIII are required for the next cloning step and are therefore included in this scheme. The two sequence-bearing vectors are digested with BseRI/BsaI and BsaI/BsgI, respectively. These fragments are then ligated to create a new pCS vector comprising the fused sequence.

Chapter 2: Recombinant cellulose-binding spider-silk fusion protein: production and characterisation

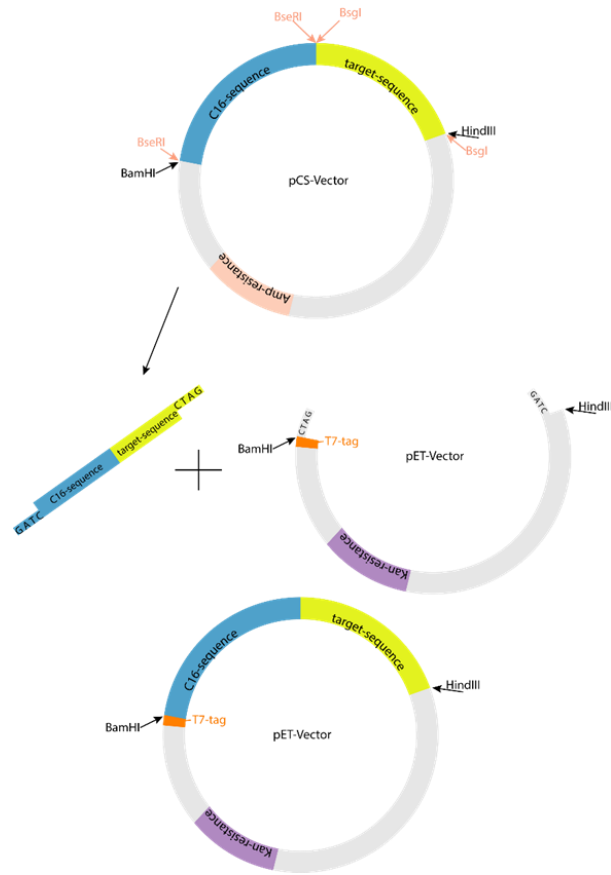


Figure 2-2: Workflow of the eADF4(C16)-target-sequence transfer into an expression vector (pET). BamHI/HindIII digested the fused sequence in the pCS vector. The sequence is then transferred into a pET vector which has been treated the same. The sticky-ends facilitate improved ligation specificity, and the kanamycin resistance of the pET vector serves as a selection marker for successful cloning attempts. A general pET vector, not including the 6-His-tag is shown.

2.2.2 Protein expression and purification

The final pET28a_eADF4(C16)-CBD plasmid was introduced into *E. coli* BL21(DE3)gold (Novagen, Germany) and cultured via fed-batch process in 1.3 L Minifors (Infors, Germany), 3.5 L Biostat (Satorius, Germany), 5 L Labfors (Infors, Germany), or 30 L Biostat (Satorius, Germany) fermenters in "modified complex medium light" (1.08 wt% tryptone/peptone, 1.65 wt% yeast extract, 10.53 mM KH₂PO₄), as previously described [74, 408]. Briefly, the complete fermentation was conducted at 30°C instead of the optimal 37°C for *E. coli* growth [409]. This alteration was introduced to prolong the cultivation overnight without reaching the decline phase. The pH was kept at a constant value of 6.7±0.1 by automatically adding (NH)₃ and H₃PO₄. Pure oxygen was introduced to maintain a set point of 40% pO₂ to sustain aerobic conditions if necessary. Furthermore, upon depletion

Chapter 2: Recombinant cellulose-binding spider-silk fusion protein: production and characterisation

of the base feed substance (glycerol), an automated feed was activated at approximately 1 mL/min. Fermentation parameters were surveilled and managed with the EVE software-platform for bioprocesses (Infors, Germany). Protein production was induced after an optical density at $\lambda=600$ nm (OD₆₀₀) of 60 was reached and was achieved by supplementing the culture to a total concentration of 0.1 mM Isopropyl β -d-1-thiogalactopyranoside (IPTG) for a duration of 1.5 hours.

Figure 2-3 shows a representative fermentation profile with the crucial factors for bacterial growth displayed. The oxygen partial pressure (pO₂) was utilized as a rough indicator of the culture process. It can be deduced that between 500-600 minutes, the bacterial mass reached a point where the oxygen content of the supplied air decreased, and the automatic oxygen supply started. The spike in pO₂ concentration around minute 950 indicates the initial feed source (glycerol) depletion and initiated an automatic feed of 4% (software-specific value, equals approximately 1mL/min) to maintain constant bacterial growth. Furthermore, it can be seen that the automatic pH adjustment relied solely on the addition of (NH)₃ starting with the additional supply of oxygen, indicating the countermeasure of the production of acidic compounds by *E.Coli* [410].

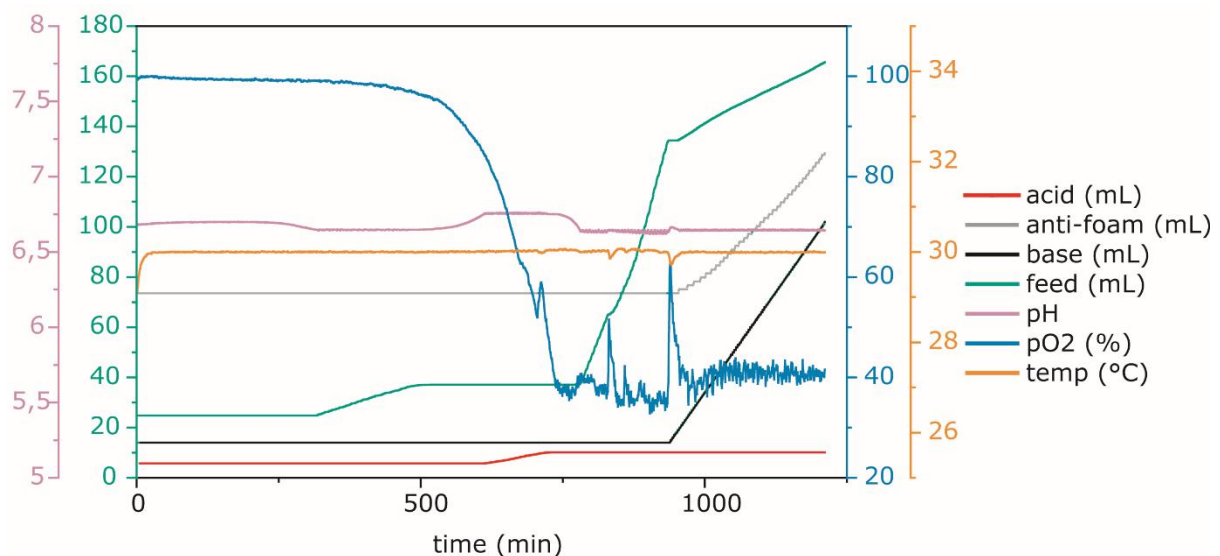


Figure 2-3: Representative fermentation profile of overnight cultivation followed by a 1.5-hour induction window of eADF4(C16)-CBD.

Chapter 2: Recombinant cellulose-binding spider-silk fusion protein: production and characterisation

Next, the final cell suspension was harvested, washed with washing buffer (10 mM Tris/HCL pH7.5, 150 mM NaCl), and then incubated with 0.2 mg/ml lysozyme (Merck, Germany) and Protease Inhibitor Mix-HP (SERVA, Germany) at 4°C for 2 hours. Cell disruption was performed using a high-pressure homogeniser Microfluidizer M110S (Microfluidics, USA-Newton) with two cycles at 150 bar. After centrifugation (30 min at 22,000 x g, 4°C), the sample underwent heat precipitation at 70°C, followed by another centrifugation step.

The supernatant was then purified using immobilised metal ion affinity chromatography (IMAC) on an Äkta purifier (GE healthcare) utilising the 6HIS-tag at the N-terminus of the protein. For this purpose, two HisTrap™ High Performance (Cytiva, Merck, Germany) columns were used in combination. The pre-conditioned cell lysate was loaded onto the column overnight at a flow rate of up to 2 mL/min. Elution occurred with an imidazole gradient in steps of 0 mM, 35 mM and 300 mM in 100 mM NaCl, 50 mM Tris/HCL pH 7.5. After IMAC, the eluate was dialysed against 300 mM NaCl, 50 mM Tris/HCL pH7.5 for short-time storage at 4°C.

Figure 2-4 depicts a representative chromatogram, where 800mL of the cell lysate was loaded overnight, followed by introducing an imidazole-free buffer until the original UV absorbance of ~0 was detected. Next, weakly bound proteins were eluted by the liquid phase containing 35 mM imidazole, indicated by the UV peak at 1500 mL. Once a stable UV signal was established, the target protein elution with 300 mM imidazole was initiated, as displayed by the UV peak at ~1850 mL. Lastly, 500 mM imidazole was used to wash off any remaining bound protein. However, the absence of a peak suggests that all bound protein was eluted at 300 mM. The yield of the purified protein was approximately 0.2 mg per gram of centrifuged bacterial mass. The display of the conductivity served as a control measure and showed no irregularities. The conductivity is higher during the loading phase due to the high amount of salts in the bacterial suspension.

Chapter 2: Recombinant cellulose-binding spider-silk fusion protein: production and characterisation

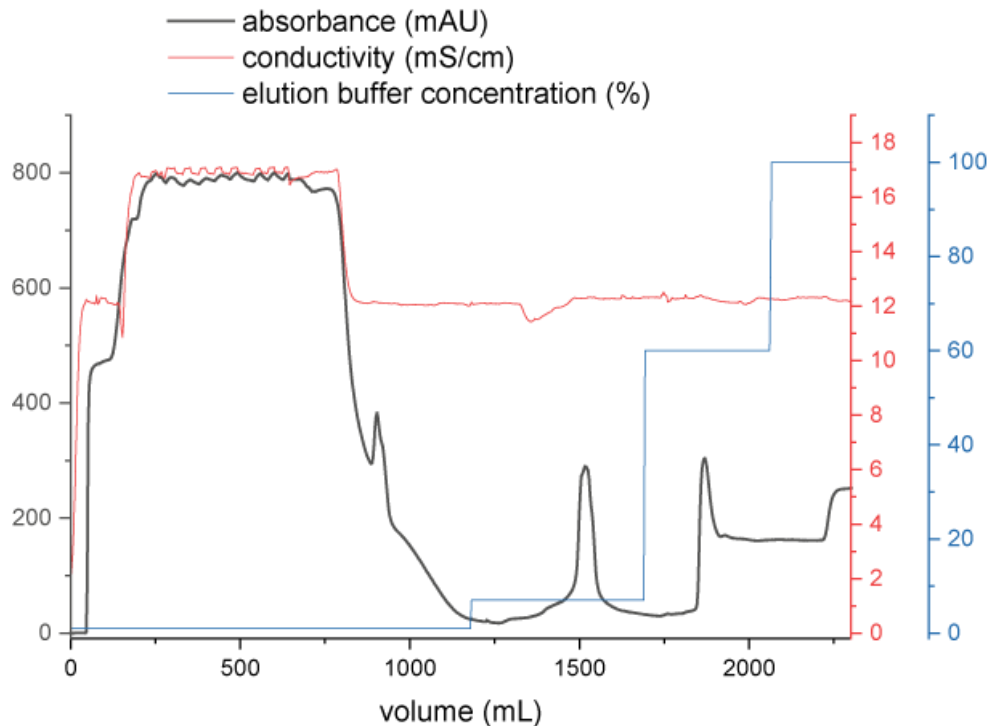


Figure 2-4: A representative chromatogram of the IMAC-purification of eADF4(C16)-CBD.

2.2.3 SDS polyacrylamide gel electrophoresis, silver staining and Western Blot

For SDS-PAGE analysis, 10% gels were cast and stored at 4°C until usage. All samples were mixed with Laemmli buffer (10 % w/v SDS, 50 % w/v glycerol, 300 mM Tris/HCl pH7.5, 0,05 % w/v bromophenol blue), supplemented with or without β -Mercaptoethanol (to a final concentration of 20% v/v), and denatured by incubating the samples for 10 min at 95°C. A molecular protein standard (0.8 μ L, SERVA dual color protein standard) and the individual samples at protein concentrations of approximately 2 μ g were loaded onto the gel, followed by gel electrophoresis for 1h (500 V, 30 mA per gel, 200 W) in running buffer (0.25 M Tris/HCl pH 6.8; 8% SDS, 40% glycerol, 0.04% bromophenol blue).

After SDS-PAGE, silver staining was performed for protein detection. First, the gels were washed with MQ-H₂O and then incubated for 10 min in FIX I buffer (30% v/v ethanol, 10% v/v acetic acid). After another wash step with MQ-H₂O the gels were incubated for 30 min in FIX II buffer (0.4 M sodium acetate; 0.5% v/v acetic acid;

Chapter 2: Recombinant cellulose-binding spider-silk fusion protein: production and characterisation

30% v/v ethanol; 3.5g Na₂SO₃), followed by four wash steps with MQ-H₂O and incubation in silver staining solution (6.5 mM AgNO₃, 50 µL formaldehyde) for 45 min in a light-proof container. After that, a small amount of developer solution (2.5 g Na₂CO₃, 100 µL formaldehyde in 50 mL H₂O) was added to precipitate free silver. The rest of the developer solution was then added. The gels were incubated until protein bands were detectable, and adding 10% glycerol stopped the developing reaction. Silver staining was carried out at room temperature, and the gels were rocked gently during incubation times.

Immunoblotting, specifically Western Blotting, reveals proteins within a protein mixture using specific antibodies. Before blotting, the SDS gel and four Whatman® filter papers in the same size as the gel (8x9 cm) were incubated in western blot transfer buffer for 5 min (50 mM Tris, 40 mM glycine, 1.3 mM SDS, 20% v/v methanol). A polyvinylidene difluoride membrane, the size of the gel, was activated by gently rocking in 100% methanol for 30 sec. Subsequently, the membrane was washed thrice with MQ-H₂O before incubation in western blot transfer buffer for 15 min. The western blot was performed by stacking the components: (top to bottom) 2 Whatman® filter papers, SDS-PAGE gel, the PVDF membrane and 2 Whatman® filter papers. The electrophoretic transfer was conducted for 1h at 0.75 mA/cm² of membrane and 8 W.

After blotting, the PVDF membrane was incubated for 1h at RT in a blocking solution (5% Casein in PBS). The membrane was washed three times with 1x PBS and the blot was subsequently incubated for 1h in 50 mL of a conjugated antibody solution (T7-HRP-antibody (Merck, Germany) in PBS +1% Casein; 1:5000). After a last wash step using PBS, the membrane was placed protein side up on a sheet of aluminium foil and incubated with ECL western blotting reagent (Promega, Germany) for 2 min, before detection of the luminol-based chemiluminescence with an Ettan DIGE imager (GE healthcare).

Figure 2-5 summarizes the observations from silver staining and Western Blot for the target protein used to determine protein purity. Furthermore, the corresponding western blot identified the protein band at the 300 mM imidazole lane as eADF4(C16)-CBD by T7-specific antibody detection. The protein band of the flow-through sample showed a protein mixture flowing through the column

Chapter 2: Recombinant cellulose-binding spider-silk fusion protein: production and characterisation

without interaction, and the Western Blot confirms that no eADF4(C16)-CBD is present, therefore suggesting that the capacity of the column was not depleted and all available target protein bound to the column. The 35 mM imidazole lane shows some protein bands, most likely representing weak, non-specific binding of *E.coli* proteins. Lastly, the 300 mM lane showed one distinctive protein band, which could be identified as eADF4(C16)-CBD by the Western Blot.

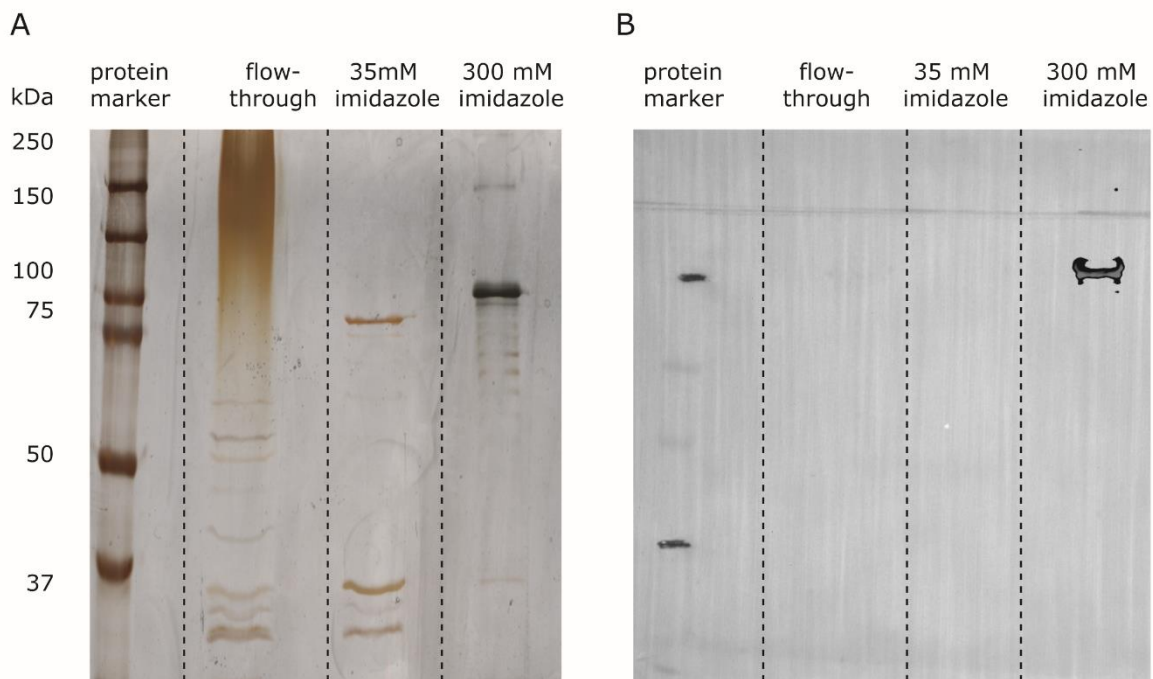


Figure 2-5: A: Silver stained SDS-gel of samples taken from IMAC-purification of eADF4(C16)-CBD and B: corresponding Western Blot with T7-HRP-antibody detection.

2.2.4 MALDI-TOF

The eADF4(C16)-CBD protein exhibited an unexpected phenomenon of reduced mobility, showing a protein band between 75 and 100 kDa, commonly observed in proteins rich in alanine and acidic residues [411]. Therefore, MALDI-TOF analysis was performed to verify the correct protein size, and the obtained results (**Figure 2-6**) confirmed a protein size of 60.7 kDa based on the m/z value for the +1 charge. Another peak at half the size represents the +2 charge and further indicates protein purity. These findings support the notion that the observed low mobility is a consequence of the properties of the eADF4(C16)-CBD protein.

Chapter 2: Recombinant cellulose-binding spider-silk fusion protein: production and characterisation

MALDI-TOF analysis was conducted using a Bruker MALDI-TOF Autoflex (Bruker, Germany) equipped with a 337 nm N₂ laser and operated at an acceleration voltage of 20 kV. Protein samples dissolved in 3 M guanidinium isothiocyanate were desalted using ZipTip C4 and co-eluted with the matrix consisting of sinapinic acid (20 mg/mL) in 60% acetonitrile and 0.1% trifluoroacetic acid. The processed data were analysed using mMass v5.5.0 software [412].

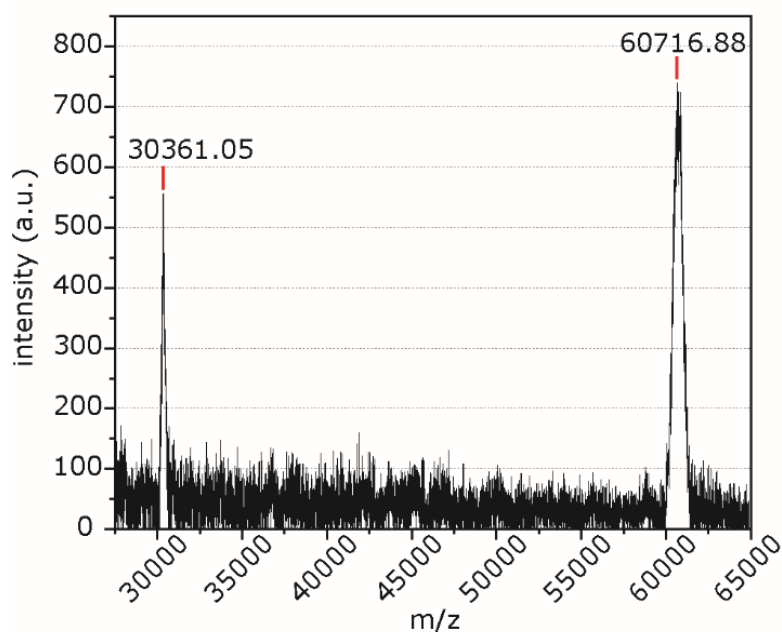


Figure 2-6: MALDI-TOF of eADF4(C16)-CBD in aqueous solution showing a +1 peak at 60716 m/z and a +2 peak at 30361 m/z.

2.2.5 Circular Dichroism (CD) spectroscopy

For near-UV measurements, protein solutions were prepared at 1 mg/mL concentrations in analytically pure 10 mM Tris/HCl (pH 7.5) containing 150 mM NaCl. The solutions were obtained by ultracentrifugation at 55,000 rpm for 30 minutes using an Optima MAX-XP centrifuge (Beckman Coulter). Near-UV measurements were performed at 20 °C using a 1 cm pathway quartz cuvette at intervals of 10 °C for thermal degradation. Chemical denaturation experiments involved mixing the stock protein solution with guanidinium chloride (GdmCl) in ratios to maintain the final protein concentration of 1 mg/mL. Far-UV CD spectra were recorded with 0.1 mg/mL protein concentrations using a 1 mm pathway

Chapter 2: Recombinant cellulose-binding spider-silk fusion protein: production and characterisation

cuvette. All spectra were obtained as an average of five scans using a Jasco J815 spectrometer (Jasco, Germany).

2.2.6 Fluorescence spectroscopy

Fluorescence spectra were obtained by recording the emission spectra from protein solutions at a 0.5 mg/mL concentration. The solutions were prepared in analytically pure 10 mM Tris/HCl (pH 7.5) containing 150 mM NaCl and placed in quartz cuvettes. A fluorescence spectrometer, FluoroMax-3 (Jobin-Yvon Inc.), was used for the measurements with excitation set at a wavelength of 295 nm.

2.2.7 Cellulose-binding assay

A simplistic approach was chosen for the initial observation of the cellulose-binding activity of the fusion. Therefore, 1 mg/mL of cellulose fibres (C6288, Sigma-Aldrich, Merck, Germany) was incubated with eADF4(C16)-CBD and eADF4(C16) solutions in varying buffer compositions on a shaking thermoblock (450 rpm at 37 °C) for 30 minutes. After incubation, the suspension was centrifuged for 30 minutes at 13,000 x g, and the supernatant was analysed for UV absorption at 280 nm.

2.2.8 Spin-coating

To cellulose-coat 14mm gold QCM-D chips (QuartzPro, Sweden), they were ozone-treated for 10 minutes using a PSD-UV ozone cleaner (Novascan Technologies, USA). Subsequently, 20 µL of a 0.05% w/v cellulose solution was applied to the chips, which were then spun for 60 seconds at 67 rps with an acceleration time of 5 seconds using a spin coater (SCI-30, Quantum Design, Germany). Following spin-coating, the chips were dried for 10 minutes on a heating plate at 100°C (EchoTherm™ HP40, Torrey Pines Scientific, CA). Lastly, they were washed in MQ-H₂O for 3 minutes and air-dried.

Chapter 2: Recombinant cellulose-binding spider-silk fusion protein: production and characterisation

2.2.9 QCM-D measurements

Using a Q-Sense Analyser setup, QCM-D measurements were carried out with cellulose-coated 14 mm gold sensors (QuartzPro, Sweden) mounted in 4 humidity Modules (Biolin Scientific, Sweden). Buffer solution (10 mM Tris/HCL pH7.5, 150 mM NaCl) and protein solutions (0.25 mg/mL) were introduced to the humidity modules, maintaining a 100 μ L/min flow rate. Analysis and calculations were carried out with the Qtools software (Biolin Scientific, Sweden).

2.3 Results and Discussion

2.3.1 Designing eADF4(C16)-CBD

The first step in creating a novel cellulose-binding fusion protein is identifying a feasible fusion partner. As highlighted in the literature review (**1.6.3**) the area of cellulose-binding domains (CBD) is plentiful and spread across various species [289]. Due to the established production of eADF4(C16) [12] in *E. coli*, a bacterial CBD [26, 290, 413] for streamlined production in the same host was targeted [290]. Furthermore, as the fusion protein was created with mechanically enhanced composites, especially hydrogels, in mind, irreversible binding mechanisms were favoured [289, 414]. Finally, the established variants and modifications of eADF4(C16) contain a T7 tag for identification purposes at the N-terminus, further narrowing down the amount of suitable CBD candidates to c-terminally located domains, which ultimately led to focusing on the CBD derived from the exoglucanase enzyme in *Cellulomonas fimi*, CBD_{CEX} [406].

Furthermore, *C. fimi* is, like *E. coli*, a gram-positive, rod-shaped bacterium, minimizing the risk of cross species expression. *C. fimi* is known for its ability to metabolise cellulosic material and is typically found in soil [415]. The cellulose-binding domain CBD_{CEX} has been shown to interact with cellulose through an entropically driven process. This binding mechanism is attributed to the reduced conformational flexibility of the binding partners [293].

The first iteration of the eADF4(C16)-CBD fusion protein was designed by the addition of the CBD moiety to the eADF4(C16) sequence without a linker

Chapter 2: Recombinant cellulose-binding spider-silk fusion protein: production and characterisation

sequence, which is found in the natural cellulase enzyme, separating the catalytic from the binding domain. The resulting product from the fermentation and purification process was only discovered within inclusion bodies, a sign of improperly folded, water-insoluble protein moieties [416]. Consequently, no cellulose-binding capabilities were detected (data of this variant not included). As CBD_{CEX} contains β -sheets crucial for cellulose-binding, this discovery, combined with the absence of cellulose-binding activity, suggested a different approach.

As the linker sequence mentioned above is typical for most naturally occurring cellulase enzymes [417], the faulty protein production was hypothesised to be caused by the lack of such a spacer.

Previous studies reported reduced catalytic activity when linker regions were deleted in enzymes such as cellobiohydrolase I of *Trichoderma reesei* [418] and Endoglucanase A (CenA) of *C. fimi* [419]. However, the impact of linker modifications on fusion proteins remains highly variable, depending on the specific fusion partner. Therefore, a modified linker sequence consisting of tyrosine and proline, which closely resembles the natural linker in CBD_{CEX} [418, 419], was introduced. Additionally, a 6His-tag was incorporated at the C-terminus of the fusion to enable IMAC. The resulting fusion protein variant and the individual amino acid motifs, is depicted in **Figure 2-7**.

Chapter 2: Recombinant cellulose-binding spider-silk fusion protein: production and characterisation

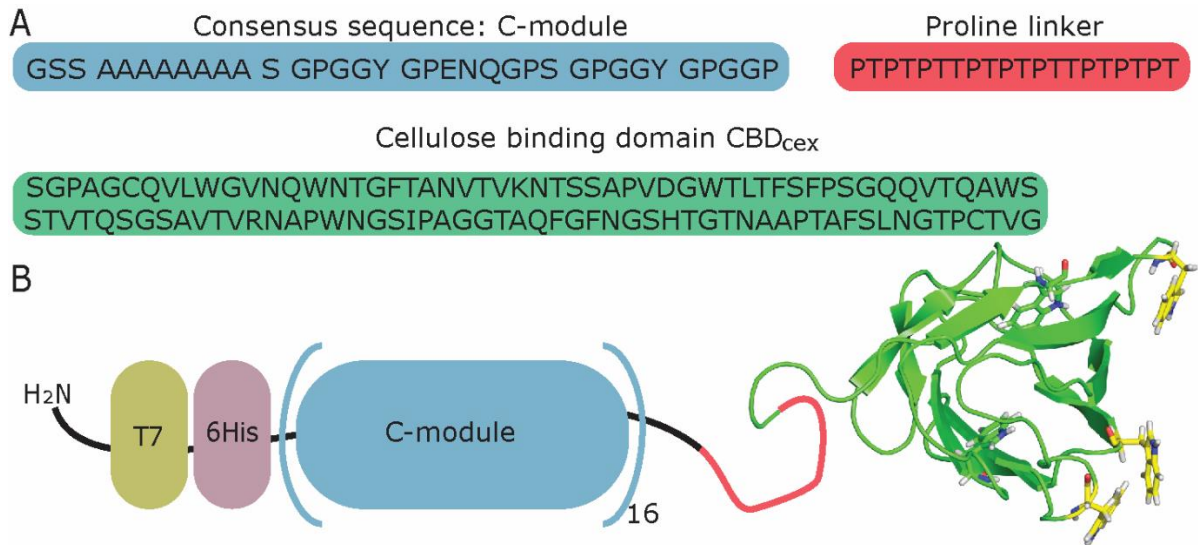


Figure 2-7: A) The amino acid motifs of the hybrid spider silk-cellulose binding protein. B) Schematic structure of the fusion protein eADF4(C16)-CBD. Domain structure reproduced by PDB ID 3.2.1.91. The exposed tryptophan residues W17, W54, and W72, responsible for binding cellulose, are highlighted yellow. The proline-linker is demonstrated as a red string, and eADF4(C16) is shown in block form with the attached T7- and His-tag at the n-terminus

2.3.2 Proper folding of the CBD

Once the genetic modifications of eADF4(C16)-CBD were incorporated and the protein was produced and purified, the next steps involved validating its ability to bind to cellulose substrates and assessing whether the fusion retained its capacity to form hydrogels at high concentrations.

As the cellulose binding mechanism relies heavily on a native structure of the CBD moiety [420], secondary and tertiary protein structure analysis techniques have been employed. This approach exploited that eADF4(C16) is intrinsically unfolded in aqueous solutions [19], and the CBD consists of short β -sheet structures and contains five tryptophane residues [406].

First, as a direct comparison to unmodified eADF4(C16), far-UV circular dichroism (CD) spectroscopy has been conducted. **Figure 2-8** shows the resulting spectra between 250-195 nm, where no significant distinction between both proteins can be observed. As typical for eADF4(C16) and variants thereof, a minimum at 200 nm can be observed in the overall random coil indicating spectrum [74]

Chapter 2: Recombinant cellulose-binding spider-silk fusion protein: production and characterisation

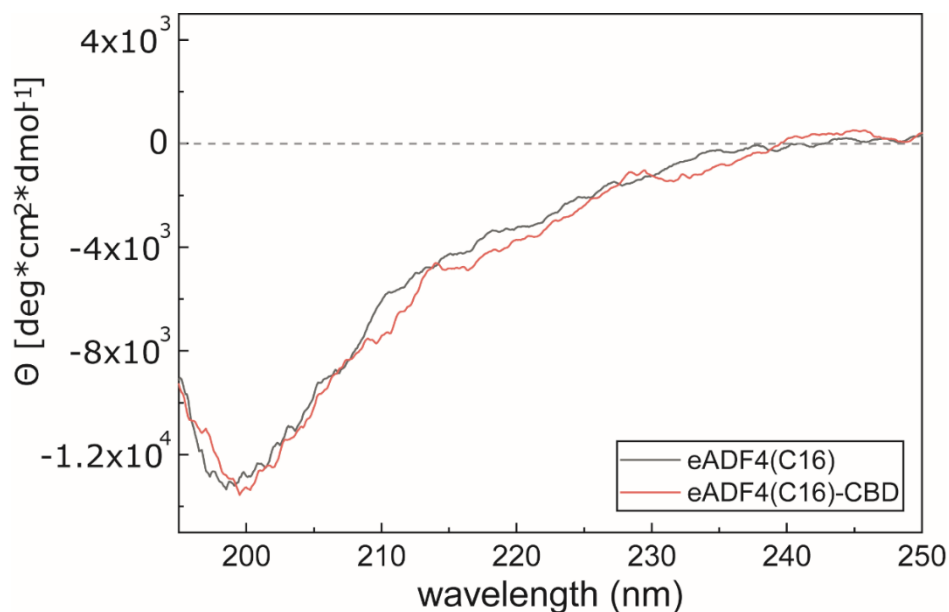


Figure 2-8: Far-UV CD spectra of eADF4(C16) and the CBD-modified variant.

The limited contribution of the CBD can be attributed to its relatively small proportion within the fusion protein (62 amino acids out of 726 amino acids). These findings align with the results *Humenik et al.* [78] obtained for their GFP fusion. Although eADF4(C16)-GFP comprises β -sheets in a more significant ratio, the fusion's far-UV spectra only exhibited slight changes in intensity while maintaining the overall shape and characteristic minimum at 200nm.

Consequently, near-UV observations, ensuring its native conformation, were employed to observe the unfolding of the globular CBD.

Both the eADF4(C16) moiety and the linker lack tertiary structures in aqueous solutions. Therefore, any observed changes in protein structure could be attributed to the denaturation of the CBD. Additionally, since neither eADF4(C16) nor the linker contain tryptophan residues [15, 228], any alterations in tryptophan signals could also be attributed to changes in the CBD structure.

Near-UV CD measurements revealed that the overall protein structure, particularly the peak at 290 nm associated with tryptophan residues [421], exhibited a decrease in intensity upon denaturation by guanidinium chloride (GdmCl) (**Figure 2-9A**) or with increasing temperature (**Figure 2-9B**) indicating a loss of tertiary structure [422]. Furthermore, **Figure 2-9B** includes the shape of a near-UV spectra of eADF4(C16) in an aqueous solution, where the characteristic

Chapter 2: Recombinant cellulose-binding spider-silk fusion protein: production and characterisation

fingerprint, including the 290 nm peak, is absent, closely resembling the spectra of eADF4(C16)-CBD denatured by 3 M GdmCl.

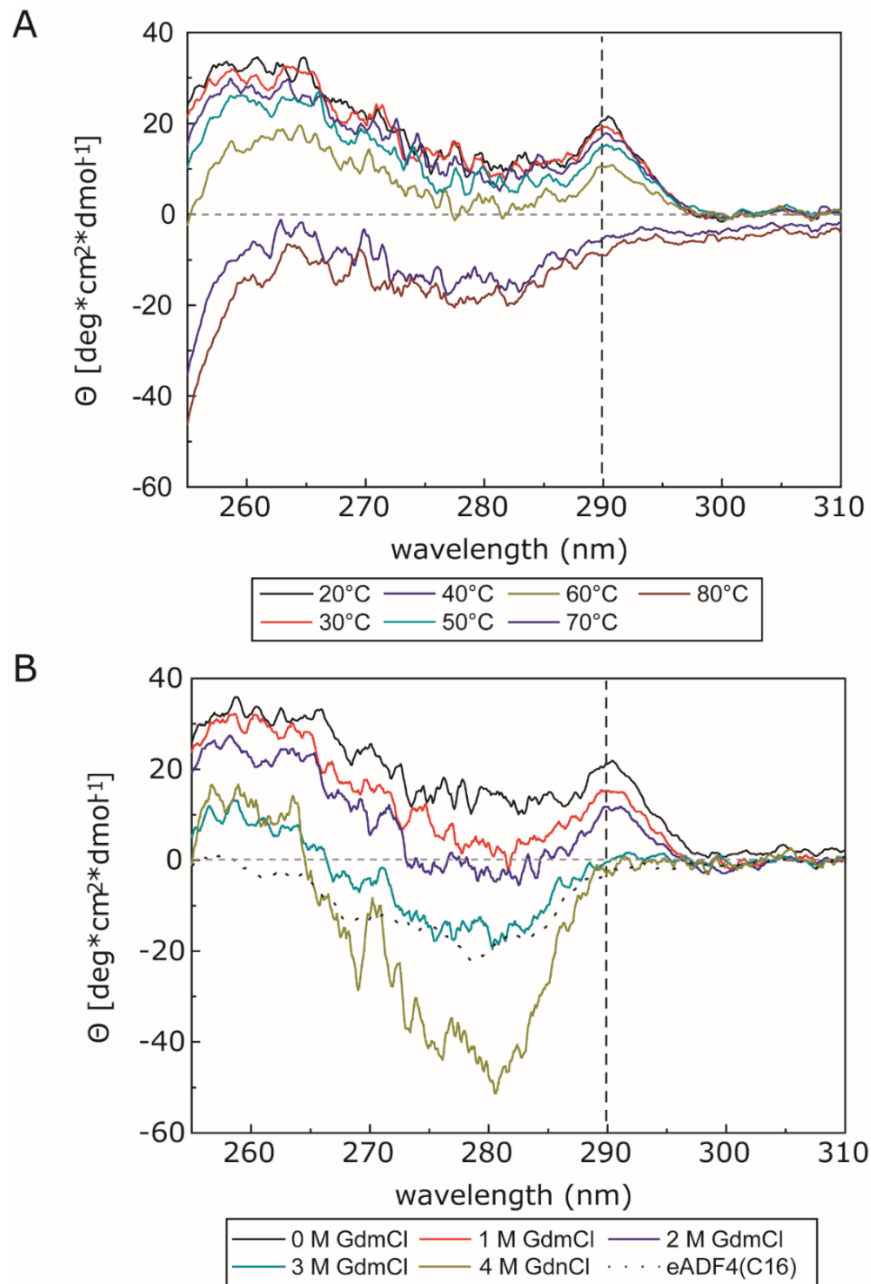


Figure 2-9: Near UV- CD spectra of eADF4(C16)-CBD denatured by a temperature gradient (A) and a GdmCl gradient (B). The vertical dotted line represents the tryptophan peak at 290 nm, which decreases in intensity by proceeding denaturation.

Lastly, fluorescence spectroscopy, utilising an excitation wavelength of 295 nm (**Figure 2-10**), demonstrated a red-shift and enhanced emission spectra intensity with increasing GdmCl concentration. This can be attributed to the exposure of two of the five tryptophan residues, which were previously buried within the native

Chapter 2: Recombinant cellulose-binding spider-silk fusion protein: production and characterisation

structure of the domain, during the denaturation process. Additionally, the denaturation of the protein by GdmCl leads to a reduction in protein aggregation [423].

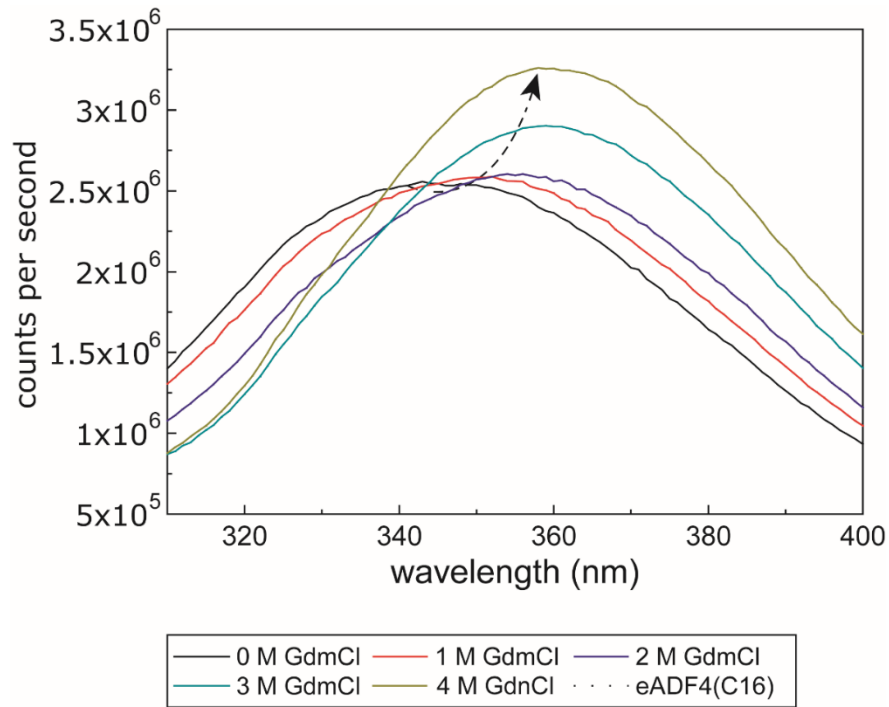


Figure 2-10: Fluorescence spectra of eADF4(C16)-PL-CBD in the presence of different GdmCl concentrations.

These findings combined suggest that the CBD of the fusion protein can be denatured and, therefore, maintains its native structure throughout the production and purification processes.

Chapter 2: Recombinant cellulose-binding spider-silk fusion protein: production and characterisation

2.3.3 Cellulose binding

Finally, the ability of the fusion to bind to cellulose substrates was evaluated through two approaches. Firstly, an incubation assay was conducted to assess whether the protein concentration of a solution decreased due to protein binding to cellulose fibres (CF). **Figure 2-11** summarises the concentration differences observed after a 30-minute incubation period.

The protein concentration remained unchanged for all control conditions without added CF, confirming the stability of the protein solution in all buffer conditions for up to 30 minutes at 37 °C.

Furthermore, incubation of CF with eADF(C16) did not exhibit a decrease in protein concentration after 30 minutes, indicating the inability of the unmodified variant to bind to cellulose. In contrast, all tested buffer conditions for eADF4(C16)-CBD showed decreased protein concentrations after centrifugation. Furthermore, when examining the binding activity of eADF4(C16)-CBD in different buffer compositions (0 mM, 150 mM, and 300 mM NaCl), it was observed that higher ionic strength, represented by the 150 mM and 300 mM NaCl conditions, appeared to enhance the binding activity of eADF4(C16)-CBD to cellulose.

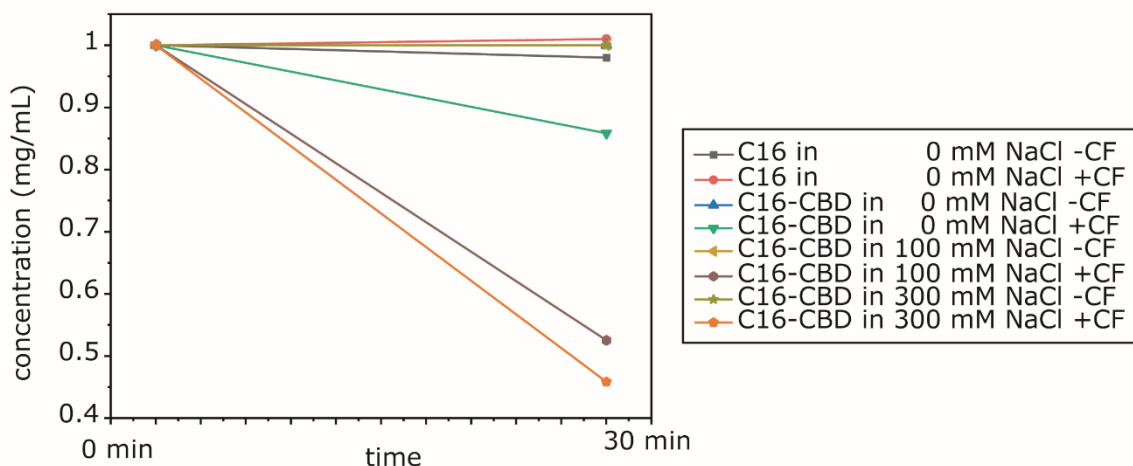


Figure 2-11: Cellulose-binding assay. Concentration change after a 30-minute incubation of cellulose fibres with eADF4(C16) based protein solutions.

Chapter 2: Recombinant cellulose-binding spider-silk fusion protein: production and characterisation

This initial observation of the binding capacity was then confirmed with QCM-D measurements. Cellulose coated QCM-D chips were incubated with protein solutions of eADF4(C16) and the CBD variant. **Figure 2-12** shows the resulting frequency change of this procedure, directly correlating to adsorbed protein to the cellulose surface on the chip. After an equilibration time of the coated chips in the buffer system (not shown in **Figure 2-12**), the protein solution was introduced at minute 1.5, as indicated by the first red line in the graph.

The frequency shift revealed notable differences between eADF4(C16)-CBD and eADF4(C16) samples. The eADF4(C16)-CBD sample exhibited a significant decrease in frequency by approximately 65 Hz, whereas the frequency change was much less pronounced, around 15 Hz, for the sample incubated with eADF4(C16). Moreover, when the protein solution was replaced with a buffer solution, the frequency change of the eADF4(C16) samples reversed to approximately 10 Hz, indicating that weakly adhered protein was washed off the surface.

In contrast, the frequency change for the cellulose binding variant remained around 65 Hz even after introducing the buffer. By applying the Sauerbrey approximation, the total mass adsorption for eADF4(C16)-CBD was determined to be $\sim 375 \text{ ng/cm}^2$, significantly higher than the value of $\sim 50 \text{ ng/cm}^2$ observed for eADF4(C16). These findings strongly support the capability of the fusion protein to bind to the cellulose substrate specifically, providing further evidence for the hypothesis of cellulose fibre-enhanced hydrogel formation.

Chapter 2: Recombinant cellulose-binding spider-silk fusion protein: production and characterisation

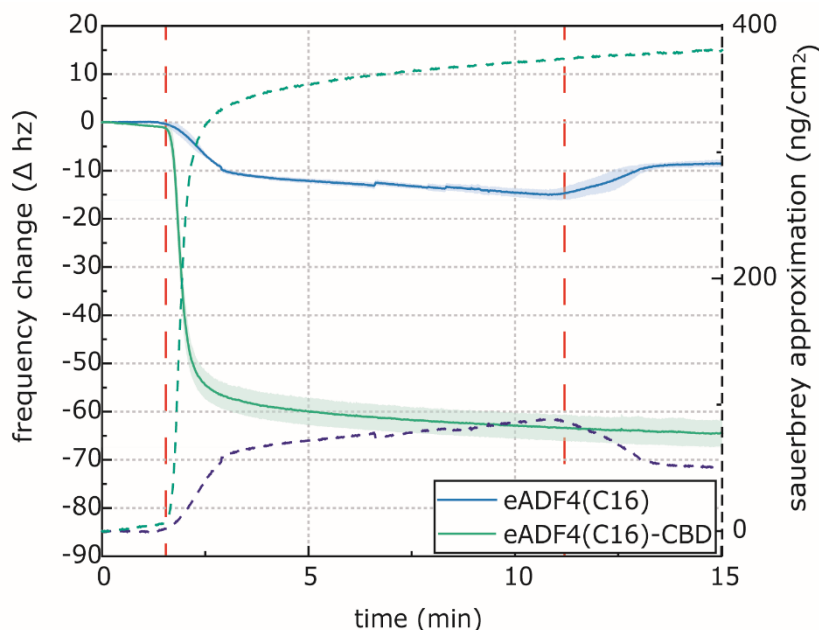


Figure 2-12: QCM-D measurements of 0.125 mg/mL eADF4(C16)-CBD and eADF4(C16) on cellulose films. Dashed red lines indicate a change of the introduced solution. The first line shows the change from the buffer to the protein solution, and the second line indicates the buffer wash following protein incubation. Dashed lines indicate the Sauerbrey approximation for adsorbed protein mass on the surface of the chip. ($n=3$)

2.4 Conclusion

Chapter 2 demonstrated the successful production of the cellulose-binding recombinant spider silk eADF4(C16)-CBD via fed-batch fermentations in *E. coli*. Furthermore, the fusion protein was purified via IMAC. The resulting yield of 0.2 mg per gram of bacteria is relatively low, and further studies should focus on optimising the production and purification process as the ultimate yield from a standard 5L fermentation was approximately 80-100 mg. For the target application of hydrogels, such an amount is sufficient for analysis and small-scale experiments. However, more extensive experiments cannot be conducted with the same batch of protein. Therefore the production and purification with higher yields would be highly desirable for future applications.

Structural analysis of the fusion was occupied, confirming changes in the tertiary protein structure upon denaturation conditions, suggesting an unfolding of the CBD. This leads to the assumption that the domain was correctly folded into its

Chapter 2: Recombinant cellulose-binding spider-silk fusion protein: production and characterisation

native state during protein production and retained the structure throughout the purification process.

Lastly, the fusion protein showed cellulose binding activity in two independent experiments, suggesting an active binding domain.

Chapter 3 Hydrogels from recombinant cellulose-binding spider-silk fusion proteins

3.1 Introduction

After the successful production and characterization of eADF4(C16)-CBD in Chapter 2, the next step is to evaluate the protein's capabilities in forming cellulose-fibre enhanced hydrogels and discuss its potential application in tissue engineering (TE). The unique properties of eADF4(C16)-CBD make it an exciting candidate for hydrogel formation, combining the mechanical strength of spider silk proteins with the functional benefits of cellulose binding.

Cellulose-embedded hydrogels are particularly promising for bone TE due to several key attributes. Cellulose, a natural polymer, provides excellent biocompatibility, minimal cytotoxicity, and is readily available [424]. When integrated into hydrogels, cellulose fibres enhance the mechanical properties, providing the necessary stiffness and structural integrity that are critical for supporting bone tissue regeneration [425]. The presence of cellulose also improves the hydrogel's stability and porosity, which are essential for nutrient diffusion and cell proliferation [426].

To this end, initial experiments utilized 3D bioprinting to create cylindrical structures, allowing for a visual assessment of shape fidelity and the printing behavior of the gel formulations. 3D printing was specifically chosen for this phase to observe how the hydrogels could be manipulated and formed under conditions simulating injectable applications. Understanding the printing and injection behavior is crucial for applications where precise placement and structural integrity are paramount, such as in minimally invasive surgical procedures.

Following the 3D printing experiments, a thorough discussion was carried out using plate-plate rheology to compare the mechanical properties of pure eADF4(C16), eADF4(C16)-CBD gels, and their cellulose fibre blended variants.

Chapter 3: Hydrogels from recombinant cellulose-binding spider-silk fusion proteins

This step was essential to validate the observations from 3D printing and to provide a detailed analysis of the gels' rheological properties.

Scanning Electron Microscopy (SEM) was employed to examine the freeze-dried structures of the gels, offering insights into the microstructural organization and the interactions between the protein and cellulose fibres. This analysis provided a deeper understanding of how the cellulose fibres enhance the mechanical stability and structural integrity of the hydrogels.

Lastly, the potential for TE applications was evaluated by encapsulating MG63 osteoblast-like cells within the gels. The biocompatibility and effectiveness of the hydrogels were assessed using live/dead staining and a proliferation assay over an 8-day period. These experiments aimed to demonstrate the hydrogels' ability to support cell viability and proliferation, key factors for their use in tissue regeneration.

This chapter thus combines advanced fabrication techniques with comprehensive mechanical and biological assessments to establish the viability of eADF4(C16)-CBD hydrogels for tissue engineering applications.

3.2 Material and Methods

Chemicals used in the experiments of this chapter were purchased from Roth (Karlsruhe, Germany) if not stated otherwise. eADF4(C16) was purchased from AMSilk GmbH (Planegg/ Munich, Germany).

3.2.1 Hydrogel preparation

Aqueous eADF4(C16)-based protein solutions were dialysed against a 20% w/v PEG 40000 solution in 10 mM Tris/HCl pH 7.5, 150 mM NaCl, supplemented with 5 mM DTT to concentrated protein solutions through the hygroscopic effect of the PEG solution. The dialysis process was performed using 6-8 kDa cutoff dialysis tubes to maintain slow up-concentration and low-shear. After dialysis, the protein solution was further dialysed against a volume ratio of at least 1:1000 in 10 mM Tris/HCl pH 7.5 buffer for 30 minutes to remove excess salts. The dialysed protein solution was then incubated at 37 °C to induce hydrogel formation for up to 16 hours. The highly concentrated protein solutions were gently mixed with up to 3

Chapter 3: Hydrogels from recombinant cellulose-binding spider-silk fusion proteins

mg/mL CF (C6288, Sigma-Aldrich, Merck, Germany) before gelation for the processing of Cellulose fibre-blended gels.

3.2.2 Rheology

Rheological measurements of the prepared hydrogels were conducted using a TA Instruments DHR2 Rheometer (TA instruments, Germany) with a 25 mm plate-plate geometry and a 0.4 mm gap, employing a lab-made solvent trap to prevent drying of the gels at room temperature. Oscillation mode was used for all pre-formed hydrogels. First, a frequency sweep ranging from 0.1 to 100 rad/s was performed to determine the viscoelastic region of each gel variant. Subsequently, amplitude sweeps were conducted, covering a range of 0.01 to 1000% strain at a frequency of 10 rad/s. Viscosity measurements were obtained using a flow ramp for 500 seconds, with the shear rate gradually increasing from 0.001 to 100/s.

3.2.3 3D printing

Hollow cylinders with a 5 mm diameter and a single filament wall were 3D printed using a pneumatic extrusion bioprinter (3D Discovery Bioplotter RegenHU, Villaz-Saint-Pierre, Switzerland). The printing process involved using 2% w/v eADF4(C16) and eADF4(C16)-CBD gels and was guided by an STL file of a hollow cylinder with a 5 mm diameter, generated with the MM Converter software. Printing was conducted at 10 mm/s, deploying pneumatic print heads equipped with a 3cc (Drifton, Denmark) cartridge and a 27G tapered tip with a 0.2 mm inner diameter (Cellink, Sweden) for precise gel deposition.

3.2.4 Cell culture: viability and proliferation of MG63 cells

The MG63 cell line (ATCC® CRL-1427™) was maintained in culture using Eagle's Minimum Essential Medium (EMEM) supplemented with 10% fetal calf serum (FCS) (SAFC, 12133C), 1% non-essential amino acids (Gibco, Thermo-Fisher, Germany), 2 mM Glutamine, and 50 mM Gentamycin (Gibco, Thermo-Fisher, Germany).

Chapter 3: Hydrogels from recombinant cellulose-binding spider-silk fusion proteins

Routine sub-culturing was performed when cells reached 80-90% confluency. The cells were rinsed with 1x Dulbecco's Phosphate-Buffered Saline (DPBS) and detached using 0.25% Trypsin/EDTA (Gibco, Thermo-Fisher, Germany) for subsequent passages.

For the cell proliferation assay, cells were harvested and counted using a Neubauer haemocytometer. The desired cell count of 8.5×10^5 cells per mL of hydrogel was achieved by transferring the appropriate volume of cell suspension into a centrifuge tube and centrifuging at $300 \times g$ for 5 minutes. The supernatant was removed, and the cells were resuspended in the appropriate volume of growth media to prepare a final media content of 15% v/v in all hydrogel formulations. Pre-gelled silk solutions were carefully mixed with the cell suspension to obtain a final protein concentration of 20 mg/mL.

To initiate the proliferation assay, 75 μL of the gel/cells mixture was transferred to a 96-well plate and allowed to gel completely at 37°C , 5% CO_2 for 1 hour in a cell culture incubator. After gelation, 100 μL cell culture media was added, and metabolic activity was assessed on days 1, 3, 5, and 7 using AlamarBlue™ cell viability reagent. Before a 2.5-hour incubation with the reagent (1:10 dilution in growth media) at 37°C and 5% CO_2 , the wells were rinsed twice with 100 μL DPBS. Fluorescence intensity at 590 nm (Ex.: 530-560 nm) was measured using a plate reader. The remaining reaction solution was replaced with fresh culture media for further incubation.

150 μL of cell-laden bioink was spread into $\mu\text{-Slide 8 Well Glass Bottom}$ wells for live-dead staining. The staining was performed on days 1 and 7 using 1 $\mu\text{g/mL}$ Calcein-AM and 1 $\mu\text{g/mL}$ Ethidium homodimer-1 (EthD-1) in 1x DPBS. After 1-2 hours of incubation at 37°C and 5% CO_2 , cells were washed twice with DPBS and imaged using confocal laser scanning microscopy (CLSM) with a DMI8 microscope (Leica, Germany).

Chapter 3: Hydrogels from recombinant cellulose-binding spider-silk fusion proteins

3.2.5 SEM imaging

The bulk hydrogel was rapidly frozen in liquid nitrogen to prepare samples for SEM imaging and subjected to overnight freeze-drying (Christ Alpha LD plus, Germany). The dried samples were then carefully fractured embedded in carbon cement (Leit-C, PLANO GmbH, Wetzlar, Germany) with the fractured sides facing upward. To enhance conductivity, a thin layer of platinum with a thickness of 1.3 nm was deposited onto the samples using an EM ACE600 sputter coater (Leica, Germany). The SEM images were captured using an Apreo VolumeScope SEM (FEI Thermo Fischer Scientific Inc., MA, USA). The SEM was operated at an acceleration voltage of 2.0 kV and a beam current of 25 pA.

3.2.6 Statistical analysis

Statistical analysis was conducted using OriginPro 2020b software. To assess the statistical significance of differences between groups, analysis of variance (ANOVA) was employed. Post-hoc tests were performed using the Tukey HSD (honestly significant difference) test.

3.3 Results and discussion

3.3.1 Hydrogel formation

After the successful production and characterisation of the cellulose-binding recombinant spider silk protein eADF4(C16)-CBD, the gelation and printability properties were evaluated to assess its potential for hydrogel-based applications. The fusion protein exhibited self-assembly into fibrils when processed and exposed to shear in buffers with low ionic strength, similar to previous observations for eADF4(C16) [56] and its GFP fusion counterpart [74]. This self-assembly phenomenon created soft hydrogels with elastic moduli from 0.2 to 110 kPa for chemically cross-linked gels between 1-7% w/v comparable to soft human tissues [24]. However, for eADF4(C16)-CBD, even in high ionic strength environments

Chapter 3: Hydrogels from recombinant cellulose-binding spider-silk fusion proteins

(≥ 150 mM NaCl), the maximum achievable concentration for eADF4(C16)-CBD solutions was limited to approximately 2% w/v before precipitation occurred.

Surprisingly, the 2% w/v eADF4(C16)-CBD hydrogel demonstrated superior shape fidelity and print accuracy compared to 2% w/v eADF4(C16) hydrogels. Figure 3-1 illustrates the striking difference, as the eADF4(C16) gel print was interrupted due to cylinder collapse after a few layers, while the 2% w/v fusion-gel was printed up to an entire hollow cylinder structure. This improved printability of the fusion protein could be attributed to dimer formation, as previous studies have shown that CBD-spider silk fusion proteins readily form disulphide bridge-driven dimers, enabled by two cysteine residues in the CBD domain [216]. Although different recombinant spider silk and CBD sources were used in those studies, the dimerisation of various CBDs has been reported in the literature [427, 428]. Additionally, non-reducing SDS-PAGE analysis revealed the presence of dimers in the eADF4(C16)-CBD fusion protein (**Figure 3-1E**).

Consequently, dithiothreitol (DTT) was introduced as a reducing agent to prevent dimerisation during the dialysis steps. Notably, the half-life of DTT is significantly decreased during the gelation process at 37°C [429], rendering it inactive within a few hours. Therefore, the dimerisation process was enabled during gelation, enhancing the cross-linking of the hydrogels, leading to a more densely linked gel.

Chapter 3: Hydrogels from recombinant cellulose-binding spider-silk fusion proteins

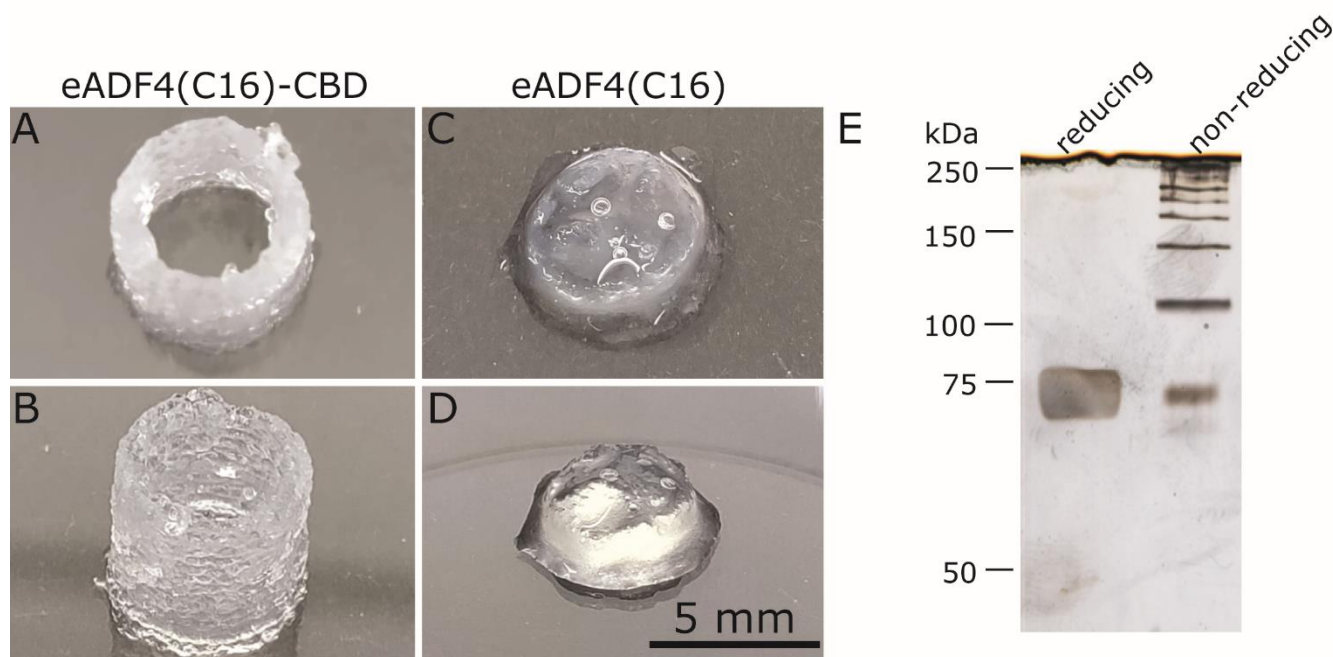


Figure 3-1: 3D-bioprinted hydrogels from eADF4(C16)-CBD (A+B) and eADF4(C16) (C+D). Both gels are at 2% w/v protein concentration and were printed as a hollow cylinder with 5 mm in diameter. E: Silver stained SDS-gel of eADF4(C16)-CBD in reducing and non-reducing conditions.

3.3.2 Enhanced Stiffness of eADF4(C16)-CBD Hydrogels through Cellulose Microfiber Blending

Next, the focus shifted to enhancing the stiffness of the hydrogels, which is crucial for tailoring their mechanical properties to specific applications, particularly in TE. The goal was to create cellulose fibre-enhanced hydrogels to modulate the stiffness and promote improved cell viability and integration. Rheological data provided valuable insights into the viscoelastic properties of these gels and evaluated their suitability for specific applications.

The utilized cellulose fibres were acquired from Merck, Germany and are depicted in **Figure 3-2**. Labelled as „cellulose fibres-medium“, they show an average length of 100 μm , per the manufacturer data and confirmed by SEM images. However, the thickness and uniformity appear to be random, which might be attributed to the manufacturing process. These fibres represent one of the simplest and cheapest forms of cellulose fibres, being processed from plant material and purified to be used in chromatography.

Chapter 3: Hydrogels from recombinant cellulose-binding spider-silk fusion proteins

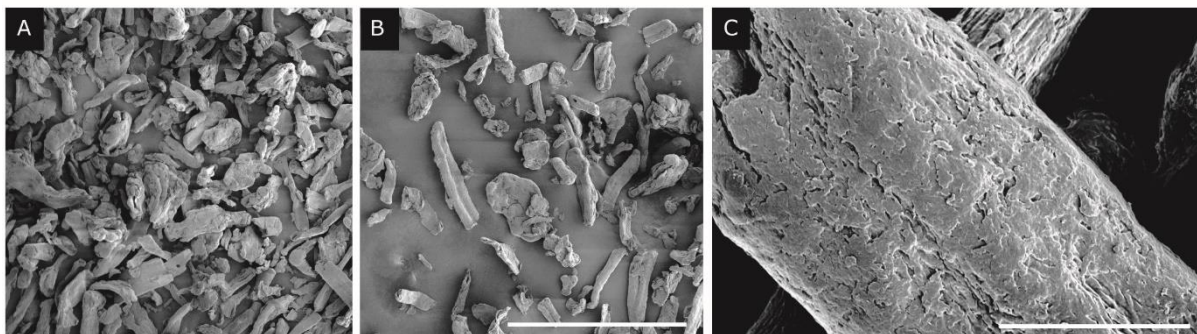


Figure 3-2: SEM micrographs of the used CF to blend with eADF4(C16)-CBD for size analysis. Scale bars: A+B: 200 μm ; C: 20 μm .

Figure 3-3 presents the amplitude sweeps of 2% w/v eADF4(C16) (**Figure 3-3A**) and eADF4(C16)-CBD (**Figure 3-3B**) hydrogels with and without 3 mg/mL cellulose fibres (CF). The resulting moduli exhibited typical profiles for soft hydrogels, similar to those observed for eADF4(C16) hydrogels in previous studies [24, 56].

The amplitude sweep shows elevated moduli for both eADF4(C16)-CBD with and without cellulose-fibre reinforcement throughout the linear viscoelastic region from approximately 0.05 to 2% strain. Furthermore, the flow point for both these gels occurred at a higher strain of $\sim 40\%$ compared to between 10-20% for eADF4(C16) gels, indicating stiffer, more stable gels [430].

Chapter 3: Hydrogels from recombinant cellulose-binding spider-silk fusion proteins

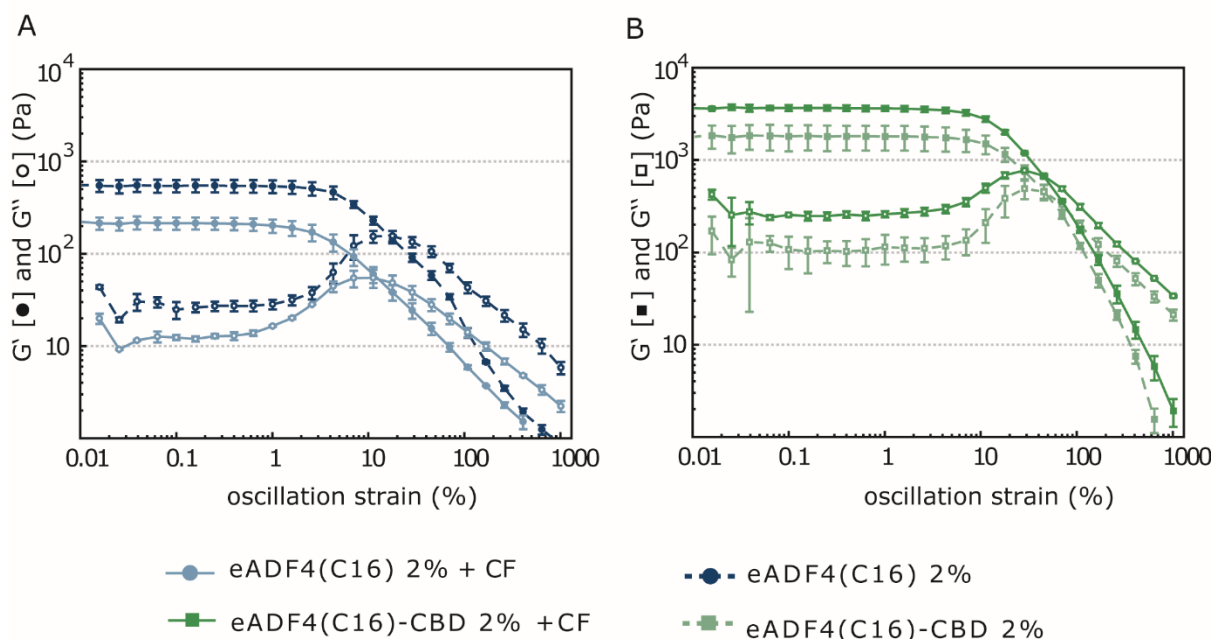


Figure 3-3: Amplitude sweep of 2% w/v eADF4(C16) (A) and eADF4(C16)-CBD (B) with and without 3 mg/mL cellulose fibres (CF). ($n=2$)

The printability results (**Figure 3-1**) suggested that the cellulose-binding hydrogels had higher moduli and a flow point at higher strain rates than unmodified hydrogels. This behaviour aligns with the observations made for stiffer gels of unmodified eADF4(C16) at higher concentrations [58]. Notably, with eADF4(C16)-CBD, the increase in stiffness could be achieved while keeping the protein concentration the same, which is suggested to be more favourable for TE applications. Higher protein concentrations can lower water content and pore size, potentially hindering cell viability [431, 432].

The stiffness of eADF4(C16)-CBD hydrogels, as displayed as elastic modulus in **Figure 3-4** and evidenced by the stress-strain behaviour in **Figure 3-5**, significantly increased compared to the unmodified protein. Moreover, the mechanical properties of the cellulose-binding variant were further enhanced upon blending with cellulose fibres. In contrast, hydrogels formed by eADF4(C16) showed decreased stiffness upon blending, which could be attributed to the disruption of physical cross-linking by the binding to cellulose fibres when blended with 3 mg/mL.

Chapter 3: Hydrogels from recombinant cellulose-binding spider-silk fusion proteins

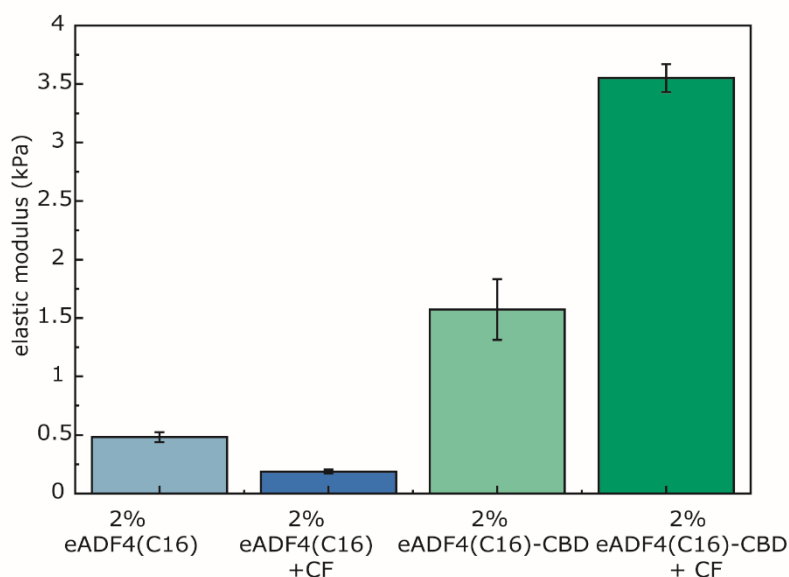


Figure 3-4: Stiffness of 2% w/v hydrogels of eADF4(C16) and CF-enhanced eADF4(C16)-CBD ($n=3$).

Interestingly, even without the incorporation of cellulose fibres, eADF4(C16)-CBD hydrogels at a concentration of 2% w/v exhibited a higher stiffness than the GFP fusion hydrogels presented by Humenik et al. [78] by surpassing a maximal shear stress of 250 Pa. This observation was attributed to the dimerisation capabilities of eADF4(C16)-CBD combined with the physical cross-linking that occurs in all eADF4(C16)-based hydrogels.

Notably, the cellulose fibre-enhanced hydrogels showed a nearly 100% increase in yield stress compared to the GFP variant, indicating a significant improvement in mechanical strength. This increase was attributed to the additional binding of the fusion protein to CF, which act as a semi-chemical cross-linking agent.

Figure 3-5B illustrates the viscosity profile of the four tested gel variations, confirming their shear-thinning behaviour, which is essential for successful 3D printing processes [58]. Interestingly, the eADF4(C16)-CBD hydrogels exhibited a unique viscosity profile, showing no significant differences between cellulose fibre-blended and unblended gels. In contrast, eADF4(C16) hydrogels exhibited higher viscosity upon blending with cellulose fibres than their unblended counterparts.

Chapter 3: Hydrogels from recombinant cellulose-binding spider-silk fusion proteins

These observations could be explained by the role of cellulose fibres in the gel structure. Specifically, the presence of CF contributes to increased resistance to flow within the gel, leading to higher viscosity [433]. However, these fibres may also disrupt the physical cross-linking between fibrils in eADF4(C16) hydrogels. In CBD gels, conversely, the cellulose-binding domain of the fusion protein exhibits an affinity for cellulose fibres, enabling the protein to form tight connections with the cellulose, thereby maintaining the overall structure and cross-linking density of the gel. As a result, the increased resistance to flow expected when adding cellulose fibres may be counteracted by the more robust cross-linking and interconnected network in the CBD gels, resulting in minimal changes to the viscosity profile.

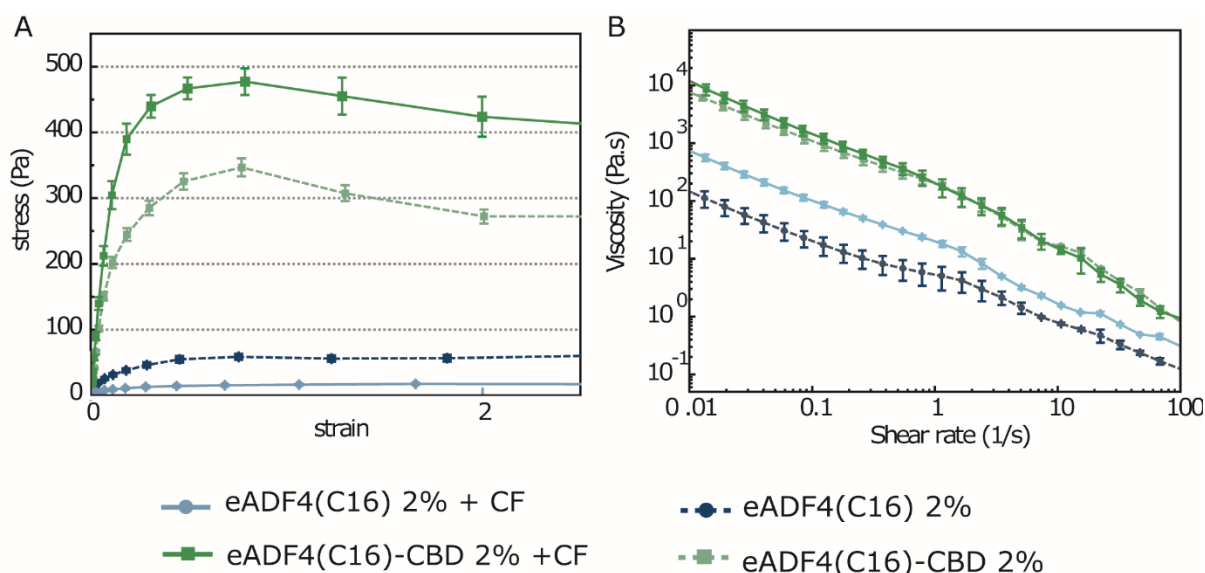


Figure 3-5: A: Stress-strain behaviour, and B: Viscosities of the different hydrogel blends. $n=2$

Figure 3-6 depicts the hypothesised gelation process involving eADF4(C16)-CBD and cellulose fibres, forming a "double cross-linked" hydrogel with enhanced mechanical properties. The process can be divided into two main steps that elucidate the hydrogel formation:

- i) Mixing cellulose fibres and concentrated eADF4(C16)-CBD in an aqueous solution initiates the interaction between the cellulose fibres and eADF4(C16)-CBD fusions.

Chapter 3: Hydrogels from recombinant cellulose-binding spider-silk fusion proteins

ii) Due to the binding between protein and cellulose, the local density of protein bound to cellulose rapidly increases. This leads to the formation of numerous network cross-links and subsequent self-assembly of the protein into fibrils, similar to the process observed in unmodified eADF4(C16) hydrogels [24].

The resulting hydrogels possess a "double cross-linked" network structure, where interactions between the CBD and cellulose occur on one side, while hydrophobic interactions between the fibrils contribute to the overall gel structure on the other side. This double cross-linking mechanism enhances the mechanical properties of the hydrogel.

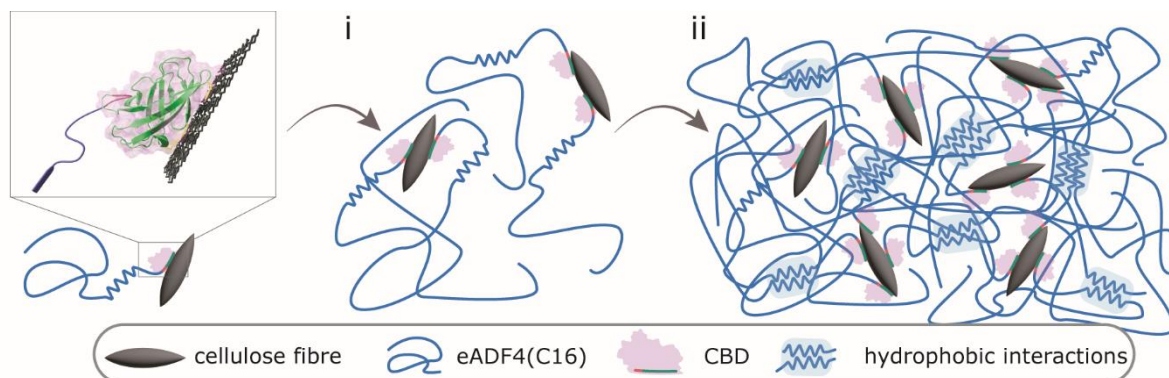


Figure 3-6: Schematic of the hypothesised gelation process. *i)* The eADF4(C16)-CBD protein (blue: eADF4(C16) moiety, green with purple cloud: CBD) binds to cellulose particles (black) in the solution. *ii)* The dense protein-cellulose network is further cross-linked via hydrophobic interactions of the protein fibrils (blue boxes).

SEM imaging of the freeze-dried bioink formulations (**Figure 3-7**) provided insights into the microstructure of the hydrogels. Both eADF4(C16) and cellulose fibre-enhanced eADF4(C16)-CBD hydrogels exhibited a similar overall structure with consistent pore sizes. The SEM images revealed the presence of cellulose fibres deeply embedded within the proteinaceous matrix, indicating close interaction between cellulose and eADF4(C16)-CBD. This finding supports the hypothesis that the CF can serve as anchoring points for cells within the gel matrix and act as integrated mechanical enhancers within the gel network.

However, it is essential to note that the SEM images depict the freeze-dried state of the hydrogels, and the actual matrix structure in its hydrated state will differ. A hydrated gel would show larger and more flexible pore structures. Furthermore, it should be noted, that no cell-containing hydrogels have been imaged via SEM. The combination of sample preparation for cells for SEM, involving dehydration steps

Chapter 3: Hydrogels from recombinant cellulose-binding spider-silk fusion proteins

and the proteinaceous matrix structure of the protein pose a challenge in imaging both in a near-native state as the dehydrating steps would shrink down the pore size. Simultaneously, freeze-drying of the cells would alter their morphology. Nonetheless, these observations provide valuable insights into the structural characteristics of the hydrogels and support their potential as injectable biomaterials for treating small and potentially deeply located defects in bone and cartilage.

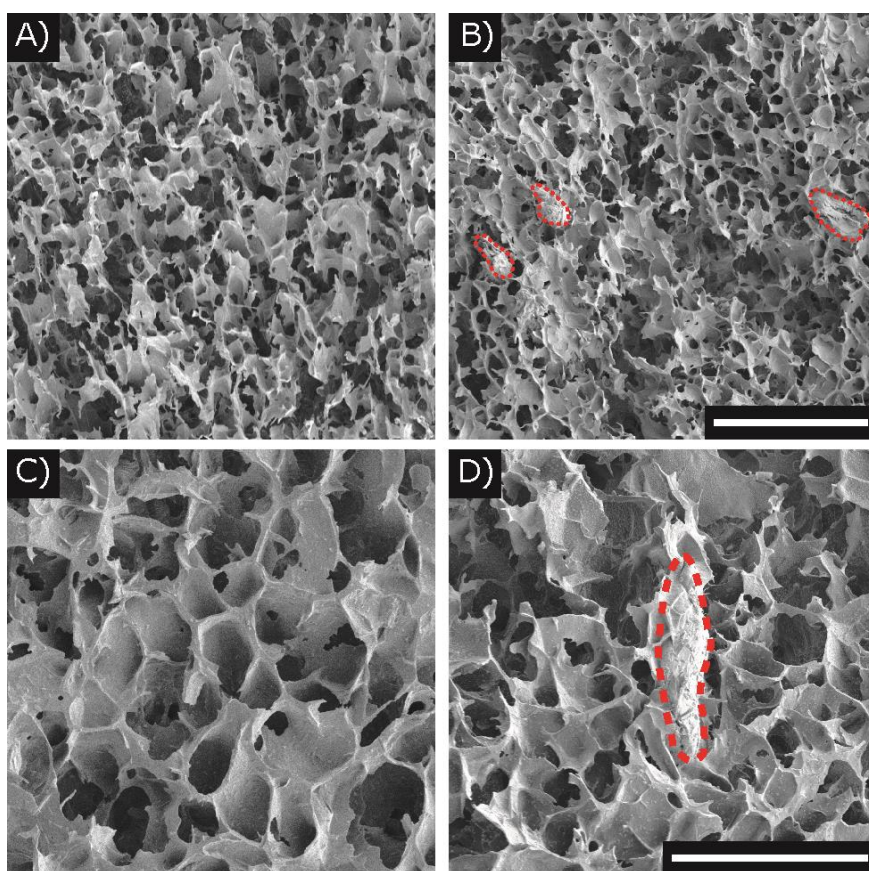


Figure 3-7: SEM images of the freeze-dried bioink formulations. A)+C) eADF4(C16); B)+D) eADF4(C16)-CBD. Red dotted lines highlight incorporated cellulose fibres; scale bars: A)+B): 100 μm ; C)+D): 50 μm .

3.3.3 Application in Tissue Engineering: Injectable hydrogels for bone defects

So far, cellulose-fibre-enhanced eADF4(C16)-CBD hydrogels demonstrated improved mechanical properties compared to hydrogels from eADF4(C16) at the same protein concentration. Furthermore, the printability, and thus potential

Chapter 3: Hydrogels from recombinant cellulose-binding spider-silk fusion proteins

injectability of the fusion, was maintained, showing enhanced resolution and shape fidelity. These findings suggested that these hydrogels could pose a suitable scaffold for TE when injected into, for example, bone defects or when used for cartilage repair without extensive incisions into the patient's body. Therefore, Cell viability and proliferation examinations have been conducted as a first approximation to potential future applications using the MG63 osteosarcoma-derived cell line [434]. **Figure 3-8** summarises the findings with a proliferation assay over the period of 8 days (**Figure 3-8A**). Here, the proliferation rate was compared between 2 % w/v eADF4(C16) and fibre-enhanced eADF4(C16)-CBD gels, showing no significant difference after one day of cultivation. However, starting at day three until the end of the experiment on day 8, the proliferation rate was significantly elevated for cells growing in the eADF4(C16)-CBD gels compared to the unmodified counterpart, indicating a more suitable environment for tissue development.

Furthermore, Live/dead staining revealed minimal dead cells in both ink formulations (**Figure 3-8B-E**). Previous studies on cell proliferation in eADF4(C16) hydrogels have shown only a slight increase in cell number, which could be marginally improved by incorporating the cell adhesion peptide RGD [57, 59]. Additionally, the results of these studies indicated a round morphology of the encapsulated cells, a characteristic hypothesized to be enhanced by incorporating solid anchor points into the ink formulation. Many studies have demonstrated this strategy's effectiveness in varying hydrogel formulations [435-437], suggesting the potential of using blended cellulose fibres as these anchoring sites.

Interestingly, the presence of cellulose fibres in eADF4(C16)-CBD hydrogels not only increased the proliferation rate compared to eADF4(C16) gels but also resulted in significant changes in cell morphology (**Figure 3-8F+G**). As hypothesised before, this indicates that the cells attached to the micropatterned cellulose fibres within the gel, which are approximately 50-100 μm long, as shown in **Figure 3-2**. This attachment allows the cells to spread and develop their morphology, a phenomenon suggested in the literature before [438, 439].

Chapter 3: Hydrogels from recombinant cellulose-binding spider-silk fusion proteins

A crucial aspect of the enhanced cell spreading and growth observed in cellulose-embedded hydrogels can be attributed to the phenomenon of biofouling. Biofouling refers to the accumulation of microorganisms, cells, and biological molecules on a surface, which can significantly influence the biological interactions at the material interface. In the context of tissue engineering, biofouling of cellulose fibers within hydrogels can play a beneficial role. Cellulose, being a natural polysaccharide, provides an excellent substrate for protein adsorption from the surrounding biological environment or cell culture media [440]. These adsorbed proteins can act as mediators for cell adhesion, promoting integrin binding and subsequent cell spreading. Furthermore, the natural hydrophilicity and rough surface texture of cellulose fibers enhance initial cell attachment and proliferation [441]. The inherent biocompatibility and minimal cytotoxicity of cellulose ensure that these biofouling interactions do not elicit adverse immune responses, making cellulose-embedded hydrogels an ideal scaffold material for supporting osteoblast activity and bone tissue growth.

In contrast to 2D osteoblast cell culture observations on the surface of hydrogels, where stiff matrices have shown favourable outcomes in terms of attachment and proliferation [113, 442, 443], further studies suggested that highly porous and comparatively soft hydrogels are suitable biinks for encapsulated osteoblasts [431, 432]. In 3D environments, the stiffness of the matrix was shown to have limited effects compared to factors such as mass transfer and available area for proliferation, which seem to have a more significant impact on cell fate [113].

Nevertheless, eADF4(C16)-CBD-based hydrogels for TE can never be load-bearing due to their limited mechanics. However, other applications where the load is not crucial can be targeted due to the exceptional ECM-mimicking properties of hydrogels. Furthermore, softer gels have been demonstrated to promote mineralisation [431], potentially stiffening the gels *in vivo* once the tissue signals its need.

However, regardless of whether softer or stiffer matrices are utilised, encapsulated osteoblasts have mainly exhibited spherical morphology and decreased cell numbers over time without the addition of solid anchor points [113, 444-446].

Chapter 3: Hydrogels from recombinant cellulose-binding spider-silk fusion proteins

This novel bioink formulation meets the suggested requirements, as even the stiffer CF-blended eADF4(C16)-CBD hydrogels (~ 3.5 kPa, **Figure 3-4**) remain relatively soft compared to alternatives found in the literature (several 100 kPa [113]). Considering these aspects, it is remarkable that a steady proliferation profile and observable cell spreading in an injectable and form-stable hydrogel could be observed simultaneously.

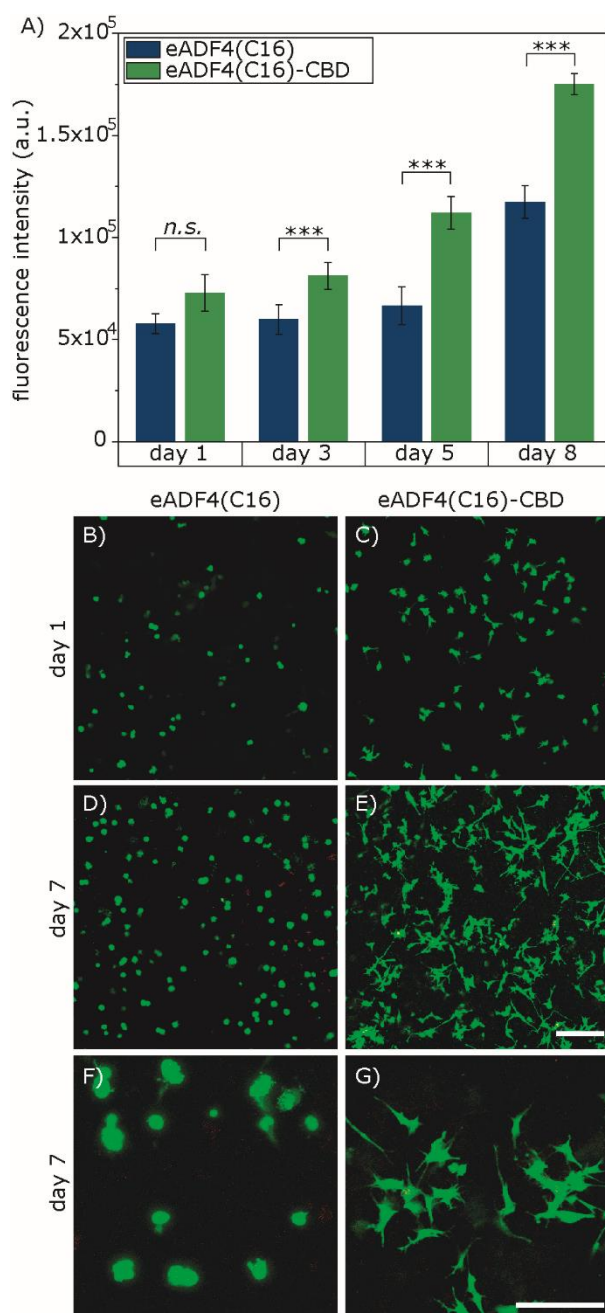


Figure 3-8: MG63 cell culture on 2% (w/v) eADF4(C16) and eADF4(C16)-CBD (blended with 0.3% (w/v) cellulose fibres) hydrogels. A): Proliferation assay of MG63 cells in the bioink formulations

Chapter 3: Hydrogels from recombinant cellulose-binding spider-silk fusion proteins

over 8 days; *** $p \leq 0.001$. B)-E): Confocal micrographs of Live (green)/Dead (red) stained MG63 cells in the bioinks after 1 and 7 days; Scale bar: 200 μm . F)+G): magnified micrographs of the cell morphology at day 7; scale bar: 200 μm .

3.4 Conclusion

Chapter 3 delved into utilising the novel cellulose-binding fusion protein eADF4(C16)-CBD for hydrogel applications. The investigation revealed promising properties and capabilities of the fusion protein in the context of hydrogel engineering.

The findings demonstrated that eADF4(C16)-CBD retains the inherent ability of the unmodified protein to form hydrogels and surpasses it in terms of printability and shape fidelity. This suggests that the fusion protein offers a solid foundation for designing and fabricating hydrogels with precise geometries and structures.

Moreover, rheological evaluations unveiled that incorporating cellulose fibres into eADF4(C16)-CBD hydrogels further enhances their mechanical properties. The presence of cellulose fibres results in a double cross-linked network, combining the hydrophobic interactions characteristic of the unmodified gels with the cellulose-binding capabilities of the fusion proteins CBD. This unique combination of interactions imparts the hydrogels with increased stiffness and improved mechanical integrity.

To assess the suitability of eADF4(C16)-CBD hydrogels for Tissue Engineering applications, *in vitro* experiments were conducted using the MG63 cell line. The results revealed significantly improved cell proliferation rates and distinctive cell morphologies within the cellulose fibre-enhanced eADF4(C16)-CBD hydrogels compared to eADF4(C16) hydrogels of the same concentration. This suggests that incorporating cellulose fibres provides anchor points for cells, promoting cell attachment, spreading, and morphological development. These findings highlight the potential of eADF4(C16)-CBD hydrogels as injectable biomaterials.

However, there are limitations of the eADF4(C16)-CBD-based gel formulations in regards to bone TE. More precisely, the bioprinting approach described in chapter

Chapter 3: Hydrogels from recombinant cellulose-binding spider-silk fusion proteins

3.3.1 has not been carried out with cells in the gel formation. It needs to be verified that the incorporated cellulose-fibres do not negatively impact the cell viability upon the shear-inducing printing procedure. Additionally, to further research the suitability of the gel formulation for TE approaches, different cell types should be introduced and evaluated, potentially looking in other fields than bone-related TE with a high focus on stiff gels. As described in 3.3.3, the hydrogels presented here are, despite the increased stiffness profile, still in the low-stiffness regime of hydrogels for TE. Considering this, applications related to brain TE might be relevant for this gel formulation. However, only for in vitro and research/diagnostic purposes as the introduction of non-degradable cellulose-fibres in brain tissue should be avoided at all cost.

Lastly, while cellulose offers numerous advantages for TE, one significant challenge is its lack of biodegradability in human systems. Humans do not possess the necessary enzymes, such as cellulases, to break down cellulose into its constituent sugars. This means that cellulose-based scaffolds can persist in the body for extended periods, which can be both beneficial and problematic. On the one hand, the persistence of cellulose can provide long-term structural support, which is particularly advantageous in bone tissue engineering where gradual scaffold degradation and replacement by natural bone can be desirable. On the other hand, the inability to degrade cellulose may lead to potential issues with scaffold clearance and integration. Over time, the accumulation of non-degradable cellulose could provoke a foreign body response, leading to chronic inflammation or fibrous encapsulation.

In summary, this chapter showcased the promising properties and capabilities of eADF4(C16)-CBD for hydrogel applications. The fusion protein combines the unique features of the unmodified eADF4(C16) protein with cellulose-binding capabilities, resulting in hydrogels with enhanced printability, mechanical properties, and cellular compatibility. These findings lay the foundation for further exploration and development of eADF4(C16)-CBD hydrogels for various tissue engineering and regenerative medicine applications, where controlled mechanical properties and cell interactions are crucial for successful tissue regeneration.

Chapter 3: Hydrogels from recombinant cellulose-binding spider-silk fusion proteins

Chapter 4 Endothelial cell-selective recombinant spider silk fusion protein: production and characterisation

4.1 Introduction

Chapter 4 focuses on the REDV-modified recombinant spider silk variant, eADF4(C16)-REDV, as a coating material for drug-eluting stents (DES). For this purpose, first, the design, production and purification of the protein are described in this chapter, before **Chapter 5** governs the application thereof as a potential drug-eluting coating.

First, the eADF4(C16)-REDV protein was synthesised leveraging an *E. coli* expression system and purified from inclusion bodies. Next, the characterisations conducted in this chapter include observations regarding protein identity using MALDI-TOF, SDS-PAGE and CD spectroscopy. Furthermore, the purity of the obtained protein was confirmed by these measurements and additional fluorescence spectroscopy. Lastly, the peptide modification's feasibility with the REDV sequence was examined by cell culture experiments comprising of attachment and proliferation studies.

Chapter 5 will follow up these characterisations in applying the protein as films and coatings for cell culture or to provide coatings on 316L stainless steel, chosen as a representative material for metal stents. A series of biological assays were conducted to demonstrate the potential of eADF4(C16)-REDV as a suitable coating material for drug-eluting stents. These assays included cell adhesion and growth tests, hemocompatibility with human whole blood, enzymatic degradation, and drug elution.

Chapter 4: Endothelial cell-selective recombinant spider silk fusion protein: production and characterisation

4.2 Material and Methods

Chemicals for the conduction of the experiments of this chapter were purchased from Roth (Karlsruhe, Germany) if not stated otherwise. eADF4(C16) was purchased from AMSilk GmbH (Planegg/ Munich, Germany). All nucleotide sequences were acquired from Eurofins Genomics (Germany). Enzymes were acquired from New England Biolabs (Germany) and used according to the manufacturer's protocol.

4.2.1 Cloning of the REDV-modified eADF4(C16) protein

The cloning of eADF4(C16)-REDV was conducted using the same method described in **2.2.1**. The sequence used for further modification on the C-terminus of eADF4(C16) was: GGGGS GREDVYG. The short, glycine-rich sequence serves as a spacer between both fusion partners. Furthermore, the target sequence was incorporated into a pET29 vector instead of pET28a.

4.2.2 Protein Production and inclusion body purification

Modified recombinant spider silk proteins were produced using an *E. coli* expression system. The eADF4(C16)-RGD fusion protein was synthesised by using the BL21 gold (DE3) (Novagen, Germany) strain of *E. coli* in a fed-batch fermentation process, as detailed in prior literature [303].

The fermentation process was carried out as described in **2.2.2**. However, the production process was initiated by introducing a 1M concentration of isopropyl-beta-D-thiogalactopyranoside (IPTG) over 16 hours, and the growth phase was maintained at 37°C.

A representative fermentation monitoring is shown in **Figure 4-1** where a typical profile for an overnight inclusion body-producing profile is depicted. The start of the growth phase is observable from 0 to approximately 250 minutes, where the temperature was at a constant 37°C. This period is shorter than for producing eADF4(C16)-CBD, as described in **chapter 2.2.2**, because the initial inoculum

Chapter 4: Endothelial cell-selective recombinant spider silk fusion protein: production and characterisation

volume was greater, and the temperature was at the ideal value for fast *E. coli* growth. This process was chosen to achieve a sufficient cell number in the first hours to enable the following induction with 1M IPTG at 30°C overnight. Doing so initiated the overexpression of the protein and storage in inclusion bodies. In contrary to eADF4(C16)-CBD, eADF4(C16)-REDV does not feature any secondary structures in the solution, eliminating the need for delicate induction time monitoring to avoid misfolding and inclusion body formation. Therefore, the high yield of an inclusion body fermentation could be exploited with up to 20 hours of induction times being employed without risking obtaining non-functional products [174]. The fermentation profile shown in **Figure 4-1** closely resembles the one shown in **Figure 2-3**. However, the temperature profile varies, resulting in a spike in pO₂ around 450 minutes when the temperature was regulated from 37°C to 30°C, as oxygen has a higher solubility at higher temperatures and additional O₂ was already supplied to maintain the set value of 40%. The feed was set to 4% for the remaining ~1100 minutes, and the profile showed no irregularity, suggesting continuous aerobic protein production.

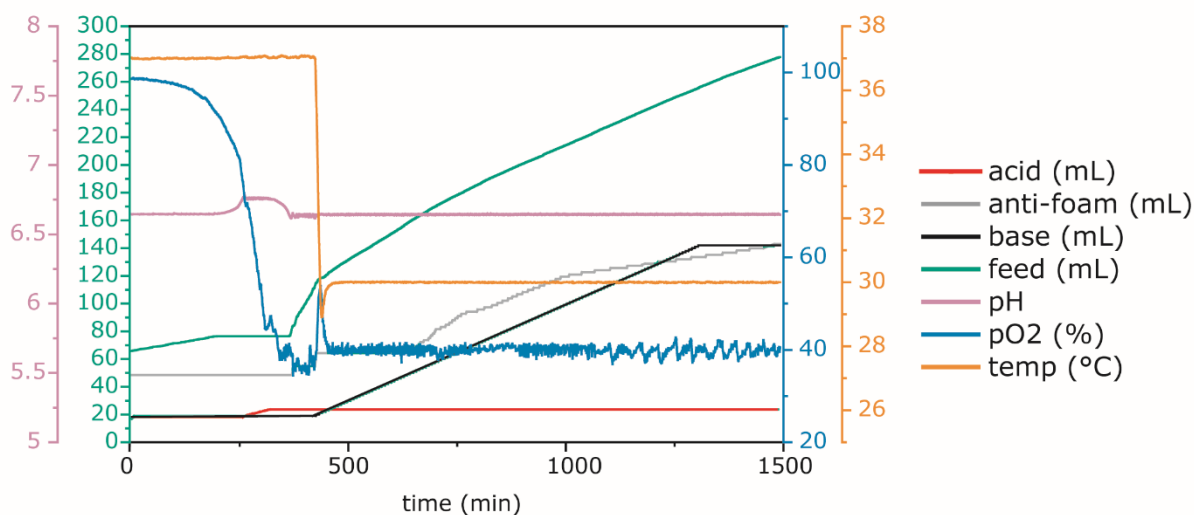


Figure 4-1: Representative fermentation profile of overnight induction for the high-yield production of eADF4(C16)-REDV.

For protein purification from inclusion bodies, the harvested bacterial suspension underwent two rounds of washing using a buffer solution of 150 mM NaCl and 10

Chapter 4: Endothelial cell-selective recombinant spider silk fusion protein: production and characterisation

mM Tris/HCl at a pH of 7.5 following the fermentation and harvest processes. Subsequently, the cellular structures were disrupted for 4 hours through the introduction of lysozyme at a concentration of 0.2 mg/mL within a solution containing 5 mM ethylenediaminetetraacetic acid (EDTA) and 1 mM phenylmethylsulfonyl fluoride (PMSF). Next, the cells were subjected to disruption using a high-pressure homogeniser (Niro Soavi, Italy, model NS1001L2K) with two cycles of 150 bar. The homogenised suspension underwent centrifugation at 4°C and 22,000 x g for 45 minutes. Isolation of the released inclusion bodies was achieved by first suspending the remaining pellet in a detergent buffer with a ratio of 1:10 (60 mM EDTA, 2% (v/v) Triton X-100, 1.5 M NaCl) and allowing it to incubate for 30 minutes. Initially, the dispersion was centrifuged at 4°C 22,000 x g for 15 minutes. Subsequently, the resulting pellet was resuspended in a Tris-EDTA buffer containing 1 mM EDTA, 100 mM Tris-HCl at a pH of 7.5, and 100 mM NaCl. Next, a 30% ammonium sulphate precipitation was carried out overnight. Subsequently, the precipitate underwent centrifugation at 4°C and 22,000 x g for 45 minutes. The resulting pellet was washed using 8M carbonyl diamide (urea) for 1 hour, followed by another round of centrifugation. The process of urea washing was repeated twice more. The pellet was subjected to a series of water washes until the absence of DNA contamination was confirmed by observing the absorbance at a wavelength of 260 nm using a NanoDrop 1000 (Peqlab, Germany) spectrophotometer. Subsequently, the obtained material underwent lyophilisation (Alpha 1-2 Ldplus, Christ, Germany) for long-time storage of the purified eADF4(C16)-REDV product.

The inclusion body purification yielded up to 30 mg of protein per gram of bacteria and was further lyophilised for long-time storage. **Figure 4-2A** shows a schematic of the eADF4(C16)-REDV protein with a T7-tag at the N-terminus, and the REDV peptide on the C-terminus of the 16 C-modules. The purity of the lyophilised protein was confirmed by SDS-Page, followed by silver staining (**Figure 4-2B**), as no additional bands are visible. eADF4(C16)-REDV showed no difference to eADF4(C16) in its mobility during electrophoresis, suggesting the same or very similar molecular weight, as expected for such a short peptide modification. However, as discussed in **2.2.4**, eADF4(C16)-based proteins display an intriguing

Chapter 4: Endothelial cell-selective recombinant spider silk fusion protein: production and characterisation

characteristic of reduced mobility. This is evidenced by observing a protein band between 50 and 75 kDa during gel electrophoresis.

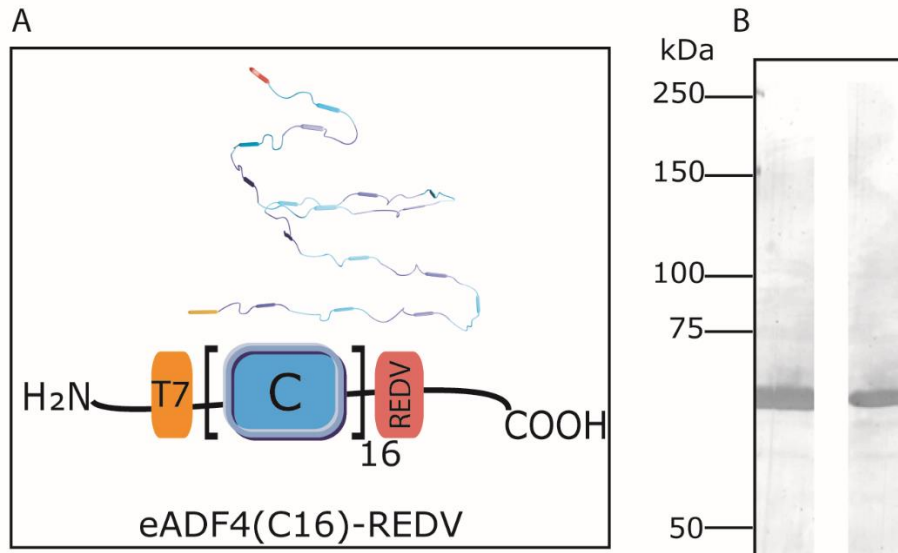


Figure 4-2: A) A schematic of the fusion protein eADF4(C16)-REDV. The individual C-modules are shown in light and dark blue, the N-terminal T7-tag is highlighted in orange and the C-terminal REDV peptide in red. B) The silver-stained SDS-PAGE gels of eADF4(C16) (left) and eADF4(C16)-REDV (right) show the purity of the product and similar molecular weights.

Due to the inaccurate size display of both protein variants in the SDS-gel, MALDI-TOF (**Figure 4-3**) has been conducted to confirm the identity of the product and the purchased control protein eADF4(C16). The theoretical molecular weight of eADF4(C16)-REDV is 48.7 kDa and 47.6 kDa for eADF4(C16) as computed with the GENTle software.

Chapter 4: Endothelial cell-selective recombinant spider silk fusion protein: production and characterisation

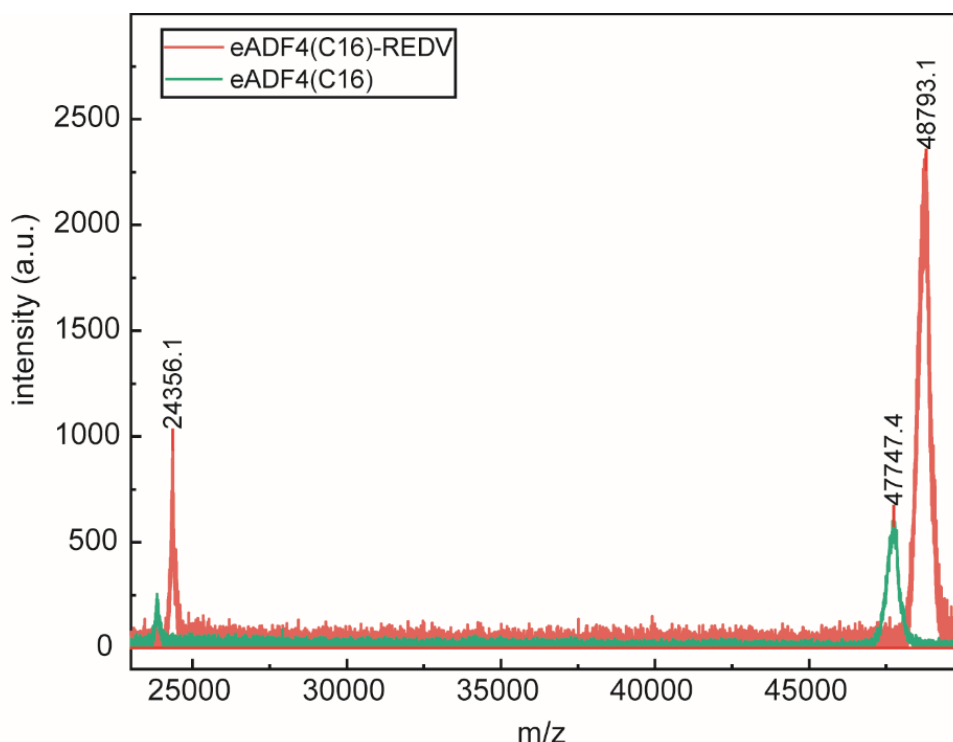


Figure 4-3: MALDI-TOF was used to determine the molecular weight of eADF4(C16) (green) and the REDV variant (red). Results indicate that eADF4(C16) and eADF4(C16)-REDV molecular weights are 47.7 kDa and 48.7 kDa, respectively. A smaller peak at one-half the molecular weight corresponds to molecules with a z value of 2.

4.2.3 Preparation of aqueous eADF4(C16) solutions

Given their water-insoluble nature, a two-step process is employed to achieve aqueous solutions for all eADF4(C16)-based proteins intended for characterisation measurements. First, the proteins are solubilised in a 6M guanidinium thiocyanate (GdmSCN) solution. Subsequently, they are dialysed against a 10 mM Tris/HCl buffer at pH 7.5. The dialysis is carried out in a buffer volume that is always at least 100 times the volume of the protein solution, with the buffer being changed at least three times to ensure efficient removal of GdmSCN.

Chapter 4: Endothelial cell-selective recombinant spider silk fusion protein: production and characterisation

4.2.4 Protein characterisation

Protein characterisation was carried out by far-UV CD (2.2.5), SDS-Page (0) and MALDI-TOF (2.2.4) under the same conditions, as described in their respective chapters.

Additionally, fluorescence spectroscopy was carried out to validate the proteins' purity. Therefore, spectra were obtained by recording the emission of protein solutions from 300 nm to 450 nm at a 0.5 mg/mL concentration. The solutions were prepared in analytically pure 10 mM Tris/HCl (pH 7.5) and measured in quartz cuvettes. A fluorescence spectrometer, FluoroMax-3 (Jobin-Yvon Inc.), was used for the measurements with excitation wavelengths set at 280 nm for tryptophan residues and 220 nm for tyrosine residues.

4.2.5 Cell culture: adhesion and proliferation

For all cell culture experiments, thin films of eADF4(C16) and modifications thereof were produced by casting from hexafluoroisopropanol (HFIP, Merck, Australia). 10 mg/mL solutions were cast directly into the wells of tissue culture-treated 48-well plates (Corning Costar TC-Treated Multiple Well Plates, Merck, Australia) and allowed to dry overnight. The coated wells were then post-treated by incubating with 80% w/v ethanol for 30 minutes, followed by a rinsing step with MQ-H₂O.

For the cell culture experiments, three distinct cell types were used: human umbilical vein endothelial cells (HUVEC, C2519AS, Lonza, Australia), human coronary artery smooth muscle cells (HCASMC, FC-0031, Lifeline Cell Technology, USA), and neonatal human dermal fibroblasts (NHDF, CC-2509 Lonza, Australia). Maintenance and expansion of the cells was executed at 37 °C in a 5% CO₂, humidity-controlled environment (SafeGrow Pro, Bioari, Italy), utilising their respective growth media: EGM-2 BulletKit Medium (Lonza, Australia), Vasculife SMC Complete Kit (FC-0031, Lifeline Cell Technology, USA), and FGM-2 Fibroblast Growth Medium-2 BulletKit (CC-2509 Lonza, Australia). Passaging of the cells was occupied once a confluence of 70-80% was reached, and no passage after 9 cycles was utilised for experiments.

Chapter 4: Endothelial cell-selective recombinant spider silk fusion protein: production and characterisation

Cell adhesion was assessed on silk substrates by seeding 30,000 cells in 200 μ L of corresponding cell culture media into wells of a 48-well tissue culture treated plate (Corning Costar TC-Treated Multiple Well Plates, Merck, Australia). The wells were protein-coated, with uncoated tissue-treated wells serving as controls. After an incubation period of 4 hours, the wells underwent a wash procedure with phosphate-buffered saline (PBS, Gibco, 100110023, Merck, Australia) to eradicate non-adherent cells. The relative cell attachment was quantified using the CellTiter-Glo assay [447] with a GloMax Discover Microplate reader (Promega, Australia) guided by the manufacturer's protocol.

In the proliferation assay, each well was seeded with a suspension of 3,000 cells in 200 μ L medium. The culture media was replaced every 48 hours. At specified intervals for measurement, the wells were rinsed with PBS and subjected to the CellTiter-Glo assay, as detailed by the manufacturer's protocol.

Simultaneously, additional cell-seeded wells were prepared for microscopy on each measurement day by undergoing fluorescent staining. These wells were washed and fixed using 3.7% paraformaldehyde (Merck, Australia) and permeabilised with 0.1% Triton X-100 (Merck, Australia) in PBS. Staining procedures involved the use of 300 nM 4',6-diamidino-2-phenylindole and dihydrochloride (DAPI, Merck, Australia) for cell nuclei, phalloidin-rhodamine (ActinRed™ 555 ReadyProbes, Thermo Fisher, Australia) for F-actin, and Anti-CD31 antibodies conjugated with Alexa Fluor® 488 [JC/70A] ab215911 (abcam, USA) for the PECAM-1 molecule within endothelial cell walls. These staining steps were conducted in alignment with the instructions provided by the manufacturers.

4.2.6 Statistical analysis

Statistical analysis was conducted using OriginPro 2020b software. To assess the statistical significance of differences between groups, analysis of variance (ANOVA) was employed. Post-hoc tests were performed using the Tukey HSD (honestly significant difference) test.

Chapter 4: Endothelial cell-selective recombinant spider silk fusion protein: production and characterisation

4.3 Results and discussion

4.3.1 Protein characterisation

Circular dichroism (CD) spectra (**Figure 4-4A**) showed no discernible differences between eADF4(C16) and the REDV variant, indicating that the REDV modification did not have a significant impact on secondary protein structure showing a minimum at 220 nm, which is in accordance with other peptide modified sequences such as eADF4(C16)-RGD which yield intrinsically unfolded structures in aqueous solutions [303].

Additionally, the absence of tryptophane residues in eADF4(C16)-REDV enabled the usage of fluorescence spectroscopy to confirm the product purity. **Figure 4-4B** shows a the combined emission spectra of excited tyrosine and tryptophane residues with a peak for tyrosine, which is present in the protein structure, and no signal for tryptophane. The missing signal for tryptophane is an indicator of protein purity, as most *E.coli* proteins comprise tryptophan residues [174]

These results combined demonstrate that the novel REDV-spider silk fusion protein was successfully produced and isolated using an *E. coli* expression system.

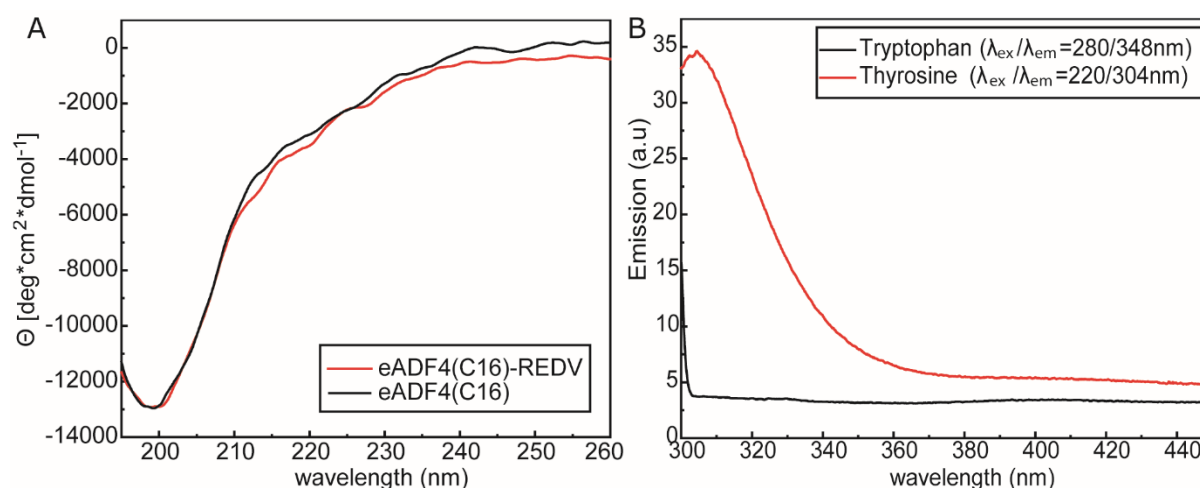


Figure 4-4: A): The CD-spectra of both eADF4(C16) variants from 195 to 260 nm show no significant changes caused by the peptide modification. B): Fluorescence spectra of eADF4(C16)-REDV displaying a Thyrosine peak and no Tryptophane emission peak.

Chapter 4: Endothelial cell-selective recombinant spider silk fusion protein: production and characterisation

4.3.2 Cell selectivity

The presence of endothelium is crucial in our native blood vessels as it serves to prevent thrombosis and neointimal hyperplasia. The endothelial cells form a lining within the blood vessels, playing a significant role in maintaining vascular homeostasis and preventing the formation of blood clots and excessive cell proliferation in the vessel wall. As a protective barrier, the endothelium helps regulate blood flow, inhibits platelet aggregation, and maintains a healthy vascular environment. Thus, endothelial cells' presence and proper function are essential for maintaining the integrity and functionality of the blood vessel [448-450]. This challenge could potentially be overcome by exploiting the naturally inferior cell adhesion properties of ADF4(C16) towards most tested cell types thus far [16, 21, 232, 303], combined with the endothelial cell-selective properties of the REDV peptide.

The REDV motif has been demonstrated to selectively interact with endothelial cells in the cardiovascular system through the $\alpha 4\beta 1$ integrin receptor [451]. This ligand is found in the III-CS domain of human plasma fibronectin [30]. Although the $\alpha 4\beta 1$ integrin is present in various human cell types, including cells of neural crest origin, melanoma cells, lymphocytes, and hematopoietic stem cells [30], it has been successfully employed to enhance the specific endothelialization of surfaces both *in vitro* and *in vivo*. Additionally, it has been used as a targeting ligand on particle systems to deliver payloads specifically to endothelial cells [452].

To assess the cell selectivity of the new protein, cell adhesion tests have been performed with endothelial cells (EC), smooth muscle cells (SMC) and fibroblasts (FB) as the most common cell types surrounding vessel structures. The minimally adhesive eADF4(C16) variant was employed as negative controls, following previous studies [16, 21, 232, 303]. On the other hand, the highly-adhesive RGD-functionalized silk, eADF4(C16)-RGD [16, 21, 232, 303], and fibronectin-coated tissue culture plates (TCP) were utilised as positive controls. To assess cell adhesion after 4 hours, the metabolic activity of the cells was measured using the CellTiter-Glo Assay, with ATP-dependent luminescence serving as a proxy for cell number.

Chapter 4: Endothelial cell-selective recombinant spider silk fusion protein: production and characterisation

The cell attachment data presented in **Figure 4-5** provides compelling evidence that the REDV-functionalized silk adheres explicitly to endothelial cells. The results reveal distinct patterns of cell attachment for the different surfaces investigated.

The TCP and RGD-functionalized surfaces demonstrated strong attachment of all cell types, and no statistically significant differences were observed between them. These findings indicate that both surfaces effectively support cell attachment and exhibit comparable adhesive properties.

In contrast, the unmodified silk exhibited minimal adhesion across all cell types tested, consistent with previous reports [21, 232]. This limited adhesion can be attributed to the inherent low-affinity nature of unmodified silk towards cell adhesion molecules.

Remarkably, the REDV-functionalized silk exhibited selective cell adhesion. SMC and FB did not show statistically significant differences in adhesion between the REDV-functionalized materials and the unfunctionalised silk negative control. Moreover, their adhesion was significantly lower than the positive controls ($p \leq 0.001$), underscoring the efficacy of the positive control surfaces for these particular cell types.

Notably, the HUVECs demonstrated elevated attachment to the eADF4(C16)-REDV surfaces compared to eADF4(C16) as supported by the literature in both monoculture and coculture experiments [150, 315, 453]. Although a limited number of smooth muscle cells adhered to both the unfunctionalized eADF4(C16) and the eADF4(C16)-REDV, the current clinical materials lack selectivity towards endothelial cells compared to vascular smooth muscle cells. This suggests that these spider silk materials could offer significant advantages *in vivo*.

The data support the notion that the REDV-functionalized silk promotes specific adhesion of endothelial cells while displaying reduced adhesion to other tested cell types.

Chapter 4: Endothelial cell-selective recombinant spider silk fusion protein: production and characterisation

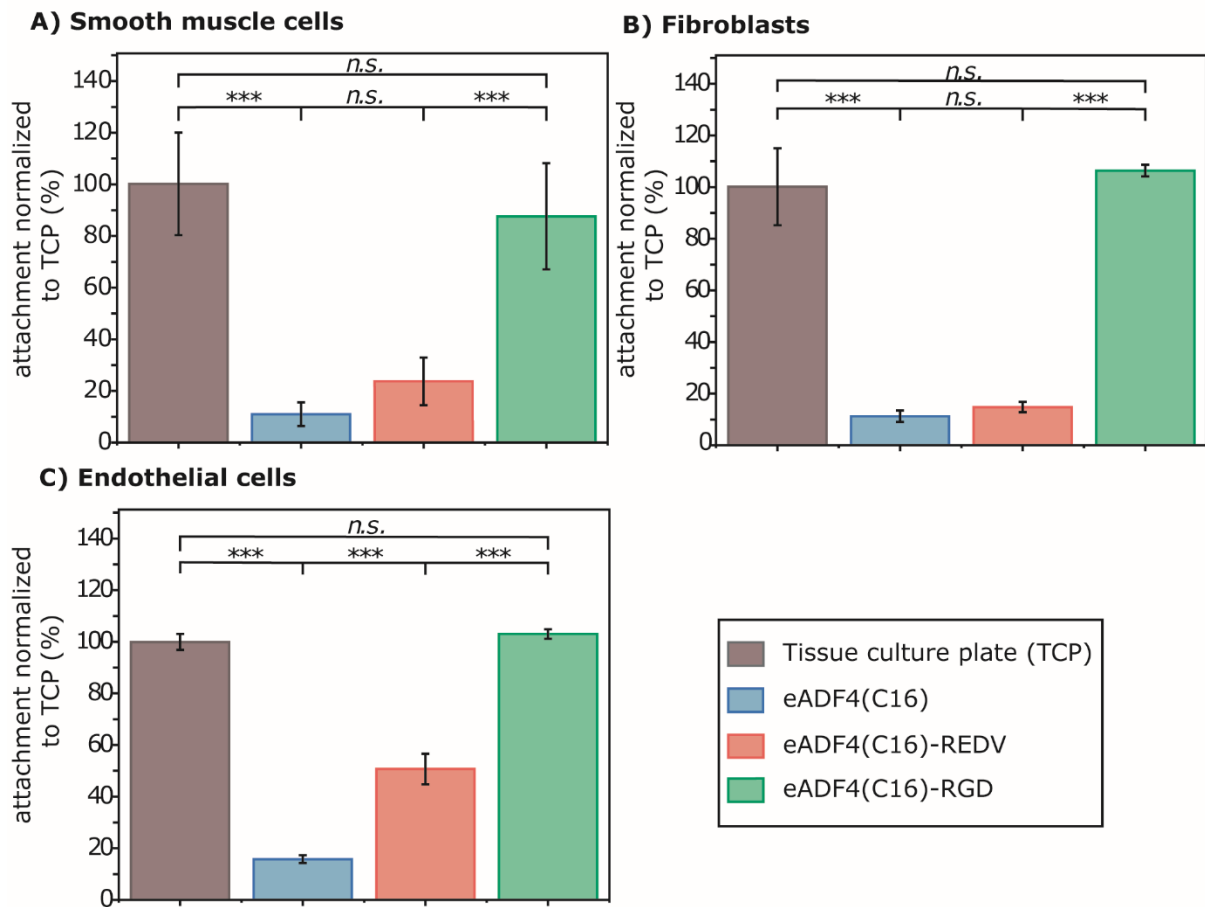


Figure 4-5: 4-hour adhesion of A) human smooth muscle cells, B) fibroblasts, and C) endothelial cells. Normalized to TCP-adhesion. *** $p \leq 0.001$.

4.3.3 HUVEC proliferation

To ensure the rapid endothelialisation of biomedical devices, endothelial cells must exhibit robust proliferation on surfaces. Therefore, the growth of endothelial cells on TCP and the silk surfaces was evaluated, as depicted in **Figure 4-6A**.

After 7 days, both TCP and RGD-functionalized surfaces demonstrated the highest population of endothelial cells. The growth curves of these surfaces began to plateau around day 5, indicating that a monolayer coverage was being approached. Notably, the surface density of HUVECs on the REDV-functionalized surfaces was statistically higher than that on the unmodified silk materials, albeit lower than that on TCP or RGD surfaces. This discrepancy could be attributed to lower initial cell adhesion or a reduced proliferation rate on the REDV-

Chapter 4: Endothelial cell-selective recombinant spider silk fusion protein: production and characterisation

functionalized surfaces. Nonetheless, the REDV-functionalized surface exhibited specificity towards endothelial cells and the ability to promote endothelium formation.

It is worth mentioning that the REDV peptide was shown to have the capability to capture endothelial progenitor cells from the blood flow, which could potentially enhance its efficacy *in vivo* [29, 453, 454]. This additional functionality further underscores the potential of the REDV-functionalized surface for applications involving endothelialisation.

These findings demonstrate that the REDV-functionalized surface exhibits specificity towards endothelial cells and supports their proliferation, highlighting its potential as a suitable substrate for promoting endothelialisation on biomedical devices.

Fluorescence microscopy was performed to further confirm the quantitative EC proliferation results shown in **Figure 4-6B**. The microscopy images revealed that only a few cells could adhere to the unfunctionalised silk surface, and minimal proliferation was observed. In contrast, the endothelial cells exhibited significant proliferation on the TCP, RGD-functionalized, and REDV-functionalized surfaces, reaching near-monolayer coverage over the 7-day experimental period.

Furthermore, CD31 staining on day 7 demonstrated the formation of a confluent endothelium, where the cells exhibited cell-cell connections. This staining supports the eADF4(C16)-REDV fusion proteins ability to promote the formation of an endothelial cell monolayer.

At early time points, cells on eADF4(C16)-REDV surfaces exhibit a qualitatively less spread morphology. This may be attributed to the REDV ligand interacting with only one known integrin, potentially restricting initial cell spreading compared to the RGD ligand, which binds to multiple integrins.

In summary, the fluorescence microscopy results complement the quantitative data on EC proliferation. The images show that the unfunctionalised silk surface had limited cell adhesion and proliferation, while the TCP, RGD-functionalized, and REDV-functionalized surfaces facilitated robust EC proliferation and the formation of a confluent endothelial monolayer. While the coverage of the eADF4(C16)-REDV

Chapter 4: Endothelial cell-selective recombinant spider silk fusion protein: production and characterisation

coated surface does not reach the same level of confluence as the positive controls by day 7, it is expected, that both surfaces will yield full coverage and plateau in a similar value of luminescence for long-term experiments.

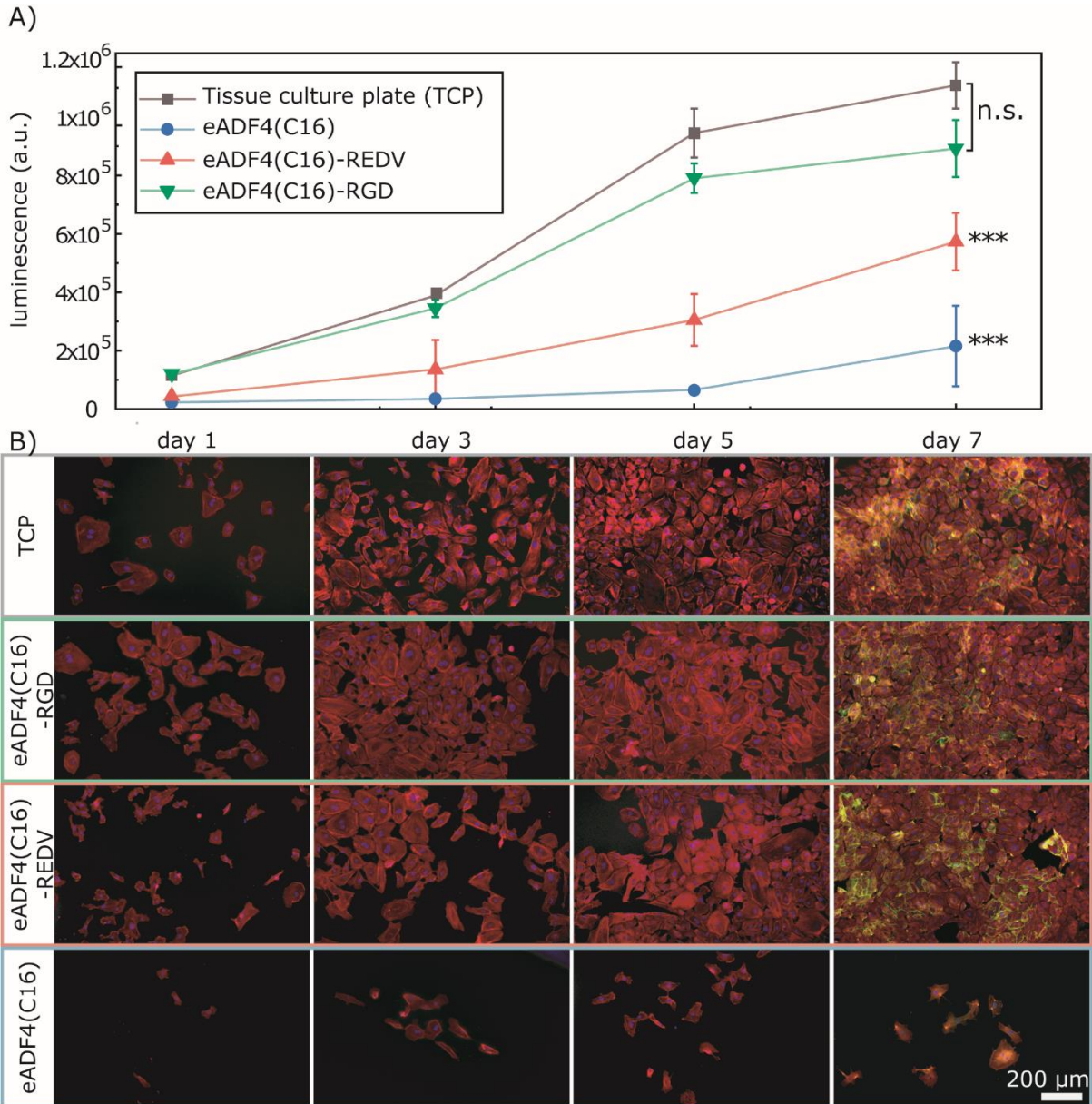


Figure 4-6: A) 7-day proliferation of human endothelial cells on fibronectin-coated TCP and films of the spider silk variants. *** $p \leq 0.001$. B) Representative fluorescence images of endothelial cells on various surfaces over 7 days. Cell nuclei were stained blue (DAPI), f-actin was stained red (rhodamine-conjugated phalloidin), and CD31 was stained green (Alexa Fluor 488-conjugated rat anti-human CD31 antibody) (on day 7 only). Scale bar for all images identical: 200 μm .

Chapter 4: Endothelial cell-selective recombinant spider silk fusion protein: production and characterisation

4.4 Conclusion

In conclusion, this chapter presents significant findings regarding the potential of the novel REDV-functionalized eADF4(C16) silk protein as a coating material for promoting endothelialisation on biomedical devices. The results highlight the endothelial cell specificity introduced by the REDV modification, demonstrating selective adhesion and proliferation of endothelial cells whilst minimising adhesion of other cell types. The REDV-functionalized surface effectively supports endothelial cell growth, forming near-monolayer coverage, characterised by cell-cell adhesions after 7 days *in vitro*.

These findings show promising first results supporting the use of eADF4(C16)-REDV as a stent coating material in regards to the hypothesized cell selectivity towards EC. The next chapter therefore will delve into hemocompatibility and more application-oriented observations regarding the coating of 316L stainless steel.

Chapter 5 Endothelial cell-selective recombinant spider silk fusion protein: application as a coating for DES

5.1 Introduction

This final research chapter combines the findings about eADF4(C16)-REDV from the previous chapter and expands into the observation as a potential coating material for drug-eluting stent applications. It features the characterisation of coatings on 316L stainless steel by SEM, water-contact angle measurements and adhesion-centered assays. Next, observations regarding their hemocompatibility, including coagulation and Factor XII activation assays on platelet-poor plasma, were conducted. Furthermore, enzymatic degradation behaviour in a simulated wound-healing enzyme mixture was observed. Lastly, everolimus drug-elution capabilities have been explored by detecting small amounts of released drug via HPLC-LCMS. Furthermore, this interdisciplinary array of experiments is a valuable example of the culmination of cooperative work within and across different universities for such tasks. For these experiments, expert knowledge from various sources was made available and significantly improved the outcome of this project.

In this manner, Dr Yukie O'Brian performed Gas chromatography measurements, Athulya Wickramasingha, under the supervision of Prof. Luke Henderson, observed the polyacrylamide coatings as an intermediate layer between steel and spider silk at Deakin University, and Prof. Anna Waterhouse provided extensive knowledge about blood-surface interactions and kindly offered her help by hosting a research stay at her group for Cardiovascular Medical Devices at the University of Sydney to conduct these experiments.

Chapter 5: Endothelial cell-selective recombinant spider silk fusion protein: application as a coating for DES

5.2 Material and Methods

Analytical grade chemicals were purchased from Merck, Australia and used as received if not stated otherwise. eADF4(C16) was purchased from AMSilk GmbH (Planegg/ Munich, Germany).

Procedures that included blood collection from healthy volunteers were conducted in alignment with the University of Sydney Human Research Ethics Committee's approval (HREC, project 2014/244), adhering strictly to the stipulations of the Helsinki Declaration. Anticoagulated whole blood, spiked with pre-loaded 0.5 U/mL heparin (Heparin Sodium Injection; SAGENT Pharmaceuticals Inc, USA) in the drawing syringe, was collected from venous blood donors who had not used any anti-thrombotic drugs within the preceding fortnight and was utilised 15 minutes after collection.

5.2.1 Coating of 316L stainless steel

For the production of spider silk coatings on 316L stainless steel sheets, the sheets were initially cut to a dimension of 6 mm x 8 mm for blood tests and 6 mm x 6 mm for drug elution and enzymatic degradation essays, followed by a cleaning procedure that involved ultrasonication baths with isopropanol, ethanol, and MQ-H₂O in 3 cycles for 30 seconds each to eliminate surface impurities. Following the cleaning and drying with nitrogen gas, a 200 mg/mL solution of the eADF4(C16) variant was used to dip-coat the steel samples at a 1 mm/min withdrawal speed with a lab-made dip coater based on a syringe pump (Harvard, PHD 22/2000, USA). Once coated, the sheets dried through solvent evaporation at ambient temperature overnight. A post-treatment step was applied on the coated sheets by incubating with 80% v/v ethanol for 30 minutes. This step was concluded with a water rinse and subsequent nitrogen gas drying.

To assess drug elution, everolimus (EVE, SML2282, Merck, Australia) was dissolved in a 200 mg/mL eADF4(C16)-REDV solution in HFIP at 10 mg/mL. This solution was used to dip-coat 316L stainless steel sheets as before. The post-

Chapter 5: Endothelial cell-selective recombinant spider silk fusion protein: application as a coating for DES

treatment of these coated sheets was conducted by exposure to an ethanol-rich atmosphere for 16 hours. This method was implemented to circumvent the solubilisation of EVE in liquid ethanol before a final rinse in water was conducted.

5.2.2 AFM

An MFP-3D Origin (Asylum Research, USA) atomic force microscope (AFM) was utilised in tapping mode to conduct AFM on silk-coated 316L stainless steel sheets that featured partly delaminated coatings for the determination of film thickness. To create the partly delaminated films, an additional 6 x 4 mm steel sheet was tightly clamped onto a 6 x 8 mm sheet to be removed after the coating process. The film was therefore only partly covering the bigger sheet and upon removal, this layer delaminated a few mm into the coating of the main sheet.

The AFM used Tap300-G cantilevers (BudgetSensors, Bulgaria) with a spring constant of 40 Nm⁻¹, with a scan size of 40 µm x 40 µm. Post-acquisition, the images were processed using the Asylum Research 14 software.

5.2.3 Bending/scratching assay

Qualitative observations of their bending behaviour and resistance to scratching have been conducted to assess the stability of the eADF4(C16)-based coatings on 316L stainless steel. For the bending behaviour, dried and wet (30-minute incubation in water at 37°C) coated 6 x 8 mm steel sheets were bent carefully by hand until the opposing 6 mm edges made contact. After a hold time of 5 seconds, the sheets were carefully released. The wet sheets were dried with nitrogen gas, and cut approximately 1 mm from the bend to minimise the sample height for SEM.

For scratching, wet (30-minute incubation in water at 37°C) and dry coated sheets were placed on a flat surface and fixated. Next, the sharp tip of self-closing forceps (F.S.T, USA) was used to create a fine scratch on the coating surface. The wet

Chapter 5: Endothelial cell-selective recombinant spider silk fusion protein: application as a coating for DES

samples were dried with nitrogen gas, and all samples were directly prepared for SEM imaging.

5.2.4 SEM

Scanning electron microscopy (SEM) was conducted on silk-coated 316L stainless steel sheets following the scratch and bending treatments, exposure to whole blood to evaluate clotting or exposure to enzymatic solutions for degradation assessment. For human blood-based samples, fixation was done using 2.5% w/v glutaraldehyde, followed by post-fixation with 1% v/v osmium tetroxide, subsequent dehydration in a series of ascending ethanol concentrations, and final drying with hexamethyldisilazane [167]. Enzymatic degradation test samples were washed in distilled water thrice and dried in a desiccator for two weeks. All samples were sputter-coated with 5 nm of gold using a Safematic CCU-010 (Safematic, Switzerland) before imaging with a Teneo VolumeScope (FEI, USA).

5.2.5 Water contact angle

Measurements of water contact angles were undertaken on silk-coated stainless steel sheets using an OCA 20 tensiometer (Dataphysics, Germany). The procedure involved dispersing 8 μ L of water onto the surface. The contact angle was recorded following a 5-second equilibration period.

5.2.6 Gas chromatography

Gas chromatography was carried out to identify if HFIP traces remained in the protein coatings after post-treatment. Therefore, post-treated sheets were incubated in 100% methanol overnight. The methanol was then analysed for any remaining HFIP. Furthermore, standard samples with 0.1, 0.01, 0.001 and 0.0001 % v/v HFIP were prepared by a dilution series. Gas chromatography was carried out by Dr. Yukie O'Brian of the University of Melbourne TrACEES platform, who kindly provided the SOP of the conducted measurement:

Chapter 5: Endothelial cell-selective recombinant spider silk fusion protein: application as a coating for DES

The gas chromatography analysis was carried out using an SGE BPX-VOL column with dimensions of 30 m length and 0.25 mm inner diameter, and a particle size of 1.4 μm . Helium was used as the carrier gas at a 1.0 mL/min flow rate. The injection volume was set to 1 μL . The inlet temperature was maintained at 270°C, and a split ratio of 50:1 was applied.

The oven temperature program consisted of an initial temperature of 40°C for 1 minute, followed by a temperature ramp of 10°C/min until reaching 270°C. The final temperature was held at 270°C for 2 minutes.

For mass spectrometry (MS) analysis, electron impact ionisation mode was employed. The source temperature was set to 180°C, while the interface temperature was maintained at 200°C. The mass range was selected from 30 to 500 m/z.

The above parameters were used to ensure accurate and efficient separation, detection, and analysis of the target compounds using gas chromatography coupled with mass spectrometry.

5.2.7 Polyacrylamide functionalisation and lap shear test

The functionalisation with an intermediate acrylamide layer was observed to examine the potential of an additional polymer layer between silk and steel. The experiments were conducted according to *Emonson et al.*[157].

An electrochemical cell was initially set up for functionalising stainless steel plates with a diazonium compound and acrylamide. A glass beaker was filled with a 350 mL solution consisting of H_2SO_4 (0.01 M, 350 mL), 4-nitrobenzene diazonium tetrafluoroborate (20 mM), and acrylamide (1 M, 24.8 g, 0.35 M).

The cell used a set of 10 stainless steel plates (25 mm \times 85 mm \times 2 mm), each spaced 4 mm apart, as the counter electrode. Another identical set of plates with the same spacing served as the working electrode. The counter and working electrodes were placed 4 cm apart, with an Ag/AgCl reference electrode in the centre.

Chapter 5: Endothelial cell-selective recombinant spider silk fusion protein: application as a coating for DES

After functionalisation, the steel plates were cleaned by sonicating in 150 mL of ethanol for 5 minutes. This ensured that any adsorbed material was thoroughly washed away. After this step, the samples were dried and stored at room temperature until further analyses were conducted.

The shear strength of the adhesive bond created between metal and eADF4(C16)-REDV was assessed in adherence to the standard methodology outlined in ASTM D1002-10 [157]. Functionalised steel plates were glued together with 100 μ L of a 200 mg/mL eADF4(C16)-REDV solution and were allowed to dry for two weeks. Therefore, a customised 3D-printed mold was utilised to ensure a uniform overlapping area of 25 mm x 25 mm between bonded samples. An applied mass of 150 g was used during bonding to maintain a consistent, flat contact area at the bond interface. Pre- and post-adhesion weights of the samples were obtained to monitor the precise quantity of silk fibroin used in the bonding process by the weight difference.

Upon completion of the drying process, the samples were carefully extracted from their holders and placed into a 10 kN Instron universal microtester for mechanical testing. To avoid any torsional stresses induced by the tensile testing clamps, a metal wire was threaded through the top sample's water jet cut hole and secured to this wire for testing.

The rate of tensile extension during the test was set at 0.5 mm/min. Lap shear strength σ of specimens was calculated by **Equation 5-1**, with **F** representing the maximum force at failure (N), and **A** denoting the bonding area between metal specimens (m^2).

$$\sigma = \frac{F}{A} \quad (5-1)$$

Given the inherent challenges of applying precise amounts of viscous silk solution onto a metal surface, all σ values were normalised by the calculated weight difference. This normalised lap shear strength (σ_N) is presented in MPa/g and used to mitigate data variations caused by differences in adhesive quantity.

Chapter 5: Endothelial cell-selective recombinant spider silk fusion protein: application as a coating for DES

5.2.8 QCM-D measurements

Initial hemocompatibility experiments included the observation of fibrinogen adhesion onto eADF4(C16)-based coatings. Therefore, QCM-D chips were spin-coated with a 10 mg/mL protein solution in HFIP, according to **2.2.8**. The QCM-D measurements have been conducted as described in **2.2.9** with PBS as a buffer system and 1 mg/mL human fibrinogen (F3879, Merck, Australia) in PBS as an incubation medium.

5.2.9 Factor XIIa activation

For the quantitative observation of blood coagulation, previously established protocols were used, according to *Ruhoff et al [455]*.

Material-induced factor XII (FXII) activation was assessed using the chromogenic FXIIa substrate S-2302 (HD-Pro-Phe-Arg-pNA·2HCl) (Chromogenix, Diapharma, USA) as previously described [455]. Human platelet-poor plasma (PPP, acid citrate dextrose), obtained from the Australian Red Cross Lifeblood (with informed consent, 19-08NSW-02), was incubated for 10min at 37 °C in Bovine serum albumin (BSA, Merck, Australia)-blocked wells containing samples prior to S-2302 addition (0.4mM in 50 mM Tris, 150 mM NaCl buffer, pH 7.7). Activated FXII production of p-nitroaniline from S-2302 cleavage was measured at 405 nm every 30 seconds using a microplate reader (CLARIOstar, BMG LabTech, Germany). Linear least-squares regression was performed on the linear portion (0–10 min) of the curve, and the slope was used to quantify the substrate cleavage rate (each replicate was analysed separately).

5.2.10 Turbidity assay

The clotting time assay was performed with PPP (n = 5 donors), according to a previously established protocol by *Ruhoff et al [455]*. PPP was centrifuged twice at 1700 × g for 20 min at 37 °C, checked for a platelet count of < 1 × 10³ μL⁻¹

Chapter 5: Endothelial cell-selective recombinant spider silk fusion protein: application as a coating for DES

using a Sysmex KX21 hematology analyser (Sysmex Corporation, Japan), then pooled and frozen at $-80\text{ }^{\circ}\text{C}$ (1 mL aliquots) until use.

To measure coagulation, materials were pre-incubated with PPP at $37\text{ }^{\circ}\text{C}$ for 10 min to allow surface-induced FXIIa generation prior to adding CaCl_2 (1 mM final, 50% final plasma concentration) to allow coagulation to progress. Absorbance (405 nm) was monitored every 30 seconds, using a microplate reader (CLARIOstar, BMG LabTech, Germany) and clotting time was calculated at 50% maximal absorbance.

5.2.11 Whole blood rocking assay

To evaluate the coatings' hemocompatibility in a more application-oriented environment, whole-blood rocking assays have been conducted, as previously described [456]. Therefore, 316L stainless steel ($0.6 \times 0.8\text{ cm}^2$) and eADF4(C16)- (and its REDV and RGD modified variants) coated steel sheets were employed as substrates. BSA (3% w/v) in saline solution was used to pre-incubate the 24-well plate overnight at $4\text{ }^{\circ}\text{C}$ to diminish non-specific protein adsorption. After a wash with pre-warmed saline (3x, 1 mL, $37\text{ }^{\circ}\text{C}$, 0.9% saline, Baxter, USA), the samples were incorporated into the wells and incubated with anticoagulated whole blood (800 μL , 0.5 U mL^{-1} heparin, $n = 3$ individual donors) in a shaking incubator at $37\text{ }^{\circ}\text{C}$ with 120 rpm, (Multitron, Infors HT) for specific time intervals. 15 $\mu\text{g}/\text{mL}$ Alexa Fluor-647 human fibrinogen (Invitrogen, F35200 Lot#2489019) was added to the blood to enable fluorescence detection and quantification of the fibrin clot. After blood incubation, samples were washed thrice with pre-warmed saline and then fixed in a 2.5% glutaraldehyde solution in 0.1 M phosphate buffer for an hour in the dark. After washing with 0.1 M phosphate buffer (3x, 5 min), samples were preserved in 0.1 M phosphate buffer solution and fluorescence readings were recorded with a microplate reader (CLARIOstar, BMG LabTech, Germany).

Chapter 5: Endothelial cell-selective recombinant spider silk fusion protein: application as a coating for DES

5.2.12 Modified chandler loop

Modified Chandler loop experiments were carried out per ISO 10993-4 [457]. Segments of Tygon tubing (ND-100-65, internal diameter 0.250 inches, outer diameter 0.312 inches, SDR Scientific, Australia) measuring 23 cm in length were used. Sheets of spider silk-coated and uncoated 316L stainless steel, measuring 0.6 x 1.2 cm², were inserted approximately 2-3 cm into the tube opening and tightly aligned to the tube wall. Human whole blood was added to the tubes and sealed with 2.5 cm long silicone tubing (Masterflex L/S 18 96410-18, Cole Palmer, Australia). The tubes were maintained at 37°C and rotated at 30 rpm. Samples were collected after 30 minutes by filtering the blood through 40 µm filters (CLS431750, Sigma Aldrich) and gently immersed in a saline solution to rinse off non-adherent blood. Any filtered blood clots were washed thrice with saline, and the resultant weight of the steel sheets was used to calculate the final weight increase of the sample.

5.2.13 Enzymatic degradation

For the degradation study, spider silk-coated stainless steel samples were incubated with a solution of matrix metalloprotease-2 (MMP-2 human, Merck, Australia) and human elastase (human Neutrophil Elastase protein (Active) (ab280938), abcam, USA). Both enzymes were used at a concentration of 250 ng/mL each in enzyme buffer (50 mM Tris/HCL pH 7.5, 10mM CaCl, 150mM NaCL, 0.05% Tween-20). This degradation process was tracked over 29 days. Spider silk-coated steel sheets incubated in buffer without enzyme served as the control.

Sample collections and buffer/enzyme exchanges were performed thrice weekly (Mon-Wed-Fri). The degradation process was quantified as mass loss of the protein coating by measuring the concentration of the released protein, using a NanoDrop 1000 (Peqlab, Germany) at a wavelength of 280 nm, therefore giving an indirect degradation rate based on the mass loss of the coating.

Chapter 5: Endothelial cell-selective recombinant spider silk fusion protein: application as a coating for DES

5.2.14 Everolimus elution

Everolimus (EVE) elution into PBS was tracked by incubating the coated sheets at 37°C. Buffer changes were performed at each measurement point. Measurements were taken at 1, 2, 3, 4, and 5 hours on the first day, every 48 hours until day 14, and on day 21 and day 29. This sampling schedule was based on the expected burst release as suggested by previous studies which eluted everolimus and its derivatives into PBS [96, 151, 458, 459].

The total amount of loaded EVE was determined by dissolving the post-treated and drug-loaded specimens in 100 µL HFIP, followed by the addition of 900 µL methanol for HPLC detection. The concentration was then computed using pre-established standards.

5.2.15 HPLC-MS

Liquid drug elution samples were lyophilised (Biobase BK-FD10P, China) and re-solubilised in 200 µL methanol (HPLC grade, 67-56-1, Thermo Fisher). Following 10 minutes of centrifugation at 13,000 x g, 150 µL were transferred into HPLC vials for analysis on a Shimadzu Prep HPLC-MS (Shimadzu, Japan). Data collection and analysis were done using LabSolution software.

The sample was separated using an HPLC ACE EXCEL 5 SUPER C18 250 x 4.6mm column (Winlab, Australia) at 40°C. Elution was carried out using a gradient of buffer A (99.9% water, 0.1% formic acid) and buffer B (99.9% acetonitrile (ACN, HPLC grade, Merck, Australia), 0.1% formic acid) as described in **Table 5-1**. The flow rate was maintained at 1.5 mL/min, and the injection volume was 100 µL.

Chromatograms at UV 280 nm and m/z 975.7 were compared to a previously established EVE standard, as shown in **figure 5-1**, to determine the quantity of the drug. The total amount of drug loaded on a coating, used to compute the total release, was indirectly determined by solubilising the post-treated, drug-loaded coatings.

Chapter 5: Endothelial cell-selective recombinant spider silk fusion protein: application as a coating for DES

Table 5-1: Buffer gradient used in HPLC-MS data acquisition

Time (min)	Buffer A	Buffer B	curve
0	97 %	3 %	isocratic
0-1	10 %	90 %	linear
1-2.5	5 %	95 %	linear
2.5-3.5	5 %	95 %	Isocratic
3.5-10	97 %	3 %	isocratic

Chapter 5: Endothelial cell-selective recombinant spider silk fusion protein: application as a coating for DES

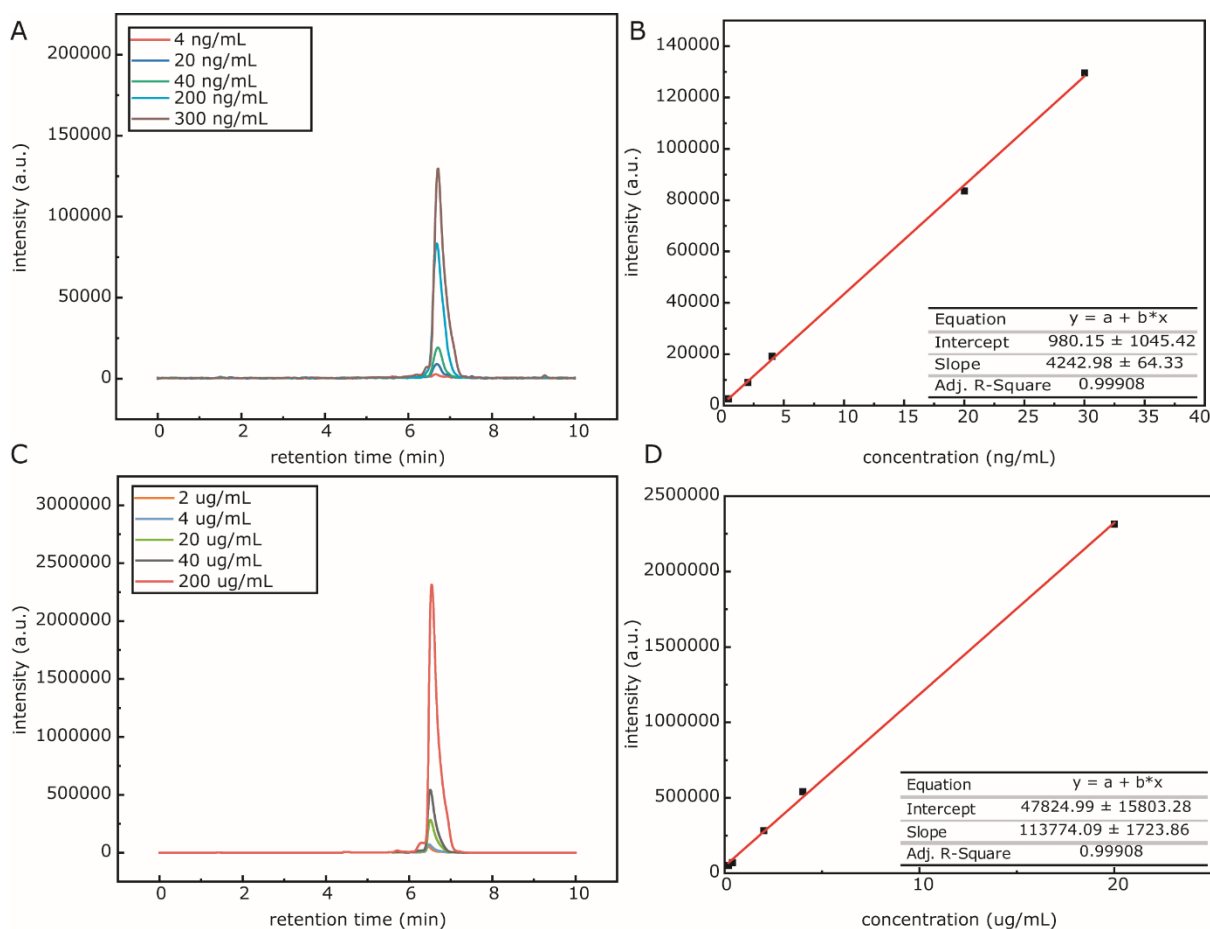


Figure 5-1: EVE-standard for HPLC-MS and UV 280nm. A) Chromatogram of EVE at 975.7 m/z with B) the standard derived from the peak values. C) the compound's photodiode array (PDA) signal at 280 nm, and D) the standard derived from the peak values thereof. Computed with the linear fit function of the Origin 2020b software.

5.2.16 Statistical analysis

Statistical analysis was conducted using OriginPro 2020b software. To assess the statistical significance of differences between groups, analysis of variance (ANOVA) was employed. Post-hoc tests were performed using the Tukey HSD (honestly significant difference) test.

Chapter 5: Endothelial cell-selective recombinant spider silk fusion protein: application as a coating for DES

5.3 Results and discussion

5.3.1 Protein processing and coating of 316L stainless steel

The prerequisite for subsequent analysis of the coating behaviour is a homogeneous, defect-free surface. SEM imaging has been conducted to observe the resulting surface structure following dip-coating and ethanol post-treatment. As shown in **Figure 5-2**, the surface of cleaned 316L stainless steel sheets features a partial wave-like structure, typical for bulk stainless steel which has been processed cold, such as the rolling and cutting for these thin sheets [460]. However, for the coated specimens, these structural patterns are entirely covered by the protein coating. The coating is homogeneous and defect-free, setting the stage for further analysis of the coating properties.

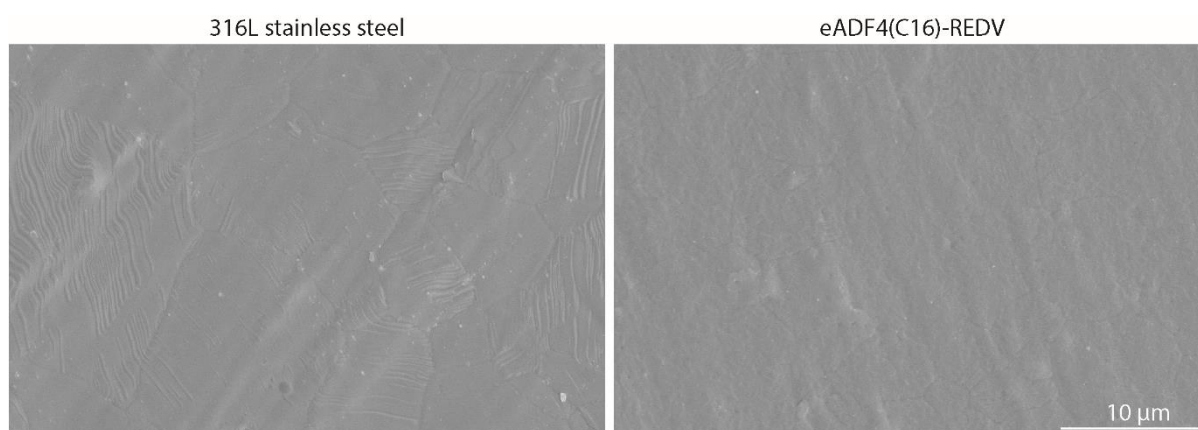


Figure 5-2: Surface characterization of spider silk coatings on 316L stainless steel. The surface topography of pristine 316L stainless steel (left) and eADF4(C16)-REDV-coated 316L stainless steel (right) was visualised scanning electron microscopy

Next, the optimal dip-coating parameters have been established to create a coating thickness mimicking the thickness found on commercially available DES.

Therefore, AFM has been employed to determine the height of the resulting coatings. As shown in **Figure 5-3**, the average coating thickness of the partially delaminated films at the established dip-coating settings was $1.5 \pm 0.3 \mu\text{m}$, averaging 100 measurements per film. Even though the exact thicknesses of commercially available stents are confidential information, according to calculations made from their data sheets and other review papers estimating the

Chapter 5: Endothelial cell-selective recombinant spider silk fusion protein: application as a coating for DES

values, it can be concluded that most DES are coated with coatings reaching from 2-5 μm [370, 461, 462]. Therefore, the coatings examined in this chapter are well within the commercially available DES coating range. However, for the translation to coating stent structures, a different approach to dip-coating needs to be evaluated as this process is limited to the viscosity of the spider silk solution and the existence of a re-solubilisation effect, which makes multiple dip-coating cycles unfeasible due to inhomogeneities occurring. Nonetheless, these model surfaces fulfil the purpose of observing the coating properties for potential applications as DES coatings.

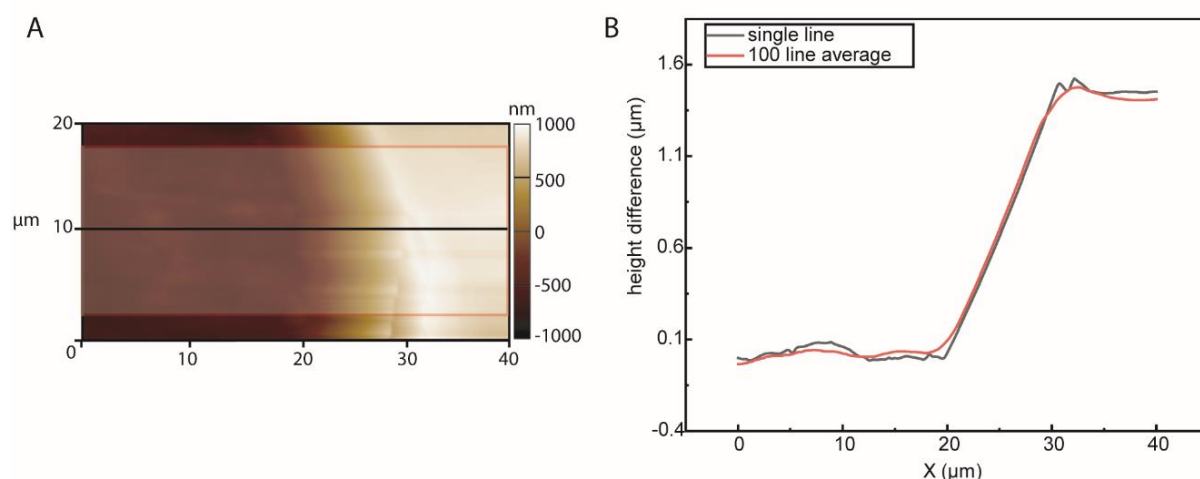


Figure 5-3: A: AFM image of a partly delaminated eADF4(C16)-REDV coating on 316L stainless steel with indication of measurement lines used to calculate the thickness of the coating. B: thickness profile obtained from 1 (black line) and the average of 100 (red line) lines of the AFM image.

After establishing the dip-coating parameters for the coating examination, water-contact angle measurements were conducted to observe how the spider silk coating influences hydrophobicity. Especially regarding hemocompatibility, the hydrophilicity of a material is crucial; however still not completely understood. Generally, more hydrophilic surfaces are considered more susceptible to fibrin clotting and Factor XIIa activation [455]. However, blood compatibility will be covered in the next chapter. On the other hand, regarding EC selectivity, more hydrophilic surfaces are more attractive for cell attachment [463], with an optimal adhesion on surfaces between 40°-70° [464].

The water-contact angles measured for eADF4(C16)-based protein coatings can be seen in **Figure 5-4**, where the average contact angle measurements on bare

Chapter 5: Endothelial cell-selective recombinant spider silk fusion protein: application as a coating for DES

316L stainless steel surfaces resulted in a value of $84.2 \pm 2^\circ$. In contrast, the contact angle for all silk coatings was approximately 40° for all variants. These findings align with previously published values [173, 465], confirming the hydrophilic nature of the silk coatings and their ability to reduce the contact angle compared to the bare metal surface.

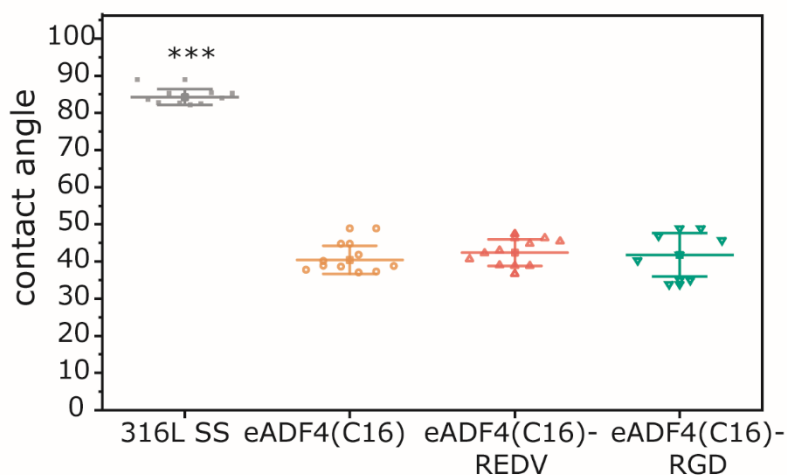


Figure 5-4: The hydrophilicity of the various surfaces was investigated by measuring the water contact using sessile droplet tensiometry. Contact angle data is presented as mean \pm standard error ($n=10$ and) and *** indicates that $p \leq 0.001$.

A possible concern of the employed coating method might be the effect of potentially remaining HFIP in the coating. HFIP is shown to be cytotoxic and would inadvertently show a negative impact on any application *in vivo* and *in vitro* [466]. Therefore, gas chromatography has been used to observe the potential HFIP-leaching of a post-treated coating overnight. **Figure 5-5** shows the resulting chromatograms with the blank sample being pure methanol. It can be deduced that no apparent peak for the sample curve is detectable in the multiple ion chromatogram, suggesting that the remaining or leaching HFIP, if present, is below the detection limit existing below 0.001%. Therefore, it can safely be claimed that the amount of HFIP is of no concern for further *in vitro* and *in vivo* experiments, as the safety data sheet of HFIP claims an LD50 of 1500 mg/kg in rats, which should be well above 0.001% v/v in any *in vivo* scenario. Furthermore, a patent filed in 2017 titled "*Method for removing organic solvent*" used air-drying as an effective way to eliminate HFIP from protein coatings overnight and also confirmed by gas chromatography that no HFIP could be detected [467].

Chapter 5: Endothelial cell-selective recombinant spider silk fusion protein: application as a coating for DES

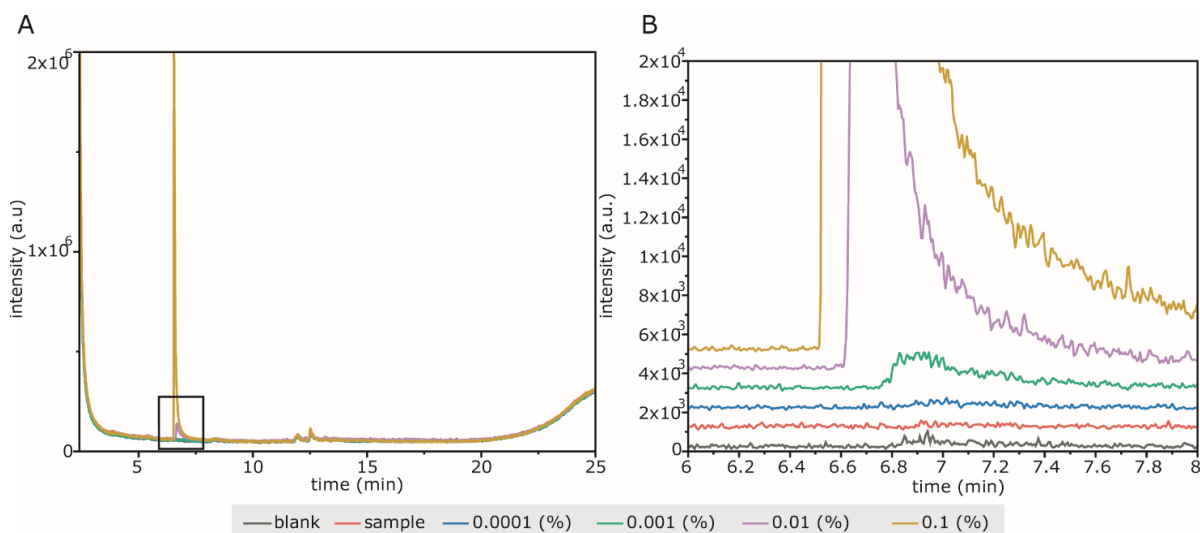


Figure 5-5: Gas chromatography of pre-determined HFIP concentrations in methanol and an overnight leaching sample of an eADF4(C16)-REDV coated 316L stainless steel sheet. A: Total ion chromatogram. B: Multiple ion chromatogram of the sum of ions $m/z = 51, 69, 99,$ and 129 as determined by a library search for the peak in A.

Lastly, after confirming the chemical viability of the protein coatings for further testing, their mechanical properties were examined qualitatively. Therefore, the coated sheets were subjected to bending and stretching tests in dry and wet, i.e. swollen, conditions. **Figure 5-6** demonstrates how the surfaces reacted to an external force. In a wet state, as would be the case for the coatings environment *in vivo* it can be seen that the coatings are not susceptible to bending (**Figure 5-6C**) and scratching leaves the surface with a removed track for the contact area (**Figure 5-6A**). However, when scratching a dry coating, a large coating area delaminates with the scratching procedure, exposing large steel areas (**Figure 5-6B**). Surprisingly, dry bending of the coatings did not lead to fracturing of the coating (**Figure 5-6D**).

Although these findings were purely qualitative and did not hold the argument to support the coatings' adhesion stability, it can be deduced that the coatings seem more resistant to defects in wet conditions, most likely due to their swelling behaviour. Therefore, enhancing the adhesion to the steel and being softer, enabling the removal of coating while scratching.

Chapter 5: Endothelial cell-selective recombinant spider silk fusion protein: application as a coating for DES

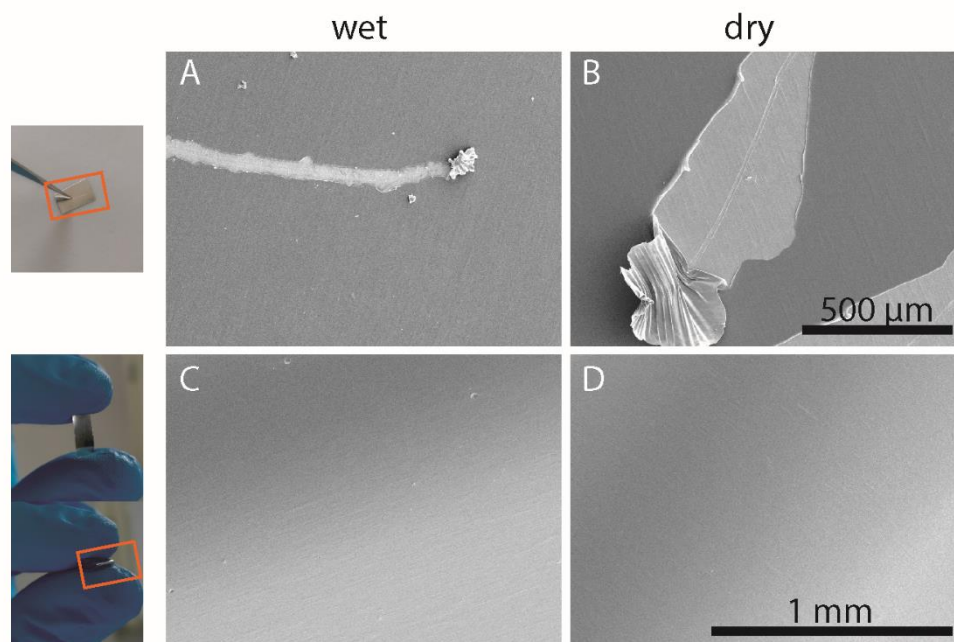


Figure 5-6: Scratching and bending behaviour of eADF4(C16)-REDV coatings. The left side inserts demonstrate how the mechanical force acted on the coatings. A: A scratch on a wet protein coating showing protein removal along the scratched path, B: A scratch on a dry protein coating, displaying large areas of delamination C: Bending of a wet and D: a dry protein coating where no apparent defects are observable.

In an attempt to increase the integrity of the coating in a dry state under mechanical stress, the potential of an additional polymer layer for enhanced adhesion was observed next. Therefore, an intermediate polyacrylamide layer deposition, as *Emonson et al.* used for *B. mori* films [157] was incorporated to enable hydrogen bonding and promote adhesion between the spider silk coating and the substrate. By utilising a modified electrochemical graft-from approach, the polyacrylamide was covalently bound to the steel, potentially enabling a stronger adhesion of the spider silk coating. **Figure 5-7** shows visual observations (A-C) of polyacrylamide functionalised steel plates glued together by an eADF4(C16)-REDV solution. **Figure 5-7A** shows a glued-together specimen for the lap shear test, holding the weight of the second steel plate (85 mm × 25.4 mm × 2 mm) and **Figure 5-7B** shows the plates after the lap-shear experiment. The images suggested that the modification significantly improved the behaviour in terms of the delamination of the coating, as this effect could not be observed. Both steel plates seem to contain protein on their respective surfaces. **Figure 5-7C** demonstrates the lap-shear setup, and **Figure 5-7D** summarises the normalised adhesive strengths according to the amount of protein used for gluing,

Chapter 5: Endothelial cell-selective recombinant spider silk fusion protein: application as a coating for DES

showcasing that the polyacrylamide functionalisation significantly increased the coatings' adhesion to the substrate.

Despite these results suggesting a better adhesion of the protein coating to the surface, it has to be considered that these measurements were conducted in a dry state due to limitations in the experimental setup. However, the scratching and bending tests, as seen in **Figure 5-6** have been conducted on these functionalised surfaces, resulting in complete delamination upon wetting of the coatings. This observation aligns with the ability of polyacrylamide to be highly soluble in water if not cross-linked [468] as, for example, in an SDS-gel. Therefore, the additional coating solubilised, leading to complete delamination.

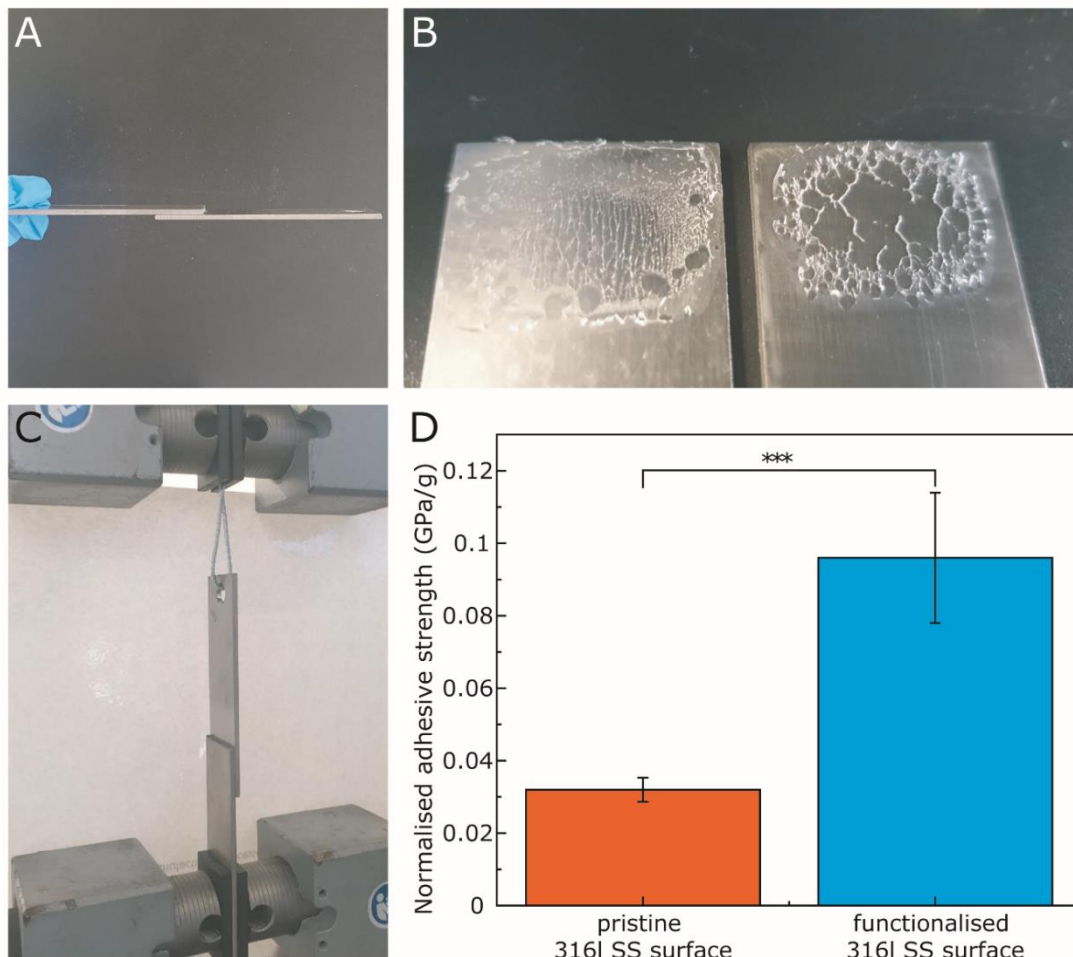


Figure 5-7: Lap-shear test of polyacrylamide functionalised steel plates glued with eADF4(C16)-REDV solution. A: photograph of a glued specimen for testing, B: Specimens after the lap-shear test, C) The experimental setup and D) Normalised adhesive strengths of pristine and functionalised steel plates coated with spider silk. . n=3, ***p<0.001.

Chapter 5: Endothelial cell-selective recombinant spider silk fusion protein: application as a coating for DES

To conclude, the surface characterisation of eADF4(C16)-based coatings showed homogeneous surfaces created by a dip-coating approach that showed reduced water-contact angle, indicating a more hydrophilic surface. Furthermore, it could be confirmed that no HFIP from the coating procedure remains after post-treatment, rendering these coatings viable for *in vitro* and *in vivo* testing.

The mechanical stability, specifically the adhesion to the steel substrate, is one remaining concern for future applications as the coatings showed good integrity in a wet state, but the dry state was very susceptible to defects from scratching. An additional polyacrylamide layer improved this; however, it simultaneously led to poor performance in the wet state.

Nonetheless, from these results, it can be derived that another, more suitable, preferably water-insoluble polymer layer could simultaneously enhance the spider silk coatings adhesion in a dry and a wet state. A natural polymer to consider would be chitosan which could be applied by electrospraying and layer-by-layer deposition, providing the sites for H-bond dependent adhesion similar to the polyacrylamide layer[469]. However, while water soluble, a chitosan layer would swell in wet state [175] and possibly lead to delamination and defects when immobilized. Two synthetic approaches could be the usage of (3-Aminopropyl)triethoxysilane (APTES) or polyvinylidene fluoride (PVDF) coatings. APTES is an aminosilane, used for the deposition of thin monolayers of alkoxy silanes for attaching organic coatings to metal surfaces[470] and has been suggested to be biocompatible[471]. PVDF is commercially used as metal coatings, especially as adhesion substrate for paints. It is a thermoplast which is highly wear and water resistant and would could possibly also provide H-bonding sites for improved spider silk adhesion. Furthermore, it is commonly spray-coated, providing thin coatings and was found to be biocompatible[472].

5.3.2 Hemocompatibility

After thorough characterisation of eADF4(C16)-based coatings for 316L stainless steel, the evaluation on the potential application as DES coating material was targeted, firstly focusing on the blood coagulation behaviour.

Chapter 5: Endothelial cell-selective recombinant spider silk fusion protein: application as a coating for DES

An optimal stent coating should minimise thrombosis, thereby reducing the occurrence of thrombus-induced restenosis, embolism, stroke and decreasing the dependence on antiplatelet therapy [167]. Therefore, as a first approximation of clotting behaviour, QCM-D measurements to assess fibrinogen adhesion, similar to the studies *Lentz et al.* [49] performed on spider silk films cast from formic acid, were conducted. Similar to their findings, the HFIP-cast films used in this study exhibited less fibrinogen adhesion than the control gold surface, as shown in **Figure 5-8**. All tested eADF4(C16) variants showed significantly less fibrinogen adhesion than the control specimen. However, to the instrumental limitation of the QCM-D device and the spin-coating setup, reliable reproducibility amongst the protein coatings was impossible to achieve. Nevertheless, the control gold surface exhibited significantly higher fibrinogen adhesion in every attempt for reproducibility (n=3).

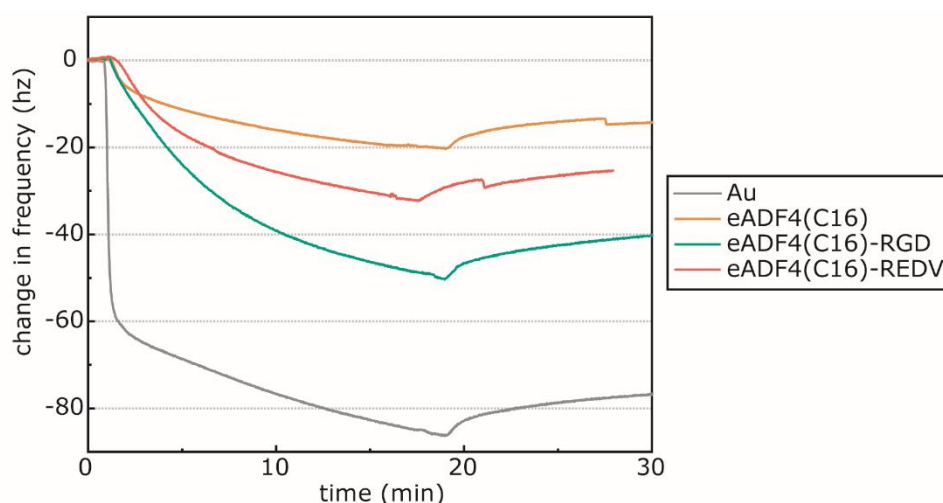


Figure 5-8: QCM-D measurements of human fibrinogen on gold (Au) QCM-D chips and eADF4(C16)-based coated chips. Graph cut to exclude equilibration time. Fibrinogen introduction after ~1 minute, PBS washing step after ~18 minutes.

The initial findings from QCM-D measurements using human fibrinogen suggested that the coatings have the potential for hemocompatibility. However, the process of thrombosis induced by biomaterials is multifaceted, involving various pathways initiated by the adsorption of procoagulant proteins such as fibrinogen, factor XII (FXII), von Willebrand factor (vWF), and complement proteins [455]. In addition, factors like shear stress can also impact the clotting process [473]. Following ISO10993-4 [473] guidelines, several blood-material assays were conducted to

Chapter 5: Endothelial cell-selective recombinant spider silk fusion protein: application as a coating for DES

assess the hemocompatibility of the spider silk materials. These assays included clotting time measurement, FXIIa activation assay, whole blood coagulation assay, and a modified Chandler loop assay [473] to examine the influence of flow on clotting. Furthermore, scanning electron microscopy was employed to visualise the surfaces in both their pristine and clotted states.

First, a clotting time assay was conducted to assess the coagulation potential of the spider silk surfaces (**Figure 5-9A**). Platelet-poor plasma (PPP) was incubated on the different surfaces, and the turbidity of the suspension was measured. A decrease in turbidity indicates clotting and the formation of fibrin clots, which occurs through contact activation via the intrinsic pathway [474]. The experiment included two control surfaces: hydrophilic (oxygen-plasma treated) polystyrene, known to strongly trigger coagulation, and unmodified polystyrene as a hydrophobic surface model. No significant difference in turbidity was observed between the negative control and the eADF4(C16) variants. However, the hydrophilic polystyrene surface exhibited noticeable clotting behavior.

A Factor XII activation assay was performed to validate the results obtained from the clotting time assay (**Figure 5-9B+C**). This assay aimed to investigate the clotting mechanism in more detail. The results revealed no detectable activation of Factor XII on the negative control and eADF4(C16) variants, while significant activation was observed on the positive hydrophilic control over a 60-minute period. These findings are particularly noteworthy because contact activation of Factor XII on negatively charged hydrophilic surfaces has been shown to accelerate the coagulation cascade [475]. The fact that the eADF4(C16) coatings, which exhibit negative charges and hydrophilicity, did not induce Factor XII activation suggests that these silk surfaces do not trigger this particular clotting pathway and possess exceptional hemocompatibility for their material category.

Chapter 5: Endothelial cell-selective recombinant spider silk fusion protein: application as a coating for DES

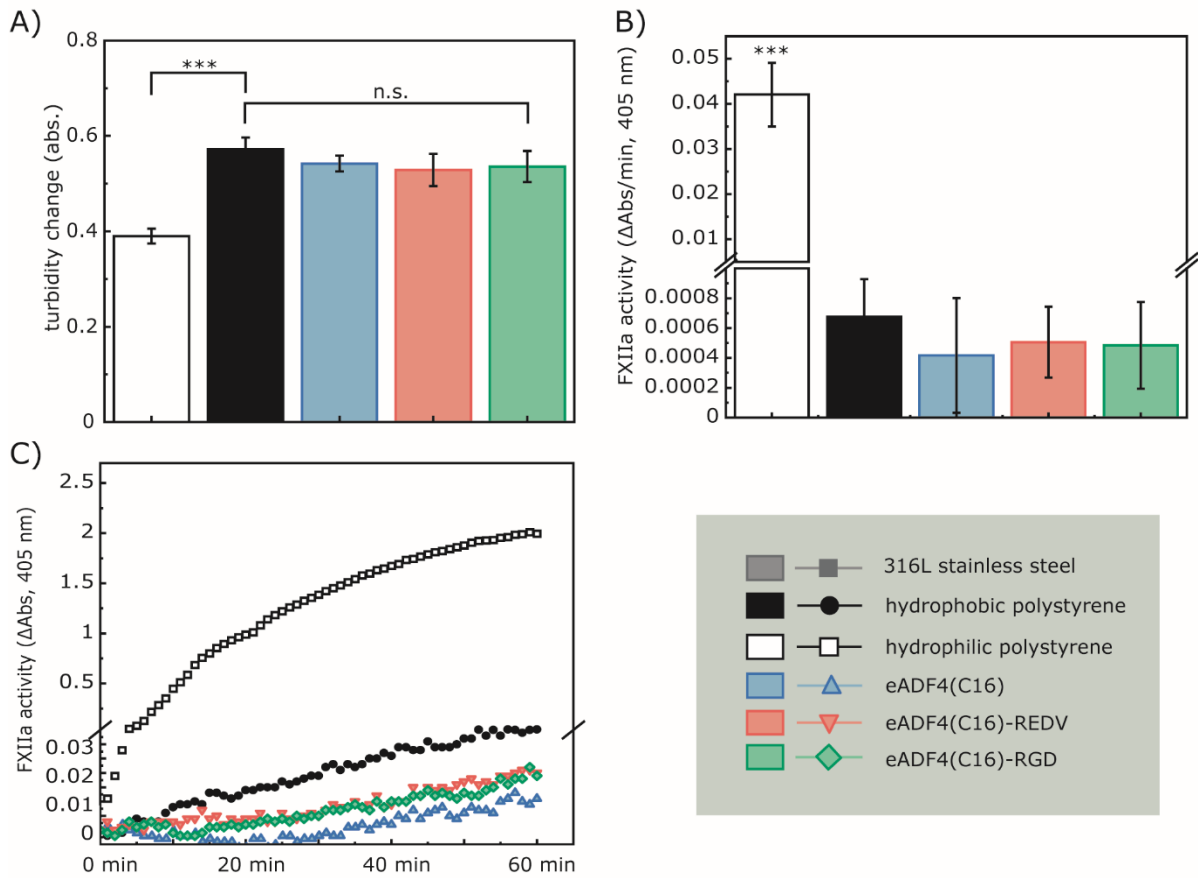


Figure 5-9: Hemocompatibility assays on spider silk coatings and control surfaces. A) Clotting was assessed by measuring the turbidity change when the various surfaces were exposed to platelet poor plasma (PPP), as an increase in turbidity indicates fibrin formation ($n=4$). B) Factor XIIa activation rate was assessed on various surfaces as it is involved in the coagulation cascade. ($n=4$). C) Representative Factor XIIa activation profiles used for determination of the slopes in panel B. $***p \leq 0.001$.

Although these results suggested very good hemocompatibility of eADF4(C16)-based coatings, blood coagulation is, as mentioned before, a very intricate mechanism and still not entirely uncovered in all its complexity. Therefore, following the plasma-based tests, human whole blood clotting assays were performed on 316L stainless steel surfaces and steel surfaces coated with the spider silk variants using whole blood spiked with fluorescent fibrinogen. This assay allows for qualitative analysis of thrombosis through visual inspection and quantitative analysis through fluorescence measurements of the clotted surfaces. Visually, the bare 316L stainless steel sheets induced significant thrombosis, while the spider silk coatings exhibited considerably reduced thrombus formation (**Figure 5-10A**). Quantitative assessment of thrombus accumulation confirmed the visual observations, as the 316L stainless steel surfaces demonstrated

Chapter 5: Endothelial cell-selective recombinant spider silk fusion protein: application as a coating for DES

substantial clotting compared to minimal clotting on the spider silk surfaces after the 60-minute experiment (**Figure 5-10B**).

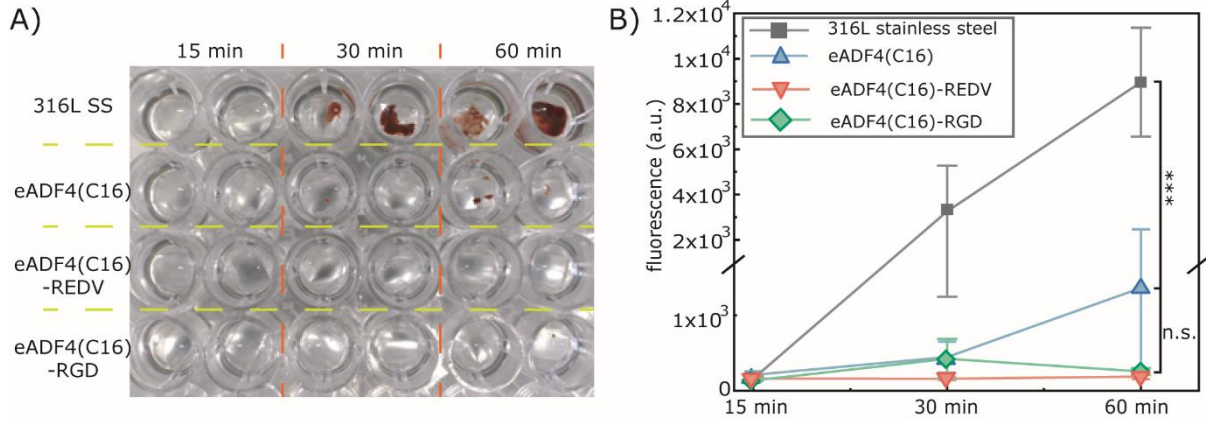


Figure 5-10: Photograph of the coagulated samples after 15-, 30-, and 60-minute exposure to human whole blood, and E) Quantification of the whole blood coagulation by measuring the fluorescence intensity of the fibrin network formed from PPP that was spiked with fluorescently labelled fibrinogen. Data is presented as mean ± standard error (n = 3 donors) p ≤ 0.001 for all statistical analyses. ***p ≤ 0.001.

Scanning electron microscopy was employed to visualize the surfaces following the whole blood coagulation assay, as depicted in **Figure 5-11**. Within 15 minutes of blood exposure, polymerized fibrin and activated platelets can be observed on the 316L stainless steel surfaces. By the 60-minute time point, an extensive fibrin network, activated platelets, and trapped red blood cells are evident on the steel surfaces. In contrast, all silk surfaces exhibit a minimal presence of platelets, white cells, and thrombus formation.

Chapter 5: Endothelial cell-selective recombinant spider silk fusion protein: application as a coating for DES

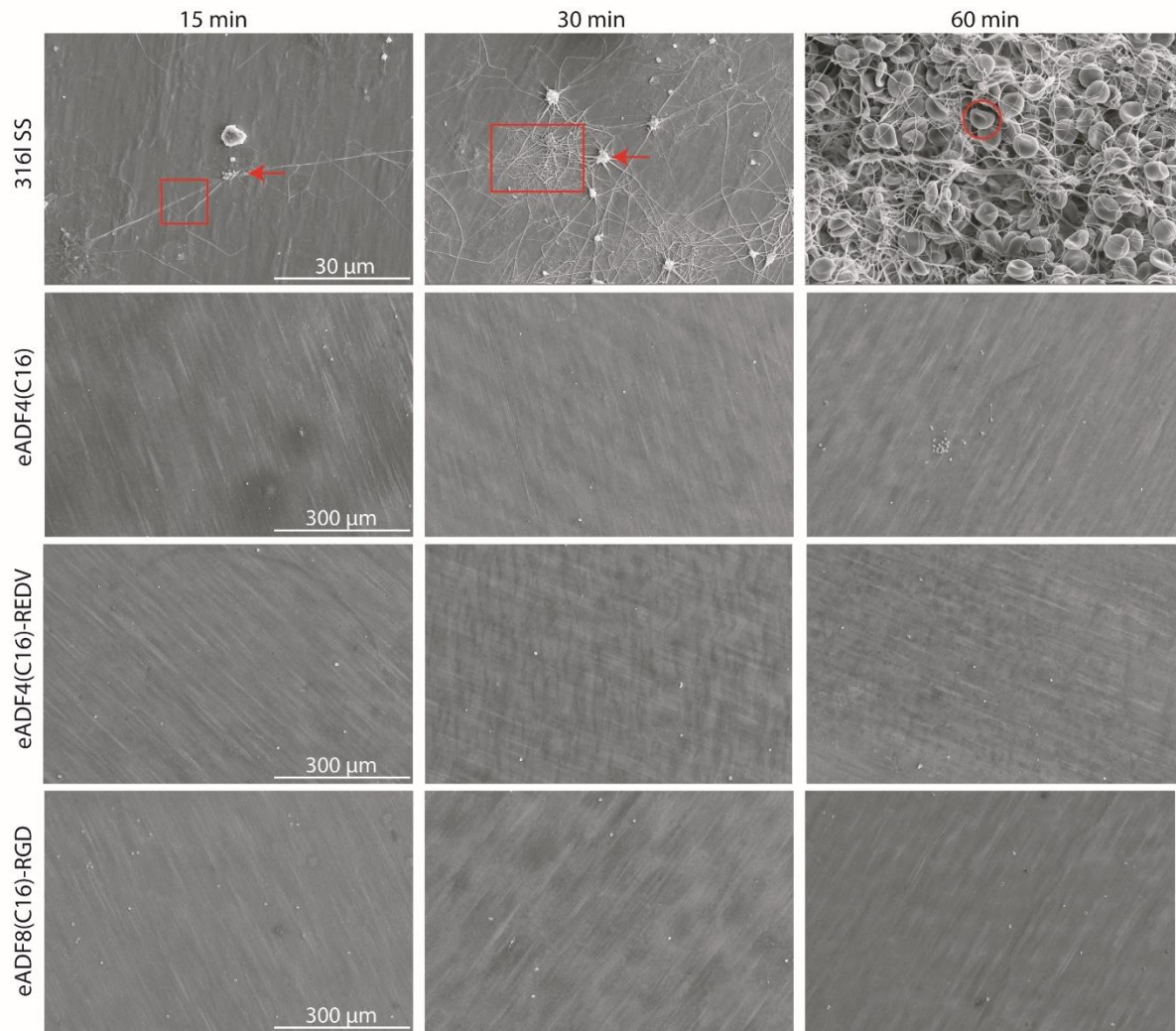


Figure 5-11: Representative scanning electron micrographs of 316L stainless steel and eADF(C16)-based surfaces after 15, 30, and 60 minutes of exposure to whole blood. Red squares highlight fibrin network formations, arrows point at activated platelets and circles denote fixed red blood cells.

Lastly, it is crucial to consider the impact of blood flow on clotting, as high shear rates can activate shear-sensitive platelets and von Willebrand Factor, while low shear rates can promote coagulation due to decreased mass transport [473]. To assess the thrombogenicity of the silk materials under blood flow conditions, the modified Chandler Loop experiment [167] was conducted (**Figure 5-12**). The results from the Chandler Loop assay align with the findings from the whole blood coagulation assay presented in **Figure 5-10** and **Figure 5-11**. Visual inspection reveals significant thrombus formation on the bare 316L stainless steel surfaces, while the spider silk surfaces exhibit minimal accumulated thrombus. The quantitative analysis of thrombus weight supports the visual observations, as all

Chapter 5: Endothelial cell-selective recombinant spider silk fusion protein: application as a coating for DES

spider silk variants demonstrate significantly lower thrombus accumulation than the stainless steel sample.

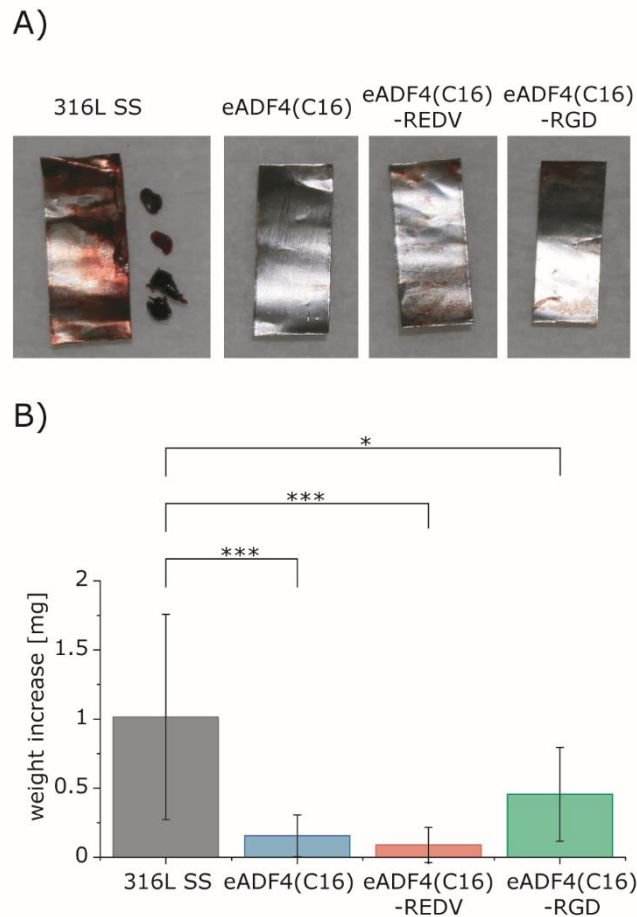


Figure 5-12: Representative photograph of samples after 30 minutes of whole blood exposure in the Chandler Loop assay. B) Quantification of modified Chandler Loop data by assessing mass gain of samples after exposure to blood. * $p < 0.05$, *** $p < 0.001$. $n = 9$

Previous research [49, 476] utilising human whole blood demonstrated initial hemocompatibility observations with eADF4(C16) particles and films. The findings presented here provide a more thorough analysis of the interactions between human blood and spider silk by examining the coagulation mechanism (activation of Factor XIIa) and the effects of shear on the clotting process (modified Chandler's loop).

The combination of thrombogenicity experiments conducted following ISO 10993-4 standards provides strong evidence that spider silk alone and its fusion variants with REDV and RGD possess low thrombogenicity compared to

Chapter 5: Endothelial cell-selective recombinant spider silk fusion protein: application as a coating for DES

hydrophilic polystyrene and stainless steel controls. Notably, all eADF4(C16) variants exhibit reduced thrombogenicity under both static and flow conditions using whole blood with minimal anticoagulation, highlighting their excellent thromboresistant properties. Overall, these findings indicate the potential of recombinant spider silk materials to exhibit exceptional thromboresistance and support their utilization in cardiovascular applications.

5.3.3 Enzymatic degradation of the coating

The polymeric stent coating is critical in releasing antiproliferative drugs in commercial drug-eluting stents. The release mechanism involves Fickian-style diffusion and drug release through polymer relaxation and degradation [477]. Therefore, it is crucial to assess the degradation of spider silk coatings under physiologically relevant conditions.

To evaluate the degradation, a mixture of human neutrophil elastase (250 ng/mL) and matrix-metalloprotease-2 (MMP-2, 250 ng/mL), two clinically-relevant human proteases were used at wound-healing concentrations [478-485]. The protein content of the coating was estimated by solubilizing post-treated steel coatings in HFIP, followed by dialysis against Tris/HCl pH 7.5, resulting in approximately 3 ± 0.3 mg protein on a 36 mm² steel sheet.

Figure 5-13A presents the mass-loss profile of eADF4(C16)-REDV coated steel sheets over a period of 29 days. The mass profile shows a relatively linear behaviour, with an approximate mass loss of 4.5 % after 29 days, aligning with previous studies on formic acid-cast films and foams in wound healing-specific enzymatic environments observing only minimal degradation [22, 49]. Furthermore, control samples incubated in buffer show no degradation throughout the experiment, supporting that the presence of enzymes had a small effect.

This slow degradation rate is preferable to synthetic coatings like PLGA, which demonstrated rapid degradation (via hydrolysis only) with mass loss of 85–90% after 30–60 days [486-488] when used as a coating. Other, more durable polymers, like coatings based on PLLA, exhibited a 15% mass loss after three

Chapter 5: Endothelial cell-selective recombinant spider silk fusion protein: application as a coating for DES

months and up to a 30% loss at month twelve [489]. This study elevated a bare metal stent to a more bulk-like method by applying a coating that was 22 m thick to it. Still, when comparing the degradation rate of DES coatings, spider silk and PLLA appear to fall into the same regime.

SEM micrographs of the spider silk surfaces during degradation are shown in **Figure 5-13B**. These micrographs support the quantitative degradation data. The control samples exhibited no significant changes, while the spider silk coatings exposed to enzymes displayed some degradation.

Chapter 5: Endothelial cell-selective recombinant spider silk fusion protein: application as a coating for DES

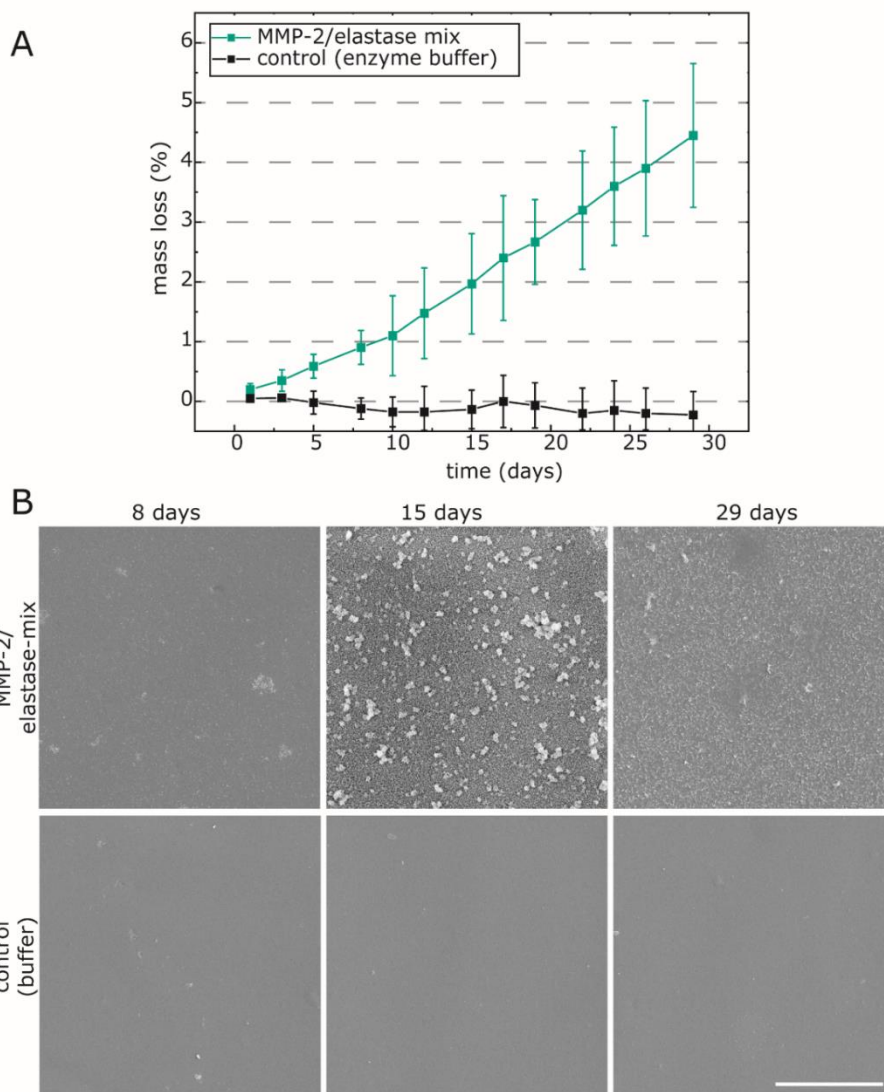


Figure 5-13: A) Degradation of eADF4(C16)-REDV coatings shown as mass loss from protein coatings over time. B) Scanning electron micrographs of silk coatings exposed to either a proteinase solution or buffer (negative control). Scale bar: 10 μm .

Interestingly, surface roughness increases in the day 15 image (magnified in **Figure 5-14**), which may be attributed to protein structure reorganization or more rapid enzymatic degradation of the amorphous protein component compared to the crystalline beta sheets. By day 29, the degraded spider silk surfaces still exhibited some surface roughness, although less pronounced than on day 15. It is important to note that spider silk degradation results in naturally occurring amino acids, which are reported to have less inflammatory potential than degradation products of commonly used polymers [490-492]. Most notably, after

Chapter 5: Endothelial cell-selective recombinant spider silk fusion protein: application as a coating for DES

29 days in a protease environment mirroring the conditions found at wound healing, approximately 95% w/w of the coating is still present on the steel sheet, displaying a homogeneous surface.

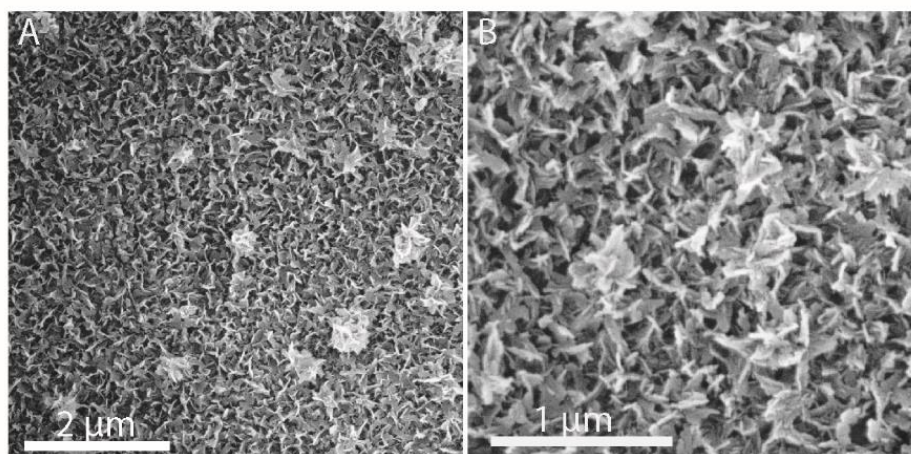


Figure 5-14: Magnified SEM micrographs from **Figure 5-13B**. Enzyme-degraded (MMP-2/elastase mix) after 15 days of incubation.

5.3.4 Drug elution properties

Present-day drug-eluting stents employ antiproliferative drugs to reduce the chance of in-stent restenosis triggered by neointimal hyperplasia [373]. Therefore, new candidates to this type of stent coating must provide elution capabilities of medically significant drugs. eADF4(C16) particles made from aqueous solution have been used before to study the transport of hydrophilic drugs [62] and β -carotin as a hydrophobic model drug [493], though DES typically comprise hydrophobic antiproliferative drugs. Consequently, this study examined the feasibility of eluting the gold standard hydrophobic antiproliferative DES-agent everolimus through eADF4(C16)-REDV coatings. Importantly, when talking about drug formulations, hydrophobic means low solubility in aqueous solutions (in the case of EVE below 1 mg/mL), whereas the solubility in non-polar solvents such as alcohols or lipids is elevated drastically[494].

Chapter 5: Endothelial cell-selective recombinant spider silk fusion protein: application as a coating for DES

Before application of the coating, the spider silk and the drug were dissolved in the shared solvent, HFIP, resulting in a transparent solution, indicating the adequate solubility of both solutes. Earlier studies confirm this finding where sirolimus (everolimus' precursor) was electrospun from an HFIP solution [373]. In this experiment, the coatings were designed to include about $0.6 \mu\text{g}/\text{mm}^2$, paralleling the drug concentration found in widely-used drug-eluting stents such as Cypher [495], Taxus™ [496], Corel-C [497], or Yinyi [498] which all average in around $1 \mu\text{g}/\text{mm}^2$.

PBS as an elution media was chosen to mimic the bodily environment in pH and salt concentration and is primarily used in *in vitro* elution studies of everolimus and sirolimus, which less water soluble than EVE [458, 461, 499].

The quantity of everolimus incorporated into the eADF4(C16)-REDV coatings on 316L stainless steel sheets with a surface area of 72 mm^2 was estimated by resolubilizing post-treated and drug-loaded coatings. The final drug concentration in the coating was $0.3 \pm 0.05 \mu\text{g}/\text{mm}^2$. Therefore, the concentration in the coating was approximately $22 \pm 4 \mu\text{g}$ ($n=2$).

Figure 5-15A details the release pattern of everolimus from the spider silk coatings into PBS, which took place over 29 days. A burst release occurred within an estimated 5 hours, releasing approximately 70% of the drug into the medium. Nevertheless, an uninterrupted release from the device was noted throughout the 29-day experiment until a final EVE concentration of approximately $3.3 \mu\text{g}$ remained in the coating (estimation of $\sim 15\%$ of $22 \mu\text{g}$ total drug loaded from solubilized coatings. Samples from the same batch).

This sustained release is crucial since the initial month is vital for curtailing neointimal hyperplasia [500, 501]. Moreover, this drug release pattern aligns with the release from PCL and other materials, showing an initial burst release followed by 3-30 days sustained release [375, 458, 502].

Despite a significant drug portion being released in the initial hours, this does not directly imply an inherent shortcoming. Commercial drug-eluting stents often release up to 90% of the drug within 48 hours. Moreover, the drug released from

Chapter 5: Endothelial cell-selective recombinant spider silk fusion protein: application as a coating for DES

those stents remained detectable in the artery wall for at least 56 days post-burst release [503].

This basic drug release approach showed the feasibility of eADF4(C16)-REDV coatings to elute the antiproliferative drug everolimus, however, several limitations regarding the assay medium and its applicability to human physiological environments need to be addressed. First, the primary medium (PBS) utilized in this assay was a simplified buffer solution, a common standard for *in vitro* experiments, which does not fully capture the complexity of the biological environment within the human body. *In vivo* conditions are significantly more complex due to the presence of various proteins and enzymes in the human system, such as albumin and proteases. These biomolecules could interact with the drug, potentially modifying the observed release kinetics.

Next, the static nature of the assay fails to replicate the dynamic conditions of blood flow present in the human body. Blood flow generates shear stress and creates a dynamic environment that can influence drug release. The absence of these conditions in the assay medium can lead to discrepancies in the observed release profiles compared to those expected in a physiological environment.

To enhance the representativeness of the drug-releasing assay, several modifications should be considered. Incorporating human plasma or serum into the assay medium would provide a more accurate representation of the protein-rich environment in the bloodstream. This modification could yield more relevant release profiles that better mimic *in vivo* conditions. Implementing bioreactors or flow chambers that simulate the shear stress and dynamic conditions of blood flow would also provide a more realistic assessment of drug release under physiological conditions. Such systems are crucial for evaluating the performance of drug-releasing coatings in a manner that closely mimics their behavior in the human body.

Various mathematical drug elution models were examined. A simple, diffusion-only model, the Korsmeyer-Peppas fit [504], was a poor match for the data with an R^2 of 0.75. However, the Peppas-Sahlin model [505], expressed in **Equation 5-2**, better matched the empirical data with an R^2 of 0.97.

Chapter 5: Endothelial cell-selective recombinant spider silk fusion protein: application as a coating for DES

$$\frac{M_t}{M_\infty} = k_1 t^m \left[1 + \frac{k_2}{k_1} t^m \right] \quad (5-2)$$

In this equation, M_t/M_∞ signifies the fraction of the drug eluted, while k_1 and k_2 , are kinetic constants, and m is the Fickian diffusion coefficient. The Peppas-Sahlin model proves beneficial when multiple kinetic processes collectively govern the release pattern. This model is often applied when the drug delivery results from an interplay between Fickian diffusion and relaxation of the polymer matrix. [505]. In the case of spider silk coatings, the polymer matrix relaxation might be partly due to the time-sensitive swelling of the polymer in the water-based environment and possibly other not-yet-defined factors [506]. This model permits the separate determination of each mechanism's contribution, as indicated in **Figure 5-15B**. Initially, drug release is primarily driven by diffusion. Over time, however, the polymer relaxation factor (i.e., swelling) grows in importance for drug delivery. It is critical to highlight that drug delivery was examined in PBS, with no proteolytic enzymes present, so the release data doesn't account for the effects of coating degradation on the release pattern. Nonetheless, the majority of drug release happens within the initial few hours, significantly quicker than the coating degradation process. Thus, the initial drug release rate likely represents the rate even if protein degradation occurred.

Chapter 5: Endothelial cell-selective recombinant spider silk fusion protein: application as a coating for DES

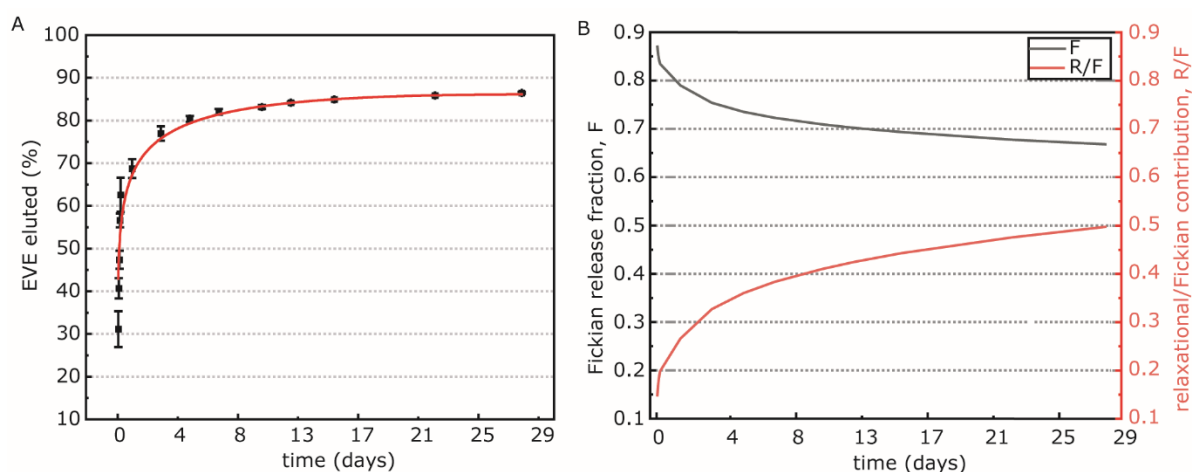


Figure 5-15: A) Drug elution of everolimus (EVE) from spider silk coatings fitted to a Pappas-Sahlin model. B) Fraction of Fickian diffusion (F ; black) and polymer relaxation (R/F ; red) over the time of drug elution according to the Peppas-Sahlin fit. Percentage estimated based on the total amount of drug from independent measurements. $n=2$

5.4 Conclusion

The data presented in Chapter 5 provides compelling evidence for the potential application of eADF4(C16)-REDV as a coating for drug-eluting stents. The unique properties exhibited by this fusion protein make it a promising candidate for enhancing the performance and safety of these medical devices.

In addition to its endothelial cell selectivity, covered in **Chapter 4**, eADF4(C16)-REDV demonstrates excellent hemocompatibility. The fusion protein exhibits excellent hemocompatibility, minimising platelet activation and thrombus formation, thus reducing the risk of stent-associated thrombosis. This feature is of utmost importance for the long-term success of drug-eluting stents, as it ensures the maintenance of blood flow and prevents adverse events.

Additionally, enzymatic degradation experiments showcased the long-term viability of eADF4(C16)-REDV-based coatings with approximately 95% of the protein mass remaining after 29 days.

Furthermore, eADF4(C16)-REDV can effectively release clinically relevant drugs over appropriate timeframes. The controlled release of therapeutic agents from

Chapter 5: Endothelial cell-selective recombinant spider silk fusion protein: application as a coating for DES

the coating allows targeted drug delivery to the site of the stent implantation, promoting local tissue healing and reducing the risk of restenosis. The release kinetics can be tailored to suit specific therapeutic requirements, ensuring optimal drug concentrations at the desired site for an extended period.

Overall, the comprehensive assessment of eADF4(C16)-REDV in these chapters highlights its potential as a coating for drug-eluting stents. Its selectivity towards endothelial cells, ability to foster a confluent endothelium, excellent hemocompatibility, and controlled drug release make it a promising candidate for improving the efficacy and safety of these medical devices. Further research and development efforts are warranted, such as more appropriate coating technologies and in vivo testing. Furthermore, blending of REDV and RGD modified protein variants could potentially further enhance the proliferation rate of the surface while maintaining selectivity towards EC. However, as the RGD peptide showed substantially increased attachment of all the tested cell types, careful investigation of a “sweet spot” blend ratio would need to be carried out to evaluate if a blend ratio is capable of improving EC attachment while at the same time not significantly enhancing the attachment of other cell types. Tackling these remaining points could pave the way to advance the translation of this innovative biomaterial into clinical applications, with the ultimate goal of enhancing patient outcomes in interventional cardiology.

Chapter 6 Summary and future outlook

6.1 Summary

This thesis has focused on developing and characterising spider silk-based biomaterials for tissue engineering applications. Two main areas were investigated: using the cellulose-binding fusion protein eADF4(C16)-CBD for hydrogel applications and developing REDV-modified silk- proteins as coatings for drug-eluting stents.

The exploration of spider silk proteins, particularly recombinant variants like eADF4(C16) and their fusion proteins (e.g., eADF4(C16)-CBD and eADF4(C16)-REDV), presents promising advancements in TE and biomedical applications. These proteins offer exceptional biocompatibility, remarkable mechanical strength, and versatility in modifications, positioning them as superior alternatives to traditional materials. Their potential for promoting tissue regeneration and improving biomedical devices, such as stents, highlights their significance in the healthcare sector.

However, several limitations must be addressed for these materials to achieve clinical success. Scaling up production to meet clinical demand remains a significant challenge, as does the high cost of production. Additionally, navigating complex regulatory pathways and ensuring long-term stability and performance *in vivo* are critical hurdles that need to be overcome. Collaborative efforts between material scientists, biologists, clinicians, and engineers will be crucial to optimize these biomaterials for clinical use.

Advanced *in vivo* models, such as small animal models and microfluidic chips, are essential for testing material properties in realistic settings. These models will help evaluate the long-term functionality and integration of the scaffolds in a physiological environment. Furthermore, detailed application-specific studies focusing on bone regeneration, wound healing, and cardiovascular stent coatings will provide tailored solutions for each clinical application.

Chapter 6: Summary and future outlook

The progress beyond the current state of the art involves enhanced mechanical properties, improved biocompatibility, and specific cell adhesion properties introduced by functional peptides like REDV. While production scalability and cost remain challenges, optimizing bioprocessing techniques and leveraging economies of scale offer potential pathways for improvement. The research presented in this thesis lays the groundwork for several clinical applications, representing significant advancements in TE and biomedical technologies.

The eADF4(C16)-CBD fusion protein was studied for its application as hydrogel materials in the first part of the thesis. Regarding the design of the fusion protein, it proved of great significance to include a linker sequence between the eADF4(C16) and the CBD moiety. Despite the recombinant spider silk's linear and not actively functional structure, only physical spacing between both fusion partners enabled a properly structured CBD, showing effective cellulose binding. Structural observations such as CD and fluorescence spectroscopy validated the adequately folded and functioning of the fusion construct. Furthermore, cellulose binding was demonstrated via an incubation assay and QCM-D measurements. The final fusion protein retained the ability of the unmodified eADF4(C16) protein's ability to form hydrogels, demonstrating improved printability and shape fidelity. Incorporating cellulose fibres further enhanced the mechanical properties of the hydrogels, resulting in increased stiffness and yield stress. The cellulose fibre-enhanced hydrogels also exhibited improved cell proliferation rates and morphological changes *in vitro*, indicating their potential for tissue engineering applications. The findings from this research highlight the suitability of eADF4(C16)-CBD hydrogels as injectable yet form-stable materials for various biomedical applications.

The second part of the thesis focused on silk-based protein constructs as coatings for drug-eluting stents.

The eADF4(C16)-REDV protein was investigated explicitly for its potential as a coating to improve drug-eluting stents' biocompatibility, tissue integration, degradability, hemocompatibility and therapeutic efficacy.

Chapter 6: Summary and future outlook

One key advantage of eADF4(C16)-REDV is its selectivity towards endothelial cells. The specific recognition and binding of the REDV peptide sequence to integrin receptors expressed on endothelial cells ensure targeted and effective interactions with the desired cell population. This selectivity promotes the formation of a confluent endothelium on the stent surface, which is crucial for facilitating proper vascular healing and minimizing the risk of complications such as thrombosis. It is important to clarify that while the REDV-functionalized surfaces demonstrated near-monolayer coverage and the formation of endothelial cell-cell adhesions after seven days *in vitro*, this does not equate to a fully functional endothelium. A fully functional endothelium involves more complex characteristics, including barrier function, anti-thrombotic properties, and the ability to respond to physiological signals.

In addition to its endothelial cell selectivity, eADF4(C16)-REDV demonstrates excellent hemocompatibility. The fusion protein exhibits a favourable interaction with blood components, minimizing platelet activation and thrombus formation, thus reducing the risk of stent-associated thrombosis. This feature is of utmost importance for the long-term success of drug-eluting stents, as it ensures the maintenance of blood flow and prevents adverse events.

Furthermore, eADF4(C16)-REDV can effectively release the clinically relevant drug everolimus over appropriate timeframes. The controlled release of therapeutic agents from the coating allows targeted drug delivery to the site of the stent implantation, promoting local tissue healing and reducing the risk of restenosis. The release kinetics can be tailored to suit specific therapeutic requirements, ensuring optimal drug concentrations at the desired site for an extended period.

While the *in vitro* results are promising, *in vivo* studies are essential to validate these findings in a more complex biological environment. The choice of *in vivo* models is crucial for understanding the behavior and efficacy of these biomaterials under physiological conditions. To assess the true potential of these materials, several experimental designs can be proposed. For instance, small animal models such as mice or rats could provide valuable data on biocompatibility, degradation, and efficacy over time. Experiments involving the implantation of eADF4(C16)-REDV coated stents in rodent models could evaluate the stent's performance in

Chapter 6: Summary and future outlook

preventing restenosis and promoting endothelialization in a living system. Advanced imaging techniques, such as intravital microscopy, could be utilized to observe the endothelialization process *in vivo*, measuring parameters such as the degree of restenosis, inflammation markers, and endothelial cell coverage over time. However, as stent structures for rodents may not be applicable, large animal models like pigs, which are more physiologically similar to humans, could be employed. These models can provide more relevant data on the long-term performance and safety of the biomaterials. Utilizing discarded human tissues from surgeries to create an *ex vivo* model can also provide a more accurate representation of how the biomaterials will perform in human patients. For instance, using segments of human veins or arteries to test the interaction of the coated stents with actual human endothelial tissues can offer critical insights.

Moreover, the development of a microfluidic chip that integrates endothelial cells forming capillary-like structures can be used to study the interaction of eADF4(C16)-REDV coatings with blood flow. This setup would allow for the real-time observation of endothelialization, drug release kinetics and the coating integrity under dynamic conditions, providing insights into how these materials interact with blood flow and cellular environments, thus mimicking *in vivo* conditions more closely than static *in vitro* assays.

Overall, this study's assessment of eADF4(C16)-REDV highlights its potential as a coating for drug-eluting stents. Its selectivity towards endothelial cells, ability to foster a confluent endothelium, excellent hemocompatibility, and controlled drug release make it a promising candidate for improving the efficacy and safety of these medical devices. Further research and development efforts are warranted to advance the translation of this innovative biomaterial into clinical applications, with the ultimate goal of enhancing patient outcomes in interventional cardiology.

These results suggest that eADF4(C16)-REDV coatings hold promise for enhancing the performance of drug-eluting stents and improving patient outcomes.

Concluding, this thesis has explored the potential of recombinant spider silk proteins, specifically eADF4(C16)-CBD and eADF4(C16)-REDV, in advancing tissue engineering and cardiovascular disease management. These proteins offer unique

Chapter 6: Summary and future outlook

properties that can address the limitations of existing treatments and open new avenues for medical interventions. The modified eADF4(C16)-CBD hydrogel presents an injectable scaffold with enhanced stiffness, cell adhesion potential, and tunable mechanical properties, making it a promising candidate for tissue engineering applications. On the other hand, the eADF4(C16)-REDV coating for drug-eluting stents offers improved biocompatibility, hemocompatibility, and endothelialization, addressing critical challenges in stenting technology. By leveraging these recombinant spider silk proteins, significant progress can be made in tissue engineering and cardiovascular disease management, bringing us closer to effective and patient-centric medical solutions.

6.2 Future perspectives

The current state of the art in tissue engineering and cardiovascular disease management involves several approaches and materials, but significant limitations persist that hinder their effectiveness and broader clinical application. For TE, existing scaffolds such as ones made from synthetic polymers and natural biopolymers often lack the ideal combination of mechanical strength, biocompatibility, and degradation profiles needed for effective tissue regeneration. Synthetic polymers, while tunable in their properties, can provoke inflammatory responses and have suboptimal degradation rates.

In the realm of cardiovascular disease management, DES have revolutionized the treatment of coronary artery disease by preventing restenosis. However, these stents often fall short in promoting rapid endothelialization and can lead to chronic inflammation and late thrombosis. Current stent coatings made from synthetic polymers or metallic surfaces struggle with hemocompatibility and fail to adequately support the formation of a functional endothelial layer.

This PhD project seeks to advance on these limitations by exploring the potential of modified recombinant spider silk proteins, specifically eADF4(C16)-CBD and eADF4(C16)-REDV, for use in both TE scaffolds and stent coatings. The unique properties of these silk proteins, such as their mechanical strength,

Chapter 6: Summary and future outlook

biocompatibility, and tunable degradation rates, position them as suitable alternatives to current materials.

For spider silk-based TE applications, the eADF4(C16)-CBD hydrogel represents a significant leap forward. By incorporating a cellulose-binding domain, the hydrogel demonstrates enhanced mechanical properties and stability, overcoming the fragility typically associated with physically crosslinked hydrogels made from recombinant spider silk proteins. This modification allows the hydrogel to maintain structural integrity under physiological conditions, making it suitable for injectable applications. Additionally, the improved cell adhesion properties of the eADF4(C16)-CBD hydrogel offer a more conducive environment for tissue regeneration, paving the way for more application-oriented experiments on this novel gel formulation. However, while the young's modulus and the corresponding stiffness could be greatly increased, it should be noted that these eADF4(C16)-based hydrogels still reign amongst the lower stiffness gels in TE and therefore should be considered for lower-stiffness applications.

In cardiovascular disease management, the eADF4(C16)-REDV functionalized coating addresses the critical challenge of promoting endothelialization while minimizing inflammation and thrombosis. The REDV peptide's selectivity for endothelial cells ensures that the coating supports the rapid formation of a functional endothelial layer, which is essential for the long-term success of stents. This approach not only reduces the risk of restenosis but also enhances the overall hemocompatibility of the stent.

Experimental findings from this thesis provide substantial evidence for the performance of these novel materials. The eADF4(C16)-CBD hydrogels exhibit excellent biocompatibility and mechanical strength, supporting cell proliferation and maintaining stability under physiological conditions *in vitro*. The eADF4(C16)-REDV coatings demonstrate selective endothelial cell adhesion and proliferation, significantly improving the formation of a confluent endothelial layer while minimizing the adhesion of non-endothelial cells. These first experiments on the new coating material for DES showed great potential and once the hurdle of coating mechanisms is improved on, follow-up *in vivo* tests could potentially lead to observations regarding clinical translation.

Chapter 6: Summary and future outlook

While this thesis has made new contributions to the field of biomaterials for TE, several avenues for future research warrant exploration. These future directions will further enhance the understanding and application of the developed biomaterials.

In the case of the eADF4(C16)-CBD hydrogel variant, future research should focus firstly on improving protein yield from the current production method. As mentioned in **2.2.2**, the yield after IMAC serves for analysis purposes but large-scale application experiments, such as *in vivo* trials or comparisons of different gel compositions, remain a hurdle with a yield this low.

Once this issue has been improved upon, different blend compositions and potentially more defined cellulose components could be utilized, as the current cellulose fibres showed a wildly varying morphology in **Figure 3-2**. By more precisely formulating the individual materials, even more defined hydrogels could be created, potentially also improving by cell adhesion peptides such as RGD to enhance cellular compatibility further. In an even more engaging project, these proteins could be combined by incorporating an RGD sequence at the N-terminus or between individual C-modules, such as between two blocks of C8, of the fusion protein.

Regarding the DES coatings, it is crucial to investigate alternative coating mechanisms. Enhancing the adhesion of the coating is of utmost importance to ensure its long-term stability and efficacy. Electrocoating involves depositing a coating material through an electrochemical process, enabling strong adhesion between the coating and the stent surface. Further investigation is required to determine if electrocoating could potentially generate covalent bonds with an intermediate layer and evaluate its feasibility as a coating method for drug-eluting stents.

The transition from coating steel sheets to the stent morphology will be the next challenge of this new material. Dip-coating is not a feasible technique for delicate structures such as stents and therefore needs to be replaced by more sophisticated methods.

Chapter 6: Summary and future outlook

Among the promising techniques are ultrasonication coating and electrospinning, each offering unique advantages for applying coatings to DES.

Ultrasonication coating utilizes high-frequency ultrasonic waves to create a fine mist of the coating solution, which can then be directed onto the stent surface. This method ensures a uniform and precise application of the coating material, even on the complex geometries characteristic of stents [507, 508]. In Fact, Ultrasonication coating is the standard of coating DES in the industry due to its fast and reproducible results.

Electrospinning uses an electric field to draw very fine fibers from a liquid polymer solution, creating nanoscale fibers that form a mesh-like coating around the stent. This method includes preparing a viscous polymer solution, using a high voltage to form fibers, and collecting these fibers on the stent through rotational movement [509]. The shortcomings of this approach however could be the limited capability to coat the inner lumen-facing surface of the stent.

These advanced coating techniques are essential for achieving the desired properties in drug-eluting stents, such as uniform coating, controlled drug release, and improved biocompatibility.

While the exploration of eADF4(C16)-REDV as a ultrasonication coated stent coating is promising, several variables and future challenges must be addressed to ensure successful application. The substrate material of the stents, typically composed of metal alloys, most commonly stainless steel or cobalt-chromium, but also other materials such as platinum-chromium or nickel-titanium, may present different surface properties that may affect the adhesion and uniformity of the spray-coated silk proteins is a different metal than 316L stainless steel is utilized. Additionally, the presence of shear forces during blood flow can impact the stability and durability of the coating. Moreover, the mechanical deformation of stents during crimping and expansion poses significant challenges, as these processes can lead to delamination or cracking of the coating. Future research must focus on optimizing the spray coating process to enhance adhesion, ensuring the coating's robustness under physiological shear conditions, and developing formulations that maintain integrity during mechanical deformation.

Chapter 6: Summary and future outlook

Furthermore, the drug-elution time-span will most likely be altered by a different deposition method, being another point of interest in the future applications of eADF4(C16)-REDV as DES coatings.

In addition to exploring different coating mechanisms, future research should investigate different drug encapsulation strategies to improve the drug loading capacity and release kinetics. The influence of coating thickness on drug release profiles should also be examined to achieve the desired therapeutic effect. Furthermore, the performance of the eADF4(C16)-REDV coating should be evaluated in *in vivo* models to assess its efficacy and safety under physiological conditions as well as to observe endothelialisation capabilities in a living organism.

The development of these biomaterials holds great promise for advancing regenerative medicine and treating various biomedical challenges, ultimately leading to improved patient outcomes. Further research and exploration of the suggested future directions will be essential in realizing the full potential of these biomaterials in clinical applications. By addressing the identified challenges and pursuing the suggested future directions, we can overcome the limitations and maximize the potential of these biomaterials, ultimately bringing us closer to realising effective tissue engineering solutions and improved patient care.

References

- [1] K.Y. Lee, D.J. Mooney, Hydrogels for Tissue Engineering, *Chemical Reviews*, 101 (2001) 1869-1880.
- [2] X. Xue, Y. Hu, S. Wang, X. Chen, Y. Jiang, J. Su, Fabrication of physical and chemical crosslinked hydrogels for bone tissue engineering, *Bioact Mater*, 12 (2022) 327-339.
- [3] Y. Liu, W. Huang, M. Meng, M. Chen, C. Cao, Progress in the application of spider silk protein in medicine, *J Biomater Appl*, 36 (2021) 859-871.
- [4] M. Ribeiro, M.A. de Moraes, M.M. Beppu, M.P. Garcia, M.H. Fernandes, F.J. Monteiro, M.P. Ferraz, Development of silk fibroin/nanohydroxyapatite composite hydrogels for bone tissue engineering, *European Polymer Journal*, 67 (2015) 66-77.
- [5] X. Yu, X. Wang, D. Li, R. Sheng, Y. Qian, R. Zhu, X. Wang, K. Lin, Mechanically reinforced injectable bioactive nanocomposite hydrogels for in-situ bone regeneration, *Chemical Engineering Journal*, 433 (2022).
- [6] J. Liu, B. Zheng, P. Wang, X. Wang, B. Zhang, Q. Shi, T. Xi, M. Chen, S. Guan, Enhanced in vitro and in vivo performance of Mg-Zn-Y-Nd alloy achieved with APTES pretreatment for drug-eluting vascular stent application, *ACS applied materials & interfaces*, 8 (2016) 17842-17858.
- [7] D. Mozaffarian, E. Benjamin, A. Go, D. Arnett, M. Blaha, M. Cushman, S. Das, S. De Ferranti, J. Despres, H. Fullerton, American heart association statistics committee; Stroke statistics subcommittee. Heart disease and stroke statistics-2016 update: a report from the American Heart Association, *Circulation*, 133 (2016) e38-e60.
- [8] S.S. Dhruva, C.S. Parzynski, G.M. Gamble, J.P. Curtis, N.R. Desai, R.W. Yeh, F.A. Masoudi, R. Kuntz, R.E. Shaw, D. Marinac-Dabic, A. Sedrakyan, S.L.T. Normand, H.M. Krumholz, J.S. Ross, Attribution of Adverse Events Following Coronary Stent Placement Identified Using Administrative Claims Data, *Journal of the American Heart Association*, 9 (2020) e013606.
- [9] L. Mao, G. Yuan, J. Niu, Y. Zong, W. Ding, In vitro degradation behavior and biocompatibility of Mg-Nd-Zn-Zr alloy by hydrofluoric acid treatment, *Materials Science and Engineering: C*, 33 (2013) 242-250.
- [10] P. Wang, P. Xiong, J. Liu, S. Gao, T. Xi, Y. Cheng, A silk-based coating containing GREDVY peptide and heparin on Mg-Zn-Y-Nd alloy: improved corrosion resistance, hemocompatibility and endothelialization, *J Mater Chem B*, 6 (2018) 966-978.
- [11] B.L. van der Hoeven, N.M. Pires, H.M. Warda, P.V. Oemrawsingh, B.J. van Vlijmen, P.H. Quax, M.J. Schalij, E.E. van der Wall, J.W. Jukema, Drug-eluting stents: results, promises and problems, *Int J Cardiol*, 99 (2005) 9-17.
- [12] T. Scheibel, Spider silks: recombinant synthesis, assembly, spinning, and engineering of synthetic proteins, *Microb Cell Fact*, 3 (2004) 14.
- [13] A. Heidebrecht, T. Scheibel, Recombinant production of spider silk proteins, *Adv Appl Microbiol*, 82 (2013) 115-153.
- [14] M. Saric, T. Scheibel, Engineering of silk proteins for materials applications, *Curr Opin Biotechnol*, 60 (2019) 213-220.

-
- [15] M. Saric, L. Eisoldt, V. Doring, T. Scheibel, Interplay of Different Major Ampullate Spidroins during Assembly and Implications for Fiber Mechanics, *Adv Mater*, (2021) e2006499.
- [16] C.B. Borkner, M.B. Elsner, T. Scheibel, Coatings and films made of silk proteins, *ACS Appl Mater Interfaces*, 6 (2014) 15611-15625.
- [17] S.T. Parker, P. Domachuk, J. Amsden, J. Bressner, J.A. Lewis, D.L. Kaplan, F.G. Omenetto, Biocompatible Silk Printed Optical Waveguides, *Advanced Materials*, 21 (2009) 2411-2415.
- [18] F. Teulé, W.A. Furin, A.R. Cooper, J.R. Duncan, R.V. Lewis, Modifications of spider silk sequences in an attempt to control the mechanical properties of the synthetic fibers, *Journal of Materials Science*, 42 (2007) 8974-8985.
- [19] D. Huemmerich, T. Scheibel, F. Vollrath, S. Cohen, U. Gat, S. Ittah, Novel assembly properties of recombinant spider dragline silk proteins, *Curr Biol*, 14 (2004) 2070-2074.
- [20] D. Steiner, G. Lang, L. Fischer, S. Winkler, T. Fey, P. Greil, T. Scheibel, R.E. Horch, A. Arkudas, Intrinsic Vascularization of Recombinant eADF4(C16) Spider Silk Matrices in the Arteriovenous Loop Model, *Tissue Eng Part A*, (2019).
- [21] A. Leal-Egaña, G. Lang, C. Mauerer, J. Wickinghoff, M. Weber, S. Geimer, T. Scheibel, Interactions of Fibroblasts with Different Morphologies Made of an Engineered Spider Silk Protein, *Advanced Engineering Materials*, 14 (2012) B67-B75.
- [22] S. Müller-Herrmann, T. Scheibel, Enzymatic Degradation of Films, Particles, and Nonwoven Meshes Made of a Recombinant Spider Silk Protein, *ACS Biomaterials Science & Engineering*, 1 (2015) 247-259.
- [23] C. Sommer, H. Bargel, N. Raßmann, T. Scheibel, Microbial repellence properties of engineered spider silk coatings prevent biofilm formation of opportunistic bacterial strains, *MRS Communications*, 11 (2021) 356-362.
- [24] K. Schacht, T. Scheibel, Controlled hydrogel formation of a recombinant spider silk protein, *Biomacromolecules*, 12 (2011) 2488-2495.
- [25] Y. Zhang, T. Nypelö, C. Salas, J. Arboleda, I.C. Hoeger, O.J. Rojas, Cellulose nanofibrils: From strong materials to bioactive surfaces, *J. Renew. Mater*, 1 (2013) 195-211.
- [26] P. Tomme, D.P. Driver, E.A. Amandoron, R.C. Miller, R. Antony, J. Warren, D.G. Kilburn, Comparison of a fungal (family I) and bacterial (family II) cellulose-binding domain, 177 (1995) 4356-4363.
- [27] R.A.J. Warren, C.F. Beck, N.R. Gilkes, D.G. Kilburn, M.L. Langsford, R.C. Miller Jr., G.P. O'Neill, M. Scheufens, W.K.R. Wong, Sequence conservation and region shuffling in an endoglucanase and an exoglucanase from *Cellulomonas fimi*, 1 (1986) 335-341.
- [28] W. Wang, L. Guo, Y. Yu, Z. Chen, R. Zhou, Z. Yuan, Peptide REDV-modified polysaccharide hydrogel with endothelial cell selectivity for the promotion of angiogenesis, *J Biomed Mater Res A*, 103 (2015) 1703-1712.
- [29] Y.I. Hsu, A. Mahara, T. Yamaoka, Identification of circulating cells interacted with integrin alpha4beta1 ligand peptides REDV or HGGVRLY, *Peptides*, 136 (2021) 170470.

-
- [30] S.P. Massia, J.A. Hubbell, Vascular endothelial cell adhesion and spreading promoted by the peptide REDV of the IIICS region of plasma fibronectin is mediated by integrin alpha 4 beta 1, *Journal of Biological Chemistry*, 267 (1992) 14019-14026.
- [31] N. Nicoli Aldini, M. Fini, R. Giardino, From Hippocrates to tissue engineering: surgical strategies in wound treatment, *World J Surg*, 32 (2008) 2114-2121.
- [32] L. Aschoff, P. Diepgen, Primitive Medizin, in: L. Aschoff, P. Diepgen (Eds.) *Kurze Übersichtstabelle zur Geschichte der Medizin*, Springer Berlin Heidelberg, Berlin, Heidelberg, 1940, pp. 1-1.
- [33] L. Aschoff, P. Diepgen, Neue Zeit, in: L. Aschoff, P. Diepgen (Eds.) *Kurze Übersichtstabelle zur Geschichte der Medizin*, Springer Berlin Heidelberg, Berlin, Heidelberg, 1940, pp. 25-72.
- [34] C.A. Vacanti, The history of tissue engineering, *J Cell Mol Med*, 10 (2006) 569-576.
- [35] L. Aschoff, P. Diepgen, Neueste Zeit, in: L. Aschoff, P. Diepgen (Eds.) *Kurze Übersichtstabelle zur Geschichte der Medizin*, Springer Berlin Heidelberg, Berlin, Heidelberg, 1940, pp. 73-76.
- [36] R. Skalak, C.F. Fox, *Tissue engineering : proceedings of a workshop, held at Granlibakken, Lake Tahoe, California, February 26-29, 1988*, Liss, New York, 1988.
- [37] M. Asadian, K.V. Chan, M. Norouzi, S. Grande, P. Cools, R. Morent, N. De Geyter, Fabrication and Plasma Modification of Nanofibrous Tissue Engineering Scaffolds, *Nanomaterials (Basel)*, 10 (2020).
- [38] M.P. Nikolova, M.S. Chavali, Recent advances in biomaterials for 3D scaffolds: A review, *Bioact Mater*, 4 (2019) 271-292.
- [39] R. Langer, J.P. Vacanti, *Tissue Engineering*, *Science*, 260 (1993) 920-926.
- [40] Y. Liu, H. Wang, H. Dou, B. Tian, L. Li, L. Jin, Z. Zhang, L. Hu, Bone regeneration capacities of alveolar bone mesenchymal stem cells sheet in rabbit calvarial bone defect, *Journal of tissue engineering*, 11 (2020) 2041731420930379.
- [41] A. Ashok, D. Choudhury, Y. Fang, W. Hunziker, Towards manufacturing of human organoids, *Biotechnology Advances*, 39 (2020) 107460.
- [42] M. Ganjibakhsh, F. Mehraein, M. Koruji, R. Aflatoonian, P. Farzaneh, Three-dimensional decellularized amnion membrane scaffold as a novel tool for cancer research; cell behavior, drug resistance and cancer stem cell content, *Materials Science and Engineering: C*, 100 (2019) 330-340.
- [43] P.X. Ma, R. Langer, Fabrication of biodegradable polymer foams for cell transplantation and tissue engineering, *Methods Mol Med*, 18 (1999) 47-56.
- [44] B.B. Mandal, S.C. Kundu, Non-bioengineered silk fibroin protein 3D scaffolds for potential biotechnological and tissue engineering applications, *Macromol Biosci*, 8 (2008) 807-818.
- [45] D.W. Hutmacher, Scaffolds in tissue engineering bone and cartilage, *Biomaterials*, 21 (2000) 2529-2543.

-
- [46] H. Kweon, M.K. Yoo, I.K. Park, T.H. Kim, H.C. Lee, H.-S. Lee, J.-S. Oh, T. Akaike, C.-S. Cho, A novel degradable polycaprolactone networks for tissue engineering, *Biomaterials*, 24 (2003) 801-808.
- [47] W.J. Li, C.T. Laurencin, E.J. Caterson, R.S. Tuan, F.K. Ko, Electrospun nanofibrous structure: a novel scaffold for tissue engineering, *Journal of biomedical materials research*, 60 (2002) 613-621.
- [48] H. Shin, S. Jo, A.G. Mikos, Biomimetic materials for tissue engineering, *Biomaterials*, 24 (2003) 4353-4364.
- [49] S. Lentz, V.T. Trossmann, C.B. Borkner, V. Beyersdorfer, M. Rottmar, T. Scheibel, Structure-Property Relationship Based on the Amino Acid Composition of Recombinant Spider Silk Proteins for Potential Biomedical Applications, *ACS Appl Mater Interfaces*, 14 (2022) 31751-31766.
- [50] T.U. Esser, V.T. Trossmann, S. Lentz, F.B. Engel, T. Scheibel, Designing of spider silk proteins for human induced pluripotent stem cell-based cardiac tissue engineering, *Mater Today Bio*, 11 (2021) 100114.
- [51] B.D. Lawrence, J.K. Marchant, M.A. Pindrus, F.G. Omenetto, D.L. Kaplan, Silk film biomaterials for cornea tissue engineering, *Biomaterials*, 30 (2009) 1299-1308.
- [52] P.H. Zeplin, N.C. Maksimovikj, M.C. Jordan, J. Nickel, G. Lang, A.H. Leimer, L. Römer, T. Scheibel, Spider Silk Coatings as a Bioshield to Reduce Periprosthetic Fibrous Capsule Formation, *Advanced Functional Materials*, 24 (2014) 2658-2666.
- [53] K.S. Koeck, S. Salehi, M. Humenik, T. Scheibel, Processing of Continuous Non-Crosslinked Collagen Fibers for Microtissue Formation at the Muscle-Tendon Interface, *Advanced Functional Materials*, 32 (2021).
- [54] A. Tamayol, M. Akbari, N. Annabi, A. Paul, A. Khademhosseini, D. Juncker, Fiber-based tissue engineering: Progress, challenges, and opportunities, *Biotechnology advances*, 31 (2013) 669-687.
- [55] R. Murugan, S. Ramakrishna, Design strategies of tissue engineering scaffolds with controlled fiber orientation, *Tissue engineering*, 13 (2007) 1845-1866.
- [56] E. DeSimone, K. Schacht, T. Scheibel, Cations influence the cross-linking of hydrogels made of recombinant, polyanionic spider silk proteins, *Materials Letters*, 183 (2016) 101-104.
- [57] V.T. Trossmann, S. Heltmann-Meyer, H. Amouei, H. Wajant, R.E. Horch, D. Steiner, T. Scheibel, Recombinant Spider Silk Bioinks for Continuous Protein Release by Encapsulated Producer Cells, *Biomacromolecules*, (2022).
- [58] A. Lechner, V.T. Trossmann, T. Scheibel, Impact of Cell Loading of Recombinant Spider Silk Based Bioinks on Gelation and Printability, *Macromol Biosci*, 22 (2022) e2100390.
- [59] D. Steiner, S. Winkler, S. Heltmann-Meyer, V.T. Trossmann, T. Fey, T. Scheibel, R.E. Horch, A. Arkudas, Enhanced vascularization and de novo tissue formation in hydrogels made of engineered RGD-tagged spider silk proteins in the arteriovenous loop model, *Biofabrication*, 13 (2021) 045003.
- [60] K. Schacht, J. Vogt, T. Scheibel, Foams Made of Engineered Recombinant Spider Silk Proteins as 3D Scaffolds for Cell Growth, *ACS Biomaterials Science & Engineering*, 2 (2016) 517-525.

-
- [61] L. Brannon-Peppas, Recent advances on the use of biodegradable microparticles and nanoparticles in controlled drug delivery, *International Journal of Pharmaceutics*, 116 (1995) 1-9.
- [62] A. Lammel, M. Schwab, M. Hofer, G. Winter, T. Scheibel, Recombinant spider silk particles as drug delivery vehicles, *Biomaterials*, 32 (2011) 2233-2240.
- [63] K. Kucharczyk, J.D. Rybka, M. Hilgendorff, M. Krupinski, M. Slachcinski, A. Mackiewicz, M. Giersig, H. Dams-Kozłowska, Composite spheres made of bioengineered spider silk and iron oxide nanoparticles for theranostics applications, *PLoS One*, 14 (2019) e0219790.
- [64] Y.B. Truong, V. Glattauer, G. Lang, K. Hands, I.L. Kyratzis, J.A. Werkmeister, J.A. Ramshaw, A comparison of the effects of fibre alignment of smooth and textured fibres in electrospun membranes on fibroblast cell adhesion, *Biomed Mater*, 5 (2010) 25005.
- [65] T. Hoshiba, H. Lu, N. Kawazoe, G. Chen, Decellularized matrices for tissue engineering, *Expert Opinion on Biological Therapy*, 10 (2010) 1717-1728.
- [66] X. Zhang, X. Chen, H. Hong, R. Hu, J. Liu, C. Liu, Decellularized extracellular matrix scaffolds: Recent trends and emerging strategies in tissue engineering, *Bioactive Materials*, 10 (2022) 15-31.
- [67] J.S. Lee, Y.S. Choi, S.-W. Cho, Decellularized Tissue Matrix for Stem Cell and Tissue Engineering, in: I. Noh (Ed.) *Biomimetic Medical Materials: From Nanotechnology to 3D Bioprinting*, Springer Singapore, Singapore, 2018, pp. 161-180.
- [68] P. Zhao, H. Gu, H. Mi, C. Rao, J. Fu, L.-s. Turng, Fabrication of scaffolds in tissue engineering: A review, *Frontiers of Mechanical Engineering*, 13 (2017) 107-119.
- [69] H.A. Tran, T.T. Hoang, A. Maraldo, T.N. Do, D.L. Kaplan, K.S. Lim, J. Rnjak-Kovacina, Emerging silk fibroin materials and their applications: New functionality arising from innovations in silk crosslinking, *Materials Today*, (2023).
- [70] A.C. Daly, K.S. Lim, High resolution lithography 3D bioprinting, *Trends in Biotechnology*, 41 (2023) 262-263.
- [71] F. Karimi, K. Lau, H.N. Kim, Z. Och, K.S. Lim, J. Whitelock, M. Lord, J. Rnjak-Kovacina, Surface Biofunctionalization of Silk Biomaterials Using Dityrosine Cross-Linking, *ACS Applied Materials & Interfaces*, 14 (2022) 31551-31566.
- [72] A.J. Guerra, P. Cano, M. Rabionet, T. Puig, J. Ciurana, 3D-Printed PCL/PLA Composite Stents: Towards a New Solution to Cardiovascular Problems, *Materials (Basel)*, 11 (2018).
- [73] A. Rohani Shirvan, N. Hemmatinejad, S.H. Bahrami, A. Bashari, A comparison between solvent casting and electrospinning methods for the fabrication of neem extract-containing buccal films, *Journal of Industrial Textiles*, 51 (2022) 311S-335S.
- [74] M. Humenik, M. Magdeburg, T. Scheibel, Influence of repeat numbers on self-assembly rates of repetitive recombinant spider silk proteins, *J Struct Biol*, 186 (2014) 431-437.
- [75] Y. Habibi, L.A. Lucia, O.J. Rojas, Cellulose nanocrystals: chemistry, self-assembly, and applications, *Chemical reviews*, 110 (2010) 3479-3500.

-
- [76] G. Askarieh, M. Hedhammar, K. Nordling, A. Saenz, C. Casals, A. Rising, J. Johansson, S.D. Knight, Self-assembly of spider silk proteins is controlled by a pH-sensitive relay, *Nature*, 465 (2010) 236-238.
- [77] R.H. Zha, P. Delparastan, T.D. Fink, J. Bauer, T. Scheibel, P.B. Messersmith, Universal nanothin silk coatings via controlled spidroin self-assembly, *Biomater Sci*, 7 (2019) 683-695.
- [78] M. Humenik, M. Mohrand, T. Scheibel, Self-Assembly of Spider Silk-Fusion Proteins Comprising Enzymatic and Fluorescence Activity, *Bioconjug Chem*, 29 (2018) 898-904.
- [79] Z. Chen, L. Wang, C. Chen, J. Sun, J. Luo, W. Cui, C. Zhu, X. Zhou, X. Liu, H. Yang, NSC-derived extracellular matrix-modified GelMA hydrogel fibrous scaffolds for spinal cord injury repair, *NPG Asia Materials*, 14 (2022) 20.
- [80] X. Shi, T. Zhou, S. Huang, Y. Yao, P. Xu, S. Hu, C. Tu, W. Yin, C. Gao, J. Ye, An electrospun scaffold functionalized with a ROS-scavenging hydrogel stimulates ocular wound healing, *Acta Biomaterialia*, (2023).
- [81] S. Heilshorn, Endothelial cell adhesion to the fibronectin CS5 domain in artificial extracellular matrix proteins, *Biomaterials*, 24 (2003) 4245-4252.
- [82] D. da Silva, M. Kaduri, M. Poley, O. Adir, N. Krinsky, J. Shainsky-Roitman, A. Schroeder, Biocompatibility, biodegradation and excretion of polylactic acid (PLA) in medical implants and theranostic systems, *Chem Eng J*, 340 (2018) 9-14.
- [83] M.A. Elsayy, K.-H. Kim, J.-W. Park, A. Deep, Hydrolytic degradation of polylactic acid (PLA) and its composites, *Renewable and Sustainable Energy Reviews*, 79 (2017) 1346-1352.
- [84] J.R.G. Carvalho, G. Conde, M.L. Antonioli, P.P. Dias, R.O. Vasconcelos, S.R. Taboga, P.A. Canola, M.A. Chinelatto, G.T. Pereira, G.C. Ferraz, Biocompatibility and biodegradation of poly(lactic acid) (PLA) and an immiscible PLA/poly(ϵ -caprolactone) (PCL) blend compatibilized by poly(ϵ -caprolactone-*b*-tetrahydrofuran) implanted in horses, *Polymer Journal*, 52 (2020) 629-643.
- [85] M. Bazgir, W. Zhang, X. Zhang, J. Elies, M. Saeinasab, P. Coates, M. Youseffi, F. Sefat, Degradation and Characterisation of Electrospun Polycaprolactone (PCL) and Poly(lactic-co-glycolic acid) (PLGA) Scaffolds for Vascular Tissue Engineering, *Materials (Basel)*, 14 (2021).
- [86] F. Karimi, A.J. O'Connor, G.G. Qiao, D.E. Heath, Integrin Clustering Matters: A Review of Biomaterials Functionalized with Multivalent Integrin-Binding Ligands to Improve Cell Adhesion, Migration, Differentiation, Angiogenesis, and Biomedical Device Integration, *Adv Healthc Mater*, 7 (2018) e1701324.
- [87] A. Shakeel, P.R. Corridon, Mitigating challenges and expanding the future of vascular tissue engineering-are we there yet?, *Front Physiol*, 13 (2022) 1079421.
- [88] A. Joshi, S. Choudhury, S.B. Gugulothu, S.S. Visweswariah, K. Chatterjee, Strategies to Promote Vascularization in 3D Printed Tissue Scaffolds: Trends and Challenges, *Biomacromolecules*, 23 (2022) 2730-2751.
- [89] J.S.K. Yuen, Jr., A.J. Stout, N.S. Kawecki, S.M. Letcher, S.K. Theodossiou, J.M. Cohen, B.M. Barrick, M.K. Saad, N.R. Rubio, J.A. Pietropinto, H. DiCindio, S.W. Zhang, A.C. Rowat, D.L. Kaplan, Perspectives on scaling production of adipose tissue for food applications, *Biomaterials*, 280 (2022) 121273.

-
- [90] A. Weekes, N. Bartnikowski, N. Pinto, J. Jenkins, C. Meinert, T.J. Klein, Biofabrication of small diameter tissue-engineered vascular grafts, *Acta Biomater*, 138 (2022) 92-111.
- [91] O.A. Sindeeva, E.S. Prikhozhdenko, I. Schurov, N. Sedykh, S. Goriainov, A. Karamyan, E.A. Mordovina, O.A. Inozemtseva, V. Kudryavtseva, L.E. Shchesnyak, R.A. Abramovich, S. Mikhajlov, G.B. Sukhorukov, Patterned Drug-Eluting Coatings for Tracheal Stents Based on PLA, PLGA, and PCL for the Granulation Formation Reduction: In Vivo Studies, *Pharmaceutics*, 13 (2021).
- [92] U. Johansson, M. Widhe, N.D. Shalaly, I.L. Arregui, L. Nilebäck, C.P. Tasiopoulos, C. Åstrand, P.-O. Berggren, C. Gasser, M. Hedhammar, Assembly of functionalized silk together with cells to obtain proliferative 3D cultures integrated in a network of ECM-like microfibers, *Scientific Reports*, 9 (2019) 6291.
- [93] M. Reimer, K. Mayer, D. Van Opdenbosch, T. Scheibel, C. Zollfrank, Biocompatible Optical Fibers Made of Regenerated Cellulose and Recombinant Cellulose-Binding Spider Silk, *Biomimetics (Basel)*, 8 (2023).
- [94] G. Rakhurst, R.J. Ploeg, *Biomaterials in modern medicine : the Groningen perspective*, World Scientific, New Jersey, 2008.
- [95] M.V. Branquinho, S.O. Ferreira, R.D. Alvites, A.F. Magueta, M. Ivanov, A.C. Sousa, I. Amorim, F. Faria, M. Fernandes, P.M. Vilarinho, In Vitro and In Vivo Characterization of PLLA-316L Stainless Steel Electromechanical Devices for Bone Tissue Engineering—A Preliminary Study, *International Journal of Molecular Sciences*, 22 (2021) 7655.
- [96] G. Mani, D.M. Johnson, D. Marton, M.D. Feldman, D. Patel, A.A. Ayon, C.M. Agrawal, Drug delivery from gold and titanium surfaces using self-assembled monolayers, *Biomaterials*, 29 (2008) 4561-4573.
- [97] S. Kulanthaivel, B. Roy, T. Agarwal, S. Giri, K. Pramanik, K. Pal, S.S. Ray, T.K. Maiti, I. Banerjee, Cobalt doped proangiogenic hydroxyapatite for bone tissue engineering application, *Materials Science and Engineering: C*, 58 (2016) 648-658.
- [98] M. Ogawa, Y. Tohma, H. Ohgushi, Y. Takakura, Y. Tanaka, Early fixation of cobalt-chromium based alloy surgical implants to bone using a tissue-engineering approach, *International Journal of Molecular Sciences*, 13 (2012) 5528-5541.
- [99] T. Ghassemi, A. Shahroodi, M.H. Ebrahimzadeh, A. Mousavian, J. Movaffagh, A. Moradi, Current concepts in scaffolding for bone tissue engineering, *Archives of bone and joint surgery*, 6 (2018) 90.
- [100] B.D. Ratner, Replacing and renewing: synthetic materials, biomimetics, and tissue engineering in implant dentistry, *Journal of dental education*, 65 (2001) 1340-1347.
- [101] M. Moravej, D. Mantovani, Biodegradable metals for cardiovascular stent application: interests and new opportunities, *Int J Mol Sci*, 12 (2011) 4250-4270.
- [102] A. Mattesini, G.G. Secco, G. Dall'Ara, M. Ghione, J.C. Rama-Merchan, A. Lupi, N. Viceconte, A.C. Lindsay, R. De Silva, N. Foin, T. Naganuma, S. Valente, A. Colombo, C. Di Mario, ABSORB biodegradable stents versus second-generation metal stents: a comparison study of 100 complex lesions treated under OCT guidance, *JACC Cardiovasc Interv*, 7 (2014) 741-750.
- [103] H. Asadi, S. Ghalei, H. Handa, R.P. Ramasamy, Cellulose nanocrystal reinforced silk fibroin coating for enhanced corrosion protection and biocompatibility of Mg-based alloys for orthopedic implant applications, *Progress in Organic Coatings*, 161 (2021).

-
- [104] H.H. Lu, S. Thomopoulos, Functional attachment of soft tissues to bone: development, healing, and tissue engineering, *Annu Rev Biomed Eng*, 15 (2013) 201-226.
- [105] C.B. Borkner, S. Wohlrab, E. Möller, G. Lang, T. Scheibel, Surface Modification of Polymeric Biomaterials Using Recombinant Spider Silk Proteins, *ACS Biomaterials Science & Engineering*, 3 (2016) 767-775.
- [106] S. McMahon, N. Bertollo, E.D.O. Cearbhaill, J. Salber, L. Pierucci, P. Duffy, T. Dürig, V. Bi, W. Wang, Bio-resorbable polymer stents: a review of material progress and prospects, *Progress in Polymer Science*, 83 (2018) 79-96.
- [107] A. Hezi-Yamit, C. Sullivan, J. Wong, L. David, M. Chen, P. Cheng, D. Shumaker, J.N. Wilcox, K. Udipi, Impact of polymer hydrophilicity on biocompatibility: implication for DES polymer design, *J Biomed Mater Res A*, 90 (2009) 133-141.
- [108] O.V. Stepanenko, M.I. Sulatsky, E.V. Mikhailova, O.V. Stepanenko, I.M. Kuznetsova, K.K. Turoverov, A.I. Sulatskaya, Trypsin Induced Degradation of Amyloid Fibrils, *Int J Mol Sci*, 22 (2021).
- [109] A. Kumar, S.S. Han, PVA-based hydrogels for tissue engineering: A review, *International Journal of Polymeric Materials and Polymeric Biomaterials*, 66 (2017) 159-182.
- [110] J. George, C.C. Hsu, L.T.B. Nguyen, H. Ye, Z. Cui, Neural tissue engineering with structured hydrogels in CNS models and therapies, *Biotechnol Adv*, 42 (2020) 107370.
- [111] T. Okaya, K. Kikuchi, Y. Morii, Polymerization of Acrylamide in Aqueous Medium Initiated with a Redox System of Cysteine and Ammonium Persulfate, *Polymer Journal*, 29 (1997) 545-549.
- [112] G. Wang, X. Wang, L. Huang, Feasibility of chitosan-alginate (Chi-Alg) hydrogel used as scaffold for neural tissue engineering: a pilot study in vitro, *Biotechnology & Biotechnological Equipment*, 31 (2017) 766-773.
- [113] T. Jiang, J. Zhao, S. Yu, Z. Mao, C. Gao, Y. Zhu, C. Mao, L. Zheng, Untangling the response of bone tumor cells and bone forming cells to matrix stiffness and adhesion ligand density by means of hydrogels, *Biomaterials*, 188 (2019) 130-143.
- [114] T.T. Hoang Thi, Y. Lee, P. Le Thi, K.D. Park, Engineered horseradish peroxidase-catalyzed hydrogels with high tissue adhesiveness for biomedical applications, *Journal of Industrial and Engineering Chemistry*, 78 (2019) 34-52.
- [115] M.D. Baumann, C.E. Kang, C.H. Tator, M.S. Shoichet, Intrathecal delivery of a polymeric nanocomposite hydrogel after spinal cord injury, *Biomaterials*, 31 (2010) 7631-7639.
- [116] G. Wang, X. Wang, L. Huang, Feasibility of chitosan-alginate (Chi-Alg) hydrogel used as scaffold for neural tissue engineering: a pilot study in vitro, *Biotechnology and Biotechnological Equipment*, 31 (2017) 766-773.
- [117] T. Kimura, S. Iwai, T. Moritan, K. Nam, S. Mutsuo, H. Yoshizawa, M. Okada, T. Furuzono, T. Fujisato, A. Kishida, Preparation of poly(vinyl alcohol)/DNA hydrogels via hydrogen bonds formed on ultra-high pressurization and controlled release of DNA from the hydrogels for gene delivery, *Journal of Artificial Organs*, 10 (2007) 104-108.
- [118] R.J.H. Stenekes, H. Talsma, W.E. Hennink, Formation of dextran hydrogels by crystallization, *Biomaterials*, 22 (2001) 1891-1898.

-
- [119] S. Kumari, H. Bargel, M.U. Anby, D. Lafargue, T. Scheibel, Recombinant Spider Silk Hydrogels for Sustained Release of Biologicals, *ACS Biomaterials Science & Engineering*, (2018) 1750–1759.
- [120] P. Sajkiewicz, Kinetics of crystallisation of polymers-a review, *Progress in Rubber Plastics and Recycling Technology*, 18 (2002) 195-215.
- [121] Y. Yu, Y. Zhang, J.A. Martin, I.T. Ozbolat, Evaluation of Cell Viability and Functionality in Vessel-like Bioprintable Cell-Laden Tubular Channels, *Journal of Biomechanical Engineering*, 135 (2013).
- [122] P. Zhai, X. Peng, B. Li, Y. Liu, H. Sun, X. Li, The application of hyaluronic acid in bone regeneration, *Int J Biol Macromol*, 151 (2020) 1224-1239.
- [123] K. Zafeiris, D. Brasinika, A. Karatza, E. Koumoulos, I. Karoussis, K. Kyriakidou, C. Charitidis, Additive manufacturing of hydroxyapatite–chitosan–genipin composite scaffolds for bone tissue engineering applications, *Materials Science and Engineering: C*, 119 (2021) 111639.
- [124] Z. Lu, S. Liu, Y. Le, Z. Qin, M. He, F. Xu, Y. Zhu, J. Zhao, C. Mao, L. Zheng, An injectable collagen-genipin-carbon dot hydrogel combined with photodynamic therapy to enhance chondrogenesis, *Biomaterials*, 218 (2019) 119190.
- [125] M.H. Nabavi, M. Salehi, A. Ehterami, F. Bastami, H. Semyari, M. Tehranchi, M.A. Nabavi, H. Semyari, A collagen-based hydrogel containing tacrolimus for bone tissue engineering, *Drug Deliv Transl Res*, 10 (2020) 108-121.
- [126] Q. Li, D.G. Barrett, P.B. Messersmith, N. Holten-Andersen, Controlling Hydrogel Mechanics via Bio-Inspired Polymer–Nanoparticle Bond Dynamics, *ACS Nano*, 10 (2016) 1317-1324.
- [127] S. Wüst, M.E. Godla, R. Müller, S. Hofmann, Tunable hydrogel composite with two-step processing in combination with innovative hardware upgrade for cell-based three-dimensional bioprinting, *Acta Biomater*, 10 (2014) 630-640.
- [128] Y.C. Chen, R.Z. Lin, H. Qi, Y. Yang, H. Bae, J.M. Melero-Martin, A. Khademhosseini, Functional Human Vascular Network Generated in Photocrosslinkable Gelatin Methacrylate Hydrogels, *Adv Funct Mater*, 22 (2012) 2027-2039.
- [129] Y.S. Zhang, A. Arneri, S. Bersini, S.R. Shin, K. Zhu, Z. Goli-Malekabadi, J. Aleman, C. Colosi, F. Busignani, V. Dell'Erba, C. Bishop, T. Shupe, D. Demarchi, M. Moretti, M. Rasponi, M.R. Dokmeci, A. Atala, A. Khademhosseini, Bioprinting 3D microfibrillar scaffolds for engineering endothelialized myocardium and heart-on-a-chip, *Biomaterials*, 110 (2016) 45-59.
- [130] R. Gaetani, D.A. Feyen, V. Verhage, R. Slaats, E. Messina, K.L. Christman, A. Giacomello, P.A. Doevendans, J.P. Sluijter, Epicardial application of cardiac progenitor cells in a 3D-printed gelatin/hyaluronic acid patch preserves cardiac function after myocardial infarction, *Biomaterials*, 61 (2015) 339-348.
- [131] P. Mistry, A. Aied, M. Alexander, K. Shakesheff, A. Bennett, J. Yang, Bioprinting Using Mechanically Robust Core-Shell Cell-Laden Hydrogel Strands, *Macromol Biosci*, 17 (2017).
- [132] W. Zhang, X. Wang, S. Wang, J. Zhao, L. Xu, C. Zhu, D. Zeng, J. Chen, Z. Zhang, D.L. Kaplan, The use of injectable sonication-induced silk hydrogel for VEGF165 and BMP-2 delivery for elevation of the maxillary sinus floor, *Biomaterials*, 32 (2011) 9415-9424.

-
- [133] K. Markstedt, A. Mantas, I. Tournier, H. Martínez Ávila, D. Hägg, P. Gatenholm, 3D Bioprinting Human Chondrocytes with Nanocellulose–Alginate Bioink for Cartilage Tissue Engineering Applications, *Biomacromolecules*, 16 (2015) 1489-1496.
- [134] H.W. Kang, S.J. Lee, I.K. Ko, C. Kengla, J.J. Yoo, A. Atala, A 3D bioprinting system to produce human-scale tissue constructs with structural integrity, *Nat Biotechnol*, 34 (2016) 312-319.
- [135] P.-H.G. Chao, S. Yodmuang, X. Wang, L. Sun, D.L. Kaplan, G. Vunjak-Novakovic, Silk hydrogel for cartilage tissue engineering, *Journal of Biomedical Materials Research Part B: Applied Biomaterials*, 95B (2010) 84-90.
- [136] H. Hong, Y.B. Seo, D.Y. Kim, J.S. Lee, Y.J. Lee, H. Lee, O. Ajiteru, M.T. Sultan, O.J. Lee, S.H. Kim, C.H. Park, Digital light processing 3D printed silk fibroin hydrogel for cartilage tissue engineering, *Biomaterials*, 232 (2020) 119679.
- [137] Y.P. Singh, N. Bhardwaj, B.B. Mandal, Potential of Agarose/Silk Fibroin Blended Hydrogel for in Vitro Cartilage Tissue Engineering, *ACS Appl Mater Interfaces*, 8 (2016) 21236-21249.
- [138] Y. Zhou, K. Liang, S. Zhao, C. Zhang, J. Li, H. Yang, X. Liu, X. Yin, D. Chen, W. Xu, P. Xiao, Photopolymerized maleilated chitosan/methacrylated silk fibroin micro/nanocomposite hydrogels as potential scaffolds for cartilage tissue engineering, *International Journal of Biological Macromolecules*, 108 (2018) 383-390.
- [139] S. Michael, H. Sorg, C.T. Peck, L. Koch, A. Deiwick, B. Chichkov, P.M. Vogt, K. Reimers, Tissue engineered skin substitutes created by laser-assisted bioprinting form skin-like structures in the dorsal skin fold chamber in mice, *PLoS One*, 8 (2013) e57741.
- [140] A. Skardal, D. Mack, E. Kapetanovic, A. Atala, J.D. Jackson, J. Yoo, S. Soker, Bioprinted amniotic fluid-derived stem cells accelerate healing of large skin wounds, *Stem Cells Transl Med*, 1 (2012) 792-802.
- [141] M. Yanez, J. Rincon, A. Dones, C. De Maria, R. Gonzales, T. Boland, In vivo assessment of printed microvasculature in a bilayer skin graft to treat full-thickness wounds, *Tissue Eng Part A*, 21 (2015) 224-233.
- [142] D. Chouhan, T.u. Lohe, P.K. Samudrala, B.B. Mandal, In situ forming injectable silk fibroin hydrogel promotes skin regeneration in full thickness burn wounds, *Advanced healthcare materials*, 7 (2018) 1801092.
- [143] T.W. Chung, W.P. Chen, P.W. Tai, H.Y. Lo, T.Y. Wu, Roles of Silk Fibroin on Characteristics of Hyaluronic Acid/Silk Fibroin Hydrogels for Tissue Engineering of Nucleus Pulposus, *Materials (Basel)*, 13 (2020).
- [144] A.M. Hopkins, L. De Laporte, F. Tortelli, E. Spedden, C. Staii, T.J. Atherton, J.A. Hubbell, D.L. Kaplan, Silk Hydrogels as Soft Substrates for Neural Tissue Engineering, *Advanced Functional Materials*, 23 (2013) 5140-5149.
- [145] D.C. Leslie, A. Waterhouse, J.B. Berthet, T.M. Valentin, A.L. Watters, A. Jain, P. Kim, B.D. Hatton, A. Nedder, K. Donovan, E.H. Super, C. Howell, C.P. Johnson, T.L. Vu, D.E. Bolgen, S. Rifai, A.R. Hansen, M. Aizenberg, M. Super, J. Aizenberg, D.E. Ingber, A bioinspired omniphobic surface coating on medical devices prevents thrombosis and biofouling, *Nat Biotechnol*, 32 (2014) 1134-1140.

-
- [146] J.P.M. Kramer, T.B. Aigner, J. Petzold, K. Roshanbinfar, T. Scheibel, F.B. Engel, Recombinant spider silk protein eADF4(C16)-RGD coatings are suitable for cardiac tissue engineering, *Sci Rep*, 10 (2020) 8789.
- [147] C. Sommer, H. Bargel, N. Raßmann, T. Scheibel, Microbial repellence properties of engineered spider silk coatings prevent biofilm formation of opportunistic bacterial strains, *MRS Communications*, (2021).
- [148] A.R. Franco, E.M. Fernandes, M.T. Rodrigues, F.J. Rodrigues, M.E. Gomes, I.B. Leonor, D.L. Kaplan, R.L. Reis, Antimicrobial coating of spider silk to prevent bacterial attachment on silk surgical sutures, *Acta Biomater*, 99 (2019) 236-246.
- [149] O.A. Sindeeva, O. Kopach, M.A. Kurochkin, A. Sapelkin, D.J. Gould, D.A. Rusakov, G.B. Sukhorukov, Polylactic Acid-Based Patterned Matrixes for Site-Specific Delivery of Neuropeptides On-Demand: Functional NGF Effects on Human Neuronal Cells, *Frontiers in Bioengineering and Biotechnology*, 8 (2020).
- [150] Y. Ji, Y. Wei, X. Liu, J. Wang, K. Ren, J. Ji, Zwitterionic polycarboxybetaine coating functionalized with REDV peptide to improve selectivity for endothelial cells, *J Biomed Mater Res A*, 100 (2012) 1387-1397.
- [151] W. Xu, K. Yagoshi, T. Asakura, M. Sasaki, T. Niidome, Silk Fibroin as a Coating Polymer for Sirolimus-Eluting Magnesium Alloy Stents, *ACS Appl Bio Mater*, 3 (2020) 531-538.
- [152] Y. Fan, Y. Zhang, Q. Zhao, Y. Xie, R. Luo, P. Yang, Y. Weng, Immobilization of nano Cu-MOFs with polydopamine coating for adaptable gasotransmitter generation and copper ion delivery on cardiovascular stents, *Biomaterials*, 204 (2019) 36-45.
- [153] K. Spieß, S. Wohlrab, T. Scheibel, Structural characterization and functionalization of engineered spider silk films, *Soft Matter*, 6 (2010).
- [154] A. Kaliyaraj Selva Kumar, Y. Zhang, D. Li, R.G. Compton, A mini-review: How reliable is the drop casting technique?, *Electrochemistry Communications*, 121 (2020) 106867.
- [155] J. Danglad-Flores, S. Eickelmann, H. Riegler, Deposition of polymer films by spin casting: A quantitative analysis, *Chemical Engineering Science*, 179 (2018) 257-264.
- [156] J. Wang, J.A. Jansen, F. Yang, Electrospraying: Possibilities and Challenges of Engineering Carriers for Biomedical Applications—A Mini Review, *Frontiers in Chemistry*, 7 (2019).
- [157] N.S. Emonson, J.D. Randall, B.J. Allardyce, M.K. Stanfield, B. Dharmasiri, F. Stojcevski, L.C. Henderson, Promoting Silk Fibroin Adhesion to Stainless Steel Surfaces by Interface Tailoring, *Chempluschem*, 88 (2023) e202200335.
- [158] S. Salehi, K. Koeck, T. Scheibel, Spider Silk for Tissue Engineering Applications, *Molecules*, 25 (2020).
- [159] X. Wang, Z. Gu, B. Jiang, L. Li, X. Yu, Surface modification of strontium-doped porous bioactive ceramic scaffolds via poly(DOPA) coating and immobilizing silk fibroin for excellent angiogenic and osteogenic properties, *Biomater Sci*, 4 (2016) 678-688.
- [160] E. Ko, K. Yang, J. Shin, S.W. Cho, Polydopamine-assisted osteoinductive peptide immobilization of polymer scaffolds for enhanced bone regeneration by human adipose-derived stem cells, *Biomacromolecules*, 14 (2013) 3202-3213.

-
- [161] R.K. Kankala, X.-M. Xu, C.-G. Liu, A.-Z. Chen, S.-B. Wang, 3D-printing of microfibrinous porous scaffolds based on hybrid approaches for bone tissue engineering, *Polymers*, 10 (2018) 807.
- [162] T.D. Stocco, P.J.G. Rodrigues, M.A. de Almeida Filho, A.O. Lobo, Nanohydroxyapatite Electrodeposition onto Electrospun Nanofibers: Technique Overview and Tissue Engineering Applications, *Bioengineering (Basel)*, 8 (2021).
- [163] R. Romero, J.K. Travers, E. Asbury, A. Pennybaker, L. Chubb, R. Rose, N.P. Ehrhart, M.J. Kipper, Combined delivery of FGF-2, TGF- β 1, and adipose-derived stem cells from an engineered periosteum to a critical-sized mouse femur defect, *Journal of Biomedical Materials Research Part A*, 105 (2017) 900-911.
- [164] D. Lukovic, N. Nyolczas, R. Hemetsberger, I.J. Pavo, A. Posa, B. Behnisch, G. Horak, K. Zlabinger, M. Gyongyosi, Human recombinant activated protein C-coated stent for the prevention of restenosis in porcine coronary arteries, *J Mater Sci Mater Med*, 26 (2015) 241.
- [165] M.K. Abraham, A. Nolte, R. Reus, A. Behring, D. Zengerle, M. Avci-Adali, J.D. Hohmann, K. Peter, C. Schlensak, H.P. Wendel, S. Krajewski, In vitro Study of a Novel Stent Coating Using Modified CD39 Messenger RNA to Potentially Reduce Stent Angioplasty-Associated Complications, *PLoS One*, 10 (2015) e0138375.
- [166] W. Zheng, Z. Wang, L. Song, Q. Zhao, J. Zhang, D. Li, S. Wang, J. Han, X.L. Zheng, Z. Yang, D. Kong, Endothelialization and patency of RGD-functionalized vascular grafts in a rabbit carotid artery model, *Biomaterials*, 33 (2012) 2880-2891.
- [167] A. Waterhouse, Y. Yin, S.G. Wise, D.V. Bax, D.R. McKenzie, M.M. Bilek, A.S. Weiss, M.K. Ng, The immobilization of recombinant human tropoelastin on metals using a plasma-activated coating to improve the biocompatibility of coronary stents, *Biomaterials*, 31 (2010) 8332-8340.
- [168] K. Ghosal, A. Manakhov, L. Zajíčková, S. Thomas, Structural and Surface Compatibility Study of Modified Electrospun Poly(ϵ -caprolactone) (PCL) Composites for Skin Tissue Engineering, *AAPS PharmSciTech*, 18 (2017) 72-81.
- [169] L. Baoyong, Z. Jian, C. Denglong, L. Min, Evaluation of a new type of wound dressing made from recombinant spider silk protein using rat models, *Burns*, 36 (2010) 891-896.
- [170] H. Xu, J.M. Holzwarth, Y. Yan, P. Xu, H. Zheng, Y. Yin, S. Li, P.X. Ma, Conductive PPY/PDLLA conduit for peripheral nerve regeneration, *Biomaterials*, 35 (2014) 225-235.
- [171] Y. Zhao, H. Liu, Z. Wang, Q. Zhang, Y. Li, W. Tian, Z. Tong, Y. Wang, C. Huselstein, X. Shi, Y. Chen, Electrodeposition to construct mechanically robust chitosan-based multi-channel conduits, *Colloids and Surfaces B: Biointerfaces*, 163 (2018) 412-418.
- [172] Y. Yang, Y. Zhang, R. Chai, Z. Gu, A Polydopamine-Functionalized Carbon Microfibrinous Scaffold Accelerates the Development of Neural Stem Cells, *Front Bioeng Biotechnol*, 8 (2020) 616.
- [173] T. Fu, C.S. Wen, J. Lu, Y.M. Zhou, S.G. Ma, B.H. Dong, B.G. Liu, Sol-gel derived TiO₂ coating on plasma nitrided 316L stainless steel, *Vacuum*, 86 (2012) 1402-1407.
- [174] D. Huemmerich, C.W. Helsen, S. Quedzuweit, J. Oschmann, R. Rudolph, T. Scheibel, Primary Structure Elements of Spider Dragline Silks and Their Contribution to Protein Solubility, *Biochemistry*, 43 (2004) 13604-13612.

-
- [175] T. Aigner, T. Scheibel, Self-Rolling Refillable Tubular Enzyme Containers Made of Recombinant Spider Silk and Chitosan, *ACS Appl Mater Interfaces*, 11 (2019) 15290-15297.
- [176] C.L. Craig, Evolution of arthropod silks, *Annu Rev Entomol*, 42 (1997) 231-267.
- [177] L. Römer, T. Scheibel, The elaborate structure of spider silk: structure and function of a natural high performance fiber, *Prion*, 2 (2008) 154-161.
- [178] T.A. Blackledge, A.P. Summers, C.Y. Hayashi, Gumfooted lines in black widow cobwebs and the mechanical properties of spider capture silk, *Zoology*, 108 (2005) 41-46.
- [179] J.M. Gosline, M.W. Denny, M.E. DeMont, Spider silk as rubber, *Nature*, 309 (1984) 551-552.
- [180] M. Heim, D. Keerl, T. Scheibel, Spider silk: from soluble protein to extraordinary fiber, *Angew Chem Int Ed Engl*, 48 (2009) 3584-3596.
- [181] E. Doblhofer, A. Heidebrecht, T. Scheibel, To spin or not to spin: spider silk fibers and more, *Appl Microbiol Biotechnol*, 99 (2015) 9361-9380.
- [182] L. Eisoldt, A. Smith, T. Scheibel, Decoding the secrets of spider silk, *Materials Today*, 14 (2011) 80-86.
- [183] C. Thamm, T. Scheibel, Recombinant Production, Characterization, and Fiber Spinning of an Engineered Short Major Ampullate Spidroin (MaSp1s), *Biomacromolecules*, 18 (2017) 1365-1372.
- [184] G.C. Candelas, J. Cintron, A spider fibroin and its synthesis, *Journal of Experimental Zoology*, 216 (1981) 1-6.
- [185] N.A. Ayoub, J.E. Garb, R.M. Tinghitella, M.A. Collin, C.Y. Hayashi, Blueprint for a High-Performance Biomaterial: Full-Length Spider Dragline Silk Genes, *PLOS ONE*, 2 (2007) e514.
- [186] S. Winkler, D. Wilson, D.L. Kaplan, Controlling β -Sheet Assembly in Genetically Engineered Silk by Enzymatic Phosphorylation/Dephosphorylation, *Biochemistry*, 39 (2000) 12739-12746.
- [187] A.H. Simmons, C.A. Michal, L.W. Jelinski, Molecular Orientation and Two-Component Nature of the Crystalline Fraction of Spider Dragline Silk, *Science*, 271 (1996) 84-87.
- [188] D.H. Hijirida, K.G. Do, C. Michal, S. Wong, D. Zax, L.W. Jelinski, ^{13}C NMR of *Nephila clavipes* major ampullate silk gland, *Biophysical Journal*, 71 (1996) 3442-3447.
- [189] J. Pérez-Rigueiro, M. Elices, G.R. Plaza, G.V. Guinea, Similarities and Differences in the Supramolecular Organization of Silkworm and Spider Silk, *Macromolecules*, 40 (2007) 5360-5365.
- [190] Y. Liu, A. Sponner, D. Porter, F. Vollrath, Proline and Processing of Spider Silks, *Biomacromolecules*, 9 (2008) 116-121.
- [191] N. Kono, H. Nakamura, R. Ohtoshi, D.A.P. Moran, A. Shinohara, Y. Yoshida, M. Fujiwara, M. Mori, M. Tomita, K. Arakawa, Orb-weaving spider *Araneus ventricosus* genome elucidates the spidroin gene catalogue, *Scientific Reports*, 9 (2019) 8380.

-
- [192] J.E. Garb, R.A. Haney, E.E. Schwager, M. Gregorič, M. Kuntner, I. Agnarsson, T.A. Blackledge, The transcriptome of Darwin's bark spider silk glands predicts proteins contributing to dragline silk toughness, *Communications Biology*, 2 (2019) 275.
- [193] N. Kono, R. Ohtoshi, A.D. Malay, M. Mori, H. Masunaga, Y. Yoshida, H. Nakamura, K. Numata, K. Arakawa, Darwin's bark spider shares a spidroin repertoire with *Caerostris extrusa* but achieves extraordinary silk toughness through gene expression, *bioRxiv*, (2021) 2021.2007.2016.452619.
- [194] F. Hagn, L. Eisoldt, J.G. Hardy, C. Vendrely, M. Coles, T. Scheibel, H. Kessler, A conserved spider silk domain acts as a molecular switch that controls fibre assembly, *Nature*, 465 (2010) 239-242.
- [195] L. Eisoldt, J.G. Hardy, M. Heim, T.R. Scheibel, The role of salt and shear on the storage and assembly of spider silk proteins, *J Struct Biol*, 170 (2010) 413-419.
- [196] F. Hagn, C. Thamm, T. Scheibel, H. Kessler, pH-dependent dimerization and salt-dependent stabilization of the N-terminal domain of spider dragline silk--implications for fiber formation, *Angew Chem Int Ed Engl*, 50 (2011) 310-313.
- [197] L. Eisoldt, C. Thamm, T. Scheibel, Review the role of terminal domains during storage and assembly of spider silk proteins, *Biopolymers*, 97 (2012) 355-361.
- [198] H. Yamada, H. Nakao, Y. Takasu, K. Tsubouchi, Preparation of undegraded native molecular fibroin solution from silkworm cocoons, *Materials Science and Engineering: C*, 14 (2001) 41-46.
- [199] F. Vollrath, Biology of spider silk, *International Journal of Biological Macromolecules*, 24 (1999) 81-88.
- [200] H. Wen, X. Lan, Y. Zhang, T. Zhao, Y. Wang, Z. Kajiura, M. Nakagaki, Transgenic silkworms (*Bombyx mori*) produce recombinant spider dragline silk in cocoons, *Molecular biology reports*, 37 (2010) 1815-1821.
- [201] H.-T. Xu, B.-L. Fan, S.-Y. Yu, Y.-H. Huang, Z.-H. Zhao, Z.-X. Lian, Y.-P. Dai, L.-L. Wang, Z.-L. Liu, J. Fei, Construct synthetic gene encoding artificial spider dragline silk protein and its expression in milk of transgenic mice, *Animal Biotechnology*, 18 (2007) 1-12.
- [202] C. Karatzas, J. Zhou, Y. Huang, F. Duguay, N. Chretien, B. Bhatia, A. Bilodeau, R. Keyston, T. Tao, C. Keefer, Production of recombinant spider silk (BioSteel®) in the milk of transgenic animals, *Transgenic Res*, 8 (1999) e477.
- [203] S.R. Fahnestock, S.L. Irwin, Synthetic spider dragline silk proteins and their production in *Escherichia coli*, *Applied Microbiology and Biotechnology*, 47 (1997) 23-32.
- [204] F. Teulé, C. Aubé, M. Ellison, A. Abbott, Biomimetic manufacturing of customised novel fibre proteins for specialised applications, *AUTEX Res J*, 3 (2003) 160-165.
- [205] I. Agapov, O. Pustovalova, M. Moisenovich, V. Bogush, O. Sokolova, V. Sevastyanov, V. Debabov, M. Kirpichnikov, Three-dimensional scaffold made from recombinant spider silk protein for tissue engineering, *Doklady. Biochemistry and biophysics*, Springer Nature BV, 2009, pp. 127.
- [206] V. Bogush, K. Sidoruk, L. Davydova, I. Zalunin, D. Kozlov, M. Moisenovich, I. Agapov, M. Kirpichnikov, V. Debabov, Recombinant analogue of spidroin 2 for biomedical materials, *Doklady. Biochemistry and biophysics*, Springer Nature BV, 2011, pp. 276.

-
- [207] K. Sidoruk, L. Davydova, D. Kozlov, D. Gubaidullin, A. Glazunov, V. Bogush, V. Debabov, Fermentation optimization of a *Saccharomyces cerevisiae* strain producing 1F9 recombinant spider silk, *Applied biochemistry and microbiology*, 51 (2015) 766-773.
- [208] J. Scheller, U. Conrad, Production of spider silk proteins in transgenic tobacco and potato, *Mol. Farming*, 19 (2005) 171-181.
- [209] J. Scheller, D. Henggeler, A. Viviani, U. Conrad, Purification of spider silk-elastin from transgenic plants and application for human chondrocyte proliferation, *Transgenic research*, 13 (2004) 51-57.
- [210] S. Ittah, S. Cohen, S. Garty, D. Cohn, U. Gat, An essential role for the C-terminal domain of a dragline spider silk protein in directing fiber formation, *Biomacromolecules*, 7 (2006) 1790-1795.
- [211] Y. Miao, Y. Zhang, K. Nakagaki, T. Zhao, A. Zhao, Y. Meng, M. Nakagaki, E.Y. Park, K. Maenaka, Expression of spider flagelliform silk protein in *Bombyx mori* cell line by a novel Bac-to-Bac/BmNPV baculovirus expression system, *Applied microbiology and biotechnology*, 71 (2006) 192-199.
- [212] K.S. Lee, B.Y. Kim, Y.H. Je, S.D. Woo, H.D. Sohn, B.R. Jin, Molecular cloning and expression of the C-terminus of spider flagelliform silk protein from *Araneus ventricosus*, *Journal of biosciences*, 32 (2007) 705-712.
- [213] Y. Zhang, J. Hu, Y. Miao, A. Zhao, T. Zhao, D. Wu, L. Liang, A. Miikura, K. Shiomi, Z. Kajiura, Expression of EGFP-spider dragline silk fusion protein in BmN cells and larvae of silkworm showed the solubility is primary limit for dragline proteins yield, *Molecular biology reports*, 35 (2008) 329-335.
- [214] D.M. Widmaier, C.A. Voigt, Quantification of the physiochemical constraints on the export of spider silk proteins by *Salmonella* type III secretion, *Microbial cell factories*, 9 (2010) 1-12.
- [215] D.M. Widmaier, D. Tullman-Ercek, E.A. Mirsky, R. Hill, S. Govindarajan, J. Minshall, C.A. Voigt, Engineering the *Salmonella* type III secretion system to export spider silk monomers, *Molecular systems biology*, 5 (2009) 309.
- [216] S. Meirovitch, Z. Shtein, T. Ben-Shalom, S. Lapidot, C. Tamburu, X. Hu, J.A. Kluge, U. Raviv, D.L. Kaplan, O. Shoseyov, Spider Silk-CBD-Cellulose Nanocrystal Composites: Mechanism of Assembly, *Int J Mol Sci*, 17 (2016).
- [217] J.T. Prince, K.P. McGrath, C.M. DiGirolamo, D.L. Kaplan, Construction, cloning, and expression of synthetic genes encoding spider dragline silk, *Biochemistry*, 34 (1995) 10879-10885.
- [218] A.E. Brooks, S.M. Stricker, S.B. Joshi, T.J. Kamerzell, C.R. Middaugh, R.V. Lewis, Properties of synthetic spider silk fibers based on *Argiope aurantia* MaSp2, *Biomacromolecules*, 9 (2008) 1506-1510.
- [219] Y. Fukushima, Genetically engineered syntheses of tandem repetitive polypeptides consisting of glycine-rich sequence of spider dragline silk, *Biopolymers: Original Research on Biomolecules*, 45 (1998) 269-279.
- [220] X.-X. Xia, Z.-G. Qian, C.S. Ki, Y.H. Park, D.L. Kaplan, S.Y. Lee, Native-sized recombinant spider silk protein produced in metabolically engineered *Escherichia coli* results in a strong fiber, *Proceedings of the National Academy of Sciences*, 107 (2010) 14059-14063.

-
- [221] S. Szela, P. Avtges, R. Valluzzi, S. Winkler, D. Wilson, D. Kirschner, D.L. Kaplan, Reduction– Oxidation Control of β -Sheet Assembly in Genetically Engineered Silk, *Biomacromolecules*, 1 (2000) 534-542.
- [222] E. Bini, C.W.P. Foo, J. Huang, V. Karageorgiou, B. Kitchel, D.L. Kaplan, RGD-functionalized bioengineered spider dragline silk biomaterial, *Biomacromolecules*, 7 (2006) 3139-3145.
- [223] J. Huang, C. Wong, A. George, D.L. Kaplan, The effect of genetically engineered spider silk-dentin matrix protein 1 chimeric protein on hydroxyapatite nucleation, *Biomaterials*, 28 (2007) 2358-2367.
- [224] C.W.P. Foo, E. Bini, J. Hensman, D. Knight, R. Lewis, D. Kaplan, Role of pH and charge on silk protein assembly in insects and spiders, *Applied Physics A*, 82 (2006) 223-233.
- [225] R.V. Lewis, M. Hinman, S. Kothakota, M.J. Fournier, Expression and purification of a spider silk protein: a new strategy for producing repetitive proteins, *Protein expression and purification*, 7 (1996) 400-406.
- [226] M. Burchinal, L. Nelson, M. Carlson, J. Brooks-Gunn, Neighborhood characteristics, and child care type and quality, *Early Education and Development*, 19 (2008) 702-725.
- [227] K.A. Padgett, J.A. Sorge, Creating seamless junctions independent of restriction sites in PCR cloning, *Gene*, 168 (1996) 31-35.
- [228] J. Bauer, T. Scheibel, Conformational Stability and Interplay of Helical N- and C-Terminal Domains with Implications on Major Ampullate Spidroin Assembly, *Biomacromolecules*, 18 (2017) 835-845.
- [229] T.B. Aigner, E.K. DeSimone, T. Scheibel, Biofabrication using recombinant spider silk proteins as a biomaterial, (2017).
- [230] S. Jokisch, M. Neuenfeldt, T. Scheibel, Silk-Based Fine Dust Filters for Air Filtration, *Advanced Sustainable Systems*, 1 (2017).
- [231] G. Lang, S. Jokisch, T. Scheibel, Air filter devices including nonwoven meshes of electrospun recombinant spider silk proteins, *J Vis Exp*, (2013) e50492.
- [232] F. Bauer, S. Wohlrab, T. Scheibel, Controllable cell adhesion, growth and orientation on layered silk protein films, *Biomater Sci*, 1 (2013) 1244-1249.
- [233] V.J. Neubauer, Rekombinante Spinnenseidenproteine und Biomineralisation für technische und biomedizinische Anwendungen., Bayreuther Graduiertenschule für Mathematik und Naturwissenschaften - BayNAT Universität Bayreuth, 2022, pp. 184.
- [234] J. Petzold, T.B. Aigner, F. Touska, K. Zimmermann, T. Scheibel, F.B. Engel, Surface Features of Recombinant Spider Silk Protein eADF4(κ 16)-Made Materials are Well-Suited for Cardiac Tissue Engineering, *Advanced Functional Materials*, 27 (2017).
- [235] T.U. Esser, V.T. Trossmann, S. Lentz, F.B. Engel, T. Scheibel, Designing of spider silk proteins for human induced pluripotent stem cell-based cardiac tissue engineering, *Materials Today Bio*, 11 (2021) 100114.
- [236] K. Pawar, G. Welzel, C. Haynl, S. Schuster, T. Scheibel, Recombinant Spider Silk and Collagen-Based Nerve Guidance Conduits Support Neuronal Cell Differentiation and Functionality in Vitro, *ACS Appl Bio Mater*, 2 (2019) 4872-4880.

-
- [237] T.B. Aigner, C. Haynl, S. Salehi, A. O'Connor, T. Scheibel, Nerve guidance conduit design based on self-rolling tubes, *Mater Today Bio*, 5 (2020) 100042.
- [238] C. Allmeling, A. Jokuszies, K. Reimers, S. Kall, P.M. Vogt, Use of spider silk fibres as an innovative material in a biocompatible artificial nerve conduit, *Journal of Cellular and Molecular Medicine*, 10 (2006) 770-777.
- [239] F. Roloff, S. Strauß, P.M. Vogt, G. Bicker, C. Radtke, Spider Silk as Guiding Biomaterial for Human Model Neurons, *BioMed Research International*, 2014 (2014) 906819.
- [240] C. Radtke, C. Allmeling, K.H. Waldmann, K. Reimers, K. Thies, H.C. Schenk, A. Hillmer, M. Guggenheim, G. Brandes, P.M. Vogt, Spider silk constructs enhance axonal regeneration and remyelination in long nerve defects in sheep, *PLoS One*, 6 (2011) e16990.
- [241] M. Lewicka, P. Rebellato, J. Lewicki, P. Uhlén, A. Rising, O. Hermanson, Recombinant spider silk protein matrices facilitate multi-analysis of calcium-signaling in neural stem cell-derived AMPA-responsive neurons, *bioRxiv*, (2019) 579292.
- [242] V.J. Neubauer, T. Scheibel, Spider Silk Fusion Proteins for Controlled Collagen Binding and Biomineralization, *ACS Biomater Sci Eng*, 6 (2020) 5599-5608.
- [243] J.G. Hardy, J.G. Torres-Rendon, A. Leal-Egana, A. Walther, H. Schlaad, H. Colfen, T.R. Scheibel, Biomineralization of Engineered Spider Silk Protein-Based Composite Materials for Bone Tissue Engineering, *Materials (Basel)*, 9 (2016).
- [244] N. Dinjaski, R. Plowright, S. Zhou, D.J. Belton, C.C. Perry, D.L. Kaplan, Osteoinductive recombinant silk fusion proteins for bone regeneration, *Acta Biomater*, 49 (2017) 127-139.
- [245] S. Gomes, I.B. Leonor, J.F. Mano, R.L. Reis, D.L. Kaplan, Spider silk-bone sialoprotein fusion proteins for bone tissue engineering, *Soft Matter*, 7 (2011).
- [246] R. Plowright, N. Dinjaski, S. Zhou, D.J. Belton, D.L. Kaplan, C.C. Perry, Influence of silk-silica fusion protein design on silica condensation in vitro and cellular calcification, *RSC Adv*, 6 (2016) 21776-21788.
- [247] A.W. Morgan, K.E. Roskov, S. Lin-Gibson, D.L. Kaplan, M.L. Becker, C.G. Simon, Jr., Characterization and optimization of RGD-containing silk blends to support osteoblastic differentiation, *Biomaterials*, 29 (2008) 2556-2563.
- [248] A. Steins, P. Dik, W.H. Müller, S.J. Vervoort, K. Reimers, J.W. Kuhbier, P.M. Vogt, A.A. van Apeldoorn, P.J. Coffey, K. Schepers, In Vitro Evaluation of Spider Silk Meshes as a Potential Biomaterial for Bladder Reconstruction, *PLoS One*, 10 (2015) e0145240.
- [249] H. Wendt, A. Hillmer, K. Reimers, J.W. Kuhbier, F. Schäfer-Nolte, C. Allmeling, C. Kasper, P.M. Vogt, Artificial Skin – Culturing of Different Skin Cell Lines for Generating an Artificial Skin Substitute on Cross-Weaved Spider Silk Fibres, *PLOS ONE*, 6 (2011) e21833.
- [250] C. Fredriksson, M. Hedhammar, R. Feinstein, K. Nordling, G. Kratz, J. Johansson, F. Huss, A. Rising, Tissue Response to Subcutaneously Implanted Recombinant Spider Silk: An in Vivo Study, *Materials*, 2 (2009) 1908-1922.
- [251] D. Chouhan, N. Thatikonda, L. Nilebäck, M. Widhe, M. Hedhammar, B.B. Mandal, Recombinant Spider Silk Functionalized Silkworm Silk Matrices as Potential Bioactive Wound Dressings and Skin Grafts, *ACS Appl Mater Interfaces*, 10 (2018) 23560-23572.

-
- [252] K. Hennecke, J. Redeker, J.W. Kuhbier, S. Strauss, C. Allmeling, C. Kasper, K. Reimers, P.M. Vogt, Bundles of Spider Silk, Braided into Sutures, Resist Basic Cyclic Tests: Potential Use for Flexor Tendon Repair, *PLOS ONE*, 8 (2013) e61100.
- [253] U. Johansson, M. Widhe, N.D. Shalaly, I.L. Arregui, L. Nilebäck, C.P. Tasiopoulos, C. Åstrand, P.O. Berggren, C. Gasser, M. Hedhammar, Assembly of functionalized silk together with cells to obtain proliferative 3D cultures integrated in a network of ECM-like microfibers, *Sci Rep*, 9 (2019) 6291.
- [254] H.X. Wang, Z.X. Xue, M.H. Wei, D.-L. Chen, M. Li, A Novel Scaffold from Recombinant Spider Silk Protein in Tissue Engineering, *Advanced Materials Research*, 152-153 (2011) 1734-1744.
- [255] K. Schacht, T. Jungst, M. Schweinlin, A. Ewald, J. Groll, T. Scheibel, Biofabrication of cell-loaded 3D spider silk constructs, *Angew Chem Int Ed Engl*, 54 (2015) 2816-2820.
- [256] L.G. Griffith, M.A. Swartz, Capturing complex 3D tissue physiology in vitro, *Nature Reviews Molecular Cell Biology*, 7 (2006) 211-224.
- [257] N.T. Elliott, F. Yuan, A Review of Three-Dimensional In Vitro Tissue Models for Drug Discovery and Transport Studies, *Journal of Pharmaceutical Sciences*, 100 (2011) 59-74.
- [258] N. Kasoju, U. Bora, Silk Fibroin in Tissue Engineering, *Advanced Healthcare Materials*, 1 (2012) 393-412.
- [259] L. Yang, M. Hedhammar, T. Blom, K. Leifer, J. Johansson, P. Habibovic, C.A. van Blitterswijk, Biomimetic calcium phosphate coatings on recombinant spider silk fibres, *Biomedical Materials*, 5 (2010) 045002.
- [260] U.-J. Kim, J. Park, C. Li, H.-J. Jin, R. Valluzzi, D.L. Kaplan, Structure and Properties of Silk Hydrogels, *Biomacromolecules*, 5 (2004) 786-792.
- [261] T. Yucel, P. Cebe, D.L. Kaplan, Vortex-Induced Injectable Silk Fibroin Hydrogels, *Biophysical Journal*, 97 (2009) 2044-2050.
- [262] X. Wang, J.A. Kluge, G.G. Leisk, D.L. Kaplan, Sonication-induced gelation of silk fibroin for cell encapsulation, *Biomaterials*, 29 (2008) 1054-1064.
- [263] X. Wang, J.A. Kluge, G.G. Leisk, D.L. Kaplan, Sonication-induced gelation of silk fibroin for cell encapsulation, *Biomaterials*, 29 (2008) 1054-1064.
- [264] R. Calabrese, D.L. Kaplan, Silk ionomers for encapsulation and differentiation of human MSCs, *Biomaterials*, 33 (2012) 7375-7385.
- [265] M. Fini, A. Motta, P. Torricelli, G. Giavaresi, N. Nicoli Aldini, M. Tschon, R. Giardino, C. Migliaresi, The healing of confined critical size cancellous defects in the presence of silk fibroin hydrogel, *Biomaterials*, 26 (2005) 3527-3536.
- [266] W. Zhang, X. Wang, S. Wang, J. Zhao, L. Xu, C. Zhu, D. Zeng, J. Chen, Z. Zhang, D.L. Kaplan, X. Jiang, The use of injectable sonication-induced silk hydrogel for VEGF(165) and BMP-2 delivery for elevation of the maxillary sinus floor, *Biomaterials*, 32 (2011) 9415-9424.
- [267] G. Manoukian, F. Hagemester, Denileukin diftitox: a novel immunotoxin, *Expert Opin Biol Ther*, 9 (2009) 1445-1451.

-
- [268] R.J. Kreitman, Immunotoxins for targeted cancer therapy, *Aaps j*, 8 (2006) E532-551.
- [269] B. Leader, Q.J. Baca, D.E. Golan, Protein therapeutics: a summary and pharmacological classification, *Nature Reviews Drug Discovery*, 7 (2008) 21-39.
- [270] M.F. McDermott, Riloncept in the treatment of chronic inflammatory disorders, *Drugs Today (Barc)*, 45 (2009) 423-430.
- [271] G. Molineux, The development of romiplostim for patients with immune thrombocytopenia, *Ann N Y Acad Sci*, 1222 (2011) 55-63.
- [272] F. Luo, Z.G. Qian, X.X. Xia, Responsive Protein Hydrogels Assembled from Spider Silk Carboxyl-Terminal Domain and Resilin Copolymers, *Polymers (Basel)*, 10 (2018).
- [273] N. Mittal, R. Jansson, M. Widhe, T. Benselfelt, K.M.O. Hakansson, F. Lundell, M. Hedhammar, L.D. Soderberg, Ultrastrong and Bioactive Nanostructured Bio-Based Composites, *ACS Nano*, 11 (2017) 5148-5159.
- [274] P. Mohammadi, A.S. Aranko, C.P. Landowski, O. Ikkala, K. Jaudzems, W. Wagermaier, M.B. Linder, Biomimetic composites with enhanced toughening using silk-inspired triblock proteins and aligned nanocellulose reinforcements, *Science Advances*, 5 (2019) eaaw2541.
- [275] P. Mohammadi, G. Beaune, B.T. Stokke, J.V.I. Timonen, M.B. Linder, Self-Coacervation of a Silk-Like Protein and Its Use As an Adhesive for Cellulosic Materials, *ACS Macro Lett*, 7 (2018) 1120-1125.
- [276] M. Bhattacharya, M.M. Malinen, P. Lauren, Y.-R. Lou, S.W. Kuisma, L. Kanninen, M. Lille, A. Corlu, C. GuGuen-Guillouzo, O. Ikkala, Nanofibrillar cellulose hydrogel promotes three-dimensional liver cell culture, *Journal of controlled release*, 164 (2012) 291-298.
- [277] S. Saska, H. Barud, A. Gaspar, R. Marchetto, S.J.L. Ribeiro, Y. Messaddeq, Bacterial cellulose-hydroxyapatite nanocomposites for bone regeneration, *International journal of biomaterials*, 2011 (2011).
- [278] S. Saska, R.M. Scarel-Caminaga, L.N. Teixeira, L.P. Franchi, R.A. Dos Santos, A.M.M. Gaspar, P.T. De Oliveira, A.L. Rosa, C.S. Takahashi, Y. Messaddeq, Characterization and in vitro evaluation of bacterial cellulose membranes functionalized with osteogenic growth peptide for bone tissue engineering, *Journal of Materials Science: Materials in Medicine*, 23 (2012) 2253-2266.
- [279] C. Ao, Y. Niu, X. Zhang, X. He, W. Zhang, C. Lu, Fabrication and characterization of electrospun cellulose/nano-hydroxyapatite nanofibers for bone tissue engineering, *International journal of biological macromolecules*, 97 (2017) 568-573.
- [280] B. Gaihre, A.C. Jayasuriya, Fabrication and characterization of carboxymethyl cellulose novel microparticles for bone tissue engineering, *Materials Science and Engineering: C*, 69 (2016) 733-743.
- [281] B. Singh, N. Panda, R. Mund, K. Pramanik, Carboxymethyl cellulose enables silk fibroin nanofibrous scaffold with enhanced biomimetic potential for bone tissue engineering application, *Carbohydrate polymers*, 151 (2016) 335-347.
- [282] S.Y. Cho, M.E. Lee, Y. Choi, H.-J. Jin, Cellulose nanofiber-reinforced silk fibroin composite film with high transparency, *Fibers and Polymers*, 15 (2014) 215-219.

-
- [283] R. Xiong, H.S. Kim, S. Zhang, S. Kim, V.F. Korolovych, R. Ma, Y.G. Yingling, C. Lu, V.V. Tsukruk, Template-Guided Assembly of Silk Fibroin on Cellulose Nanofibers for Robust Nanostructures with Ultrafast Water Transport, *ACS Nano*, 11 (2017) 12008-12019.
- [284] X. Chen, R. Zhou, B. Chen, J. Chen, Nanohydroxyapatite/cellulose nanocrystals/silk fibroin ternary scaffolds for rat calvarial defect regeneration, *RSC Advances*, 6 (2016) 35684-35691.
- [285] S. Guzman-Puyol, J.A. Heredia-Guerrero, L. Ceseracciu, H. Hajiali, C. Canale, A. Scarpellini, R. Cingolani, I.S. Bayer, A. Athanassiou, E. Mele, Low-Cost and Effective Fabrication of Biocompatible Nanofibers from Silk and Cellulose-Rich Materials, *ACS Biomaterials Science & Engineering*, 2 (2016) 526-534.
- [286] M.A. Goldstein, M. Takagi, S. Hashida, O. Shoseyov, R.H. Doi, I.H. Segel, Characterization of the cellulose-binding domain of the *Clostridium cellulovorans* cellulose-binding protein A, *J Bacteriol*, 175 (1993) 5762-5768.
- [287] D.N. Bolam, A. Ciruela, S. McQueen-Mason, P. Simpson, M.P. Williamson, J.E. Rixon, A. Boraston, G.P. Hazlewood, H.J. Gilbert, Pseudomonas cellulose-binding domains mediate their effects by increasing enzyme substrate proximity, *Biochem J*, 331 (Pt 3) (1998) 775-781.
- [288] P. Tomme, R.A. Warren, N.R. Gilkes, Cellulose hydrolysis by bacteria and fungi, *Adv Microb Physiol*, 37 (1995) 1-81.
- [289] P. Tomme, A. Boraston, B. McLean, J. Kormos, A.L. Creagh, K. Sturch, N.R. Gilkes, C.A. Haynes, R.A.J. Warren, D.G. Kilburn, Characterization and affinity applications of cellulose-binding domains Presented at the 2nd Conference on Affinity Technology, Arlington, VA, USA, September 29-30, 1997.1, *Journal of Chromatography B: Biomedical Sciences and Applications*, 715 (1998) 283-296.
- [290] I. Levy, O. Shoseyov, Cellulose-binding domains: Biotechnological applications, *Biotechnology Advances*, 20 (2002) 191-213.
- [291] N.R. Gilkes, B. Henrissat, D.G. Kilburn, R.C. Miller, R.A. Warren, Domains in microbial beta-1, 4-glycanases: sequence conservation, function, and enzyme families, 55 (1991) 303-315.
- [292] P. Tomme, R.A.J. Warren, R.C. Miller, Jr., D.G. Kilburn, N.R. Gilkes, Cellulose-Binding Domains: Classification and Properties, *Enzymatic Degradation of Insoluble Carbohydrates*, American Chemical Society 1996, pp. 142-163.
- [293] A.L. Creagh, E. Ong, E. Jervis, D.G. Kilburn, C.A. Haynes, Binding of the cellulose-binding domain of exoglucanase Cex from *Cellulomonas fimi* to insoluble microcrystalline cellulose is entropically driven, 93 (1996) 12229-12234.
- [294] F.K. Andrade, S.M. Moreira, L. Domingues, F.M. Gama, Improving the affinity of fibroblasts for bacterial cellulose using carbohydrate-binding modules fused to RGD, *J Biomed Mater Res A*, 92 (2010) 9-17.
- [295] S. Varjonen, P. Laaksonen, A. Paananen, H. Valo, H. Hähl, T. Laaksonen, M.B. Linder, Self-assembly of cellulose nanofibrils by genetically engineered fusion proteins, *Soft Matter*, 7 (2011).
- [296] Q. Xiao, J. Han, C. Jiang, M. Luo, Q. Zhang, Z. He, J. Hu, G. Wang, Novel Fusion Protein Consisting of Metallothionein, Cellulose Binding Module, and Superfolder GFP for

Lead Removal from the Water Decoction of Traditional Chinese Medicine, *ACS Omega*, 5 (2020) 2893-2898.

[297] E.A. Miller, S. Baniya, D. Osorio, Y.J. Al Maalouf, H.D. Sikes, Paper-based diagnostics in the antigen-depletion regime: High-density immobilization of rcSso7d-cellulose-binding domain fusion proteins for efficient target capture, *Biosens Bioelectron*, 102 (2018) 456-463.

[298] E. Shpigel, A. Goldlust, A. Eshel, I.K. Ber, G. Efroni, Y. Singer, I. Levy, M. Dekel, O. Shoseyov, Expression, purification and applications of staphylococcal Protein A fused to cellulose-binding domain, *Biotechnology and applied biochemistry*, 31 (2000) 197-203.

[299] S. Voutilainen, A. Paananen, M. Lille, M.B. Linder, Modular protein architectures for pH-dependent interactions and switchable assembly of nanocellulose, *International Journal of Biological Macromolecules*, 137 (2019) 270-276.

[300] L. Lemetti, J. Tersteegen, J. Sammaljärvi, A.S. Aranko, M.B. Linder, Recombinant Spider Silk Protein and Delignified Wood Form a Strong Adhesive System, *ACS Sustainable Chemistry & Engineering*, 10 (2021) 552-561.

[301] X. Chen, J.L. Zaro, W.C. Shen, Fusion protein linkers: property, design and functionality, *Adv Drug Deliv Rev*, 65 (2013) 1357-1369.

[302] U. Hersel, C. Dahmen, H. Kessler, RGD modified polymers: biomaterials for stimulated cell adhesion and beyond, *Biomaterials*, 24 (2003) 4385-4415.

[303] S. Wohlrab, S. Muller, A. Schmidt, S. Neubauer, H. Kessler, A. Leal-Egana, T. Scheibel, Cell adhesion and proliferation on RGD-modified recombinant spider silk proteins, *Biomaterials*, 33 (2012) 6650-6659.

[304] N. Doi, H. Yanagawa, STABLE: protein-DNA fusion system for screening of combinatorial protein libraries in vitro, *Febs Letters*, 457 (1999) 227-230.

[305] J.J. Dunn, F.W. Studier, M. Gottesman, Complete nucleotide sequence of bacteriophage T7 DNA and the locations of T7 genetic elements, *Journal of Molecular Biology*, 166 (1983) 477-535.

[306] W. Wang, D.I. Wang, Z. Li, Facile fabrication of recyclable and active nanobiocatalyst: purification and immobilization of enzyme in one pot with Ni-NTA functionalized magnetic nanoparticle, *Chem Commun (Camb)*, 47 (2011) 8115-8117.

[307] T. Ellinger, R. Ehricht, Single-step purification of T7 RNA polymerase with a 6-histidine tag, *Biotechniques*, 24 (1998) 718-720.

[308] J.P. Kim, K. Zhang, R.H. Kramer, T.J. Schall, D.T. Woodley, Integrin receptors and RGD sequences in human keratinocyte migration: unique antimigratory function of $\alpha 3 \beta 1$ epiligrin receptor, *J Invest Dermatol*, 98 (1992) 764-770.

[309] E. Ruoslahti, M.D. Pierschbacher, New Perspectives in Cell Adhesion: RGD and Integrins, *Science*, 238 (1987) 491-497.

[310] Y. Liu, A. Mahara, Y. Kambe, Y.I. Hsu, T. Yamaoka, Endothelial cell adhesion and blood response to hemocompatible peptide 1 (HCP-1), REDV, and RGD peptide sequences with free N-terminal amino groups immobilized on a biomedical expanded polytetrafluorethylene surface, *Biomater Sci*, 9 (2021) 1034-1043.

-
- [311] F. Karimi, V.J. Thombare, C.A. Hutton, A.J. O'Connor, G.G. Qiao, D.E. Heath, Beyond RGD; nanoclusters of syndecan- and integrin-binding ligands synergistically enhance cell/material interactions, *Biomaterials*, 187 (2018) 81-92.
- [312] D. Hunter, N. Cashman, R. Morris-Valero, J. Bullock, S. Adams, J. Sanes, An LRE (leucine-arginine-glutamate)-dependent mechanism for adhesion of neurons to S-laminin, *The Journal of Neuroscience*, 11 (1991) 3960-3971.
- [313] K.J. Tomaselli, D.E. Hall, L.A. Flier, K.R. Gehlsen, D.C. Turner, S. Carbonetto, L.F. Reichardt, A neuronal cell line (PC12) expresses two $\beta 1$ -class integrins— $\alpha 1\beta 1$, and $\alpha 3\beta 1$ —that recognize different neurite outgrowth-promoting domains in laminin, *Neuron*, 5 (1990) 651-662.
- [314] K. Hosoyama, C. Lazurko, M. Muñoz, C.D. McTiernan, E.I. Alarcon, Peptide-based functional biomaterials for soft-tissue repair, *Frontiers in bioengineering and biotechnology*, 7 (2019) 205.
- [315] S.P.M.a.J.A. Hubbell, Vascular Endothelial Cell Adhesion and Spreading Promoted by the Peptide REDV of the IIICS Region of Plasma Fibronectin Is Mediated by Integrin (1992).
- [316] S. Noel, A. Hachem, Y. Merhi, G. De Crescenzo, Development of a Polyester Coating Combining Antithrombogenic and Cell Adhesive Properties: Influence of Sequence and Surface Density of Adhesion Peptides, *Biomacromolecules*, 16 (2015) 1682-1694.
- [317] Q. Han, S. Ai, Q. Hong, C. Zhang, Y. Song, X. Wang, X. Wang, S. Cui, Z. Li, H. Zhu, Z. Yang, X. Chen, G. Cai, A supramolecular hydrogel based on the combination of YIGSR and RGD enhances mesenchymal stem cells paracrine function via integrin $\alpha 2\beta 1$ and PI3K/AKT signaling pathway for acute kidney injury therapy, *Chemical Engineering Journal*, 436 (2022) 135088.
- [318] R.M. Scarborough, J.W. Rose, M.A. Hsu, D.R. Phillips, V.A. Fried, A.M. Campbell, L. Nannizzi, I.F. Charo, Barbourin. A GPIIb-IIIa-specific integrin antagonist from the venom of *Sistrurus m. barbouri*, *The Journal of biological chemistry*, 266 (1991) 9359-9362.
- [319] N.T. Feric, C.C.H. Cheng, M.C. Goh, V. Dudnyk, V. Di Tizio, M. Radisic, Angiopoietin-1 peptide QHREDGS promotes osteoblast differentiation, bone matrix deposition and mineralization on biomedical materials, *Biomaterials Science*, 2 (2014) 1384-1398.
- [320] S. Aota, M. Nomizu, K.M. Yamada, The short amino acid sequence Pro-His-Ser-Arg-Asn in human fibronectin enhances cell-adhesive function, *Journal of Biological Chemistry*, 269 (1994) 24756-24761.
- [321] I. Kozaki, T. Suzuki, S.-C. You, K. Shimizu, H. Honda, Increasing the activity of cell adherent cyclic NGR peptides by optimizing the peptide length and amino acid character, *Journal of Peptide Science*, 27 (2021) e3287.
- [322] C.G. Knight, L.F. Morton, A.R. Peachey, D.S. Tuckwell, R.W. Farndale, M.J. Barnes, The Collagen-binding A-domains of Integrins $\alpha 1\beta 1$ and $\alpha 2\beta 1$ Recognize the Same Specific Amino Acid Sequence, GFOGER, in Native (Triple-helical) Collagens*, *Journal of Biological Chemistry*, 275 (2000) 35-40.
- [323] A.M. Wojtowicz, A. Shekaran, M.E. Oest, K.M. Dupont, K.L. Templeman, D.W. Hutmacher, R.E. Guldberg, A.J. García, Coating of biomaterial scaffolds with the collagen-mimetic peptide GFOGER for bone defect repair, *Biomaterials*, 31 (2010) 2574-2582.

-
- [324] X. Pang, X. He, Z. Qiu, H. Zhang, R. Xie, Z. Liu, Y. Gu, N. Zhao, Q. Xiang, Y. Cui, Targeting integrin pathways: mechanisms and advances in therapy, *Signal Transduction and Targeted Therapy*, 8 (2023) 1.
- [325] M. Kloczewiak, S. Timmons, T.J. Lukas, J. Hawiger, Platelet receptor recognition site on human fibrinogen. Synthesis and structure-function relationship of peptides corresponding to the carboxy-terminal segment of the .gamma. chain, *Biochemistry*, 23 (1984) 1767-1774.
- [326] C.C. Larsen, F. Kligman, C. Tang, K. Kottke-Marchant, R.E. Marchant, A biomimetic peptide fluorosurfactant polymer for endothelialization of ePTFE with limited platelet adhesion, *Biomaterials*, 28 (2007) 3537-3548.
- [327] W.D. Staatz, K.F. Fok, M.M. Zutter, S.P. Adams, B.A. Rodriguez, S.A. Santoro, Identification of a tetrapeptide recognition sequence for the alpha 2 beta 1 integrin in collagen, *Journal of Biological Chemistry*, 266 (1991) 7363-7367.
- [328] V.M. Freitas, V.F. Vilas-Boas, D.C. Pimenta, V. Loureiro, M.A. Juliano, M.R. Carvalho, J.J.V. Pinheiro, A.C.M. Camargo, A.S. Moriscot, M.P. Hoffman, R.G. Jaeger, SIKVAV, a Laminin α 1-Derived Peptide, Interacts with Integrins and Increases Protease Activity of a Human Salivary Gland Adenoid Cystic Carcinoma Cell Line through the ERK 1/2 Signaling Pathway, *The American Journal of Pathology*, 171 (2007) 124-138.
- [329] M.B. Rahmany, M. Van Dyke, Biomimetic approaches to modulate cellular adhesion in biomaterials: A review, *Acta Biomaterialia*, 9 (2013) 5431-5437.
- [330] M. Matter, G. Laurie, A novel laminin E8 cell adhesion site required for lung alveolar formation in vitro, *Journal of Cell Biology*, 124 (1994) 1083-1090.
- [331] H. Nakahara, M. Nomizu, S.K. Akiyama, Y. Yamada, Y. Yeh, W.-T. Chen, A Mechanism for Regulation of Melanoma Invasion: LIGATION OF α 6 β 1 INTEGRIN BY LAMININ G PEPTIDES*, *Journal of Biological Chemistry*, 271 (1996) 27221-27224.
- [332] M.L. Ponce, M. Nomizu, H.K. Kleinman, An angiogenic laminin site and its antagonist bind through the α v β 3 and α 5 β 1 integrins, *FASEB Journal*, 15 (2001) 1389-1397.
- [333] A.P. Mould, M.J. Humphries, Identification of a novel recognition sequence for the integrin alpha 4 beta 1 in the COOH-terminal heparin-binding domain of fibronectin, *The EMBO Journal*, 10 (1991) 4089-4095.
- [334] A. Komoriya, L.J. Green, M. Mervic, S.S. Yamada, K.M. Yamada, M.J. Humphries, The minimal essential sequence for a major cell type-specific adhesion site (CS1) within the alternatively spliced type III connecting segment domain of fibronectin is leucine-aspartic acid-valine, *Journal of Biological Chemistry*, 266 (1991) 15075-15079.
- [335] K. Klimek, G. Ginalska, Proteins and Peptides as Important Modifiers of the Polymer Scaffolds for Tissue Engineering Applications—A Review, *Polymers*, 12 (2020) 844.
- [336] V.T. Trossmann, T. Scheibel, Design of Recombinant Spider Silk Proteins for Cell Type Specific Binding, *Adv Healthc Mater*, 12 (2023) e2202660.
- [337] M. Widhe, U. Johansson, C.-O. Hillerdahl, M. Hedhammar, Recombinant spider silk with cell binding motifs for specific adherence of cells, *Biomaterials*, 34 (2013) 8223-8234.
- [338] M. Widhe, U. Johansson, C.O. Hillerdahl, M. Hedhammar, Recombinant spider silk with cell binding motifs for specific adherence of cells, *Biomaterials*, 34 (2013) 8223-8234.

-
- [339] U. Johansson, M. Ria, K. Avall, N. Dekki Shalaly, S.V. Zaitsev, P.O. Berggren, M. Hedhammar, Pancreatic Islet Survival and Engraftment Is Promoted by Culture on Functionalized Spider Silk Matrices, *PLoS One*, 10 (2015) e0130169.
- [340] A. Cassar, D.R. Holmes, Jr., C.S. Rihal, B.J. Gersh, Chronic coronary artery disease: diagnosis and management, *Mayo Clin Proc*, 84 (2009) 1130-1146.
- [341] D.Y. Kwon, J.I. Kim, D.Y. Kim, H.J. Kang, B. Lee, K.W. Lee, M.S. Kim, Biodegradable stent, *Journal of Biomedical Science and Engineering*, 05 (2012) 208-216.
- [342] H. Hermawan, D. Dube, D. Mantovani, Developments in metallic biodegradable stents, *Acta Biomater*, 6 (2010) 1693-1697.
- [343] B. O'Brien, H. Zafar, A. Ibrahim, J. Zafar, F. Sharif, Coronary Stent Materials and Coatings: A Technology and Performance Update, *Ann Biomed Eng*, 44 (2016) 523-535.
- [344] P.W. Serruys, P. De Jaegere, F. Kiemeneij, C. Macaya, W. Rutsch, G. Heyndrickx, H. Emanuelsson, J. Marco, V. Legrand, P. Materne, A comparison of balloon-expandable-stent implantation with balloon angioplasty in patients with coronary artery disease, *New England Journal of Medicine*, 331 (1994) 489-495.
- [345] L. Mauri, W.-h. Hsieh, J.M. Massaro, K.K. Ho, R. D'Agostino, D.E. Cutlip, Stent thrombosis in randomized clinical trials of drug-eluting stents, *New England Journal of Medicine*, 356 (2007) 1020-1029.
- [346] J.C. Townsend, P. Rideout, D.H. Steinberg, Everolimus-eluting stents in interventional cardiology, *Vasc Health Risk Manag*, 8 (2012) 393-404.
- [347] M.C. Morice, P.W. Serruys, J.E. Sousa, J. Fajadet, E. Ban Hayashi, M. Perin, A. Colombo, G. Schuler, P. Barragan, G. Guagliumi, F. Molnàr, R. Falotico, A randomized comparison of a sirolimus-eluting stent with a standard stent for coronary revascularization, *N Engl J Med*, 346 (2002) 1773-1780.
- [348] J.W. Moses, M.B. Leon, J.J. Popma, P.J. Fitzgerald, D.R. Holmes, C. O'Shaughnessy, R.P. Caputo, D.J. Kereiakes, D.O. Williams, P.S. Teirstein, J.L. Jaeger, R.E. Kuntz, Sirolimus-eluting stents versus standard stents in patients with stenosis in a native coronary artery, *N Engl J Med*, 349 (2003) 1315-1323.
- [349] G.W. Stone, S.G. Ellis, D.A. Cox, J. Hermiller, C. O'Shaughnessy, J.T. Mann, M. Turco, R. Caputo, P. Bergin, J. Greenberg, J.J. Popma, M.E. Russell, A polymer-based, paclitaxel-eluting stent in patients with coronary artery disease, *N Engl J Med*, 350 (2004) 221-231.
- [350] C. Vézina, A. Kudelski, S.N. Sehgal, Rapamycin (AY-22,989), a new antifungal antibiotic. I. Taxonomy of the producing streptomycete and isolation of the active principle, *J Antibiot (Tokyo)*, 28 (1975) 721-726.
- [351] J.E. Sousa, M.A. Costa, A.C. Abizaid, B.J. Rensing, A.S. Abizaid, L.F. Tanajura, K. Kozuma, G.V. Langenhove, A.G.M.R. Sousa, R. Falotico, J. Jaeger, J.J. Popma, P.W. Serruys, Sustained Suppression of Neointimal Proliferation by Sirolimus-Eluting Stents, *Circulation*, 104 (2001) 2007-2011.
- [352] D.I. Axel, W. Kunert, C. Göggelmann, M. Oberhoff, C. Herdeg, A. Küttner, D.H. Wild, B.R. Brehm, R. Riessen, G. Köveker, K.R. Karsch, Paclitaxel inhibits arterial smooth muscle cell proliferation and migration in vitro and in vivo using local drug delivery, *Circulation*, 96 (1997) 636-645.

-
- [353] M.C. Morice, A. Colombo, B. Meier, P. Serruys, C. Tamburino, G. Guagliumi, E. Sousa, H.P. Stoll, Sirolimus- vs paclitaxel-eluting stents in de novo coronary artery lesions: the REALITY trial: a randomized controlled trial, *Jama*, 295 (2006) 895-904.
- [354] A.M. Galløe, L. Thuesen, H. Kelbæk, P. Thayssen, K. Rasmussen, P.R. Hansen, N. Bligaard, K. Saunamäki, A. Junker, J. Aarøe, U. Abildgaard, J. Ravkilde, T. Engstrøm, J.S. Jensen, H.R. Andersen, H.E. Bøtker, S. Galatius, S.D. Kristensen, J.K. Madsen, L.R. Krusell, S.Z. Abildstrøm, G.B. Stephansen, J.F. Lassen, f.t. SORT OUT II Investigators, Comparison of Paclitaxel- and Sirolimus-Eluting Stents in Everyday Clinical Practice The SORT OUT II Randomized Trial, *JAMA*, 299 (2008) 409-416.
- [355] L. Räber, L. Wohlowend, M. Wigger, M. Togni, S. Wandel, P. Wenaweser, S. Cook, A. Moschovitis, R. Vogel, B. Kalesan, C. Seiler, F. Eberli, T.F. Lüscher, B. Meier, P. Jüni, S. Windecker, Five-year clinical and angiographic outcomes of a randomized comparison of sirolimus-eluting and paclitaxel-eluting stents: results of the Sirolimus-Eluting Versus Paclitaxel-Eluting Stents for Coronary Revascularization LATE trial, *Circulation*, 123 (2011) 2819-2828, 2816 p following 2828.
- [356] S. Windecker, A. Remondino, F.R. Eberli, P. Jüni, L. Räber, P. Wenaweser, M. Togni, M. Billinger, D. Tüller, C. Seiler, M. Roffi, R. Corti, G. Sütsch, W. Maier, T. Lüscher, O.M. Hess, M. Egger, B. Meier, Sirolimus-eluting and paclitaxel-eluting stents for coronary revascularization, *N Engl J Med*, 353 (2005) 653-662.
- [357] J. Fajadet, W. Wijns, G.J. Laarman, K.H. Kuck, J. Ormiston, T. Münzel, J.J. Popma, P.J. Fitzgerald, R. Bonan, R.E. Kuntz, Randomized, double-blind, multicenter study of the Endeavor zotarolimus-eluting phosphorylcholine-encapsulated stent for treatment of native coronary artery lesions. Clinical and angiographic results of the ENDEAVOR II Trial, *Minerva Cardioangiol*, 55 (2007) 1-18.
- [358] M. Joner, G. Nakazawa, A.V. Finn, S.C. Quee, L. Coleman, E. Acampado, P.S. Wilson, K. Skorija, Q. Cheng, X. Xu, Endothelial cell recovery between comparator polymer-based drug-eluting stents, *Journal of the American College of Cardiology*, 52 (2008) 333-342.
- [359] M.B. Leon, E. Nikolsky, D.E. Cutlip, L. Mauri, H. Liberman, H. Wilson, J. Patterson, J. Moses, D.E. Kandzari, E.I. Investigators, Improved late clinical safety with zotarolimus-eluting stents compared with paclitaxel-eluting stents in patients with de novo coronary lesions: 3-year follow-up from the ENDEAVOR IV (Randomized Comparison of Zotarolimus- and Paclitaxel-Eluting Stents in Patients With Coronary Artery Disease) trial, *JACC: Cardiovascular Interventions*, 3 (2010) 1043-1050.
- [360] G.W. Stone, M. Midei, W. Newman, M. Sanz, J.B. Hermiller, J. Williams, N. Farhat, R. Caputo, N. Xenopoulos, R. Applegate, Randomized comparison of everolimus-eluting and paclitaxel-eluting stents: two-year clinical follow-up from the Clinical Evaluation of the Xience V Everolimus Eluting Coronary Stent System in the Treatment of Patients with de novo Native Coronary Artery Lesions (SPIRIT) III trial, *Circulation*, 119 (2009) 680-686.
- [361] P.W. Serruys, A.T. Ong, J.J. Piek, F.J. Neumann, W.J. van der Giessen, M. Wiemer, A. Zeiher, E. Grube, J. Haase, L. Thuesen, C. Hamm, P.C. Otto-Terlouw, A randomized comparison of a durable polymer Everolimus-eluting stent with a bare metal coronary stent: The SPIRIT first trial, *EuroIntervention*, 1 (2005) 58-65.
- [362] P.W. Serruys, P. Ruygrok, J. Neuzner, J.J. Piek, A. Seth, J.J. Schofer, G. Richardt, M. Wiemer, D. Carrié, L. Thuesen, E. Boone, K. Miquel-Herbert, J. Daemen, A randomised comparison of an everolimus-eluting coronary stent with a paclitaxel-eluting coronary stent: the SPIRIT II trial, *EuroIntervention*, 2 (2006) 286-294.

-
- [363] B.E. Claessen, M.A. Beijk, V. Legrand, W. Ruzyllo, A. Manari, O. Varenne, M.J. Suttorp, J.G. Tijssen, K. Miquel-Hebert, S. Veldhof, J.P. Henriques, P.W. Serruys, J.J. Piek, Two-year clinical, angiographic, and intravascular ultrasound follow-up of the XIENCE V everolimus-eluting stent in the treatment of patients with de novo native coronary artery lesions: the SPIRIT II trial, *Circ Cardiovasc Interv*, 2 (2009) 339-347.
- [364] G.W. Stone, A. Rizvi, K. Sudhir, W. Newman, R.J. Applegate, L.A. Cannon, J.T. Maddux, D.E. Cutlip, C.A. Simonton, P. Sood, D.J. Kereiakes, Randomized comparison of everolimus- and paclitaxel-eluting stents. 2-year follow-up from the SPIRIT (Clinical Evaluation of the XIENCE V Everolimus Eluting Coronary Stent System) IV trial, *J Am Coll Cardiol*, 58 (2011) 19-25.
- [365] G.W. Stone, M. Midei, W. Newman, M. Sanz, J.B. Hermiller, J. Williams, N. Farhat, K.W. Mahaffey, D.E. Cutlip, P.J. Fitzgerald, P. Sood, X. Su, A.J. Lansky, Comparison of an everolimus-eluting stent and a paclitaxel-eluting stent in patients with coronary artery disease: a randomized trial, *Jama*, 299 (2008) 1903-1913.
- [366] G.W. Stone, A. Rizvi, W. Newman, K. Mastali, J.C. Wang, R. Caputo, J. Doostzadeh, S. Cao, C.A. Simonton, K. Sudhir, A.J. Lansky, D.E. Cutlip, D.J. Kereiakes, Everolimus-eluting versus paclitaxel-eluting stents in coronary artery disease, *N Engl J Med*, 362 (2010) 1663-1674.
- [367] Y. Onuma, N. Kukreja, N. Piazza, J. Eindhoven, C. Girasis, L. Schenkeveld, R. van Domburg, P.W. Serruys, The everolimus-eluting stent in real-world patients: 6-month follow-up of the X-SEARCH (Xience V Stent Evaluated at Rotterdam Cardiac Hospital) registry, *J Am Coll Cardiol*, 54 (2009) 269-276.
- [368] K.W. Park, I.H. Chae, D.S. Lim, K.R. Han, H.M. Yang, H.Y. Lee, H.J. Kang, B.K. Koo, T. Ahn, J.H. Yoon, M.H. Jeong, T.J. Hong, W.Y. Chung, S.H. Jo, Y.J. Choi, S.H. Hur, H.M. Kwon, D.W. Jeon, B.O. Kim, S.H. Park, N.H. Lee, H.K. Jeon, H.C. Gwon, Y.S. Jang, H.S. Kim, Everolimus-eluting versus sirolimus-eluting stents in patients undergoing percutaneous coronary intervention: the EXCELLENT (Efficacy of Xience/Promus Versus Cypher to Reduce Late Loss After Stenting) randomized trial, *J Am Coll Cardiol*, 58 (2011) 1844-1854.
- [369] P.W. Serruys, S. Silber, S. Garg, R.J. van Geuns, G. Richardt, P.E. Buszman, H. Kelbaek, A.J. van Boven, S.H. Hofma, A. Linke, V. Klauss, W. Wijns, C. Macaya, P. Garot, C. DiMario, G. Manoharan, R. Kornowski, T. Ischinger, A. Bartorelli, J. Ronden, M. Bressers, P. Gobbens, M. Negoita, F. van Leeuwen, S. Windecker, Comparison of zotarolimus-eluting and everolimus-eluting coronary stents, *N Engl J Med*, 363 (2010) 136-146.
- [370] I. Sheiban, G. Villata, M. Bollati, D. Sillano, M. Lotrionte, G. Biondi-Zoccai, Next-generation drug-eluting stents in coronary artery disease: focus on everolimus-eluting stent (Xience V®), *Vascular Health and Risk Management*, 4 (2008) 31-38.
- [371] L.O. Jensen, P. Thayssen, E.H. Christiansen, M. Maeng, J. Ravkilde, K.N. Hansen, H.S. Hansen, L. Krusell, A. Kaltoft, H.H. Tilsted, K. Berencsi, A. Junker, J.F. Lassen, Safety and Efficacy of Everolimus- Versus Sirolimus-Eluting Stents: 5-Year Results From SORT OUT IV, *Journal of the American College of Cardiology*, 67 (2016) 751-762.
- [372] G. Paramasivam, T. Devasia, S. Ubaid, A. Shetty, K. Nayak, U. Pai, M.S. Rao, In-stent restenosis of drug-eluting stents: clinical presentation and outcomes in a real-world scenario, *The Egyptian Heart Journal*, 71 (2019) 28.
- [373] S.J. Hong, M.K. Hong, Drug-eluting stents for the treatment of coronary artery disease: A review of recent advances, *Expert Opin Drug Deliv*, 19 (2022) 269-280.

-
- [374] H.-S. Kim, J. Kang, D. Hwang, J.-K. Han, H.-M. Yang, H.-J. Kang, B.-K. Koo, S.Y. Kim, K.-H. Park, S.-W. Rha, W.-Y. Shin, H.-S. Lim, K. Park, K.W. Park, Durable Polymer Versus Biodegradable Polymer Drug-Eluting Stents After Percutaneous Coronary Intervention in Patients with Acute Coronary Syndrome, *Circulation*, 143 (2021) 1081-1091.
- [375] W. Xu, M. Sasaki, T. Niidome, Sirolimus Release from Biodegradable Polymers for Coronary Stent Application: A Review, *Pharmaceutics*, 14 (2022).
- [376] Y. Han, Q. Jing, Y. Li, L. Yang, H. Liu, X. Shang, T. Jiang, Z. Li, H. Zhang, G. Yan, T.M.-C.R.o.E.B.P.D.E.S. investigators, Sustained clinical safety and efficacy of a biodegradable-polymer coated sirolimus-eluting stent in "real-world" practice: Three-year outcomes of the CREATE (multi-center registry of EXCEL biodegradable polymer drug eluting stents) study, *Catheterization and Cardiovascular Interventions*, 79 (2012) 211-216.
- [377] S. Bangalore, B. Toklu, N. Patel, F. Feit, G.W. Stone, Newer-Generation Ultrathin Strut Drug-Eluting Stents Versus Older Second-Generation Thicker Strut Drug-Eluting Stents for Coronary Artery Disease, *Circulation*, 138 (2018) 2216-2226.
- [378] K. Kadota, T. Muramatsu, M. Iwabuchi, S. Saito, Y. Hayashi, Y. Ikari, S. Nanto, K. Fujii, N. Inoue, A. Namiki, T. Kimura, K. Mitsudo, Randomized comparison of the nobori biolimus A9-eluting stent with the sirolimus-eluting stent in patients with stenosis in native coronary arteries, *Catheterization and Cardiovascular Interventions*, 80 (2012) 789-796.
- [379] B. Verma, A. Patel, D. Katyal, V.R. Singh, A.K. Singh, A. Singh, M. Kumar, P. Nagarkoti, Real World Experience of a Biodegradable Polymer Sirolimus-Eluting Stent (Yukon Choice PC Elite) in Patients with Acute ST-Segment Elevation Myocardial Infarction Undergoing Primary Angioplasty: A Multicentric Observational Study (The Elite India Study), *Open Access Maced J Med Sci*, 7 (2019) 1103-1109.
- [380] C. Li, C. Guan, R. Zhang, Y. Yang, C. Ma, H. Li, S. Chen, Y. Han, B. Xu, R. Gao, f.t.T. Investigators, Safety and efficacy of a novel abluminal groove-filled biodegradable polymer sirolimus-eluting stent for the treatment of de novo coronary lesions: Final five-year results of the patient-level pooled analysis from the TARGET I and TARGET II trials, *Catheterization and Cardiovascular Interventions*, 93 (2019) 818-824.
- [381] B. Chevalier, P.C. Smits, D. Carrié, J. Mehilli, A.J.V. Boven, E. Regar, F.J. Sawaya, D. Chamié, A.O. Kraaijeveld, T. Hovasse, G.J. Vlachojannis, Serial Assessment of Strut Coverage of Biodegradable Polymer Drug-Eluting Stent at 1, 2, and 3 Months After Stent Implantation by Optical Frequency Domain Imaging, *Circulation: Cardiovascular Interventions*, 10 (2017) e004801.
- [382] Y. Han, B. Xu, Q. Jing, S. Lu, L. Yang, K. Xu, Y. Li, J. Li, C. Guan, A.J. Kirtane, Y. Yang, A Randomized Comparison of Novel Biodegradable Polymer- and Durable Polymer-Coated Cobalt-Chromium Sirolimus-Eluting Stents, *JACC: Cardiovascular Interventions*, 7 (2014) 1352-1360.
- [383] J. Bennett, C. Dubois, A novel platinum chromium everolimus-eluting stent for the treatment of coronary artery disease, *Biologics*, 7 (2013) 149-159.
- [384] A.R. Tzafiriri, F. Garcia-Polite, X. Li, J. Keating, J.-M. Balaguer, B. Zani, L. Bailey, P. Markham, T.C. Kiorpes, W. Carlyle, E.R. Edelman, Defining drug and target protein distributions after stent-based drug release: Durable versus deployable coatings, *Journal of Controlled Release*, 274 (2018) 102-108.
- [385] B. Xu, R. Gao, Y. Yang, X. Cao, L. Qin, Y. Li, Z. Li, X. Li, H. Lin, Y. Guo, Y. Ma, J.a. Wang, S. Nie, L. Xu, E. Cao, C. Guan, G.W. Stone, Biodegradable Polymer-Based Sirolimus-

Eluting Stents With Differing Elution and Absorption Kinetics: The PANDA III Trial, *Journal of the American College of Cardiology*, 67 (2016) 2249-2258.

[386] H.Y. Ang, Y.Y. Huang, S.T. Lim, P. Wong, M. Joner, N. Foin, Mechanical behavior of polymer-based vs . metallic-based bioresorbable stents, *Journal of Thoracic Disease*, (2017) S923-S934.

[387] W. Xu, K. Sato, Y. Koga, M. Sasaki, T. Niidome, Corrosion resistance of HF-treated Mg alloy stent following balloon expansion and its improvement through biodegradable polymer coating, *Journal of Coatings Technology and Research*, 17 (2020) 1023-1032.

[388] D. Pappalardo, T. Mathisen, A. Finne-Wistrand, Biocompatibility of Resorbable Polymers: A Historical Perspective and Framework for the Future, *Biomacromolecules*, 20 (2019) 1465-1477.

[389] S. Jana, Endothelialization of cardiovascular devices, *Acta Biomater*, 99 (2019) 53-71.

[390] J. Zhang, H. Huang, R. Ju, K. Chen, S. Li, W. Wang, Y. Yan, In vivo biocompatibility and hemocompatibility of a polytetrafluoroethylene small diameter vascular graft modified with sulfonated silk fibroin, *The American Journal of Surgery*, 213 (2017) 87-93.

[391] C.-K. Yoo, J.-Y. Jeon, Y.-J. Kim, S.-G. Kim, K.-G. Hwang, Cell attachment and proliferation of osteoblast-like MG63 cells on silk fibroin membrane for guided bone regeneration, *Maxillofacial Plastic and Reconstructive Surgery*, 38 (2016) 17.

[392] Y. Gotoh, M. Tsukada, N. Minoura, Effect of the chemical modification of the arginyl residue in Bombyx mori silk fibroin on the attachment and growth of fibroblast cells, *Journal of Biomedical Materials Research: An Official Journal of The Society for Biomaterials, The Japanese Society for Biomaterials, and the Australian Society for Biomaterials*, 39 (1998) 351-357.

[393] N. Minoura, S.-I. Aiba, M. Higuchi, Y. Gotoh, M. Tsukada, Y. Imai, Attachment and growth of fibroblast cells on silk fibroin, *Biochemical and biophysical research communications*, 208 (1995) 511-516.

[394] E. Marsano, M. Canetti, G. Conio, P. Corsini, G. Freddi, Fibers based on cellulose-silk fibroin blend, *Journal of Applied Polymer Science*, 104 (2007) 2187-2196.

[395] J. Riesle, A.P. Hollander, R. Langer, L.E. Freed, G. Vunjak-Novakovic, Collagen in tissue-engineered cartilage: types, structure, and crosslinks, *J Cell Biochem*, 71 (1998) 313-327.

[396] Z.G. Qian, M.L. Zhou, W.W. Song, X.X. Xia, Dual Thermosensitive Hydrogels Assembled from the Conserved C-Terminal Domain of Spider Dragline Silk, *Biomacromolecules*, 16 (2015) 3704-3711.

[397] T.B. Aigner, E. DeSimone, T. Scheibel, Biomedical Applications of Recombinant Silk-Based Materials, *Adv Mater*, 30 (2018) e1704636.

[398] E. DeSimone, K. Schacht, A. Pellert, T. Scheibel, Recombinant spider silk-based bioinks, *Biofabrication*, 9 (2017) 044104.

[399] A.C. Weiss, H.M. Herold, S. Lentz, M. Faria, Q.A. Besford, C.-S. Ang, F. Caruso, T. Scheibel, Surface Modification of Spider Silk Particles to Direct Biomolecular Corona Formation, *ACS applied materials & interfaces*, 12 (2020) 24635-24643.

-
- [400] S. Noel, A. Hachem, Y. Merhi, G. De Crescenzo, Development of a Polyester Coating Combining Antithrombogenic and Cell Adhesive Properties: Influence of Sequence and Surface Density of Adhesion Peptides, *Biomacromolecules*, 16 (2015) 1682-1694.
- [401] H.-S. Han, S. Loffredo, I. Jun, J. Edwards, Y.-C. Kim, H.-K. Seok, F. Witte, D. Mantovani, S. Glyn-Jones, Current status and outlook on the clinical translation of biodegradable metals, *Materials Today*, 23 (2019) 57-71.
- [402] H. Hendra, D. Dominique, M. Diego, Patents on Metallic Biodegradable Stents, *Recent Patents on Materials Science*, 3 (2010) 140-145.
- [403] H. Hermawan, D. Mantovani, Process of prototyping coronary stents from biodegradable Fe-Mn alloys, *Acta Biomater*, 9 (2013) 8585-8592.
- [404] J. Yang, M. Khan, L. Zhang, X. Ren, J. Guo, Y. Feng, S. Wei, W. Zhang, Antimicrobial surfaces grafted random copolymers with REDV peptide beneficial for endothelialization, *J Mater Chem B*, 3 (2015) 7682-7697.
- [405] S. Maloy, V. Stewart, R.K. Taylor, *Genetic Analysis of Pathogenic Bacteria: A Laboratory Manual*, 1995.
- [406] E. Ong, N.R. Gilkes, R.C. Miller Jr., R.A.J. Warren, D.G. Kilburn, The cellulose-binding domain (CBDCex) of an exoglucanase from *Cellulomonas fimi*: Production in *Escherichia coli* and characterization of the polypeptide, 42 (1993) 401-409.
- [407] P.J. Shilling, K. Mirzadeh, A.J. Cumming, M. Widesheim, Z. Köck, D.O. Daley, Improved designs for pET expression plasmids increase protein production yield in *Escherichia coli*, *Communications Biology*, 3 (2020) 214.
- [408] S. Rammensee, U. Slotta, T. Scheibel, A.R. Bausch, Assembly mechanism of recombinant spider silk proteins, *Proceedings of the National Academy of Sciences*, 105 (2008) 6590-6595.
- [409] D.J. Kroll, H. Abdel-Malek Abdel-Hafiz, T. Marcell, S. Simpson, C.Y. Chen, A. Gutierrez-Hartmann, J.W. Lustbader, J.P. Hoeffler, A multifunctional prokaryotic protein expression system: overproduction, affinity purification, and selective detection, *DNA Cell Biol*, 12 (1993) 441-453.
- [410] H. Liu, J. Kang, Q. Qi, G. Chen, Production of lactate in *Escherichia coli* by redox regulation genetically and physiologically, *Appl Biochem Biotechnol*, 164 (2011) 162-169.
- [411] R.C. Beavis, B.T. Chait, H.S. Creel, M.J. Fournier, T.L. Mason, D.A. Tirrell, Analysis of artificial proteins by matrix-assisted laser desorption mass spectrometry, *Journal of the American Chemical Society*, 114 (1992) 7584-7585.
- [412] M. Strohal, M. Hassman, B. Kořata, M. Kodíček, mMass data miner: an open source alternative for mass spectrometric data analysis, *Rapid Communications in Mass Spectrometry*, 22 (2008) 905-908.
- [413] G. Carrard, A. Koivula, H. Söderlund, P. Béguin, Cellulose-binding domains promote hydrolysis of different sites on crystalline cellulose, 97 (2000) 10342-10347.
- [414] M. Linder, T.T. Teeri, The roles and function of cellulose-binding domains, *Journal of Biotechnology*, 57 (1997) 15-28.
- [415] M.L. Langsford, N.R. Gilkes, W.W. Wakarchuk, D.G. Kilburn, R.C. Miller, R.A.J. Warren, The Cellulase System of *Cellulomonas fimi*, *Microbiology*, 130 (1984) 1367-1376.

-
- [416] B. Fahnert, H. Lilie, P. Neubauer, Inclusion Bodies: Formation and Utilisation, Physiological Stress Responses in Bioprocesses: -/-, Springer Berlin Heidelberg, Berlin, Heidelberg, 2004, pp. 93-142.
- [417] N.R. Gilkes, R.A. Warren, R.C. Miller, Jr., D.G. Kilburn, Precise excision of the cellulose binding domains from two *Cellulomonas fimi* cellulases by a homologous protease and the effect on catalysis, *The Journal of biological chemistry*, 263 (1988) 10401-10407.
- [418] M. Srisodsuk, T. Reinikainen, M. Penttilä, T.T. Teeri, Role of the interdomain linker peptide of *Trichoderma reesei* cellobiohydrolase I in its interaction with crystalline cellulose, *Journal of Biological Chemistry*, 268 (1993) 20756-20761.
- [419] H. Shen, M. Schmuck, I. Pilz, N.R. Gilkes, D.G. Kilburn, R.C. Miller, R.A. Warren, Deletion of the linker connecting the catalytic and cellulose-binding domains of endoglucanase A (CenA) of *Cellulomonas fimi* alters its conformation and catalytic activity, *Journal of Biological Chemistry*, 266 (1991) 11335-11340.
- [420] J. Kormos, P.E. Johnson, E. Brun, P. Tomme, L.P. McIntosh, C.A. Haynes, D.G. Kilburn, Binding site analysis of cellulose binding domain CBD(N1) from endoglucanase C of *Cellulomonas fimi* by site-directed mutagenesis, *Biochemistry*, 39 (2000) 8844-8852.
- [421] S. Sharma, S. Sarkar, S.S. Paul, S. Roy, K. Chattopadhyay, A small molecule chemical chaperone optimizes its unfolded state contraction and denaturant like properties, *Sci Rep*, 3 (2013) 3525.
- [422] L.O. Narhi, C.H. Li, R. Ramachander, J. Svitel, Y. Jiang, Optical Spectroscopic Methods for the Analysis of Biological Macromolecules, in: N. Allewell, L.O. Narhi, I. Rayment (Eds.) *Molecular Biophysics for the Life Sciences*, Springer New York, New York, NY, 2013, pp. 33-90.
- [423] C. Duy, J. Fitter, How aggregation and conformational scrambling of unfolded states govern fluorescence emission spectra, *Biophysical journal*, 90 (2006) 3704-3711.
- [424] G. Tozzi, A. De Mori, A. Oliveira, M. Roldo, Composite Hydrogels for Bone Regeneration, *Materials*, 9 (2016) 267.
- [425] A. Kumar, K.M. Rao, S.S. Han, Synthesis of mechanically stiff and bioactive hybrid hydrogels for bone tissue engineering applications, *Chemical Engineering Journal*, 317 (2017) 119-131.
- [426] D. Burger, M. Beaumont, T. Rosenau, Y. Tamada, Porous Silk Fibroin/Cellulose Hydrogels for Bone Tissue Engineering via a Novel Combined Process Based on Sequential Regeneration and Porogen Leaching, *Molecules*, 25 (2020) 5097.
- [427] S.J. Craig, A. Shu, Y. Xu, F.C. Foong, R. Nordon, Chimeric protein for selective cell attachment onto cellulosic substrates, *Protein Eng Des Sel*, 20 (2007) 235-241.
- [428] Y. Xu, F.C. Foong, Characterization of a cellulose binding domain from *Clostridium cellulovorans* endoglucanase-xylanase D and its use as a fusion partner for soluble protein expression in *Escherichia coli*, *J Biotechnol*, 135 (2008) 319-325.
- [429] R. Stevens, L. Stevens, N.C. Price, The stabilities of various thiol compounds used in protein purifications, *Biochemical Education*, 11 (1983) 70.
- [430] G. Mazurek, M. Iwański, Modelling of Asphalt Concrete Stiffness in the Linear Viscoelastic Region, *IOP Conference Series: Materials Science and Engineering*, 245 (2017) 032029.

-
- [431] L.A. Castillo Diaz, A. Saiani, J.E. Gough, A.F. Miller, Human osteoblasts within soft peptide hydrogels promote mineralisation in vitro, *J Tissue Eng*, 5 (2014) 2041731414539344.
- [432] J. Zhang, E. Wehrle, P. Adamek, G.R. Paul, X.H. Qin, M. Rubert, R. Muller, Optimization of mechanical stiffness and cell density of 3D bioprinted cell-laden scaffolds improves extracellular matrix mineralization and cellular organization for bone tissue engineering, *Acta Biomater*, 114 (2020) 307-322.
- [433] C.G. Lopez, W. Richtering, Oscillatory rheology of carboxymethyl cellulose gels: Influence of concentration and pH, *Carbohydrate Polymers*, 267 (2021) 118117.
- [434] A. Billiau, V.G. Edy, H. Heremans, J. Van Damme, J. Desmyter, J.A. Georgiades, P. De Somer, Human interferon: mass production in a newly established cell line, MG-63, *Antimicrob Agents Chemother*, 12 (1977) 11-15.
- [435] M. Koosha, M. Raoufi, H. Moravvej, One-pot reactive electrospinning of chitosan/PVA hydrogel nanofibers reinforced by halloysite nanotubes with enhanced fibroblast cell attachment for skin tissue regeneration, *Colloids and Surfaces B: Biointerfaces*, 179 (2019) 270-279.
- [436] A.V. Nasalapure, R.K. Chalannavar, D.R. Kasai, K.R. Reddy, A.V. Raghu, Novel polymeric hydrogel composites: Synthesis, physicochemical, mechanical and biocompatible properties, *Nano Express*, 2 (2021) 030003.
- [437] Z. Montaseri, S.S. Abolmaali, A.M. Tamaddon, F. Farvadi, Composite silk fibroin hydrogel scaffolds for cartilage tissue regeneration, *Journal of Drug Delivery Science and Technology*, 79 (2023) 104018.
- [438] L. Zhang, T.J. Webster, Nanotechnology and nanomaterials: Promises for improved tissue regeneration, *Nano Today*, 4 (2009) 66-80.
- [439] Z. Zhang, M. Li, W. Chen, S. Zhu, N. Liu, L. Zhu, Immobilization of lead and cadmium from aqueous solution and contaminated sediment using nano-hydroxyapatite, *Environ Pollut*, 158 (2010) 514-519.
- [440] M.A. Sainz, S. Serena, M. Belmonte, P. Miranzo, M.I. Osendi, Protein adsorption and in vitro behavior of additively manufactured 3D-silicon nitride scaffolds intended for bone tissue engineering, *Materials Science and Engineering: C*, 115 (2020) 110734.
- [441] M. Golizadeh, A. Karimi, S. Gandomi-Ravandi, M. Vossoughi, M. Khafaji, M.T. Joghataei, F. Faghihi, Evaluation of cellular attachment and proliferation on different surface charged functional cellulose electrospun nanofibers, *Carbohydrate polymers*, 207 (2019) 796-805.
- [442] A. Gilarska, J. Lewandowska-Lancucka, W. Horak, M. Nowakowska, Collagen/chitosan/hyaluronic acid - based injectable hydrogels for tissue engineering applications - design, physicochemical and biological characterization, *Colloids Surf B Biointerfaces*, 170 (2018) 152-162.
- [443] T. Zhang, S. Lin, X. Shao, Q. Zhang, C. Xue, S. Zhang, Y. Lin, B. Zhu, X. Cai, Effect of matrix stiffness on osteoblast functionalization, *Cell Prolif*, 50 (2017).
- [444] K. Chatterjee, S. Lin-Gibson, W.E. Wallace, S.H. Parekh, Y.J. Lee, M.T. Cicerone, M.F. Young, C.G. Simon, Jr., The effect of 3D hydrogel scaffold modulus on osteoblast differentiation and mineralization revealed by combinatorial screening, *Biomaterials*, 31 (2010) 5051-5062.

-
- [445] L. Jongpaiboonkit, W.J. King, W.L. Murphy, Screening for 3D environments that support human mesenchymal stem cell viability using hydrogel arrays, *Tissue Eng Part A*, 15 (2009) 343-353.
- [446] F. You, X. Wu, N. Zhu, M. Lei, B.F. Eames, X. Chen, 3D Printing of Porous Cell-Laden Hydrogel Constructs for Potential Applications in Cartilage Tissue Engineering, *ACS Biomater Sci Eng*, 2 (2016) 1200-1210.
- [447] T.L. Riss, R.A. Moravec, Use of Multiple Assay Endpoints to Investigate the Effects of Incubation Time, Dose of Toxin, and Plating Density in Cell-Based Cytotoxicity Assays, *ASSAY and Drug Development Technologies*, 2 (2004) 51-62.
- [448] H.-F. Guo, W.-W. Dai, D.-H. Qian, Z.-X. Qin, Y. Lei, X.-Y. Hou, C. Wen, A simply prepared small-diameter artificial blood vessel that promotes in situ endothelialization, *Acta Biomaterialia*, 54 (2017) 107-116.
- [449] S. Baiguera, D. Ribatti, Endothelialization approaches for viable engineered tissues, *Angiogenesis*, 16 (2013) 1-14.
- [450] P.F. Sanchez, E.M. Brey, J.C. Briceno, Endothelialization mechanisms in vascular grafts, *J Tissue Eng Regen Med*, 12 (2018) 2164-2178.
- [451] J. Lv, X. Hao, Q. Li, M. Akpanyung, A. Nejjari, A. Neve, X. Ren, Y. Feng, C. Shi, W. Zhang, Star-shaped copolymer grafted PEI and REDV as a gene carrier to improve migration of endothelial cells, *Biomater, Sci*, 2017.
- [452] Y. Zhuang, C. Zhang, M. Cheng, J. Huang, Q. Liu, G. Yuan, K. Lin, H. Yu, Challenges and strategies for in situ endothelialization and long-term lumen patency of vascular grafts, *Bioact Mater*, 6 (2021) 1791-1809.
- [453] T. Flora, I.G. de Torre, L. Quintanilla, M. Alonso, J.C. Rodríguez-Cabello, Spatial control and cell adhesion selectivity on model gold surfaces grafted with elastin-like recombinamers, *European Polymer Journal*, 106 (2018) 19-29.
- [454] A. Mahara, K. Kitagawa, A. Otaka, T. Nakaoki, K. Ishihara, T. Yamaoka, Impact of REDV peptide density and its linker structure on the capture, movement, and adhesion of flowing endothelial progenitor cells in microfluidic devices, *Mater Sci Eng C Mater Biol Appl*, 129 (2021) 112381.
- [455] A.M. Ruhoff, J.K. Hong, L. Gao, J. Singh, C. Tran, G. Mackie, A. Waterhouse, Biomaterial Wettability Affects Fibrin Clot Structure and Fibrinolysis, *Adv Healthc Mater*, 10 (2021) e2100988.
- [456] J.K. Hong, K. Mathur, A.M. Ruhoff, B. Akhavan, A. Waterhouse, C. Neto, Design Optimization of Perfluorinated Liquid-Infused Surfaces for Blood-Contacting Applications, *Advanced Materials Interfaces*, 9 (2022) 2102214.
- [457] S. Sinn, T. Scheuermann, S. Deichelbohrer, G. Ziemer, H.P. Wendel, A novel in vitro model for preclinical testing of the hemocompatibility of intravascular stents according to ISO 10993-4, *Journal of Materials Science: Materials in Medicine*, 22 (2011) 1521-1528.
- [458] Z.K. Nazarkina, B.P. Chelobanov, V.S. Chernonosova, I.V. Romanova, A.A. Karpenko, P.P. Laktionov, Sirolimus-Eluting Electrospun-Produced Matrices as Coatings for Vascular Stents: Dependence of Drug Release on Matrix Structure and Composition of the External Environment, *Materials (Basel)*, 13 (2020).

-
- [459] A. Mirmohseni, J. Hosseini, M. Shojaei, S. Davaran, Interactions of anti-proliferative and anti-platelet drugs with self-assembled monolayers: a future strategy in stent development, *RSC Adv.*, 4 (2014) 4218-4224.
- [460] F.J. Baldenebro-Lopez, C.D. Gomez-Esparza, R. Corral-Higuera, S.P. Arredondo-Rea, M.J. Pellegrini-Cervantes, J.E. Ledezma-Sillas, R. Martinez-Sanchez, J.M. Herrera-Ramirez, Influence of Size on the Microstructure and Mechanical Properties of an AISI 304L Stainless Steel-A Comparison between Bulk and Fibers, *Materials (Basel)*, 8 (2015) 451-461.
- [461] S. Hassan, M.N. Ali, B. Ghafoor, Evolutionary perspective of drug eluting stents: from thick polymer to polymer free approach, *J Cardiothorac Surg*, 17 (2022) 65.
- [462] J.M. de la Torre Hernandez, P. Tejedor, T.G. Camarero, J.M. Duran, D.H. Lee, J. Monedero, F.S. Laso, M.A. Calderon, G. Veiga, J. Zueco, Early healing assessment with optical coherence tomography of everolimus-eluting stents with bioabsorbable polymer (synergy) at 3 and 6 months after implantation, *Catheter Cardiovasc Interv*, 88 (2016) E67-73.
- [463] N.M. Alves, I. Pashkuleva, R.L. Reis, J.F. Mano, Controlling Cell Behavior Through the Design of Polymer Surfaces, *Small*, 6 (2010) 2208-2220.
- [464] Y. Arima, H. Iwata, Effect of wettability and surface functional groups on protein adsorption and cell adhesion using well-defined mixed self-assembled monolayers, *Biomaterials*, 28 (2007) 3074-3082.
- [465] S. Wohlrab, K. Spieß, T. Scheibel, Varying surface hydrophobicities of coatings made of recombinant spider silk proteins, *Journal of Materials Chemistry*, 22 (2012) 22050-22054
- [466] J. Nam, Y. Huang, S. Agarwal, J. Lannutti, Materials selection and residual solvent retention in biodegradable electrospun fibers, *Journal of applied polymer science*, 107 (2008) 1547-1554.
- [467] S.H. OOYA, Tetsuo, METHOD FOR REMOVING ORGANIC SOLVENT, in: E.P. Office (Ed.)Germany, 2009, pp. 17.
- [468] S. Wu, R.A. Shanks, Solubility study of polyacrylamide in polar solvents, *Journal of Applied Polymer Science*, 93 (2004) 1493-1499.
- [469] H.V. Ramos Avilez, D.A. Castilla Casadiego, A.L. Vega Avila, O.J. Perales Perez, J. Almodovar, 11 - Production of chitosan coatings on metal and ceramic biomaterials, in: J.A. Jennings, J.D. Bumgardner (Eds.) *Chitosan Based Biomaterials Volume 1*, Woodhead Publishing2017, pp. 255-293.
- [470] M. Sypabekova, A. Hagemann, D. Rho, S. Kim, Review: 3-Aminopropyltriethoxysilane (APTES) Deposition Methods on Oxide Surfaces in Solution and Vapor Phases for Biosensing Applications, *Biosensors*, 13 (2023) 36.
- [471] A. Natarajan, C. Chun, J.J. Hickman, P. Molnar, Growth and electrophysiological properties of rat embryonic cardiomyocytes on hydroxyl- and carboxyl-modified surfaces, *J Biomater Sci Polym Ed*, 19 (2008) 1319-1331.
- [472] S. Houis, E.M. Engelhardt, F. Wurm, T. Gries, Application of Polyvinylidene Fluoride (PVDF) as a Biomaterial in Medical Textiles, in: S.C. Anand, J.F. Kennedy, M. Mirafteb, S. Rajendran (Eds.) *Medical and Healthcare Textiles*, Woodhead Publishing2010, pp. 342-352.

-
- [473] J.K. Hong, L. Gao, J. Singh, T. Goh, A.M. Ruhoff, C. Neto, A. Waterhouse, Evaluating medical device and material thrombosis under flow: current and emerging technologies, *Biomater Sci*, 8 (2020) 5824-5845.
- [474] A.M. Ruhoff, J.K. Hong, L. Gao, J. Singh, C. Tran, G. Mackie, A. Waterhouse, Biomaterial Wettability Affects Fibrin Clot Structure and Fibrinolysis (*Adv. Healthcare Mater.* 20/2021), *Advanced Healthcare Materials*, 10 (2021) 2170098.
- [475] R. Zhuo, C.A. Siedlecki, E.A. Vogler, Competitive-protein adsorption in contact activation of blood factor XII, *Biomaterials*, 28 (2007) 4355-4369.
- [476] A.C.G. Weiss, H.M. Herold, S. Lentz, M. Faria, Q.A. Besford, C.S. Ang, F. Caruso, T. Scheibel, Surface Modification of Spider Silk Particles to Direct Biomolecular Corona Formation, *ACS Appl Mater Interfaces*, 12 (2020) 24635-24643.
- [477] S. Commandeur, H.M. van Beusekom, W.J. van der Giessen, Polymers, drug release, and drug-eluting stents, *J Interv Cardiol*, 19 (2006) 500-506.
- [478] G.T. Karapanagiotidis, P. Antonitsis, N. Charokopos, C.N. Foroulis, K. Anastasiadis, E. Rouska, H. Argiriadou, K. Rammos, C. Papakonstantinou, Serum levels of matrix metalloproteinases-1,-2,-3 and-9 in thoracic aortic diseases and acute myocardial ischemia, *Journal of cardiothoracic surgery*, 4 (2009) 1-6.
- [479] D. Ulrich, K. Hrynyschyn, N. Pallua, Matrix metalloproteinases and tissue inhibitors of metalloproteinases in sera and tissue of patients with Dupuytren's disease, *Plastic and reconstructive surgery*, 112 (2003) 1279-1286.
- [480] D. Ulrich, F. Lichtenegger, M. Eblenkamp, D. Repper, N. Pallua, Matrix metalloproteinases, tissue inhibitors of metalloproteinases, aminoterminal propeptide of procollagen type III, and hyaluronan in sera and tissue of patients with capsular contracture after augmentation with Trilucent breast implants, *Plastic and reconstructive surgery*, 114 (2004) 229-236.
- [481] G. Morgia, M. Falsaperla, G. Malaponte, M. Madonia, M. Indelicato, S. Travali, M.C. Mazzarino, Matrix metalloproteinases as diagnostic (MMP-13) and prognostic (MMP-2, MMP-9) markers of prostate cancer, *Urological research*, 33 (2005) 44-50.
- [482] C. Wiegand, U. Schonfelder, M. Abel, P. Ruth, M. Kaatz, U.C. Hipler, Protease and pro-inflammatory cytokine concentrations are elevated in chronic compared to acute wounds and can be modulated by collagen type I in vitro, *Arch Dermatol Res*, 302 (2010) 419-428.
- [483] A. Örem, O. Değer, G. Çimşit, S. Bahadır, Plasma polymorphonuclear leukocyte elastase levels and its relation to disease activity in psoriasis, *Clinica Chimica Acta*, 264 (1997) 49-56.
- [484] H. Hofer, E. Kukovetz, W. Petek, F. Schweighofer, R. Wildburger, R. Schaur, Released PMN elastase: an indicator of postsurgical uneventful wound healing and early inflammatory complications. A contribution to the search for objective criteria in wound healing monitoring, *Injury*, 26 (1995) 103-106.
- [485] O. Değer, A. Örem, N. Akyol, S. Bahadır, S. Yildirmiş, Polymorphonuclear leukocyte elastase levels in patients with Behcet's disease, *Clinica chimica acta*, 236 (1995) 129-134.
- [486] L. Lu, C.A. Garcia, A.G. Mikos, In vitro degradation of thin poly(DL-lactic-co-glycolic acid) films, *Journal of biomedical materials research*, 46 (1999) 236-244.

-
- [487] Z. Jia, C. Ma, H. Zhang, PLGA Coatings and PLGA Drug-Loading Coatings for Cardiac Stent Samples: Degradation Characteristics and Blood Compatibility, *Coatings*, 11 (2021).
- [488] X. Ma, S. Oyamada, T. Wu, M.P. Robich, H. Wu, X. Wang, B. Buchholz, S. McCarthy, C.F. Bianchi, F.W. Sellke, R. Laham, In vitro and in vivo degradation of poly(D, L-lactide-co-glycolide)/amorphous calcium phosphate copolymer coated on metal stents, *J Biomed Mater Res A*, 96 (2011) 632-638.
- [489] K. Vano-Herrera, C. Vogt, Degradation of poly(L-lactic acid) coating on permanent coronary metal stent investigated *in vivo* by micro Raman spectroscopy, *Journal of Raman Spectroscopy*, 48 (2017) 711-719.
- [490] E. Solheim, B.r. Sudmann, G. Bang, E. Sudmann, Biocompatibility and effect on osteogenesis of poly(ortho ester) compared to poly(DL-lactic acid), *Journal of biomedical materials research*, 49 (2000) 257-263.
- [491] C. Vepari, D.L. Kaplan, Silk as a Biomaterial, *Prog Polym Sci*, 32 (2007) 991-1007.
- [492] N. Dinjaski, D. Ebrahimi, Z. Qin, J.E.M. Giordano, S. Ling, M.J. Buehler, D.L. Kaplan, Predicting rates of in vivo degradation of recombinant spider silk proteins, *J Tissue Eng Regen Med*, 12 (2018) e97-e105.
- [493] B. Liebmann, D. Hümmerich, T. Scheibel, M. Fehr, Formulation of poorly water-soluble substances using self-assembling spider silk protein, *Colloids and Surfaces A: Physicochemical and Engineering Aspects*, 331 (2008) 126-132.
- [494] W. Schuler, R. Sedrani, S. Cottens, B. Häberlin, M. Schulz, H.-J. Schuurman, G. Zenke, H.-G. Zerwes, M.H. Schreier, SDZ RAD, A NEW RAPAMYCIN DERIVATIVE: Pharmacological Properties In Vitro and In Vivo, *Transplantation*, 64 (1997) 36-42.
- [495] G. Acharya, K. Park, Mechanisms of controlled drug release from drug-eluting stents, *Advanced drug delivery reviews*, 58 (2006) 387-401.
- [496] K.R. Kamath, J.J. Barry, K.M. Miller, The Taxus™ drug-eluting stent: A new paradigm in controlled drug delivery, *Advanced drug delivery reviews*, 58 (2006) 412-436.
- [497] C.R. Kaufmann, G. Mani, D. Marton, D.M. Johnson, C.M. Agrawal, Long-term stability of self-assembled monolayers on 316L stainless steel, *Biomed Mater*, 5 (2010) 25008.
- [498] R.-y. Zhang, O. ZHANG, J.-z. Zhu, L.-l. Chen, C.-y. Zhang, X.-c. Zhou, Y. Yuan, Z.-x. Zhong, L. Li, J. Qiu, Safety and efficacy of polymer-free paclitaxel-eluting microporous stent in real-world practice: 1-year follow-up of the SERY-I registry, *Chinese medical journal*, 124 (2011) 3521-3526.
- [499] S.J. Liu, F.J. Chiang, C.Y. Hsiao, Y.C. Kau, K.S. Liu, Fabrication of balloon-expandable self-lock drug-eluting polycaprolactone stents using micro-injection molding and spray coating techniques, *Ann Biomed Eng*, 38 (2010) 3185-3194.
- [500] A.W. Heldman, L. Cheng, G.M. Jenkins, P.F. Heller, D.-W. Kim, M. Ware, C. Nater, R.H. Hruban, B. Rezai, B.S. Abella, K.E. Bunge, J.L. Kinsella, S.J. Sollott, E.G. Lakatta, J.A. Brinker, W.L. Hunter, J.P. Froehlich, Paclitaxel Stent Coating Inhibits Neointimal Hyperplasia at 4 Weeks in a Porcine Model of Coronary Restenosis, *Circulation*, 103 (2001) 2289-2295.
- [501] P.K. Shah, Inflammation, Neointimal Hyperplasia, and Restenosis, *Circulation*, 107 (2003) 2175-2177.

-
- [502] M.C. Chen, H.F. Liang, Y.L. Chiu, Y. Chang, H.J. Wei, H.W. Sung, A novel drug-eluting stent spray-coated with multi-layers of collagen and sirolimus, *J Control Release*, 108 (2005) 178-189.
- [503] M.D. Dake, W.G. Van Alstine, Q. Zhou, A.O. Ragheb, Polymer-free paclitaxel-coated Zilver PTX stents—evaluation of pharmacokinetics and comparative safety in porcine arteries, *Journal of Vascular and Interventional Radiology*, 22 (2011) 603-610.
- [504] I.Y. Wu, S. Bala, N. Skalko-Basnet, M.P. di Cagno, Interpreting non-linear drug diffusion data: Utilizing Korsmeyer-Peppas model to study drug release from liposomes, *Eur J Pharm Sci*, 138 (2019) 105026.
- [505] N.A. Peppas, J.J. Sahlin, A simple equation for the description of solute release. III. Coupling of diffusion and relaxation, *International journal of pharmaceuticals*, 57 (1989) 169-172.
- [506] P. Gupta, M. Kumar, N. Bhardwaj, J.P. Kumar, C.S. Krishnamurthy, S.K. Nandi, B.B. Mandal, Mimicking Form and Function of Native Small Diameter Vascular Conduits Using Mulberry and Non-mulberry Patterned Silk Films, *ACS Appl Mater Interfaces*, 8 (2016) 15874-15888.
- [507] S.-J. Kim, J.-G. Park, J.H. Kim, J.S. Heo, J.-W. Choi, Y.-S. Jang, J. Yoon, S.J. Lee, I.K. Kwon, Development of a biodegradable sirolimus-eluting stent coated by ultrasonic atomizing spray, *Journal of Nanoscience and Nanotechnology*, 11 (2011) 5689-5697.
- [508] G. Xingzhong, H. Jie, N. Zhonghua, Optimization of coatings for vascular stent with ultrasonic spray technology, *Advances in control and communication*, Springer, 2012, pp. 547-556.
- [509] H.R. Pant, P. Pokharel, M.K. Joshi, S. Adhikari, H.J. Kim, C.H. Park, C.S. Kim, Processing and characterization of electrospun graphene oxide/polyurethane composite nanofibers for stent coating, *Chemical Engineering Journal*, 270 (2015) 336-342.